Aus der Medizinischen Klinik und Poliklinik IV der Ludwig-Maximilians-Universität München

Direktor: Prof. Dr. med. Martin Reincke

Mesenchymal stem/stromal cells engineered to express the protease inhibitor alpha-1 antitrypsin for the treatment of inflammatory lung diseases

Dissertation

zum Erwerb des Doktorgrades der Humanbiologie

an der Medizinischen Fakultät

der Ludwig-Maximilians-Universität zu München

vorgelegt von

Sabine Geiger-Schredelseker

aus Wörgl

2017

Mit Genehmigung der Medizinischen Fakultät der Universität München

Berichterstatter:	Prof. Dr. Peter J. Nelson
Mitberichterstatter:	Prof. Dr. Regina Fluhrer
	Prof. Dr. Daniel Teupser
Dekan:	Prof. Dr.med.dent. Reinhard Hickel
Tag der mündlichen Prüfung:	16.08.2017

Eidesstattliche Versicherung

Geiger-Schredelseker, Sabine

_____

Name, Vorname

Ich erkläre hiermit an Eides statt,
dass ich die vorliegende Dissertation mit dem Thema

"Mesenchymal stem/stromal cells engineered to express the protease inhibitor alpha-1 antitrypsin for the treatment of inflammatory lung diseases"

selbständig verfasst, mich außer der angegebenen keiner weiteren Hilfsmittel bedient und alle Erkenntnisse, die aus dem Schrifttum ganz oder annähernd übernommen sind, als solche kenntlich gemacht und nach ihrer Herkunft unter Bezeichnung der Fundstelle einzeln nachgewiesen habe.

Ich erkläre des Weiteren, dass die hier vorgelegte Dissertation nicht in gleicher oder in ähnlicher Form bei einer anderen Stelle zur Erlangung eines akademischen Grades eingereicht wurde.

_____   _____

Ort, Datum   Unterschrift Doktorandin/Doktorand

Acknowledgements

Table of contents

List of figures

List of tables

Abbreviations

AAT	Alpha-1 Antitrypsin
ADA-SCID	Adenosine Deaminase-deficient Severe Combined Immunodeficiency
ADAMTS-4	A Disintegrin And Metalloproteinase with Thrombospondin Motifs 4
ANGPT1	Angiopoietin-1
ARDS	Acute Respiratory Distress Syndrome
BAL	Bronchoalveolar lavage
BALF	Bronchoalveolar lavage fluid
BHQ1	Black Hole Quencher 1
bp	Base pair(s)
CAG	CMV enhancer-chicken beta actin promoter-rabbit beta globin splice acceptor
cAMP	Cyclic Adenosine Monophosphate
CAST	Computer Assisted Stereological Toolbox
CChord	Chord Compliance
CD	Cluster of Differentiation
CDS	Coding Sequence
Cdyn	Dynamic Compliance
CF	Cystic Fibrosis
cf.	*confer*
CFU(s)	Colony Forming Unit(s)
cm^2	Square Centimeter
CMV	Cytomegalovirus
COPD	Chronic Obstructive Pulmonary Disease
Cp	Crossing point
CRP	C-Reactive Protein
DAMP(s)	Danger-Associated Molecular Pattern(s)
DC(s)	Dendritic Cell(s)
DMEM	Dulbecco's Modified Eagle's Medium
DMSO	Dimethyl Sulfoxide
DNA	Desoxyribonucleic Acid
e.g.	*exempli gratia*
ECD	Energy Coupled Dye
EF1a	Eukaryotic Translation Elongation Factor 1 alpha 1
EFS	Eukaryotic Translation Elongation Factor 1 alpha 1 (short)
EGF	Epidermal Growth Factor
eGFP	Enhanced Green Fluorescent Protein
ELISA	Enzyme-Linked Immunosorbent Assay
EMCV	Encephalomyocarditis Virus
EMEM	Eagle's Minimum Essential Medium
ER	Endoplasmic Reticulum
ERV	Expiratory Reserve Volume
ESC(s)	Embryonic Stem Cell(s)
FEV_{100ms}	Forced Expiratory Volume after 100ms
FEV_{1s}	Forced Expiratory Volume after 1s
FFP	Fresh Frozen Plasma
FGF	Fibroblast Growth Factor

FITC	Fluorescein Isothiocyanate
FRC	Functional Residual Capacity
FVC	Forced Vital Capacity
FVII	Coagulation Factor VII
g	gram
GaLV	Gibbon ape Leukemia Virus
gRV	Gamma-Retroviral Vector
GvHD	Graft versus Host Disease
h	Human
H&E	Hematoxylin and Eosin
HA	Human Albumin
HAES	Hydroxyethyl Starch
HEPES	N-2-hydroxyethylpiperazine-N-2-ethane sulfonic acid
HGF	Hepatocyte Growth Factor
HIV	Human Immunodeficiency Virus
HNE	Human Neutrophil Elastase
HSC(s)	Hematopoietic Stem Cell(s)
HSP70	Heat Shock Protein 70kDa
HSP90B1	Heat Shock Protein 90kDa Beta Member 1
i.e.	*id est*
IC	Inspiratory Capacity
IDO	Indoleamine 2,3-Dioxygenase
IFN-beta	Interferon beta
IFN-gamma	Interferon gamma
IGF-1	Insulin-like Growth Factor-1
IL-1	Interleukin 1
IL-10	Interleukin 10
IL-1ra	Interleukin 1 receptor antagonist
IL-2	Interleukin 2
IL-6	Interleukin 6
IL-8	Interleukin 8
iPSC(s)	Induced Pluripotent Stem Cell(s)
IRES	Internal Ribosome Entry Site
kb	Kilobase pair(s)
kg	Kilogram
KGF	Keratinocyte Growth Factor
L	Liter
LAM PCR	Linear Amplification Mediated Polymerase Chain Reaction
LB	Luria-Bertani medium
LTR(s)	Long Terminal Repeat(s)
luc	Firefly luciferase 2
LV	Lentiviral Vector
MCP-1	Monocyte Chemoattractant Protein-1
MCS	Multiple cloning site
MFI(s)	Mean Fluorescence Intensity/Intensities
miRNA(s)	MicroRNA(s)
mL	Milliliter

MLV	Murine Leukemia Virus
MMP-9	Matrix Metallopeptidase-9
MOI	Multiplicity Of Infection
ms	Millisecond(s)
MSC(s)	Mesenchymal Stem/Stromal Cell(s)
N.a.	Not applicable
n.d.	No date
NCBI	National Center for Biotechnology Information
NE	Neutrophil Elastase
NEAA	Non-Essential Amino Acids
NF-kappaB	Nuclear Factor kappa-light-chain-enhancer of activated B cells
NK cells	Natural Killer Cell(s)
ns	Not significant
oPRE	Optimized Posttranscriptional Regulatory Element
p	Promoter
pac	Puromycin N-acetyltransferase
PAR(s)	Protease Activated Receptor(s)
PBMC(s)	Peripheral Blood Mononuclear Cell(s)
PBS	Phosphate Buffered Saline
PC7	Phycoerythrin-Cyanin-7
PCR	Polymerase Chain Reaction
PDGF	Platelet-Derived Growth Factor
PE	R-Phycoerythrin
PGE2	Prostaglandin E2
PGK	Phosphoglycerate Kinase
PL	Platelet Lysate
PLL	Poly-L-Lysin
PPE	Porcine Pancreatic Elastase
qPCR(s)	Quantitative Polymerase Chain Reaction(s)
RCL	Replication-Competent Lentivirus
RCR	Replication-Competent Retrovirus
RFU	Relative Fluorescence Units
ROS	Reactive Oxygen Species
rpm	Revolutions per minute
RPMI	Roswell Park Memorial Institute
RSV	Rous Sarcoma Virus
SD	Standard Deviation
SDF-1	Stromal Cell Derived Factor-1
SEC	Serpine Enzyme Complex
SERPINA1	Serpin Peptidase Inhibitor, clade A (alpha-1 antiproteinase, antitrypsin), member 1
SFFV	Spleen Focus Forming Virus
SIN	Self-inactivating
SV40	Simian vacuolating Virus 40
TD	Transduction
TGF-beta	Transforming Growth Factor-beta
Th	T helper
TNF-alpha	Tumor Necrosis Factor-alpha

Treg(s)	Regulatory T lymphocyte(s)
TSG-6	TNF-alpha-stimulated gene 6
TU	Transducing Units
UTR	Untranslated Region
VC	Vital Capacity
VCN(s)	Vector Copy Number(s)
VEGF	Vascular Endothelial Growth Factor
vs.	*versus*
VSV.G	Vesicular Stomatitis Virus Protein G
WBC(s)	White Blood Cell(s)
WP(s)	Work package(s)
wPRE	Woodchuck Hepatitis Virus Posttranscriptional Regulatory Element
µL	Microliter
Ψ, psi	Packaging signal

Abstract

Chronic inflammatory diseases are a growing global health problem. Chronic obstructive pulmonary disease (COPD) represents a major cause of morbidity and mortality, and is currently the third leading cause of death worldwide. COPD is a devastating progressive lung disease characterized by airflow limitation, chronic bronchitis and bronchiolitis, emphysema, and small airway remodeling. There are no curative options for COPD to date, thus there is a desperate need for novel approaches and treatments. To this end, the goal of this thesis work was to develop and evaluate a novel cell product composed of mesenchymal stem/stromal cells (MSCs) genetically modified to express the protease inhibitor alpha-1 antitrypsin (AAT), thus combining the potent immunomodulatory and cytoprotective properties of MSCs, and of AAT. A major focus was the development of an optimized expression construct/vector system for MSC engineering. Eight versions of gamma-retroviral-based vectors were designed and tested for optimal transgenic expression of human AAT and puromycin-N-acetyltransferase (*pac*) for antibiotic selection. The constructs differed in the gene promoter used for driving AAT expression, and in the relative position of the expression cassettes within the vector backbone. The vectors were then compared with regards to viral titers, transduction efficacy of primary human MSCs, AAT expression in the supernatant of transduced cells, and cell yield after antibiotic selection. The best results for all parameters were obtained when AAT was expressed from the human eukaryotic translation elongation factor 1 alpha 1 short (EFS) promoter, and the *pac* gene was linked via an internal ribosome entry site (IRES) sequence. This lead candidate expression cassette was then transferred to a lentiviral backbone to assess if transduction and AAT expression from MSCs could be further increased by using this viral system. While values were higher with the gamma-retroviral vector at low multiplicities of infection (MOIs), transduction reached a plateau and no further increase was possible even when higher MOIs were used. Transduction with the lentiviral construct, however, followed a clear dose-response, reaching transduction efficacies >80% at the highest MOI tested. *In vitro* functionality of the protease inhibitor AAT expressed from MSCs was confirmed using a neutrophil elastase inhibition assay. A process for large scale transduction and expansion of gene-modified MSCs was subsequently developed. To evaluate the potential therapeutic benefit of AAT-MSCs *in vivo*, a mouse model of elastase-induced emphysema was used. Treatment of the mice with AAT-MSCs resulted in significant improvement of pulmonary function parameters, while only a slight functional amelioration was observed after treatment with non-modified MSCs. Histopathologic examination of AAT-MSC-treated mice revealed a significant decrease of airspace enlargement, indicating regeneration of pulmonary tissue. Again, the effect was smaller after treatment with non-modified MSCs, demonstrating a more than additive effect of

combining AAT and MSCs. In conclusion, the present study provides the first *in vivo* proof of concept for the treatment of emphysematous COPD using engineered AAT-MSCs.

Zusammenfassung

Chronisch entzündliche Erkrankungen sind heutzutage ein globales, im Steigen begriffenes Gesundheitsproblem. Ein wichtiges Beispiel ist die chronisch obstruktive Lungenerkrankung (COPD), eine verheerende, fortschreitende Erkrankung der Lunge mit hoher Morbidität und Mortalität, gegenwärtig die dritthäufigste Todesursache weltweit. Symptome der COPD sind Atemnot, eine chronische Entzündung der Bronchien und Bronchiolen, die Entwicklung eines Emphysems und ein Umbau der engen Atemwege. Da bislang eine Heilung der COPD nicht möglich ist, besteht ein dringender Bedarf an innovativen Therapieansätzen. Wir entwickelten ein neuartiges Zellprodukt, basierend auf mesenchymalen Stamm-/Stromazellen (MSCs), die genetisch modifiziert wurden, sodass sie den Protease-Inhibitor Alpha-1 Antitrypsin (AAT) exprimieren. Diese Kombination ermöglicht es, die immunmodulatorischen und zytoprotektiven Eigenschaften der MSCs mit jenen von AAT in einem Produkt zu vereinen. Dabei wurde in der vorliegenden Arbeit ein Fokus auf die Entwicklung eines optimierten Expressionskonstruktes gelegt. Es wurden acht gamma-retrovirale Vektoren für die Expression von AAT und Puromycin-N-Acetyltransferase (*pac*), das eine Antibiotikaselektion genmodifizierter Zellen erlaubt, konzipiert und kloniert. Diese Konstrukte unterscheiden sich sowohl im Promoter, der für die AAT-Expression verwendet wird, als auch in der relativen Anordnung der Expressionskassetten im Plasmid. Die Auswahl des besten Konstrukts wurde anhand eines Vergleichs der Vektoren hinsichtlich der erzielten viralen Titer, der Transduktionseffizienz von primären humanen MSCs, des AAT-Gehalts im Zellkulturüberstand von transduzierten MSCs sowie der Zellausbeute nach Antibiotikaselektion durchgeführt. Die jeweils besten Ergebnisse wurden erzielt, wenn AAT von der kurzen Form des Promoters des humanen eukaryotischen Translationselongationsfaktors 1 alpha 1 (EFS) exprimiert wurde, und das *pac* Gen durch eine interne ribosomale Eintrittsstelle- (IRES)-Sequenz verknüpft war. Diese favorisierte Expressionskassette wurde in ein lentivirales Plasmid transferiert, um zu untersuchen, ob Transduktion und AAT-Expression in einem solchen System weiter verbessert werden können. Es zeigte sich, dass mittels des gamma-retroviralen Vektors größere Transduktionseffizienzen und AAT-Mengen bei niedriger Multiplizität der Infektion (MOI) erzielt werden konnten, aber bei höheren MOIs keine zusätzliche Verbesserung zu erreichen war. Im Gegensatz dazu folgten Transduktion und AAT-Expression mittels des lentiviralen Vektors einer eindeutigen Dosis-Wirkung, die bei hohen MOIs in Transduktionseffizienzen von >80% resultierte. Ein Neutrophile Elastase Inhibitionstest bestätigte die *in vitro* Funktionalität von MSC-sezerniertem AAT als Proteaseinhibitor, bevor Transduktions- und Expansionsprozesse zur Herstellung von AAT-MSCs im Großformat etabliert wurden. Um die therapeutische Wirkung von AAT-MSCs *in vivo* zu untersuchen, wurde ein Mausmodell eines Elastase-induzierten Emphysems durchgeführt. Es zeigte sich, dass die Behandlung von Mäusen mit AAT-MSCs zu einer signifikanten Verbesserung der Lungenfunktion der Tiere führte, während nicht-

modifizierte MSCs nur eine geringfügige Wiederherstellung der pulmonalen Funktion bewirkten. Die histopathologische Analyse ergab, dass die Überblähung der Lunge durch die Applikation von AAT-MSCs signifikant vermindert werden konnte, was auf eine Regeneration des Lungengewebes hindeutet. Auch in dieser Auswertung fiel der durch die Behandlung mit nicht-modifizierten MSCs erzielte Effekt geringer aus, was eine additive Wirkung von AAT und MSCs nahelegt. Zusammenfassend kann festgestellt werden, dass die vorliegende Arbeit einen ersten Nachweis des Wirkkonzepts von AAT-MSCs für die Behandlung von entzündlichen Lungenerkrankungen wie emphysematöser COPD erbringen konnte.

1. Introduction

1.1. Chronic obstructive pulmonary disease

1.1.1. Epidemiology and economics

Chronic inflammatory diseases are a growing health problem worldwide, imposing an increasing burden on individuals, populations, and economies [1]. Among them, chronic obstructive pulmonary disease (COPD) must be given a central role. It is a heterogeneous, common, and complex disorder that is at present the third leading cause of mortality globally, being responsible for more than three million deaths worldwide (equal to 6% of all deaths) in 2012 [2]. Since mild disease often goes unrecognized and thus undiagnosed, it is difficult to obtain prevalence data for COPD [3]. It is, however, estimated that in 2013 COPD affected 329 million people or nearly 5% of the global population [4,5]. COPD is also associated with a substantial economic burden. As of 2010, COPD is believed to result in global economic costs of $2.1 trillion, where $1.9 trillion are direct costs such as medical care, and $0.2 trillion are indirect costs such as missed work [6]. In the European Union, COPD accounts for 56% of all costs related to respiratory diseases, amounting to €38.6 billion, where exacerbations account for the majority of the total health costs related to COPD [7].

1.1.2. Pathophysiology

COPD is a progressive obstructive lung disease that is characterized by airflow limitation, an excessive chronic inflammatory response to noxious particles in the large and small airways of the lungs (bronchitis and bronchiolitis, respectively), with fibrosis and airway remodeling, alveolar destruction with airspace enlargement (emphysema), and mucus hypersecretion [3,8,9]. COPD is pathologically and histologically heterogeneous, and the symptoms vary in proportion between affected individuals [10]. Furthermore, the clinical picture can often be accompanied by cardiovascular disease, fatigue, depression, musculoskeletal dysfunction, weight loss, and osteoporosis [3,11]. The severity of the disease is currently categorized based on GOLD (Global initiative for chronic Obstructive Lung Disease) criteria on a 0–4 scale, depending on symptoms and the decline in lung function [8]. Patients suffering from advanced disease (GOLD score 2 and higher) progressively experience more frequent and severe acute exacerbations as their condition continues to deteriorate [12]. These exacerbations are most often the result of viral or bacterial chest infections or environmental pollutants [8].

Classically, COPD is diagnosed by spirometry, with the clinical criteria defining COPD comprising a forced expiratory volume after one second (FEV_1) value of <80% predicted, and a post-bronchodilator FEV_1:FVC (forced vital capacity) ratio <0.70 [13].

1.1.3. Risk factors for COPD development

The most important risk factor for the development of COPD is tobacco smoking, probably accounting for 80–95% of all COPD cases in industrialized countries [10,14,15]; however, only 15–25% of smokers develop COPD [16–18]. Other environmental factors such as increasing air pollution, whose connection to lung disease was established during the London smog years of the 1950s [19], occupational exposure to fumes and particulates [20], as well as the inhalation of domestic and cooking fumes, have also been linked to an increased risk of COPD development [21,22]. These risk factors can lead to an accelerated progression of the disease in combination with cigarette smoking.

It is commonly accepted that the chronic inflammation seen in the respiratory tract of patients suffering from COPD results from an excessive immune response to chronic irritants such as tobacco smoke. The reasons for this inflammation are not yet fully understood, but could be in part genetically determined, since there clearly are COPD patients who are non-smokers, and there are also many smokers who never develop COPD, despite having chronic lung inflammation that continues for many years even after smoking cessation [7,15]. Moreover, COPD is known to cluster in families, strongly hinting at the involvement of genetic factors [11]. Indeed, accumulating evidence suggests that there might be a genetic predisposition to COPD [23–27]. One candidate gene is *SERPINA1*, the gene encoding for the protein alpha-1 Antitrypsin (AAT, for more details please see chapter 1.4). The potential correlation of AAT deficiency and COPD was first suggested by Lomas and colleagues in 2006 [28], their theory has found support in several studies during the last decade, and it is now generally accepted that carrier status of AAT deficiency alleles is a strong genetic factor associated with the development of COPD [12,29–33].

1.1.4. Pathogenesis

The pathogenesis of COPD is hypothesized to result from three major pathways: (1) dysregulation of tissue homeostasis within the lung, (2) oxidative stress, and (3) protease-antiprotease imbalance [3]. However, the interplay of these pathways and the molecular mechanisms leading to COPD are still incompletely understood [11].

1.1.4.1. Inflammatory cells and mediators

A plethora of cell types are involved in the pathogenesis of COPD, with neutrophilic granulocytes and alveolar macrophages thought to represent very important cell types in the disease. In comparison to normal smokers, patients with COPD have 5- to 10-fold elevated macrophage levels in their airways, lung parenchyma, bronchoalveolar lavage fluid (BALF) and sputum [34,35], and macrophage numbers strongly correlate with disease severity [36]. Macrophages are potent immune effector cells, and upon contact with cigarette smoke or other noxious substances they can secrete inflammatory mediators such as tumor necrosis factor-alpha (TNF-alpha), monocyte chemoattractant protein-1 (MCP-1),

reactive oxygen species (ROS), chemotactic factors for neutrophilic granulocytes such as interleukin 8 (IL-8), and a number of elastolytic enzymes like matrix metalloproteinases or cathepsins, which are involved in the destruction of the lung tissue leading to emphysema [14]. Patients suffering from COPD also have elevated levels of neutrophils which are linked to the severity of the disease [34], and with deterioration of lung function [37]. Neutrophils are powerful immune cells that can secrete a variety of inflammatory mediators such as tissue proteases like neutrophil elastase, proteinase-3 and cathepsin G, all of which can lead to destruction of the lung parenchyma, and ROS or lipid mediators [38,39]. Cells of the adaptive immune system are also associated with COPD inflammation, with CD8+ T cells and T helper (Th) 17 cells thought to be the most clinically important [40,41].

1.1.4.2. Oxidative stress

A second important aspect in the pathogenesis of COPD is oxidative stress, a very important factor to consider with regards to the massive oxidant burden seen in smokers. Cigarette smoke comprises over 4700 chemical compounds and more than 10^{15} free radicals and oxidants, which can give rise to damaging levels of ROS produced by inflammatory and epithelial cells [42]. Generation of ROS further exacerbates inflammatory processes, leads to DNA damage, lipid peroxidation, and protein denaturation [43]. An interesting aspect that again underscores the potential importance of AAT in the pathogenesis of COPD, especially in patients who smoke, is that cigarette smoke has been shown to result in oxidation of the critical methionine at position 358 of AAT [44]. This modification renders the protein non-functional as an inhibitor of neutrophil elastase, thereby contributing to the proteinase-antiproteinase imbalance thought to play a role in the development of emphysema [44–46].

1.1.4.3. Proteinases in COPD

As detailed above, a variety of proteinases are secreted from immune cells such as neutrophils and macrophages as part of the excessive inflammatory response in COPD. Due to an imbalance between proteinases and endogenous inhibitors, which normally have a protective effect on the lung tissue, extracellular matrix (specifically elastin) in the lung parenchyma is destroyed by action of the proteinases resulting in airspace enlargement and emphysema [47]. The major proteinases involved in COPD are neutrophil elastase, proteinase-3 and various matrix metalloproteinases [48,49]. With regards to the present work, it is important to point out that AAT acts as a major endogenous serine proteinase inhibitor and thus plays an important role in counterbalancing the excessive release of proteinases. As described above, patients suffering from AAT deficiency are at increased risk of developing emphysema and COPD [28,31,50]. AAT may also have additional modes of action relevant for emphysema and COPD apart from its function as protease inhibitor, since mutations in AAT clearly are associated with these diseases, while mutations in neutrophil elastase are not [3].

1.1.5. Treatment

To date, there is no cure for COPD [13]. However, the major cause of the disease and means of prevention are well recognized. COPD is thought to be largely preventable, or at least its progression can be decelerated, by smoking cessation [51,52]. Due to the addictive nature of tobacco, attempts in quitting over five years are successful in only 37% of cases [53]. Additional preventive measures include improving air quality [51], as well as influenza and pneumococcus vaccinations for patients already suffering from COPD and experiencing exacerbations [54,55].

Once patients are diagnosed with COPD, the focus of therapy is on managing the disease and treating the symptoms, preventing and treating acute exacerbations, as well as controlling associated illnesses [56]. The only therapeutic approaches that have been described to reduce COPD mortality are supplemental oxygen and smoking cessation, of which the latter can decrease the risk of death by 18% [57,58]. Other current standard pharmacologic medications are primarily used to reduce symptoms and improve lung function; however, to date there are no drugs found that can significantly limit disease progression [9]. Drugs that can provide a measure of help include inhaled short-acting and long-acting bronchodilators. They are the most commonly used and usually yield a small overall benefit for patients by helping to alleviate shortness of breath, resulting in an improvement in quality of life [59,60]. Inhaled corticosteroids are typically added to the bronchodilators [57], which can work fairly well in controlling acute exacerbations, especially in patients with either moderate or severe COPD [61]. Additional treatment options include antibiotics, which are mainly used in patients suffering from two or more acute exacerbations per year [62,63]. The last treatment option for patients with severe COPD is surgery. This can be either lung volume reduction surgery to remove the parts of the lung that are destroyed by emphysema and thus allow the remaining parts of the lung to work more effectively, or – in very severe cases, and primarily in younger subjects – lung transplantation [64,65]. However, despite improved survival rates after lung transplantation, this is unfortunately not an option for most patients due to the increasing demand and the scarcity of donor organs [65,66].

During the last decade, new therapeutic strategies such as TNF-alpha antagonism [67–69] or IL-8 antagonism [70] have been tested in clinical trials; however, despite TNF-alpha and IL-8 clearly being involved in the pathogenesis of COPD, none of the studies showed subjective or objective long-term improvements. Moreover, the blockage of single key cytokines raises questions regarding long-term safety, *i.e.* a possibly increased likelihood of developing infections or malignancies [9]. Thus, there is a compelling need for the development of novel, improved therapeutic strategies for the treatment of inflammatory lung diseases such as COPD that aim at persistently controlling the underlying inflammatory processes, while at the same time leading to regeneration of the damaged lung tissue. This thesis presents an innovative cell therapy-based approach to accomplish this task.

1.2. Cell therapy and mesenchymal stem/stromal cells

Since the first successful hematopoietic stem cell (HSC) transplantation reported in 1959 [71], there has been a continuing expansion in the number of clinical trials investigating the application of stem cells [72]. In addition to HSCs, embryonic stem cells (ESCs) [73,74], induced pluripotent stem cells (iPSCs) [75], limbal stem cells [76], neural stem cells [77,78], and endothelial stem and progenitor cells [79,80] are currently being tested in clinical trials for the treatment of a variety of diseases including macular degeneration, corneal destruction, repair of the central nervous system, and critical limb ischemia. The clinical use of ESCs and iPSCs has been impeded by ethical issues, the risk of genomic instability, teratoma formation as well as allogeneic rejection problems [81,82].

In addition to HSCs, mesenchymal stem/stromal cells (MSCs) are currently the most favored cell type under investigation, with as many as 520 registered clinical trials (studies with unknown status excluded) listed in the NIH clinical trial database on June 15, 2016 [83]. Due to their broad repertoire of beneficial features including immunomodulation, growth factor production, anti-fibrosis and anti-apoptosis, angiogenesis, and neuroprotection, MSCs are under clinical trial for the treatment of diverse diseases, and the results to date have been highly encouraging in the potential treatment of Graft versus Host Disease (GvHD) [84,85], type 1 diabetes [86], transplant rejection [87,88], myocardial ischemia and infarction [89,90], and Crohn's disease [91,92]. MSCs are also being investigated for therapy of lung diseases such as acute respiratory distress syndrome (ARDS) [93], and COPD [94], thus far demonstrating an excellent safety profile. These studies are only in the early phases of testing and thus not yet empowered to assess efficacy [94]. However, positive outcomes indicative of potential efficacy have been seen, as for instance a significant reduction of C-reactive protein (CRP) levels in a subgroup of patients who had elevated levels at baseline in a clinical trial of MSCs in COPD [94].

The following section sets out to describe the biology of MSCs in greater detail and to highlight features specifically important to the treatment of inflammatory lung diseases such as COPD.

1.2.1. General MSC biology

MSCs are multipotent progenitor cells of non-hematopoietic origin that were first described by Friedenstein and colleagues in the late 1960s as the "colony-forming unit fibroblast" [95]. They described adult, plastic-adherent, spindle-shaped, fibroblast-like cells which were defined by their capacity to form new bone when transplanted to an ectopic site [96,97]. These cells were later renamed "mesenchymal stem cells" and their differentiation potential expanded to "tri-lineage" mesenchymal tissues; bone, cartilage, and fat [98]. However, their level of "stemness" is still a matter of debate among scientists as *in vivo* confirmation of their stem cell characteristics has not been established [99]. The International Society for Cellular Therapy (ISCT) published a statement paper in 2005 addressing this inconsistency between nomenclature and biologic characteristics, suggesting that the term

"stem cell" should be only used when specified stem cell criteria have been confirmed, while all other cells should be named "multipotent mesenchymal stromal cells" [100]. It was suggested that the commonly used acronym "MSC" should be employed for both cell populations, as subsequently done in the present work. It is important to note that the various clinical values of MSCs described to date do seem to be largely independent of potential stem cell properties [99].

One major advantage MSCs have regarding their clinical utilization with respect to other stem cell types is their ease of accessibility for isolation: MSCs have successfully been isolated and expanded from various tissues including bone marrow, umbilical cord, adipose tissue, dental pulp, and placenta [101,102]. It is thought that most organs have endogenous populations of MSCs, and that MSCs may have a perivascular origin [103,104]. In the bone marrow, MSCs can be found in the so-called HSC niche, where they support the survival, self-renewal, migration, and differentiation of HSCs and precursor cells [105]. In lung tissue, MSCs are predominantly localized to the perivascular region [106,107]. Since there is no distinct surface marker defining MSCs, and MSCs are represented by a fairly heterogeneous population of cells, the ISCT issued another position paper in 2006 proposing three minimal criteria defining MSCs to avoid ambiguities and inconsistencies in the field [108]. A summary of the benchmark values is shown in Table 1.

Table 1: **The minimal criteria defining MSCs according to ISCT.**

1	Adherence to plastic in standard culture conditions	
2 Phenotype	Positive (≥95%+)	Negative (≤2%+)
	CD105	CD45
	CD73	CD34
	CD90	CD14 or CD11b
		CD79a or CD19
		HLA-DR
3	*In vitro* differentiation into osteoblasts, adipocytes, and chondroblasts	

1.2.2. Mode of action of MSCs

In early MSC research it was thought that the beneficial effect of MSCs is mainly derived from their supportive action on HSCs [109], their co-localization and engraftment at the site of injury, and replacement of damaged tissue [110]. However, the field has since undergone a paradigm shift. Today more emphasis has been placed on the trophic and immunomodulatory capabilities of MSCs, their secretion of a plethora of cytokines, growth factors, and of extracellular vesicles [99,111–114]. It is now thought that the cells may only briefly interact with injured tissues, but in this time they act on inflammatory and damaged cells to dampen inflammation, limit tissue destruction, and enhance repair [109], a mechanism that has been referred to as "hit-and-run" by some researchers. Interestingly, recent data show that even though MSCs do not persist *in vivo*, the beneficial effects they exert can

remain detectable long after the cells have disappeared [115,116]. Support of this hypothesis is found in a recent work by Dos Santos and colleagues, who described that after application of MSCs in a mouse model of sepsis, 13% of the mouse genome was transcriptionally reprogrammed [117]. They observed a change in transcriptional activity of genes involved in mitochondrial-related functional derangement, innate immune pro-inflammatory responses, and vascular integrity, leading to significant MSC-induced amelioration of sepsis [117].

1.2.3. MSCs and tissue repair by paracrine signaling

Due to their wide tissue distribution, and their multipotent differentiation capabilities, MSCs are thought to play important roles in the repair of damaged tissues [118]. During tissue injury, such as the emphysema present in COPD, immune cells are recruited to the site of damage by factors secreted from apoptotic and necrotic cells, injured microvasculature, and stroma, so-called damage-associated molecular patterns (DAMPs) [119–121]. These inflammatory cells in turn produce pro-inflammatory cytokines such as interleukin 1-beta (IL-1beta), interferon gamma (IFN-gamma), and TNF-alpha, chemokines, and free radicals, which conversely induce the secretion of growth factors from MSCs, including interleukin 6 (IL-6), epidermal growth factor (EGF), fibroblast growth factor (FGF), platelet-derived growth factor (PDGF), vascular endothelial growth factor (VEGF), hepatocyte growth factor (HGF), keratinocyte growth factor (KGF), insulin-like growth factor-1 (IGF-1), antiopoietin-1 (ANGPT1), stromal cell derived factor-1 (SDF-1), and transforming growth factor-beta (TGF-beta) [122–125]. These molecules orchestrate a molecular program that leads to a support of the development of myofibroblasts, endothelial cells as well as tissue progenitor cells, resulting in tissue regeneration and repair, amelioration of tissue integrity and support of angiogenesis [126–132]. A paracrine factor which seems to be specifically important in regard to lung injury is HGF, which has been shown to not only restore integrity and permeability of endothelial cells, but to also ameliorate lung injury in models of both emphysema and pulmonary fibrosis [133–135]. Another cytokine crucial for MSC-induced tissue regeneration is IL-6, which has been recently described to support the regeneration of airway ciliated cells from basal stem cells *in vivo* [136].

Apart from classical growth factors and cytokines, MSCs also secrete other types of molecules such as the anti-microbial peptide LL37 [137] and Lipoxin A4, a lipid mediator which has recently been described to lead to significant amelioration of acute lung injury [138]. These molecules could be especially important in light of the treatment of COPD patients suffering from acute exacerbations of disease due to bacterial and viral infections.

1.2.4. Immunomodulatory properties of MSCs

MSCs possess highly effective immunoregulatory properties, affecting both the innate and adaptive immune system [111]. It is important to note that there is a plasticity of MSCs in immunomodulation

that is dependent on the microenvironment [139,140]. In the context of inflammation, MSCs are predominantly instructing anti-inflammatory functions, while in an anti-inflammatory environment they support pro-inflammatory actions of immune cells, providing a mechanism to maintain a balanced immune response [141].

In co-culture experiments MSCs have been shown to have the ability to modulate a variety of immune cells, including T cells, B cells, neutrophils, macrophages, natural killer (NK) cells, and dendritic cells (DCs) [142,143]. These effects are thought to be primarily mediated via a number of soluble factors secreted by MSCs including: indoleamine 2,3-dioxygenase (IDO), prostaglandin E2 (PGE2), interleukin 10 (IL-10), IL-1 receptor antagonist (IL-1ra), TGF-beta, HLA-G5, and TNF-alpha-stimulated gene 6 (TSG-6) [141]. These paracrine factors can influence immune processes as demonstrated by the example of IL-1ra secreted by MSCs, shown to mediate both anti-inflammatory and anti-fibrotic processes in a mouse model of bleomycin-induced lung fibrosis [144]. However, cell-cell contact leading to FAS/FAS ligand or the programmed cell death protein-1 (PD-1)/ programmed death-ligand 1 (PD-L1) pathway activation has also been linked to immunomodulation by MSCs [145,146]. MSCs can directly inhibit T cell function in an inflammatory milieu, rendering T cells anergic, or they can help induce a shift towards a regulatory T cell phenotype, even in the case of Th17 effector cells [147–150]. Interestingly, these effects of MSCs on T cell biology have also been described in models of allergic airway inflammation and acute lung injury [151,152]. Direct cell-cell contact via the FAS/FAS ligand death pathway is thought to play a role in the induction of apoptosis of T cells by MSCs as described in mouse models of systemic sclerosis and experimental colitis [153]. Furthermore, MSCs have been shown to suppress B cell proliferation and differentiation towards plasma cells [154,155], and to induce the development of IL-10-secreting regulatory B cells [156].

In addition, MSCs have the ability to regulate T and B cells through their effects on antigen-presenting cells, such as DCs or monocytes, both of which adopt a suppressive, IL-10-producing phenotype in the presence of MSCs [157–159].

As detailed above, macrophages and neutrophils, cells of the innate immune system, are thought to represent major effector immune cell types involved in the pathogenesis of COPD. MSCs can also regulate macrophage and neutrophil biology [142,143]. Upon exposure to MSCs, macrophages undergo a phenotypic switch from classically activated pro-inflammatory macrophages (M1), to alternatively activated anti-inflammatory macrophages (M2), in response to PGE2 and TSG-6 secreted by MSCs under inflammatory conditions [160,161]. Accordingly, MSCs have been described to alleviate emphysema and airway inflammation in a rat model through their interaction with alveolar macrophages [162]. It has furthermore been shown that MSCs effectively decrease neutrophil infiltration in mouse models of experimental emphysema and obliterative bronchiolitis [163,164] and inhibit neutrophil-mediated tissue damage in a murine model of vasculitis [165].

A newly discovered mechanism of cell communication is based on their secretion of extracellular vesicles or exosomes which contain proteins, RNAs, lipids, and other bioactive factors [166]. Microvesicles derived from human MSCs have been reported to exert positive effects on pulmonary edema and decreased neutrophil infiltration when applied intratracheally to mice in a model of acute lung injury [167].

Taken together, MSCs exert a plethora of immunomodulatory and regenerative functions that have been shown to be beneficial in a variety of inflammatory diseases.

1.2.5. Advantages of MSCs for clinical use

Apart from their outstanding immunomodulatory and tissue-protective functions, MSCs have additional characteristics that make them very attractive candidate cells for clinical use. As described above, one is their ease of access. They can be isolated from a variety of different tissues, some of which otherwise would even be subject to discard, such as adipose tissue or placenta. Moreover, they can readily be expanded using basic standard cell culture methods, which to date is not possible to that extent for many other cell types such as *e.g.* HSCs [168]. Furthermore, in comparison to ESCs, there are no ethical issues associated with the clinical use of MSCs, and as opposed to iPSCs, MSCs do not entail the risk of teratoma formation due to the fact that they are not pluripotent [169]. Owing to their limited lifespan and other intrinsic factors, also the overall risk of tumorigenicity seems to be negligible [170]. Another advantage MSCs have in contrast to other cell types is the fact that due to their immunomodulatory properties, they are immune-evasive and can be administered in an allogeneic setting [99]. In fact, most patients in clinical trials receive allogeneic MSCs [171], and their application seems to be feasible and safe so far [115,172]. One major advantage MSCs have in comparison to other therapies, such as small molecules or biologics, is that based on their intrinsic ability to home to sites of injury and inflammation, they exert their effects locally, thus minimizing the toxicity oftentimes seen with the first-mentioned substances [173]. Moreover, while many non-cell-based medications have to be applied many times to yield a therapeutic benefit due to their short half-life, it is thought that even a single application of MSCs is beneficial due to their "hit-and-run" mode of action [115,116,174,175]. All these features taken together make MSCs an extremely attractive candidate cell for clinical applications.

MSCs seem ideally suited as therapy vehicles for the treatment of COPD due to their potent immunomodulatory and regenerative properties combined with their ease of clinical applicability. Recently, gene modification has emerged as a potent tool to modulate cell therapy products. The goal of this thesis is focused at exploring the potential of genetically modified MSCs as an optimized cell product for the treatment of COPD.

1.3. Cell-based gene therapy

Cell-based gene therapy is described as the introduction of genetic material into cells, and the use of these gene-modified cells with their new or enhanced therapeutic properties for the prevention, alleviation, or cure of a disease. The most common strategy employed for the introduction of transgenes into cells makes use of integrating viral vectors such as gamma-retroviral or lentiviral vectors [176,177]. Since its infancy in the 1970s, when the first clinical trials using gene therapy approaches were performed [178–181], gene therapy has undergone great ups and downs, but in May 2016 the first *ex vivo* stem cell gene therapy product received marketing authorization by the European Commission [182]. However, as straight forward as this approach sounds, the obstacles of putting it into practice are extremely challenging. New genetic information must be introduced into the target cells past complicated cellular barriers; the transgene has to be expressed at sufficient levels to yield a therapeutic benefit without disrupting important regulatory mechanisms; the genetically modified cells must then be produced in sufficient amounts; and when applied to the patient, the cells must evade the patient's immunological surveillance long enough to be able to exert their therapeutic effects [177]. Thus it is not surprising that only a limited number of clinical gene therapy trials performed during the last two decades were able to demonstrate clear benefits for the patients [183,184]. In some, the patients even experienced severe adverse events such as the development of leukemia due to vector integration near oncogenes during their long-term follow-up [185–187], which led to increased skepticism towards this therapeutic approach [177]. More recently there has been a shift in attitudes towards gene therapy, due in large part to several recent pivotal studies reporting remarkable efficacy and also safety of gene therapy approaches, enabling the treatment of life-threatening diseases like primary immunodeficiencies [184,188,189], Wiskott-Aldrich syndrome [190], thalassemia [191], and neurodegenerative storage diseases [192,193]. These have been made possible by the development of viral vectors with improved safety and efficacy, such as self-inactivating (SIN) vectors and split-genome conditional packaging systems [194,195]. To date, most of the stem cell-based clinical gene therapy trials, including those mentioned above, have made use of HSCs.

MSCs have only very recently appeared on the gene-therapy field. However, gene-modified MSCs, for example armed with a suicide gene, are currently in a first-in-human phase I/II study for advanced gastrointestinal tumors [196] and have demonstrated an excellent safety profile so far (C. Günther, personal communication). Of course, suicide genes represent only one approach for genetically modifying MSCs with to give them additional features. The potential importance of AAT for inflammatory lung diseases, especially emphysematous COPD, has been laid out above. Thus, out of the plethora of potentially beneficial genes that could be used to equip MSCs for the enhanced treatment of inflammatory diseases, we chose AAT based on its variety of functions described in the following section.

1.4. Alpha-1 antitrypsin

1.4.1. The discovery of AAT

The ability of human plasma to inhibit proteases was first described in 1894 [197]. It was not until 1955 that Schultze and colleagues discovered the protein responsible for this anti-protease activity. They gave it the name "alpha-1 antitrypsin" since it moved within the alpha-1 globulin fraction in serum protein electrophoresis, and had the ability to inhibit trypsin [198]. In the 1960s it was found that the absence of the AAT band from the alpha-1 globulin fraction was linked to an inherited deficiency and associated with severe and early-onset lung emphysema [199,200], suggesting the general importance of this protein for human health and disease. At the same time it was described that intratracheal instillation of papain, a protease present in the fruit papaya, caused emphysema in rats [201]. Both studies taken together supported the hypothesis of a proteolytic pathogenetic mechanism resulting from the lack of sufficient inhibition of proteases by AAT, leading to a breakdown of lung tissue and the destruction of alveolar integrity in the development of emphysema in AAT-deficient patients [202]. These publications provided the basis for subsequent studies that identified elastase released from neutrophilic granulocytes as a major cause of emphysema in AAT-deficient patients, and a target of AAT action [203–206]. At the same time, a close link between smoking and the development of emphysema was identified [207,208]. In further studies, a protease-antiprotease imbalance was hypothesized as the cause of emphysema not only for patients suffering from AAT deficiency, but also by extension, for COPD patients [45,209,210]. Supported by the work of Gadek and colleagues [211], the US Food and Drug Administration approved the marketing of AAT purified from human plasma for replacement therapy in patients with severe AAT deficiency and emphysema in 1987 [212,213]. Since that time, major progress has been made regarding the mechanism and epidemiology of the disease [214,215] as well as in the understanding of novel characteristics of AAT [202,216–218].

1.4.2. AAT deficiency

AAT deficiency is a genetic disorder marked by production of defective AAT protein, decreased serum AAT concentrations, and accumulation of misfolded protein in the endoplasmic reticulum (ER) of hepatocytes [219]. The most severe variant, the so-called Z-phenotype, affects approximately 1 in 2000 North European Caucasians [220]. Clinically, this archetypal conformational serpinopathy is characterized by early-onset panlobular basal lung emphysema due to uninhibited breakdown of lung tissue by proteases [200,221]. As such, AAT deficiency is the only known genetic cause of emphysema [3] and the only recognized genetic factor that increases the predisposition to develop COPD [222,223]. In addition to lung disease, patients carrying the severe Z deficiency allele often suffer from neonatal hepatitis, cirrhosis, and hepatocellular carcinoma [224,225]. Furthermore, AAT deficiency has been linked to several inflammatory diseases such as panniculitis, vasculitis (in particular

Wegener's granulomatosis), bronchiectasis, and ulcerative colitis, suggesting that neutrophil proteases are also involved in the pathogenesis of these diseases [226], and demonstrating the importance of AAT in maintaining tissue homeostasis and controlling inflammation.

1.4.3. Biochemical characteristics of AAT

AAT, also termed alpha-1 proteinase inhibitor (A1PI), is a 52kDa, water-soluble and tissue-diffusible 394-amino acid circulating glycoprotein encoded by the *SERPINA1* gene [227–229]. AAT is the prototypic member of the serine protease inhibitor (SERPIN) superfamily [230]. Serpins are protease inhibitors found in all kingdoms of life that play important roles in a variety of biological processes including the control of inflammation or coagulation [231,232]. Despite its name, the major target of this inhibitor is the serine protease elastase released from neutrophils during inflammation, and AAT binds to it with one of the highest association rate constants observed in biology [233]. In addition, AAT can also block proteinase 3, myeloperoxidase, and cathepsin G secreted by neutrophils, the coagulation cascade proteinases plasmin, thrombin, urokinase, and factor Xa, the kallikreins 7 and 14, cell-surface proteases such as matriptase, and the cysteine proteinase caspase-3 [234–237], thus accounting for more than 90% of the antiproteinase activity in human plasma [229].

More than 80% of AAT is produced and secreted by hepatocytes; however, pulmonary alveolar cells, monocytes, macrophages, neutrophils, endothelial cells, intestinal paneth cells, pancreatic islet cells and some types of cancer cells can produce small amounts of the protein, mainly in a tissue-specific context during inflammatory reactions [216,238–242]. Bone marrow-derived MSCs do not appear to express AAT [243]. Humans produce large amounts (*i.e.* 34mg AAT/kg/day) resulting in plasma concentrations as high as 0.9–1.75g/L [216], and the protein is cleared with a half-life of 3–5 days [244,245]. From the plasma, 80% of AAT diffuse to interstitial tissues, while the rest reaches body fluids such as saliva, tears, milk, semen, urine, bile, and cerebrospinal fluid [246–250]. The distribution of the protein is not uniform, since *e.g.* in the epithelial lining fluid of the lower respiratory tract, the concentration of AAT is believed to be only 10% of that seen in plasma levels [251], suggesting that even small amounts of AAT may have strong local effects.

1.4.4. Mechanism of proteinase inhibition

The irreversible suicide substrate-like inhibitory mechanism that AAT is well-known for is linked to its tertiary structure, which is highly similar among all serpins. It consists of three beta sheets (named A, B, and C), 9 alpha helices (A–I), and an exposed 9-amino acid C-terminal reactive center loop (RCL, Figure 1A) [252]. Contained within this RCL is the protease recognition site centered at residues Met[358]–Ser[359] [253,254], which is presented to the protease like a "bait". Cleavage of the targeted peptide bond at this recognition site by *e.g.* elastase leads to an irreversible binding of the protease to the serpin (Figure 1B) and initiates a dramatic conformational change for both AAT as well as the protease

(Figure 1C). During this so-called stressed to relaxed transition, the covalently bound protease is transferred from one pole of the AAT protein to the other by the RCL. This mousetrap-like mechanism is a suicide interaction for both parties involved and results in an energetically favorable conformation of the serpin and complete distortion of the structure of the protease, thereby inactivating it and at the same time inducing clearing pathways to degrade the inactivated serpin-protease-complex [216,255,256].
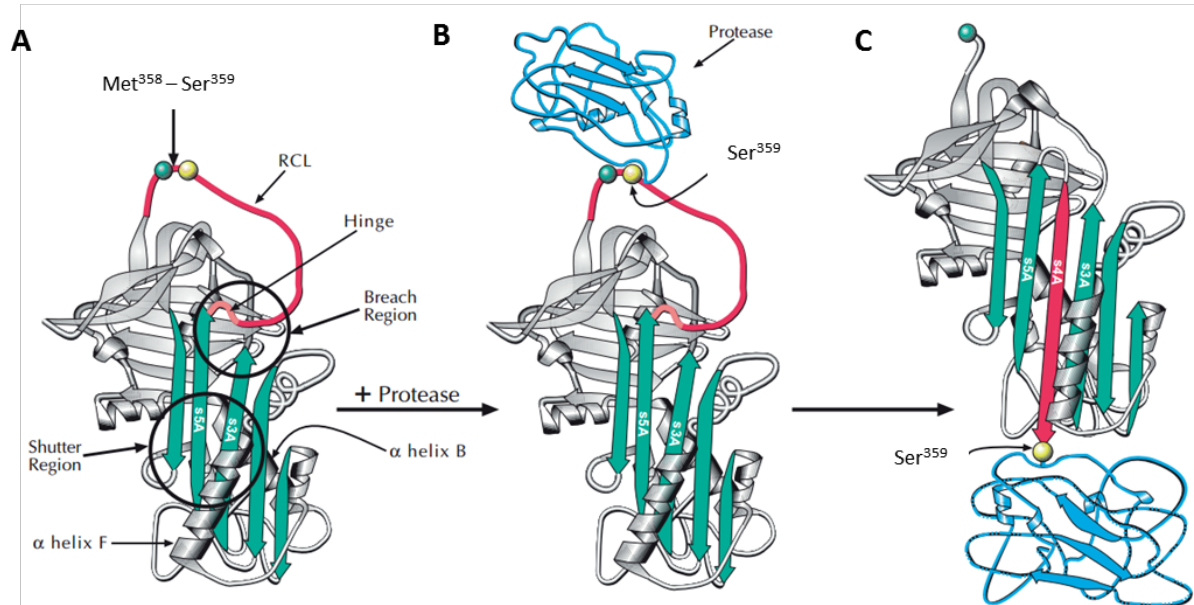
Figure 1: **Proteases are inhibited by AAT by a suicide substrate-like mechanism. A: Tertiary structure of AAT.** Indicated are the RCL (red) with the reactive site centered at $Met^{358} – Ser^{359}$ (green and yellow balls, respectively). **B: AAT-protease docking complex.** The protease binds to Ser^{359} in an attempt to cleave the reactive site bond between $Met^{358} – Ser^{359}$. **C: Final AAT-protease complex.** After cleaving the reactive site bond, the protease remains stably bound to Ser^{359}, while AAT undergoes a conformational change, leading to structural distortion and inactivation of the protease. Figure modified from PeproTechFocus. Serpins, Serpinopathies, and Conformational Diseases (n.d.)[252].

1.4.5. Anti-inflammatory and immunomodulatory properties of AAT

Solely considering the name of the protein, one is tempted to assume that the anti-inflammatory activity of AAT is purely biochemical and related to the inhibition of proteases during inflammatory processes. However, during the last decade it has been recognized that AAT not only is a potent protease inhibitor protecting tissues from the damaging effect of enzymes excessively released from inflammatory cells, but also has powerful immunomodulatory and tissue-protective properties, some of which are most likely independent of its function as a protease inhibitor [216,257]. However, the mechanisms underlying these favorable functions of AAT are still a field of intense research [242]. The following section provides an overview of the current state of our knowledge.

1.4.5.1. AAT as acute phase protein – anti-inflammatory effects

AAT is a hepatic acute phase protein with an inflammation-, cortisol- and hypoxia-inducible gene promoter [258]. Upon induction, its concentration can increase more than 4-fold in plasma, and up to 11-fold in tissues such as the lung, pancreas or intestine due to it being locally synthesized by inflammatory cells as a protective response to infection and inflammation [251,259–263]. AAT levels in the circulation also rise during pregnancy, a state in which the induction of tolerance is especially important [264].

Many of the anti-inflammatory functions of AAT are related to its ability to inhibit proteases. It has *e.g.* been described that serine proteases activate IL-1 precursor proteins exposed from necrotic cells, which is diminished in the presence of increased levels of AAT [265]. This mechanism is of particular importance for the present work, since it is commonly accepted that IL-1 is one of the major pro-inflammatory cytokines involved in the pathogenesis of smoke-induced COPD [266]. It has also been suggested that the anti-inflammatory potential of AAT is mediated by the inactivation of serine proteases which signal via a group of membrane protein receptors named protease-activated receptors (PARs), such as for example trypsin or neutrophil elastase [216]. PARs are described to be essential for various inflammatory processes including the release of MCP-1, IL-1, IL-6, and TNF-alpha from inflammatory cells, increased neutrophil migration, and the maturation of DCs [267–271]. Many of these processes play crucial roles in the excessive inflammation present in COPD [266]. Surprisingly, AAT also targets some proteins that are not serine proteases, such as a disintegrin and metalloproteinase with thrombospondin motifs 4 (ADAMTS-4), a protein involved in rheumatoid arthritis, or matrix metallopeptidase-9 (MMP-9), which is related to COPD [272–274].

Furthermore, AAT has been described to have anti-inflammatory functions that are independent of protease inhibition. The binding of IL-8, the major neutrophil chemoattractant, seems to function without utilizing the protease binding site of AAT, and leads to disrupted migration of neutrophils [275]. As described earlier, neutrophils are crucially involved in the pathogenesis of COPD [8,39]. Accordingly, the lack of AAT in the lungs of patients suffering from AAT deficiency results in excessive mobilization of neutrophils into the pulmonary parenchyma [216]. Moreover, it has been shown that AAT binds heat shock proteins like heat shock protein 90kDa beta member 1 (HSP90B1) and heat shock protein 70kDa (HSP70), indicating that it also plays a role in diminishing immune responses to DAMP molecules [276,277]. AAT has also been described to bind both receptors of TNF-alpha, although at a low affinity, indicating that this anti-inflammatory mechanism is important mainly during phases in which AAT is present at high levels, such as acute phase reactions [258,278].

1.4.5.2. Effects on innate immunity

It is thought that AAT has the ability to shift local, as well as systemic cytokine environments from pro- to anti-inflammatory [257]. This is thought to be mediated by effects on cells of the innate immune system such as monocytes/macrophages and neutrophils – cell types significantly associated with the pathogenesis of COPD [266]. It has been shown in numerous studies that AAT has a potent inhibitory effect on the production of pro-inflammatory cytokines such as IL-1beta, TNF-alpha, and IL-8 by either monocytes or PBMCs, while at the same time promoting the secretion of anti-inflammatory molecules like IL-10 and IL-1ra [279–286]. The second cell type strongly influenced by AAT is neutrophilic granulocytes. Several groups have described a suppressive effect of AAT on neutrophil activation and chemotaxis [284,287–289]. The mechanism underlying the latter effect was associated with binding by AAT to a major chemoattractant for neutrophils, the cytokine IL-8 [275]. The same group recently showed that AAT regulates TNF-alpha-induced degranulation of neutrophils, and thus the release of elastase [278].

AAT also exerts tolerance-inducing effects on DCs and macrophages. Recently, it was reported that in the presence of AAT, the expression of CD40, CD84 and major histocompatibility complex (MHC) class II in stimulated DCs is reduced. At the same time, IL-10 production is increased and the expansion of regulatory T lymphocytes (Tregs) promoted [290]. An interesting finding is that the inflammation-driven migratory capacity of the DCs was not blunted by AAT, allowing them to reach the draining lymph nodes and exert their tolerogenic function there [290].

NK cells are crucial for the response against viral infection and tumor development and have recently been described to exert functions attributable to both the innate and adaptive immunity [291]. It might be assumed that just like with the many cell types described above, AAT would also interfere with NK cell function, resulting in an increase in viral infections or elevated tumor incidence. This would be a major problem, especially for COPD patients suffering from acute exacerbations [292]. However, although DC-derived IL-15-related NK cell responses are reduced in the presence of AAT [293], patients suffering from AAT-deficiency are at increased risk of developing various types of cancer compared to individuals with normal AAT levels [294–296]. Moreover, AAT has been described to mediate anti-viral and anti-tumor effects [297–300]. The hypothesized underlying mechanism is that the effect of AAT on NK cells is immune permissive in the case of infected or transformed cells, but suppressive if the target cells are healthy and the immune signal predominantly antigen presenting cell-mediated [258].

1.4.5.3. Effects on adaptive immunity

Numerous studies have confirmed the hypothesis that AAT has no direct effects on T cells *in vitro*, as indicated by persisting levels of interleukin 2 (IL-2) and related responses in the presence of AAT in cell culture experiments [301,302]; however, a growing body of knowledge indicates that AAT treatment influences T cells in an indirect manner, leading to a reduction in T cell infiltrates, alteration of the T

cell receptor repertoire and expansion of Tregs in models of autoimmunity or allotransplantation [285,286,290,303–306]. It is suspected that all these effects on the adaptive immune system result from a shift of the cytokine environment from pro- to anti-inflammatory and from the induction of tolerogenic, IL-10-secreting DCs [257,290]. Another effect AAT appears to exert on cells of the adaptive immune system is a suppression of the activation and proliferation of B lymphocytes, as recently shown in a model of allogeneic skin transplantation [307]. Surprisingly, antigen-specific antibody production remained intact in the presence of high AAT levels; however, an isotype switching towards an IgM-high/IgG-low phenotype was observed. Furthermore, an IL-10-expressing regulatory subpopulation of B cells considered to be highly important in alloantigen tolerance seems to be expanded by treatment with AAT, and this cell population was shown to be required for AAT-induced Treg expansion [307,308].

1.4.6. Anti-apoptotic and regenerative effects

Of special importance for the present work is the observation that AAT has significant anti-apoptotic and cytoprotective effects in addition to its anti-inflammatory potential. Petrache and colleagues showed that AAT is able to inhibit pulmonary alveolar cell apoptosis by suppression of caspase-3 activation and oxidative stress, and attenuate emphysema development in animal models of apoptosis-dependent emphysema lacking neutrophilic inflammation [237,309]. Furthermore, two separate clinical trials of i.v. AAT augmentation therapy for genetic AAT-deficient lung emphysema confirmed this cytoprotective potential in the human setting as seen by a significant reduction of the decline in lung density and an arrest of emphysema development [310]. Moreover, it has been shown that AAT exerts anti-apoptotic functions on endothelial cells and vascular smooth muscle cells[311–313], while also inducing the production and preventing the elastase-dependent degradation of VEGF, thereby contributing to tissue neovascularization and regeneration [314,315].

1.4.7. Anti-microbial functions

In addition to its immunomodulatory and regenerative properties, AAT has been described to exert anti-bacterial and anti-viral functions. Shapiro and colleagues initially found that while *in vitro* infection of human whole blood with the human immunodeficiency virus (HIV) does not occur, whole blood from AAT-deficient patients is readily infected [316]. Later, the same group described that HIV infection is linked to reduced serum AAT levels [317] and that patients suffering from AAT deficiency might be at higher risk for acquiring HIV infection [299]. Furthermore, aerosolized AAT has been shown to be able to suppress *Pseudomonas aeruginosa* proliferation in a rat model of chronic lung infection[318] and in patients suffering from cystic fibrosis [319]. Another anti-bacterial property associated with AAT is its binding to the secreted enteropathogenic *Escherichia coli* proteins B and D (EspB, EspD), thereby potently inhibiting hemolysis of red blood cells [320]. These anti-microbial

properties could be especially important with regards to the treatment of acute exacerbations, since these oftentimes life-threatening complications in patients with severe COPD are mostly caused by bacterial or viral infections [292].

1.4.8. Summary

Taken together, AAT is not a prototypic anti-inflammatory molecule that blocks the activity of immune cells, but rather an immune modulator that permits an effective immune reaction, while at the same time limits an excessive inflammatory response, induces immunological tolerance that is persisting and specific, protects noninvolved bystander cells, and moreover has anti-microbial properties. These unique features together with the outstanding safety profile for AAT augmentation therapy as seen for AAT deficiency [321] make AAT an attractive candidate for the treatment of diseases with an underlying inflammatory or autoimmune pathology. Indeed, as recombinant AAT is currently being tested in clinical trials for indications such as COPD and pulmonary fibrosis, new-onset diabetes type 1, cystic fibrosis, sarcoidosis, solid organ and islet cell transplantation, HIV disease and GvHD with very promising results so far [319,321–324], it represents an excellent candidate molecule to combine with MSC-based approaches for the potential treatment of chronic airway disorders.

1.5. Summary and rationale of the present study

- Chronic inflammatory diseases such as COPD are a major health problem today and pose an increasing burden on individuals, patients and economies. COPD is the third leading cause of mortality worldwide to date and affects more than 300 million people, and since there is no cure today, novel therapeutic approaches are desperately needed.

- MSCs have been shown to exert extremely potent immunomodulatory and regenerative functions on a variety of cells in response to inflammatory stimuli. Moreover, they have been proven to be anti-microbial and hypoimmunogenic when used in an allogeneic setting. They are currently being investigated in more than 500 clinical trials, most of them related to inflammatory diseases including COPD, with very promising results and an excellent safety profile so far. Compared to other stem cell types or small molecules and biologics, MSCs have several advantages regarding their clinical usability.

- AAT is an acute phase protein and the prototypic serine protease inhibitor in the human body, protecting tissues from the damaging effect of enzymes secreted by immune cells during inflammation. Moreover, AAT has lately also been recognized as a protein with very potent regenerative, anti-inflammatory and immunoregulatory functions affecting all parts of the immune system. It has also been shown to efficiently prevent viral and bacterial infections. AAT has been used for the chronic treatment of AAT deficiency for almost three

decades now, with an outstanding safety profile and a beneficial effect on emphysema, and is currently tested for a plethora of inflammatory and autoimmune diseases in clinical trials.

- Cell-based gene therapy has yielded striking results in the treatment of various previously incurable diseases during the last years. This innovative therapeutic approach offers the possibility of combining the function of one or more transgenes with the cells' endogenous properties, resulting in a more potent cell product for the treatment of various diseases. It was only very recently that the first *ex vivo* stem cell-based gene therapy product received market authorization by the European Commission for the treatment of the so far hopeless disease adenosine deaminase-deficient severe combined immunodeficiency (ADA-SCID)[182,325].

Taken together, our hypothesis is that for the treatment of diseases as complex as emphysematous COPD, for which no cure exists so far, the effects of MSCs or AAT alone might not be sufficient to achieve an amelioration of the illness, but that combining the properties of MSCs with those of AAT may achieve a therapeutic benefit (Figure 2). Thus, this pilot study was aimed at finding a way to modify MSCs using viral vectors to optimally express transgenic AAT, and to deliver a first proof of concept that this cell product could show benefit for the treatment of inflammatory lung diseases such as COPD.
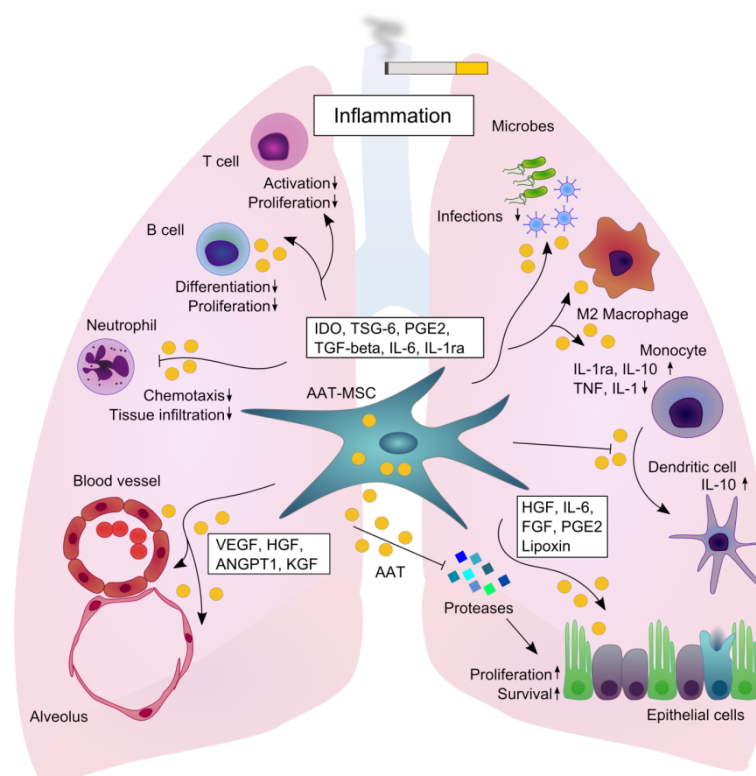
Figure 2: **Overview of the synergistic mechanisms of a combination of AAT and MSCs (AAT-MSCs) using the example of inflammatory lung diseases.**

1.6. Specific aims and scope

The following specific goals provided a framework for the present work:

- **Design of gamma-retroviral constructs for the permanent expression of *SERPINA1* and *pac* in primary human MSCs.** To generate an optimized construct for the transgenic expression of AAT in MSCs, eight gamma-retroviral vectors were planned and would be compared with regards to viral titers, transduction efficacy, and AAT expression. Three different human physiological gene promoters would be tested in parallel for driving *SERPINA1* expression. The *pac* gene enabling selection of gene-modified cells using the antibiotic puromycin should be driven either by a second promoter, or expressed via an internal ribosome entry site (IRES) sequence 3' of the *SERPINA1* gene. In case of constructs containing two promoters, different configurations of the expression cassettes should be assessed, *i.e.* the *SERPINA1* cassette would be placed 5' of the *pac* cassette in some constructs, and 3' in others.

- **Generation of functional viral supernatants and titration on HT1080 fibrosarcoma cells.** Viral supernatants of the eight transfer plasmids in combination with the respective helper plasmids should be generated, and their functionality and titers determined first by transduction of HT1080 fibrosarcoma cells. Later, primary human MSCs should be transduced at comparable multiplicities of infection (MOIs).

- **Selection of the expression cassette lead candidate.** Depending on transduction of primary human MSCs and transgenic AAT expression, the best constructs will be subjected to testing in further experiments.

- **Comparison of best expression cassette in gamma-retroviral *vs.* lentiviral backbone.** To assess if the performance of the expression cassette lead candidate in a gamma-retroviral vector could be further improved, the cassette will be cloned into a lentiviral backbone, and the plasmids compared regarding transduction efficacy and AAT expression.

- ***In vitro* confirmation of functionality of transgenic AAT expressed from MSCs.** To assess if AAT transgenically expressed from MSCs is functional with regards to its protease inhibitor capacity, an *in vitro* assay should be established, and MSC-AAT compared to natural human AAT isolated from plasma.

- **Process up-scaling, batch production and characterization.** Large scale procedures for MSC transduction, antibiotic selection and expansion should be established to be able to provide high numbers of gene-modified MSCs from the same batch for *in vivo* studies.

- **Confirmation of efficacy of AAT-MSCs in an *in vivo* model of lung emphysema.** Finally, it should be assessed if therapy with AAT-MSCs was able to improve lung function and histological parameters in a mouse model of elastase-induced pulmonary emphysema.

2. Materials and Methods

2.1. Materials

2.1.1. Bacteria

Name	Company and genotype
MAX Efficiency DH5α Competent Cells Genotype	Thermo Fisher Scientific *F- Φ80lacZΔM15 Δ(lacZYA-argF) U169 recA1 endA1 hsdR17 (rk-, mk+) phoA supE44 λ-thi-1 gyrA96 relA1*
One Shot Stbl3 Chemically Competent E. coli Genotype	Thermo Fisher Scientific *F-mcrB mrrhsdS20(rB-, mB-) recA13 supE44 ara-14 galK2 lacY1 proA2 rpsL20(StrR) xyl-5 λ-leumtl-1*

2.1.2. Restriction enzymes

Name	Company
AgeI	New England Biolabs
BamHI	New England Biolabs
ClaI	New England Biolabs
PacI	New England Biolabs
PmeI	New England Biolabs
SalI	New England Biolabs
SnaBI	New England Biolabs

2.1.3. Primers

Primers were designed following general primer design rules [326], checked for hairpin structure and dimer formation using Metabion's Oligonucleotide Properties Calculator (http://www.metabion.com/biocalc/index.html), and ordered from Metabion.

Application	Name	Sequence
Insertion of a PacI recognition site	Mutagenesis_PacI_F	5'-AACTGAGCAGATCTTAATTAAAATTCCTGCAGTAAA-3'
	Mutagenesis_PacI_R	5'-TTTACTGCAGGAATTTTAATTAAGATCTGCTCAGTT-3'
	Mutagenesis_Vector_F	5'-TCA GTG GAA CGA AAA CTC ACG TTA AGG GAT-3'
	Mutagenesis_Vector_R	5'-ATC CCT TAA CGT GAG TTT TCG TTC CAC TGA-3'
Transfer of optimized cassette into lentiviral backbone	Inf_EFS_SERPINA1_F	5'-TTCAAAATTTTATCGATGGCTCCGGTGCCCGTCAG-3'
	Inf_EFS_SERPINA1_R	5'-TCATTGGTCTTAAAGGTACCGACAACACCACGGAATTATC-3'
Primers and probe for VCN determination	human_FVII_for	5'-GCCAAGCAAGGCACTATCTC-3'
	human_FVII_rev	5'-GGCTGTGCCGAAGTAGATTC-3'
	FVII Probe	5'-Yakima Yellow-AGGACCTCCGCCAGGGTTCA-BHQ1-3'
	oPRE_WPRE_VCN fw	5'-GCTATTGCTTCCCGTACG-3'
	WPRE (Roche) rev	5'-AAAGAGACAGCAACCAGGATTT-3'
	Probe #63 Roche UPL	Proprietary (Roche)
Primers and probe for RCR determination	gag_eu_fw	5'-AGAGGAGAACGGCCACTATTG-3'
	gag_eu_rev	5'-ACTCCACTACCTCGCAGGCAT-3'
	gag_eu_probe	5'-TGTCCGTTTCCTCCTGCGCGG-3'

Primers and probe for RCL determination	HIV-1 gag F	CAGAATGGGATAGAGTGCATCCA
	HIV-1 gag R	TACTGGGATAGGTGGATTATGTGT
	HIV-1 gag P	5'-FAM-AGTTCCTGCTATGTCACTTCCCCTTG-TAMRA-3'

2.1.4. Plasmids

Number	Name	Application
#110	pSERS11_pPGK_IFNb_fw_IRES_pac	Backbone used for "1st generation" constructs
#112	pSERS11_pEF1a_IFNb_fw_IRES_pac	
#153	pMA-RQ_pEFS_pPGK_Kozak_pac	GeneArt plasmid containing promoter, Kozak and pac sequences
#168	pSERS11_pEFS_luc2_P2A_eGPF_IRES_pac	Corrected backbone used for "2nd generation" constructs
#172	pCCL-c-EFS-hADA_WPRE	Plasmid providing lentiviral backbone
#70	pcDNA3-MLV-gagpol	Helper plasmids for production of gamma-retroviral supernatants
#39	pALF-PERV A_GaLV	
#170	pCMV-dR8.91	Helper plasmids for production of lentiviral supernatants
#171	pCAGGS-VSVG	
#154	pSERS11_pPGK_SERPINA1	Intermediates
#155	pSERS11_pEF1a_SERPINA1	
#156	pSERS11_pEFS_SERPINA	
#159	pSERS11_pPGK_SERPINA1_pEFS_pac	Final gamma-retroviral *SERPINA1* expression constructs
#160	pSERS11_pEFS_SERPINA1_pPGK_pac	
#161	pSERS11_pEF1a_SEPRINA1_pPGK_pac	
#162	pSERS11_pEFS_pac_pPGK_SERPINA1	
#163	pSERS11_pPGK_pac_pEFS_SERPINA1	
#164	pSERS11_pPGK_pac_pEF1a_SERPINA1	
#193	pSERS11_pPGK_SERPINA1_IRES_pac	
#194	pSERS11_pEFS_SERPINA1_IRES_pac	
#215	pCCL_pEFS_SERPINA1_IRES_pac	Final lentiviral *SERPINA1* expression construct

2.1.5. Kits

Name	Company
Calcium Phosphate Transfection Kit	Sigma
CompactPrep Plasmid Midi Kit	Qiagen
DNeasy Blood & Tissue Kit	Qiagen
GeneArt Site-Directed Mutagenesis PLUS Kit	Thermo Fisher Scientific
GeneJET Plasmid Miniprep Kit	Thermo Fisher Scientific
Human alpha 1 Antitrypsin ELISA Kit (SERPINA1)	abcam
Immunoperoxidase Assay for Determination of Alpha 1-Antitrypsin in Human Samples	GenWay
In-Fusion HD Cloning Kit	Clontech
Microsart RESEARCH Mycoplasma Detection Kit for qPCR	Sartorius
Neutrophil Elastase Inhibitor Screening Kit (Fluorometric)	abcam
Plasmid Plus Maxi Kit	Qiagen
Plasmid Plus Midi Kit	Qiagen

QIAprep Spin Miniprep Kit	Qiagen
QIAquick Gel Extraction Kit	Qiagen
Quick Ligation Kit	NEB

2.1.6. Reagents

Reagent	Company
10% Formalin, neutral buffered	Sigma Aldrich
100X GlutaMAX	Gibco
2-Propanol 99.9%	Carl Roth
6X Orange DNA Loading Dye	Fermentas
Alizarin Red S	Sigma Aldrich
Alpha 1 Antitrypsin, Human Plasma	Athens Research & Technology
Ampicillin	Genaxxon Biosciences
BacT/ALERT SA, Standard Aerobic	bioMérieux
BacT/ALERT SN, Standard Anaerobic	bioMérieux
Chloroquine	Sigma Aldrich
Circlegrow Bacterial Growth Medium	MP Biomedicals
Cytofix/Cytoperm Fixation and Permeabilization Solution	BD Biosciences
DMEM, +D-glucose[1.0g/L], + stable glutamine, no phenol red	Merck Millipore
DMEM, +D-glucose[4.5g/L], + stable glutamine	Merck Millipore
DMEM, low glucose, pyruvate, no glutamine, no phenol red	Gibco
DMSO	WAK-Chemie Medical GmbH
Elastase from porcine pancreas	Sigma Aldrich
EMEM, with stable L-glutamine	ATCC
Ethidiumbromid	Genaxxon Biosciences
FBS, Origin: EU-approved countries	Merck Millipore
GeneJet Wash Solution	Thermo Fisher Scientific
Glycerol	Carl Roth
GolgiPlug Protein Transport Inhibitor	BD Biosciences
H_2O ROTIPURAN - low organic	Carl Roth
HA ([50g/L] in isotonic saline solution)	Baxter
HAES (10% in isotonic saline solution)	Fresenius Kabi
HEPES Buffer Solution [1M]	Gibco
Kanamycin	Genaxxon Biosciences
LB-Agar Powder according to Miller	Genaxxon Biosciences
LB-Medium - high salt	Genaxxon Biosciences
LightCycler 480 Probes Master	Roche
Mayer's Hematoxylin	Sigma Aldrich
MEM Non-Essential Amino Acids Solution (100X)	Gibco
Natural human alpha 1 Antitrypsin protein	abcam
O'GeneRuler 100bp	Fermentas
O'GeneRuler 1kb	Fermentas
Oil Red O	Sigma Aldrich
PBS	Merck Millipore

peqGREEN (DNA & RNA Dye)	Peqlab
Perm/Wash Buffer	BD Biosciences
PLL solution 0.01% [100µg/mL], sterile-filtered	Sigma Aldrich
Puromycin dihydrochloride from Streptomyces alboniger	Sigma Aldrich
RPMI	Lonza
SeaKem LE Agarose	Lonza
Sodium Pyruvate	Gibco
Sodium Pyruvate [100 mM]	Gibco
StemMACS AdipoDiff Media, human	Miltenyi Biotec
StemMACS OsteoDiff Media, human	Miltenyi Biotec
T4 DNA Ligase	NEB
TAE buffer (50X)	Genaxxon Biosciences
Trypan Blue	Sigma Aldrich
TrypLE select	Gibco

2.1.7. Antibodies

Antibody name	Company
Goat polyclonal to alpha 1 Antitrypsin (FITC), human	abcam
CD45-ECD	Beckman-Coulter
HLA-DR-ECD	Beckman-Coulter
IgG1-ECD	Beckman-Coulter
CD3-FITC	Beckman-Coulter
CD41-FITC	Beckman-Coulter
CD90-FITC	Beckman-Coulter
CD235a-FITC	Beckman-Coulter
IgG1-FITC	Beckman-Coulter
CD19-PC7	Beckman-Coulter
CD34-PC7	Beckman-Coulter
CD61-PC7	Beckman-Coulter
IgG1-PC7	Beckman-Coulter
CD14-PE	Beckman-Coulter
CD73-PE	BD Pharmingen
CD105-PE	Beckman-Coulter
IgG1-PE	Beckman-Coulter
IgG2a-PE	Beckman-Coulter
IgG3-PE	Southern Biotech
7-AAD	Beckman-Coulter

2.1.8. Consumable materials

Consumable	Company
1.5mL, 2mL, and 5mL microcentrifuge tubes	Eppendorf, Sarstedt
10cm dishes, TC-treated	Corning
10µL, 20µL, 100µL, 200µL, and 1000µL pipette tips	Greiner Bio One

15mL and 50mL centrifuge tubes	Corning
2mL, 5mL, 10mL, 25mL, and 50mL serological pipettes	Corning
6-, 12-, 24-, 48-, and 96-well plates, TC-treated	Corning
96-well flat clear bottom black polystyrene plates	Greiner Bio One
C-Chip Disposable Hemocytometer	NanoEnTek
CellSTACK cell culture chambers (1, 2 or 5 chambers)	Corning
LightCycler 480 Multiwell Plate 96	Roche
Syringe filters 0.22µM and 0.45µM	Merck Millipore
T25, T75, T175, and T225 culture flasks, TC-treated	Corning

2.1.9. Equipment

Equipment	Company
Buxco forced pulmonary maneuver system	DSI
BX51 microscope	Olympus
Centrifuge 5810R	Eppendorf
Centrifuge Heraeus Fresco 21	Thermo Fisher Scientific
Cytomics FC500 flow cytometer	Beckman Coulter
DMI6000B microscope	Leica
Incubator Heraeus BBD6220	Thermo Fisher Scientific
Incubator Heraeus Function Line	Thermo Fisher Scientific
Incubator MCO-20AIC	Sanyo
Incubator shaker KS-15 A Control	Edmund Bühler GmbH
Laminar air flow Herasafe HS15	Thermo Fisher Scientific
LightCycler 480 Instrument II	Roche
Mr. Frosty Freezing Container	Thermo Fisher Scientific
NanoPhotometer	Implen
Plate Reader Spark 10M	TECAN
Precision scale EW 600 2M	Kern
Sub-Cell GT electrophoresis system	Bio-Rad
Uvipro Chemi gel documentation system	Biometra
Water bath	Memmert WNB 14

2.1.10. Tumor cell lines

Name and cell type	Company
HT1080 human fibrosarcoma cells	ATCC
293T human embryonic kidney cells	ATCC

2.1.11. Software

Software name	Company
Kaluza	Beckman Coulter
Las X	Leica
Lasergene 12 Core Suite	DNASTAR
LightCycler 480 Software	Roche

Mendeley Desktop free reference manager	Mendeley Ltd.
new-CAST	Visiopharm
Prism 6	GraphPad Software, Inc.
SnapGene Viewer	GSL Biotech LLC

2.2. Methods

2.2.1. Design and molecular cloning strategy of viral expression plasmids

2.2.1.1. Gamma-retroviral plasmids

The *in vitro* synthesized 5' UTR and CDS of the human *SERPINA1* cDNA transcript 1 were purchased from GeneArt, with the following sequence modifications: A BamHI restriction enzyme recognition site present in the 5'UTR was destroyed by replacing a cytosine by an adenine at position 181 of the 5' UTR (GGATCA instead of GGATCC). A modified Kozak consensus sequence (GCCACC) was inserted at the 3' end of the 5'UTR sequence, immediately 5' of the *SERPINA1* start codon for efficient initiation of translation [327]. The *SERPINA1* CDS was codon optimized for *Homo sapiens* to increase protein production. Two additional stop codons were added 3' of the *SERPINA1* stop codon to ensure efficient release of the amino acid chain from the ribosome during translation. An AgeI site was added to the 5' end of the cassette, and a PacI site to the 3' to enable easy transfer of this expression cassette into retroviral expression plasmids containing different promoters that were previously cloned at apceth. Figure 3 shows a schematic of the *SERPINA1* expression cassette.
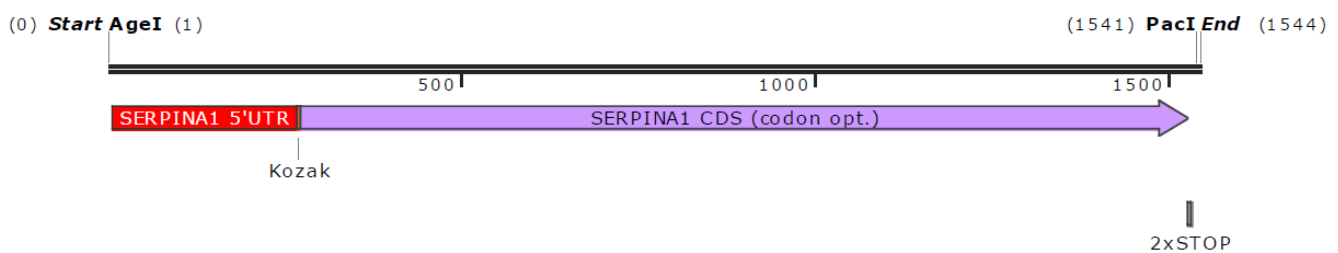
Figure 3: **Schematic of the *SERPINA1* expression cassette.**

Cloning of "1st generation" AAT constructs

Plasmid numbers represent apceth's internal plasmid denomination and will be used hereafter for simplicity. The gamma-retroviral backbone used to generate all transfer plasmids is pSERS11 [328]. The 5'-LTR comprises a simian vacuolating virus 40 (SV40) enhancer fused to the Rous sarcoma virus (RSV) promoter, and the spleen focus forming virus (SFFVp) R and U5 regions. The 3' long terminal repeat (LTR) contains an SFFVp U3 region that has a deletion and thus renders the vector self-inactivating, SFFV R and U5 regions as well as a PolyA signal. To clone plasmid #114 pSERS11_pPGK_SERPINA1_IRES_pac, in a first step a unique PacI restriction site was generated in a plasmid previously cloned at apceth (#110 pSERS11_pPGK_IFN-beta_fw_IRES_pac, Supplemental figure 1) by site-directed mutagenesis using the GeneArt Site-Directed Mutagenesis PLUS Kit and primers Mutagenesis_PacI_F, Mutagenesis_PacI_R, Mutagenesis_Vector_F, Mutagenesis_Vector_R (*cf.* 2.1.3 for sequences). Utilizing this newly created restriction site 3' of the interferon-beta (IFN-

beta) cassette present in plasmid #110, the IFN-beta cassette was replaced by the *SERPINA1* expression cassette ordered from GeneArt using restriction enzymes PacI and AgeI. After the integrity of this first construct was confirmed by analytical restriction enzyme digestion, in a next step the phosphoglycerate kinase (PGK) promoter was replaced by the eukaryotic translation elongation factor 1 alpha 1 (EF1a) promoter present in another plasmid previously cloned at apceth, #112 pSERS11_pEF1a_IFN-beta_fw_IRES_pac Supplemental figure 2), using the restriction sites SalI and AgeI, yielding construct #115 pSERS11_pEF1a_SERPINA1_IRES_pac. In order to clone construct #116 in which the *SERPINA1* cDNA is driven by the CAG promoter, in which the CMV enhancer is followed by the chicken beta actin promoter and the rabbit beta globin splice acceptor, a cassette of the configuration SalI-pCAG-AgeI was ordered from GeneArt and transferred to plasmid #114 by digesting both plasmids with SalI and AgeI, thereby replacing the PGK promoter present in plasmid #114 with the CAG promoter. The same strategy was used to generate the fourth construct, #129, in which the short intron-less form of EF1a (EFS [329]) is driving the *SERPINA1* cDNA. The SalI-pEFS-AgeI cassette was ordered from GeneArt with one modification (A79T) compared to the published sequence to remove an AgeI site present in pEFS, and SalI and AgeI were used to remove the PGK promoter present in plasmid #114 and to insert the EFS promoter. Before maxipreps and viral supernatants were generated, all four plasmids were sequenced to confirm their integrity.

Cloning of "2nd generation" AAT constructs

In order to clone plasmids #159–164 listed in Figure 6, a *pac* gene expression cassette of the following configuration was ordered from GeneArt (plasmid #153 pMA-RQ_pEFS_pPGK_Kozak_pac, Figure 4):
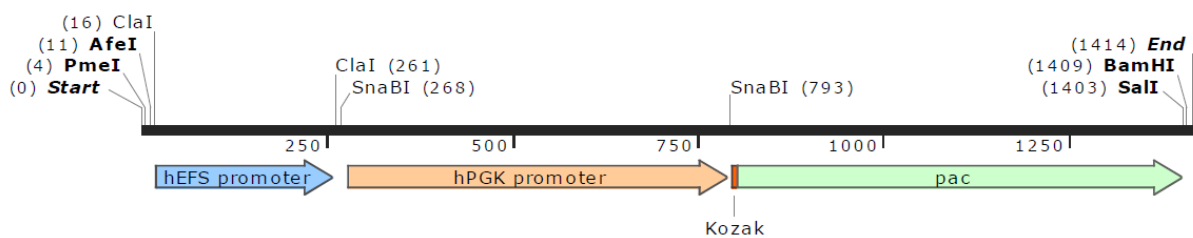
Figure 4: **Schematic representation of the *pac* gene expression cassette.**

In a first step, plasmids #114, #115, and #129 described above were digested using SalI and PacI, and the resulting insert (promoter_SERPINA1) was transferred to the optimized retroviral backbone (plasmid #139 pSERS11_Leader_MCS_oPRE, Supplemental figure 3) that had been linearized using the same restriction enzymes. The resulting intermediate constructs were #154 pSERS11_pPGK_SERPINA1, #155 pSERS11_pEF1a_SERPINA1, and #156 pSERS11_pEFS_SERPINA1. To remove pEFS and pPGK from GeneArt cassette #153, the plasmid was digested with ClaI and SnaBI, respectively, and the remaining plasmid was re-ligated. The promoter_pac cassettes were then

transferred to plasmids #154, #155, and #156. To insert them 5' of the SERPINA1 cassette, both plasmids were digested with AfeI and SalI, to insert them 3' of the SERPINA1 cassette, enzymes PmeI and BamHI were used. To generate plasmids #193 and #194, plasmid #168 (Supplemental figure 4) previously cloned at apceth was utilized. Plasmid #168 was derived from the corrected and optimized retroviral backbone (*c.f.* 3.1.3) and contains the following elements: pEFS_Luc_P2A_eGFP_IRES_pac. Digestion of this plasmid with AgeI and PacI results in the generation of a backbone including the EFS promoter (pSERS11_pEFS_IRES_pac), digestion with SalI and PacI yields a backbone only containing the IRES and the *pac* gene (pSERS11_IRES_pac). The *SERPINA1* cassette was then transferred to these plasmids by restriction enzyme digest of plasmid #159 with AgeI and PacI to generate plasmid #194 pSERS11_pEFS_SERPINA1_IRES_pac, and with SalI and PacI to generate plasmid #193 pSERS11_pPGK_SERPINA1_pac.

2.2.1.2. Lentiviral plasmid

The pEFS_SERPINA1_IRES_pac_oPRE cassette was transferred from plasmid #194 to the lentiviral pCCL backbone [194,330] by In-Fusion Cloning using the In-Fusion HD Cloning Kit. The pCCL 5'-LTR contains a cytomegalovirus (CMV) promoter and the HIV-1 R and U5 regions, followed by the HIV-1 packaging signal (Ψ). The 3'-LTR comprises an HIV-1 U3 region that has a deletion and thus renders the vector self-inactivating, an HIV-1 R and U5 region as well as a PolyA signal. The lentiviral construct #172 pCCL-c-EFS-hADA_WPRE (Supplemental figure 5) was kindly provided by Donald Kohn, UCLA, and linearized using the restriction enzymes KpnI and ClaI. The primer design, PCR, recombination reaction (using 100ng of purified PCR fragment and 100ng of linearized vector), and transformation of bacteria were all carried out following manufacturer's specifications (Protocol I), with the only modification that 50ng of plasmid #194 template were used in the PCR reaction to generate homology arms on the insert instead of 1ng as recommended (Table 2). For primer sequences please *cf.* 2.1.3. A plasmid map of the resulting lentiviral AAT transfer plasmid #215 pCCL_pEFS_SERPINA1_IRES_pac is depicted in Supplemental figure 18.

Table 2: **PCR master mix composition and cycling conditions for the In-Fusion cloning PCR.**

PCR In-Fusion cloning #215

Component	Amount [µL]	Final concentration
CloneAmp HiFi PCR Premix (2X)	12,5	1X
Primer 1 [10µM]	0,5	[200nM]
Primer 2 [10µM]	0,5	[200nM]
Template (Plasmid DNA)	1,0	50ng
H$_2$O	10,5	
Total volume	25,0	

Cycling conditions

Temperature	Time	
98°C	10 sec	
55°C	10 sec	30 cycles
72°C	20 sec	

2.2.2. Molecular cloning

2.2.2.1. Production of LB medium/circlegrow medium for *E.coli*

25g of high salt Luria-Bertani (LB) medium powder or 40g of circlegrow medium powder, respectively, were weighed into a 1 liter (L) bottle, 1L deionized water was added, and the medium was autoclaved. When required, medium was allowed to cool down to <60°C, and antibiotics – Ampicillin to a final concentration of [100µg/mL], Kanamycin to a final concentration of [50µg/mL] – were added.

2.2.2.2. Production of agar plates

40g of LB Agar Powder were added to a 1L shaking flask, 1L deionized water was added, and the mixture was autoclaved. The agar solution was allowed to cool down to <60°C. When required, antibiotics were added to the same final concentrations as mentioned above, and the agar solution was poured into 10cm ∅ petri dishes at approximately 20 milliliter (mL) per dish. After the agar had hardened, plates were packaged into plastic bags and stored at 4°C.

2.2.2.3. Cultivation of *E.coli*

Generally, DH5α and Stbl3 cells were cultured in LB medium at 37°C and 225 revolutions per minute (rpm) shaking. When problems cultivating *E.coli* in LB medium occurred, the richer circlegrow medium was used instead.

2.2.2.4. Preparation and inoculation of glycerol stocks

For the long-term storage of bacteria, glycerol stocks were prepared by mixing 250µL of autoclaved glycerol with 750µL of an overnight bacterial culture. The mix was stored at -80°C until re-initiation of the culture. To inoculate a new culture from the glycerol stock, the vial was removed from the freezer without letting it thaw. Using an inoculation loop, a small amount of frozen bacteria was streaked out onto an agar plate containing the respective antibiotic. After an overnight incubation at 37°C, a single bacterial colony was picked to inoculate a small-scale liquid culture.

2.2.2.5. Restriction enzyme digestion

All restriction enzymes and reaction buffers used in this work were purchased from New England Biolabs. Restriction enzyme digests were performed according to the following table (Table 3) provided by the manufacturer. If <1µg DNA was digested, volumes were down-scaled accordingly; if >1µg DNA was used in the reaction, volumes were up-scaled.

Table 3: **Composition of a typical restriction enzyme digestion reaction** (from: https://www.neb.com/protocols/2012/12/07/optimizing-restriction-endonuclease-reactions).

Component	Amount
Restriction Enzyme	10 units is sufficient, generally 1µL is used
DNA	1µg
10X NEBuffer	5µL (1X)
Total Reaction Volume	50µL
Incubation Time	1 hour
Incubation Temperature	Enzyme-dependent, generally 37°C

2.2.2.6. Gel electrophoresis

DNA samples were mixed with the respective volume of 6X loading dye before gel electrophoresis. A 100 base pair (bp) or 1 kilobase (kb) ladder was also run on the gel for sizing and approximate quantification of the DNA bands. Agarose gels were prepared by mixing agarose with 1X TAE Buffer in a shaking flask and bringing the solution to a boil. Percentages of agarose gels were chosen depending on the expected DNA fragment sizes; generally, concentrations ranging from 0.8% to 2% were used. After a short cool-down of the liquid gel, ethidium bromide or peqGREEN were added at concentrations recommended by the manufacturers for visualization of DNA in the gel. Gels were cast and run using the BIO-RAD Horizontal Electrophoresis Systems at voltages ranging from 100V to 120V depending on the size of the gel. Gels were imaged on a Biometra UviproChemi system.

2.2.2.7. Gel extraction

Gel pieces of interest were cut out of the agarose gel using a scalpel, and subsequent gel extraction was performed according to manufacturer's instructions.

2.2.2.8. Determination of DNA concentration

Measurement of DNA concentration was performed using Implen's NanoPhotometer according to manufacturer's instructions for use.

2.2.2.9. Ligation

For all ligation reactions performed, NEB's Quick Ligation Kit was used according to manufacturer's recommendations with the only modification that a 5-fold molar excess of insert was used instead of a 3-fold molar excess as suggested.

2.2.2.10. Transformation

Transformation of DH5α as well as Stbl3 *E.coli* was carried out following manufacturer's specifications. When bacteria were being transformed with ligation reactions, the maximum volume of ligation reaction used was 1/10 of the bacterial volume.

2.2.2.11. Miniprep/Midiprep/Maxiprep

Minipreps, midipreps, and maxipreps were performed according to manufacturer's instructions. Bacterial culture sizes used were generally 3mL for minipreps, 40mL for midipreps, and 200mL for

maxipreps. For the inoculation of midi- and maxipreps, a small-scale bacterial overnight culture (started from a single colony on the agar plate) was used at a ratio of 1:500–1:1000.

2.2.2.12. Sequencing of plasmids

All transfer plasmids used to generate viral supernatants were fully sequenced at Microsynth AG, using custom primers (listed in Table 4).

Table 4: **Primers used for sequencing final viral expression plasmids.**

Sequence	Name
5'-GTAAAACGACGGCCAG-3'	M13for
5'-CAGGAAACAGCTATGAC-3'	M13rev
5'-CCGACGGCAGTTGGGATTC-3'	SeqRANTESPromfor
5'-AAGCTTTCATATTCTGTAACTTTTGTG-3'	RANTESPromfor
5'-GGACAAACCACAACTAGAATGC-3'	SeqZSG2rev
5'-GACATTGATTATTGACTAGTTATTAATAGTAATCAATTACG-3'	pCAGfor
5'-CCAAGTAGGAAAGTCCCATAAGG-3'	SeqpCAG2rev
5'-ACTCATGGTTATGGCAGCACTGC-3'	Amp_for
5'-CGAAAGGGAAACCAGAGGAGC-3'	plentiPACKfor
5'-GAGCTCGGTACCTTTAAGACCAATGAC-3'	plenti3´LTRfor
5'-GGAATGTGTGTCAGTTAGGGT-3'	pBABErev
5'-ACCCTAACTGACACACATTCC-3'	pBABErevneu
5'-AAAGAGACAGCAACCAGGATTT-3'	WPRE(Roche)rev
5'-GATATTCTTAACTATGTTGCTCC-3'	wPRE_for
5'-TCATAAAGAGACAGCAACCAGG-3'	wPRE_Rev
5'-AAGAACTGACGAGTTCGTATTCC-3'	gPsi_for
5'-CAAAAAGTCCGACTCGGGTAGG-3'	gPsi_rev
5'-GCCGCTTACCGGATACCTGTCC-3'	Backb_for1
5'-CATACCTCGCTCTGCTAATCC-3'	Backb_rev1
5'-GATATCAAGCTTAACACGAGCC-3'	3ÕLTR_for
5'-ATTTCGTTCATCCATAGTTGCC-3'	Backb_for2
5'-CAATAGCGGCTGCTCAGCGG-3'	Seqpgkfor
5'-CGGTCACAGCTTGTCTGTAAGC-3'	bactBB2_for
5'-GTCGGCCACCCACACTTTGCC-3'	pac_rev2
5'-TGTATCCGCTCATGAGACAAT-3'	SeqblaF
5'-GAGTAAACTTGGTCTGACAG-3'	SeqKanR
5'-ACCGTGAACTTCGGCGACAC-3'	serpina1_for
5'-ATCTGCACACTGGTATTTCGG-3'	EF1alpha_for
5'-AGAGTTCGAGGCCTTGCG-3'	EF1alpha_1
5'-TGAAGGCGAACTCGGCCA-3'	serpina1_2_rev
5'-TGGCCGAGTTCGCCTTCA-3'	serpina1_2_for
5'-ACCGTGAAGGTGCCCATGAT-3'	serpina1_3_for
5'-ACCAGTACCACCACGAACAAG-3'	IRES_f
5'-ATCGAGAGAGTGACCGAGCT-3'	pac_f
5'-ACGCTCTGTTCCTGTTAATCAA-3'	PRE_f
5'-TACAATGACTCCTTTCGGTAAGT-3'	SERPINA1_5UTR_f
5'-AACCTGCCCTTCTACGAGC-3'	pac_f_2

5'-GGTGTTCCGCATTCTGCAAGC-3'	IFNbeta_f
5'-CATCTTCGCCATCTTCCGGCA-3'	IFNbeta
5'-TTAATTGCGTTGCGCTCACTGC-3'	bactBB3_for
5'-GTCTTGTCTGCTGCAGCATCG-3'	EFS_Defensin_f
5'-CCGTCTTTTGGCAATGTGAGG-3'	IRES_pac_f
5'-CCTGGATGGAGTGGGACAGAGAAAT-3'	pCCL_fw
5'-AGTGAGGAGGCTTTTTTGGAGGCCT-3'	pCCL_fw2
5'-GGAGCTAGAACGATTCGCAGTTA-3'	pCCL_fw3
5'-GGTTGTAGCTGTCCCAGTATTTGTC-3'	pCCL_fw4
5'-GATGGCCCACTACGTGAAC-3'	pCCL_rev
5'-CTTTCGCTTTCTTCCCTTCC-3'	pCCL_fw5

2.2.3. Production of gamma-retroviral and lentiviral supernatants

Gamma-retroviral supernatants were generated by transient triple transfection of 293T human embryonic kidney cells. Cells were seeded on the day prior to transfection at 5×10^6 cells/10cm $\varnothing$ dish in 10mL 293T medium. On the day of transfection, medium was exchanged for 5mL 293T medium containing 25µM chloroquine, and cells were cultured in the presence of chloroquine for at least 1 hour before transfection. Transfection was performed using Sigma's Calcium Phosphate Transfection Kit according to manufacturer's instructions. 12.5µg pCDNA3-MLV-gagpol (Supplemental figure 6), 2.0µg pALF-PERV A_GaLV envelope plasmid (Supplemental figure 7), and 7.5µg of retroviral transfer plasmid were used for the transfection of one 10cm $\varnothing$ dish. Medium was replaced with 6mL basal 293T medium 6 hours after addition of calcium phosphate-DNA precipitates. Viral supernatants were collected 2 days after transfection for the first time; 6mL fresh 293T medium was added to cells, and collected supernatants were stored at 4°C until the second harvest, one day later. Supernatants collected on both days were pooled, filtered using a 0.45µM syringe filter and cryopreserved in 1–2mL aliquots at -80°C.

Lentiviral supernatants were produced as described above; lentiviral packaging plasmids #170 pCMV-dR8.91 (10µg, Supplemental figure 8) expressing HIV-1 gagpol and #171 pCAGGS-VSVG (2µg, Supplemental figure 9) encoding the VSV.G envelope (both kindly provided by Donald Kohn, UCLA) were used in combination with 10µg lentiviral transfer plasmid #215 pCCL_pEFS_SERPINA1_IRES_pac for triple transfection of one 10cm $\varnothing$ dish.

2.2.4. Titration of gamma-retroviral and lentiviral supernatants on HT1080 cells

In order to determine viral titers, 2×10^4 HT1080 fibrosarcoma cells were seeded in a volume of 1mL HT1080 medium per well of a 12-well plate on day 1 and incubated at 37°C, 5% CO_2 in a humidified atmosphere overnight. To be able to accurately determine cell numbers on the day of transduction, three extra wells were plated as counting controls. On day 2, cells in the three counting wells were enzymatically detached using TrypLE Select, 1mL PBS was added to each well, and cells were

transferred to a 1.5mL microcentrifuge tube and pelleted by centrifugation at 500xg for 5 minutes. Supernatants were removed carefully, and cell pellets were resuspended in 50µL PBS each. Exact volumes were determined by using a micropipette. 10µL of each cell suspension were counted using a Neubauer hemocytometer, and cell numbers were recorded. The average of the three counts was used to calculate viral titers later on. For transduction, viral supernatants were diluted in 293T medium over a range from 1:2–1:200, and at least three different dilutions were test in duplicate; medium on HT1080 cells was discarded and replaced with 800µL diluted viral supernatant. Two wells were kept as non-transduced negative controls, and 800µL 293T medium was added to each of those wells. Cells were incubated at 37°C, 5% CO_2 in a humidified atmosphere overnight. On day three, diluted viral supernatants and 293T medium, respectively, were replaced with fresh HT1080 medium. Three days after transduction, transduction efficiency was analyzed by an intracellular flow cytometry assay detecting transgenic human AAT protein.

Titers in [transducing units (TU)/mL] were calculated as follows:

$$\text{Titer} \left[\frac{\text{TU}}{\text{mL}}\right] = \frac{\% \text{ AAT positive cells} * \text{number of cells seeded} * \text{dilution}}{100 * 0.8 \text{ (volume of viral supernatant)}}$$

2.2.5. Isolation of primary human MSCs from human bone marrow

Bone marrow was harvested from healthy donors after informed consent had been obtained. Routinely, tests for sterility, white blood cell (WBC) count, assessment of the morphology of bone marrow cells, and CFU assay were performed by apceth's Quality Control Department to assess the quality of the bone marrow.

Cells were then seeded in cell stack chambers in Bio-1 medium (cf. Table 5). A first complete medium change was conducted 3–5 days after seeding, and every 3–5 days thereafter half of the medium was exchanged for fresh medium. After a culture period of 10–14 days, when multiple large colonies of adherent, spindle-shaped cells were visible, cells were enzymatically detached using TrypLE select, and cryopreserved in either 90% FBS + 10% dimethyl sulfoxide (DMSO) or apceth's cryopreservation solution consisting of 45% of hydroxyethyl starch (HAES) injection solution (10% in isotonic saline solution), 45% human albumin (HA) injection solution ([50g/L] in isotonic saline solution), and 10% DMSO in aliquots of $1x10^6$-$5x10^6$ cells (P0).

2.2.6. Culture of primary human MSCs

MSCs were generally cultured in Bio-M or Bio-1 culture medium (cf. Table 5) at 37°C and 5% CO_2 in a humidified atmosphere. Care was taken to never let MSCs grow to complete confluency to avoid contact inhibition of growth and differentiation of the cells. In order to propagate MSCs, cells were washed once with PBS before enzymatic detachment using TrypLE select for 10 minutes at 37°C. The

reaction was stopped using Bio-M culture medium. Cells were then either diluted in Bio-M/Bio-1 (if volume of fresh medium was at least 5 times the initial volume) or centrifuged at 300xg for 5 minutes, and the cell pellet resuspended in fresh medium before seeding into appropriate culture vessels.

Table 5: **Culture and cryopreservation media used for MSCs and tumor cell lines.**

	Manufacturer	**Final Concentration**
Bio-M		
DMEM low glucose	Biochrom	87.5%
FBS	Biochrom	10%
HEPES [1M]	Gibco	25mM
Bio-1	apceth's proprietary cell culture medium	
293T medium		
DMEM high glucose	Biochrom	90%
FBS	Biochrom	10%
HT1080 medium		
EMEM	Lonza	90%
FBS	Biochrom	10%
Cryopreservation solution		
HAES 10%	Fresenius Kabi	45%
HA	Baxter	45%
DMSO	Wak-Chemie	10%

2.2.7. Culture of tumor cell lines

Tumor cell lines were cultured under equal conditions as MSCs in their respective medium (Table 5) and cryopreserved in 90% FBS + 10% DMSO.

2.2.8. Cell counting

Determination of cell numbers was performed by manual counting using a Neubauer hemocytometer in all experiments performed. In some experiments, cells were diluted in Trypan Blue before counting to analyze cell viability.

2.2.9. Cryopreservation of cells

MSCs were cryopreserved in either 90% FBS + 10% DMSO or cryopreservation solution (Table 5) at a concentration of $5x10^6$ cells/mL; aliquot sizes were ranging from $1–5x10^6$ cells/vial. Tumor cell lines were frozen in 90% FBS + 10% DMSO at the same concentration and aliquot sizes as MSCs. Cryovials

containing cells in their respective cryopreservation solution were immediately transferred to a Mr. Frosty Freezing Container and stored at -80°C overnight before being moved to the vapor phase of liquid nitrogen the next day.

2.2.10. Thawing of cells

Vials were quickly removed from the liquid nitrogen tank and immediately transferred to a water bath pre-heated to 37°C. When still some small ice clumps were visible in the vial, it was moved to the laminar air flow cabinet, and the cell solution was pipetted into the respective culture vessel already containing culture medium.

2.2.11. Transduction of MSCs by centrifugation of viral supernatants onto PLL-coated plates

Wells of 6- or 12-well plates were coated with Poly-L-Lysin (PLL) diluted 1:10 in PBS to a final concentration of [10µg/mL] for at least one hour. PLL was discarded, and wells were carefully washed with PBS before viral supernatant was added. The amount of viral supernatant needed for transduction was calculated based on the cell number to be transduced, the desired MOI, and the titer of the viral supernatant. Viral supernatant was added to the PLL-coated plates; in some experiments, the supernatant was diluted with 293T medium. 293T medium only was added to two wells serving as negative control wells later, one as a control for intracellular flow cytometry to analyze transduction efficacy, the other one as control for antibiotic selection. Plates containing viral supernatant and 293T medium were centrifuged in a pre-cooled centrifuge at 2000xg and 4°C for 30 minutes. During the centrifugation, cells to be transduced were enzymatically detached and counted. After completion of the centrifugation step, viral supernatant and 293T medium, respectively, were removed from the wells carefully, and cells resuspended in Bio-M were added. Cells were incubated overnight, and medium was exchanged for fresh Bio-M the next day.

2.2.12. Transduction of MSCs by direct seeding

Cells were enzymatically detached using TrypLE select, resuspended in PBS, counted, spun down at 300xg for 5 minutes, and resuspended in PBS. The amount of viral supernatant needed for transduction was calculated based on the cell number, the desired MOI, and the titer of the viral supernatant. In a first step, PLL [100µg/mL] was added to the viral supernatant at a ratio of 1:100 yielding a final concentration of PLL of [1µg/mL]. In the next step, the cells were added to the PLL-viral supernatant mixture, and the transduction mix was seeded into appropriate culture vessels. One small extra flask of transduced cells was usually plated for the flow cytometric assessment of transduction efficacy before antibiotic selection, so that the transduced batch did not have to be disturbed for this analysis. After three hours of incubation, the same amount of culture medium was

added to the 2X transduction mix, and the cells were cultured overnight. Non-transduced cells were seeded into two wells of a 6-well plate to serve as a negative control for flow cytometric analyses and as a control for the subsequent antibiotic selection.

2.2.13. Detection of transgenic AAT by intracellular flow cytometry

Cells were analyzed for the expression of transgenic intracellular (ic) AAT 48–72 hours after transduction. To enhance the detection of the protein, HT1080 cells were treated with 1µL and MSCs with 10µL, respectively, of GolgiPlug Protein Transport Inhibitor per mL medium for 16–24 hours before the staining, so that proteins were accumulated in the Golgi complex and not secreted. Cells were detached by trypsinization, counted, washed once with 1mL PBS, and up to $1x10^6$ cells were permeabilized using 250µL BD Cytofix/Cytoperm Fixation and Permeabilization Solution for 20 minutes at 4°C. After 2 washes with 1mL 1X Perm/Wash Buffer and centrifugation at 500xg for 5 minutes each, the cell pellet was resuspended in 100µL Perm/Wash Buffer and stained with a polyclonal FITC-conjugated Anti-alpha 1 Antitrypsin antibody (1µL antibody/100µL cell suspension) for 20–30 minutes at 4°C in the dark. After the incubation, cells were washed with 1mL 1X Perm/Wash Buffer, resuspended in 400µL PBS, and analyzed on a Beckman Coulter FC500 flow cytometer. Non-transduced cells were treated as described above and used as negative controls for gating. In titration experiments, only values <25% intracellular AAT-positive cells were included in titer calculations.

2.2.14. Antibiotic selection

Antibiotic selection of transduced cells was started 48–72 hours after transduction. Puromycin was diluted in fresh Bio-M medium to a final concentration of [3µg/mL], and medium on the cells was replaced with medium containing puromycin. Medium was exchanged for fresh puromycin-containing medium after 2–3 days, and cells were selected for a total of 5 days. After visual inspection of the control well and confirmation that all plated non-transduced MSCs were dead, medium was replaced with regular Bio-M for subsequent expansion of the cells.

2.2.15. Determination of VCN

DNA of transduced, puromycin-selected MSCs and non-transduced control cells was extracted using Qiagen's DNeasy Blood & Tissue Kit following manufacturer's recommendations. To determine the average vector copy number (VCN) in the bulk cell population, two singleplex quantitative polymerase chain reactions (qPCRs) were carried out for each DNA sample: One primer and probe set was detecting the optimized posttranscriptional regulatory element (oPRE) sequence, a part of the viral vector that is integrated into the genome of the cell after transduction, a second set was recognizing factor VII (FVII), a human single copy gene, that was utilized as a reference gene to

correct for variability in DNA amounts used in the qPCR. Plasmid standard curves ranging from 1–$1x10^5$ copies were included in the experiments to determine qPCR efficiencies of the two primer and probe sets. Sequences of the primers are listed in 2.1.3, composition of master mixes as well as cycling conditions are mentioned in Table 6 and Table 7. All samples were measured in triplicate on a LightCycler 480 Instrument II. A calibrator DNA extracted from an HT1080 cell clone with one single viral integration as confirmed by linear amplification mediated (LAM) PCR was included in each experiment. After completion of the qPCR run, VCNs were calculated by means of relative quantification and comparison of the calculated values to that derived from the calibrator (set to be VCN = 1).

Table 6: **Composition of qPCR master mixes for oPRE and FVII for VCN determination.**

oPRE	µL [1 reaction]	final conc.
H_2O	4.10	
Primer 275 (oPRE_WPRE_VCN fw) [20µM]	0.30	[300nM]
Primer 142 (WPRE rev) [20µM]	0.30	[300nM]
Probe 63 (UPL) [10µM]	0.30	[150nM]
2X Probes Master 480	10.00	1X
DNA [4-60ng/µL]	5.00	
Sum	20.00	

FVII	µL [1 reaction]	final conc.
H_2O	4.25	
Primer 91 (FVII for) [20µM]	0.30	[300nM]
Primer 92 (FVII rev) [20µM]	0.30	[300nM]
Probe 187 (FVII probe) [20µM]	0.15	[150nM]
2X Probes Master 480	10.00	1X
DNA [4-60ng/µL]	5.00	
Sum	20.00	

Table 7: **Cycling conditions for VCN qPCR (oPRE and FVII).**

Step	Temperature	Duration	Cycles
Initial denaturation	95°C	10 minutes	1
Denaturation	95°C	10 seconds	45
Annealing/Elongation	60°C	30 seconds	
Cooling	40°C	30 seconds	1

2.2.16. AAT ELISA

Transduced, puromycin-selected MSCs were seeded at a concentration of $1x10^4$ cells and 250µL Bio-M/cm^2 in wells of 6-, 12- or 24-well plates. After cells had adhered (approximately 4–6 hours after seeding), medium was replaced with fresh Bio-M. Cells were then incubated for 48 hours at 37°C and

5% CO_2 in a humidified atmosphere. After incubation, supernatants were cryopreserved in aliquots at -80°C until further use. On the day of the experiment, supernatants were thawed on ice and centrifuged at 3000xg for 10 minutes to remove cell debris. The AAT ELISA was performed according to manufacturer's instructions; sample pre-dilutions were usually 1:200 in Diluent N.

2.2.17. Neutrophil elastase inhibitor screening assay

2.2.17.1. Production of cell culture supernatants for neutrophil elastase inhibitor screening assay

Transduced and puromycin-selected MSCs were seeded at a concentration of $1x10^4$ cells and 250µL Bio-M/cm^2 in an appropriate culture vessel. After cells had grown to 90–100% confluency, cells were washed 5 times with PBS to remove any residual bovine AAT present in FBS that would have been picked up by the assay. Cells were cultured in Dulbecco's Modified Eagle's Medium (DMEM) supplemented with 1X GlutaMAX and 1mM Sodium Pyruvate for 16–24 hours at 37°C and 5% CO_2 in a humidified atmosphere. After incubation, supernatants were cryopreserved in aliquots at -80°C until further use. In some experiments, supernatants were concentrated using Amicon Ultra 4mL Centrifugal Filters before cryopreservation.

2.2.17.2. Neutrophil elastase inhibitor screening assay

The neutrophil elastase inhibitor screening assay was performed according to manufacturer's instructions with minor modifications, *i.e.* instead of the positive control included in the kit (SPCK), active natural AAT full length protein purified from human plasma in four different concentrations ranging from [250–2000ng/µL] was used as a more commensurable positive control.

In brief, neutrophil elastase (NE) assay buffer and substrate included in the kit were thawed; aliquots were prepared and stored at -20°C. Neutrophil elastase was reconstituted in 220µL of NE assay buffer; aliquots were prepared and stored at -80°C. Active AAT full length protein was reconstituted in ddH$_2$O to yield a concentration of [1µg/µL]; aliquots were prepared and stored at -80°C until further use. On the day of the assay, MSC supernatants were thawed, and dilutions were prepared in DMEM supplemented with 1X GlutaMAX and 1mM Sodium Pyruvate. Active full length AAT was thawed and diluted in DMEM supplemented with 1X GlutaMAX and 1mM Sodium Pyruvate to yield concentrations of [2000ng/mL], [1000ng/mL], [500ng/mL], and [250ng/mL]. Undiluted, concentrated supernatant from non-transduced MSCs was included as a negative control. The substrate was diluted 1:12.5 in NE assay buffer and kept at room temperature in the dark until further use. Immediately before starting the assay, neutrophil elastase was diluted 1:25 in NE assay buffer, and 50µL diluted elastase working solution were added per well of a 96-well flat clear bottom black polystyrene plate. 25µL of positive and negative control samples and MSC supernatant dilutions, respectively, were added and mixed by pipetting up and down carefully. All samples were measured in duplicate. After an incubation of 5 minutes at 37°C, 25µL diluted substrate working solution were

added to each well, and the fluorescence output R1 (Ex/Em = 400/505nm) was measured on a TECAN plate reader immediately. The plate was then incubated for 20 minutes at 37°C, and after that measured again at Ex/Em = 400/505nm (R2). The relative fluorescence units (RFU) generated by hydrolyzation of the substrate was calculated as ΔRFU = R2 − R1. The ΔRFU of the negative control (DMEM) was set as the 100% relative activity value, and the relative remaining neutrophil elastase activity after treatment with potential inhibitors was calculated as follows:

$$\frac{\text{RFU test inhibitor } (e.\,g.\,\text{AAT} - \text{MSC supernatant})}{\text{RFU DMEM}} * 100$$

2.2.18. Generation of large MSC batches for *in vitro* and *in vivo* experiments

2.2.18.1. Process description

P0-MSCs were generally thawed on a Friday, and the cells were cultured in 750mL Bio-1 in a CellSTACK cell culture system with 5 chambers. Cells were transduced as described in "Transduction of primary human MSCs by direct seeding" on the following Tuesday. Transduction efficacy was analyzed by intracellular flow cytometry for AAT protein 72 hours after transduction using the cells plated in the extra flask on the day of transduction. On the same day, puromycin selection was started. Depending on the confluency rate, cells were expanded either already also on Friday or on the following Monday. For propagation, cells were enzymatically detached, spun down at 300xg for 5 minutes, and distributed in 3–6 CellSTACK cell culture systems with 5 chambers in Bio-1 containing puromycin each. Cells received fresh Bio-1 containing puromycin again on Monday. When the cells in the selection control well (non-transduced MSCs) were completely dead (usually after 5 days of selection), medium was exchanged for basal Bio-1. Cells were cultured to confluency, when they were harvested, checked for complete antibiotic selection by intracellular staining for AAT and flow cytometric analysis and cryopreserved in aliquots ranging from 1×10^6–5×10^6 cells in cryopreservation medium.

To generate large batches of non-transduced MSCs, cells from the same thawing process were used, and the same culture and splitting scheme as described above was followed: On Tuesday, 2.5×10^6–1×10^7 cells were seeded in a CellSTACK culture system with 5 chambers in Bio-1, on Friday or Monday MSCs were expanded onto 3–6 CellSTACK systems and cryopreserved after growing to confluency in cryopreservation solution.

2.2.18.2. Quality control assays for batches

To assess if MSCs fulfilled apceth's quality standards, one vial of cryopreserved MSCs of each batch was thawed, and a panel of standard quality control assays was performed. Standard assays and required specifications are listed in Table 8. In addition to these tests which were carried out for all

batches produced, genetically modified batches were additionally analyzed for percentage of AAT positive MSCs pre- and post-selection, VCN, amount of AAT protein expressed per $1x10^5$ cells in 48 hours normalized to VCN, capability of the cells to inhibit neutrophil elastase in comparison to natural AAT purified from human plasma, and the presence of replication-competent retrovirus (RCR) and lentivirus (RCL).

Table 8: **Standard quality control assays performed for each batch of MSCs produced.**

Parameter	Result
Sterility	No growth of bacteria and fungi
Surface marker expression	All surface makers within specification
Adipogenic differentiation	Several adipocytes visible
Osteogenic differentiation	Osteogenic mineralization visible
Testing for Mollicutes	Negative

Sterility

MSCs were cultured for at least 48 hours after thawing, and 10mL of cell supernatant was injected into BacT/ALERT Culture Media Standard Aerobic and Standard Anaerobic bottles, respectively, and sent to synlab for analysis.

MSC surface marker flow cytometry

MSCs were enzymatically detached, counted, washed once with 1mL PBS, and resuspended in PBS so that $5x10^4$–$2x10^5$ cells were added to each of five microcentrifuge tubes in a volume of 100µL. Fluorescently labeled antibodies were added to the tubes according to the scheme depicted in Table 9, the tubes were vortexed and incubated for 20 ± 5 minutes at room temperature in the dark. After the incubation, cells were washed with 1mL PBS, and the pellets were resuspended in 100µL of a 1:5 dilution of 7-AAD Viability Dye in PBS each. After a 10-minute incubation step at room temperature in the dark, 200–400µL of PBS were added to each sample, and cells were analyzed on a Beckman Coulter FC500 flow cytometer.

Table 9 **Antibody mixes for immunofluorescent staining of MSC surface markers.**

Tube 1	Amount [µL]	Tube 2	Amount [µL]	Tube 3	Amount [µL]	Tube 4	Amount [µL]	Tube 5	Amount [µL]
IgG1-FITC	20	CD90-FITC	20	CD235a-FITC	20	CD3-FITC	20	CD41-FITC	20
IgG1-PE	20	CD73-PE	20	CD105-PE	20	CD14-PE	20	CD105-PE	20
IgG2a-PE	20	CD45-ECD	10	CD45-ECD	10	CD45-ECD	10	HLA-DR-ECD	10
IgG3-PE	10	CD34-PC7	10	CD34-PC7	10	CD19-PC7	10	CD61-PC7	10
IgG1-ECD	10								
IgG1-PC7	10								

Adipogenic and osteogenic differentiation

Plating and differentiation of MSCs

3×10^4 MSCs were seeded per well in 5 wells each of two 24-well plates (one for adipogenic differentiation, one for osteogenic differentiation) in 1mL Bio-M or Bio-1 and cultured until complete confluency (1–3 days). Bio-M/Bio-1 was then replaced by 1mL of StemMACS AdipoDiff Media for adipogenic differentiation and 1mL of StemMACS OsteoDiff Media for osteogenic differentiation, respectively, on three wells per respective plate. Two wells served as control wells and received fresh Bio-M/Bio-1. Fresh differentiation media and Bio-M/Bio-1, respectively, were added every 3–5 days for a minimum of two weeks. Cells were then stained with Oil Red O to assess differentiation into adipocytes, and with Alizarin Red to confirm osteogenic mineralization.

Oil Red O Staining (adipogenic differentiation)

All fixation and staining steps were performed at room temperature. Oil Red O staining working solution was prepared by mixing 6mL filtered Oil Red O staining stock solution [3mg/mL in 2-Propanol] with 4mL de-ionized water. The solution was incubated for 10 minutes after mixing and then filtered. Cells on the 24-well plate for adipogenic differentiation were washed twice with PBS and fixed with 2mL 10% Formalin for 30–45 minutes. In a second step, the Formalin solution was removed; cells were washed twice with 2mL tap water, and fixed again with 1mL 60% 2-Propanol for 3–5 minutes. After discarding the 60% 2-Propanol, 1mL Oil Red staining working solution was added to each well, and cells were incubated for 5–10 minutes. After 2 washes with PBS, 1mL filtered Mayer's Hematoxylin staining solution was added and kept on the cells for 1–5 minutes. After two washes with 2mL tap water each, 1mL PBS was added to each well, and photos were taken using a Leica DMI6000B microscope and LAS X software.

Alizarin Red Staining (osteogenic differentiation)

All fixation and staining steps were performed at room temperature. Cells on the 24-well plate for osteogenic differentiation were washed twice with PBS and fixed with 2mL 10% Formalin for 30–45 minutes. After discarding the Formalin solution, cells were washed twice with 2mL de-ionized water, and 1mL filtered Alizarin Red staining solution [20mg/mL in de-ionized water] was added and kept on the cells for 30–45 minutes. After incubation, the Alizarin Red staining solution was removed, and cells were washed 4 times with 1mL de-ionized water. 1mL PBS was added to each well, and photos were taken using a Leica DMI6000B microscope and LAS X software.

Testing for Mollicutes

Detection of possible Mollicutes (Mycoplasma, Acholeplasma, Spiroplasma) contamination in cell cultures was performed using the Microsart RESEARCH Mycoplasma Detection Kit for qPCR following manufacturer's recommendations using DNA extracted from MSCs (isolated using Qiagen's DNeasy Blood & Tissue Kit according to manufacturer's instructions) as template.

Testing for RCR/RCL

MSC-DNA was extracted using Qiagen's DNeasy Blood & Tissue Kit following manufacturer's recommendations. To test for RCR/RCL, qPCR assays detecting the gag sequence of MLV and HIV-1, respectively, using 50-400ng of template DNA were performed. Sequences of the primers are listed in 2.1.3; compositions of master mixes as well as cycling conditions are mentioned in Table 10 and Table 11. All samples were measured in triplicate on a LightCycler 480 Instrument II. Commercially available human genomic DNA and DNA extracted from HT1080 cells served as negative controls, pCDNA3-MLV-gagpol and pCMV-dR8.91 plasmid DNA [5 copies/µL], respectively, was used as a positive control. After completion of the qPCR run, crossing point (Cp) values were calculated by means of absolute quantification. Samples yielding Cp values <39 were considered negative.

Table 10: **Master mix compositions for MLV gag and HIV-1 gag qPCRs for detection of RCR/RCL.**

RCR	µL [1 reaction]	final conc.
H$_2$O	3.90	
Primer 214 gag_eu_for [20µM]	0.60	[600nM]
Primer 215 gag_eu_rev [20µM]	0.30	[300nM]
Probe 216 gag_eu_probe [20µM]	0.20	[200nM]
2X Probes Master 480	10.00	
DNA [10-80ng/µL]	5.00	
Sum	20.00	

RCL	µL [1 reaction]	final conc.
H$_2$O	3.90	
Primer 376 HIV-1 gag F [20µM]	0.60	[600nM]
Primer 377 HIV-1 gag R [20µM]	0.30	[300nM]
Probe 375 HIV-1 gag P [20µM]	0.20	[200nM]
2X Probes Master 480	10.00	
DNA [10-80ng/µL]	5.00	
Sum	20.00	

Table 11: **Cycling conditions for MLV gag and HIV-1 gag qPCRs.**

Step	Temperature	Duration	Cycles
Initial denaturation	95°C	10 minutes	1
Denaturation	95°C	10 seconds	45
Annealing/Elongation	60°C	30 seconds	
Cooling	40°C	30 seconds	1

2.2.19. *In vivo* experiments

The mouse experiments were performed in collaboration with Dr. Yildirim from the Comprehensive Pneumology Center at the Helmholtz Zentrum München.

2.2.19.1. Preparation of cells

For each of the two cell applications, three vials [$5x10^6$ cells/vial] each of a quality-controlled native MSC batch and a quality-controlled batch of MSCs transduced with gamma-retroviral supernatant #194, respectively, were thawed and cultured in one CellSTACK culture system with 5 chambers in 750mL Bio-M each for 48 hours. Cells were enzymatically detached using TrypLE, counted, resuspended in PBS to yield a concentration of $5x10^6$ cells/mL, and transferred to the Helmholtz Zentrum on ice for immediate intratracheal injection.

2.2.19.2. Elastase-induced emphysema mouse model

Female C57BL/6N mice aged 8–10 weeks were housed under specific pathogen free conditions, exposed to a 12-hour light cycle with access to food and water *ad libitum*, in rooms maintained at a constant temperature and humidity. Mice were divided into 4 groups consisting of 6 mice per group (Table 12). Mice in groups 2–4 were oropharyngeally exposed to a single application of 40 units/kilogram (kg) body weight porcine pancreatic elastase in 80μL volume on day 0. Control mice were treated with 80μL of PBS. On day 7, mice in groups 3 and 4 were treated with one oropharyngeal application of $5x10^5$ native MSCs or $5x10^5$ MSCs transduced with a gamma-retroviral vector to express AAT. Mice in control groups 1 and 2 received saline instead of the cells. Mice in groups 3 and 4 were additionally treated with a second oropharyngeal application of $5x10^5$ native MSCs or $5x10^5$ AAT-MSCs on day 14 after elastase treatment. All mice were analyzed on day 21.

Table 12: **Mouse groups and respective treatments.**

Group	Treatment 1	Treatment 2	Cell dose/ mouse	Application volume cells/mouse [μL]	Administration route	Animals/ group
1	PBS	Saline	N.a.	100	Oropharyngeal	6
2	Elastase	Saline	N.a.	100	Oropharyngeal	6
3	Elastase	MSCs	$5x10^5$ (2x)	100	Oropharyngeal	6
4	Elastase	AAT-MSCs	$5x10^5$ (2x)	100	Oropharyngeal	6

2.2.19.3. Pulmonary function measurements

Mice were anesthetized with an intraperitoneal injection of 130 mg/kg ketamine and 8.5 mg/kg xylazine to maintain spontaneous breathing under anesthesia. Tracheostomy was performed with a standard catheter. After intubation, mice were placed in a body plethysmograph and connected to a computer-controlled ventilator (forced pulmonary maneuver system, Buxco research systems). This laboratory set-up semi-automatically provides three different maneuvers: Boyle's Law functional

residual capacity, quasistatic pressure volume and fast flow volume maneuver.

A breathing frequency of 150 breaths/minute was imposed by pressure control ventilation until a regular breathing pattern and complete expiration at each breathing cycle were obtained. To measure functional residual capacity (FRC), ventilation was stopped at the end of expiration with an immediate closure of a valve located proximally to the endotracheal tube. Spontaneous breathing maneuvers against a closed valve with consequent pressure changes were then recorded. To measure inspiratory capacity (IC) and vital capacity (VC), the quasistatic pressure volume maneuver was performed, which inflates the lungs to a standard pressure of +30cm H_2O and then slowly exhales until a negative pressure of -30cm H_2O is reached. With the fast flow volume maneuver, lungs were first inflated to +30cm H_2O and immediately afterwards connected to a highly negative pressure in order to enforce expiration. Forced vital capacity (FVC), forced expiratory volume at 100ms (FEV_{100ms}), and peak expiratory flow (PEF) were recorded during this maneuver. In every animal, each maneuver was repeated until three acceptable measurements were recorded, of which the average was then calculated.

2.2.19.4. BALF and serum

Bronchoalveolar lavage fluid (BALF) was obtained for total and differential cell counts to assess inflammatory cell recruitment of macrophages, neutrophils and lymphocytes to the lungs. Lavage was performed using 3×500µL of PBS. Cells were pelleted at 400xg, the supernatant stored at −80°C, and the cells were resuspended in RPMI-1640 medium for total cell count using a hemocytometer. Cytospins of the cell suspension were prepared and stained using May–Grünwald–Giemsa staining mixes for differential cell counting (200 cells/sample) using morphological criteria. Serum was collected for chemokine and cytokine analysis. Mice were bled from the femoral artery; blood was left to clot for several hours and then centrifuged at 1300xg for 15 minutes. Serum was stored in aliquots at -80°C.

2.2.19.5. Lung processing

The left lung was fixed under a constant pressure of 20cm fluid column by intratracheal instillation of 6% paraformaldehyde and embedded into paraffin for hematoxylin and eosin (H&E) staining analysis using systematic uniform random sampling according to standard methods as described by Yildirim and colleagues [331].

2.2.19.6. Histology

<u>Emphysema scoring</u>

To quantify emphysema development, an emphysema state was ascribed to each H&E-stained sample in a blinded fashion by a pathologist. The score of elastase induced-emphysema was determined as follows: 0 – normal; 1 – up to 10% loss of septal tissue; 2 – 11-20% loss of septal tissue; 3 – 21-40% loss of septal tissue; 4 – 41-60% loss of septal tissue; 5 – >60% loss of septal tissue.

The slides were randomly examined in more than 10 fields of view in a blinded fashion.

<u>Inflammation scoring</u>

To quantify the inflammatory state, an inflammatory score was assigned to each H&E-stained sample in a blinded fashion by a pathologist. The score of peribronchiolar and perivascular inflammation was determined as follows: 0 – normal; 1 – few cells; 2 – a ring of inflammatory cells one to two cell layer-deep; 3 – a ring of inflammatory cells three or more than three cell layer-deep. The slides were randomly examined in more than 10 fields of view in a blinded fashion.

2.2.20. Statistical analyses

Data is depicted as mean $\pm$ standard deviation (SD). Statistical analyses were performed using GraphPad Prism Version 7.0. Tests for statistical significance are indicated in the text. Statistical significance levels are expressed as * $P < 0.05$, ** $P < 0.01$, *** $P < 0.001$, **** $P < 0.0001$.

3. Results

3.1. Design and cloning of gamma-retroviral AAT expression constructs

3.1.1. Design of the *SERPINA1* expression cassette

For the design of the AAT expression cassette, the human *SERPINA1* cDNA transcript variant 1 (NCBI Reference Sequence: NM_000295.4) was chosen from the 11 transcript variants of *SERPINA1* listed on NCBI's Nucleotide. This transcript variant encodes for the same protein as the other 10 variants of the gene; all 10 additional variants differ solely in the 5' UTR as compared to transcript variant 1. The coding sequence (CDS) comprises bases 262 to 1518 of the full reference sequence published at http://www.ncbi.nlm.nih.gov/nuccore/NM_000295.4. Bases 1 to 261 were included in the expression cassette to preserve the physiological *SERPINA1* transcript variant 1 5' UTR. The 3' UTR was not included due to size restrictions of the viral backbone. To increase protein expression, a Kozak consensus sequence [327] was inserted 5' of the *SERPINA1* start codon, and the cDNA was codon-optimized for *Homo sapiens*. For a graphical representation, please *cf.* Figure 3.

3.1.2. Cloning of four "1ˢᵗ generation" gamma-retroviral expression plasmids

Plasmid numbers mentioned throughout this work represent apceth's internal plasmid numbering and will be used below for the sake of simplicity.

As the influence of different promoters on the expression of transgenic AAT from primary MSCs was one variable to be tested in this work, the first four constructs cloned made use of four different promoters (pPGK, pEF1a, pCAG, and pEFS) to drive the *SERPINA1* expression cassette, followed by an IRES sequence and the *pac* gene in the pSERS11 backbone [328]. The plasmids were cloned as described in 2.2.1. Briefly, an *IFN-beta* expression cassette present in a plasmid previously cloned at apceth for a different project was replaced with the *SERPINA1* expression cassette, yielding plasmid #114 pPGK_SERPINA1_IRES_pac; as a next step, the PGK promoter present in plasmid #114 was exchanged for promoters EF1a, CAG, or EFS, resulting in plasmids #115, #116, and #129. Figure 5 shows a schematic representation of the 4 gamma-retroviral plasmids.

After transduction of primary human MSCs with the four viral supernatants generated using the plasmids described above, it was possible to confirm transgenic AAT expression by intracellular flow cytometry, but selection of the cells with puromycin in concentrations ranging from [0.5–3.0µg/mL] lead to a complete kill of the cells (data not shown). These experiments indicated that the *pac* gene was not expressed in sufficient amounts. After a thorough investigation and the performance of multiple experiments, it was discovered that this phenomenon was due to a non-functional IRES sequence used to design and clone the original retroviral plasmid containing the *IFN-beta* expression cassette. Consequently, the retroviral backbone was corrected using a published IRES sequence

derived from the encephalomyocarditis virus (EMCV) [332,333], and the integrity of the complete backbone checked by sequencing. Additional modifications to improve the backbone were included, such as exchanging the wPRE sequence for an optimized version, the oPRE sequence described by Schambach and colleagues [334]. This optimized backbone was subsequently used to clone all "2nd generation" constructs.
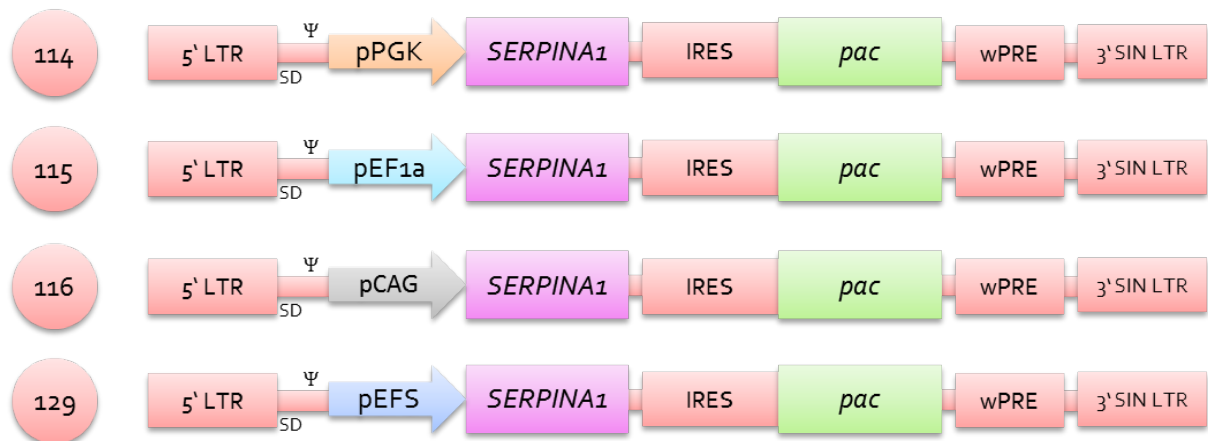
Figure 5: **Schematic representation of the "1st generation" plasmids.** Four different promoters were used to drive the expression of *SERPINA1* and *pac* (pPGK, pEF1a, pCAG, and pEFS), which were linked by an IRES sequence. A wPRE sequence was cloned 3' of the *pac* gene to increase mRNA stability and protein yield. Ψ: Packaging Signal; SD: Splice Donor.

3.1.3. Cloning of eight "2nd generation" gamma-retroviral expression plasmids

Titration and preliminary transduction experiments were performed in order to compare the different constructs using the four "1st generation" gamma-retroviral supernatants. The results indicated that although the CAG promoter led to high levels of AAT expression as was expected [335], the titer of supernatant #116 as well as transduction efficacies achieved on MSCs using that supernatant were unacceptably low (data not shown). Thus, it was decided to not include the CAG promoter in subsequent cloning strategies. Instead the influence of the remaining three promoters on AAT expression were analyzed, while at the same time different configurations of the *SERPINA1* and *pac* expression cassettes were assessed. In the first three "2nd generation" constructs cloned, pPGK, pEFS, and pEF1a were used to drive *SERPINA1* gene expression, followed by either pEFS or pPGK expressing *pac* (constructs #159, #160, and #161). To avoid unwanted recombination events in the viral vector, the same promoter was never used twice in one plasmid. To determine possible position effects of the expression cassettes within the viral vector on AAT expression, a second set of three plasmids was cloned in which the *pac* cassette was positioned 5' of the *SERPINA1* cassette (constructs #162, #163, and #164). To circumvent the possible problem of transcriptional interference [336,337], two more constructs were cloned in which an EMCV IRES sequence was used to initiate cap-independent translation of the *pac* mRNA, thereby eliminating the need for a second

promoter. The detailed cloning strategy is described in 2.2.1. Figure 6 shows a schematic representation of the eight "2nd generation" gamma-retroviral transfer plasmids; more detailed plasmid maps are depicted in the supplementary material (6.4).
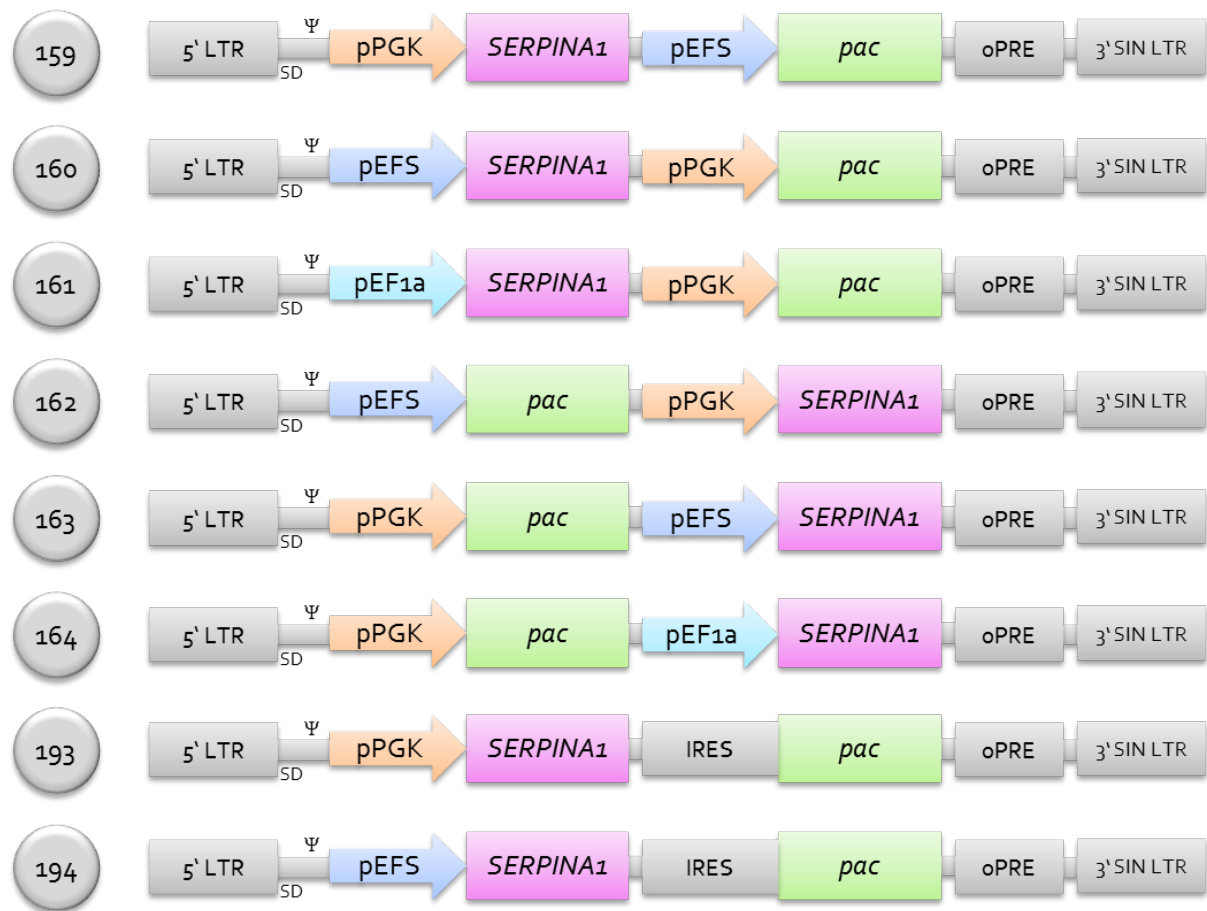
Figure 6: **Schematic representation of the eight "2nd generation" plasmids.** Three different promoters (pPGK, pEFS, and pEF1a) were used to drive the expression of *SERPINA1; pac* was expressed from either pPGK or pEFS, depending on which promoter was used for the expression of *SEPRINA1*. In constructs #159, #160, and #161, the *SERPINA1* expression cassette was positioned 5' of the *pac* cassette, in constructs #162, #163, and #164, the cassettes were swapped, so that *SERPINA1* was now 3' of *pac*. Two more constructs were cloned in which *SERPINA1* was either driven by pPGK (construct #193) or pEFS (construct #194), and *pac* was linked by an EMCV IRES sequence. An oPRE sequence was added 3' of the expression cassette(s) to increase expression and viral titers. Ψ: Packaging Signal; SD: Splice Donor.

3.2. Comparison of constructs and selection of lead candidate

3.2.1. Viral vectors are functional on HT1080 cells

In the next set of experiments, the general goal was to determine which of the constructs described above was most suitable for the transduction of human cells and the expression of transgenic AAT. Thus, as a first step, gamma-retroviral supernatants of all 2nd generation transfer plasmids cloned were produced by transient triple transfection of 293T cells as described in detail in 2.2.3. To be able

to transduce human MSCs with comparable MOIs in subsequent experiments, viral titers were first determined by transduction of HT1080 fibrosarcoma cells with a minimum of three different dilutions in duplicate per each supernatant. Transduction efficacies were analyzed by flow cytometry to detect transgenic intracellular human AAT protein, and viral titers were calculated as described in 2.2.4. All viral supernatants generated were functional on the HT1080 cells. As depicted in Figure 7A, the highest average titer of $[3 \times 10^5$ TU/mL] was achieved for viral supernatant #159 (pPGK_SERPINA1_pEFS_pac), followed by #160 (pEFS_SERPINA1_pPGK_pac), #163 (pPGK_pac_pEFS_SERPINA1), #194 (pEFS_SERPINA1_IRES_pac), and #193 (pPGK_SERPINA1_IRES_pac); supernatant #162 (pEFS_pac_pPGK_SERPINA1) yielded intermediate results, and titers of viral supernatants #161 and #164 (both constructs in which pEF1a was used to drive *SERPINA1* expression) were almost two log units lower as compared to the highest titer. Due to the size of the full-length EF1a promoter – these plasmids are approximately 1000 bases larger than the other constructs (Figure 7B) – we compared plasmid sizes with viral titers and found a negative correlation (Figure 7C, R^2 = 0.78, P = 0.035). This result suggests that higher genetic payload and resulting larger transfer plasmids can lead to decreased titers and is in line with findings published for retroviral vectors [338,339].

3.2.2. Viral vectors are functional on primary human MSCs

3.2.2.1. Constructs containing the EFS promoter to drive *SERPINA1* expression yield the highest transduction efficacy

In the next step, the viral supernatants titrated above were used for transduction of primary human MSCs at comparable MOIs to assess which construct would yield best transduction efficacy and AAT expression. Primary human MSCs were produced as described in detail in 2.2.5 and transduced at a constant MOI of 0.25 using viral supernatants #159–#194 by either direct seeding or centrifugation of viral supernatants onto PLL-coated plates. To assess transduction efficacies achieved with the various viral supernatants, cells were intracellularly stained for transgenic human AAT protein 48–72 hours post-transduction. The results are provided in Figure 8A. Normalized transduction efficacies were comparable for constructs #160, #163, #194 (the three vectors containing pEFS for *SERPINA1* expression), and #193 (pPGK_SERPINA1_IRES_pac). Results seen with #159 and #162 (constructs containing pPGK to drive *SERPINA1* expression) showed a decreased efficiency of approximately 30%, and transduction efficacies using supernatants #161 and #164 (constructs in which *SERPINA1* is driven by pEF1a) were only 30% (P < 0.01) and 10% (P < 0.001), respectively, of those achieved with the best supernatants. This was unexpected as the same amount of viral particles had been used for each transduction; however, the volumes of the supernatants that had to be used to achieve comparable MOIs were different by up to factor ~30 due to the enormous differences in viral titers. By comparing viral titers with the transduction efficacies achieved, a positive correlation was found

(Figure 8B, R^2 = 0.73, P = 0.0066), suggesting that the number of viral particles used for transduction determined transduction efficacies, but that there was a potential negative impact of large volumes of viral supernatant on transduction.
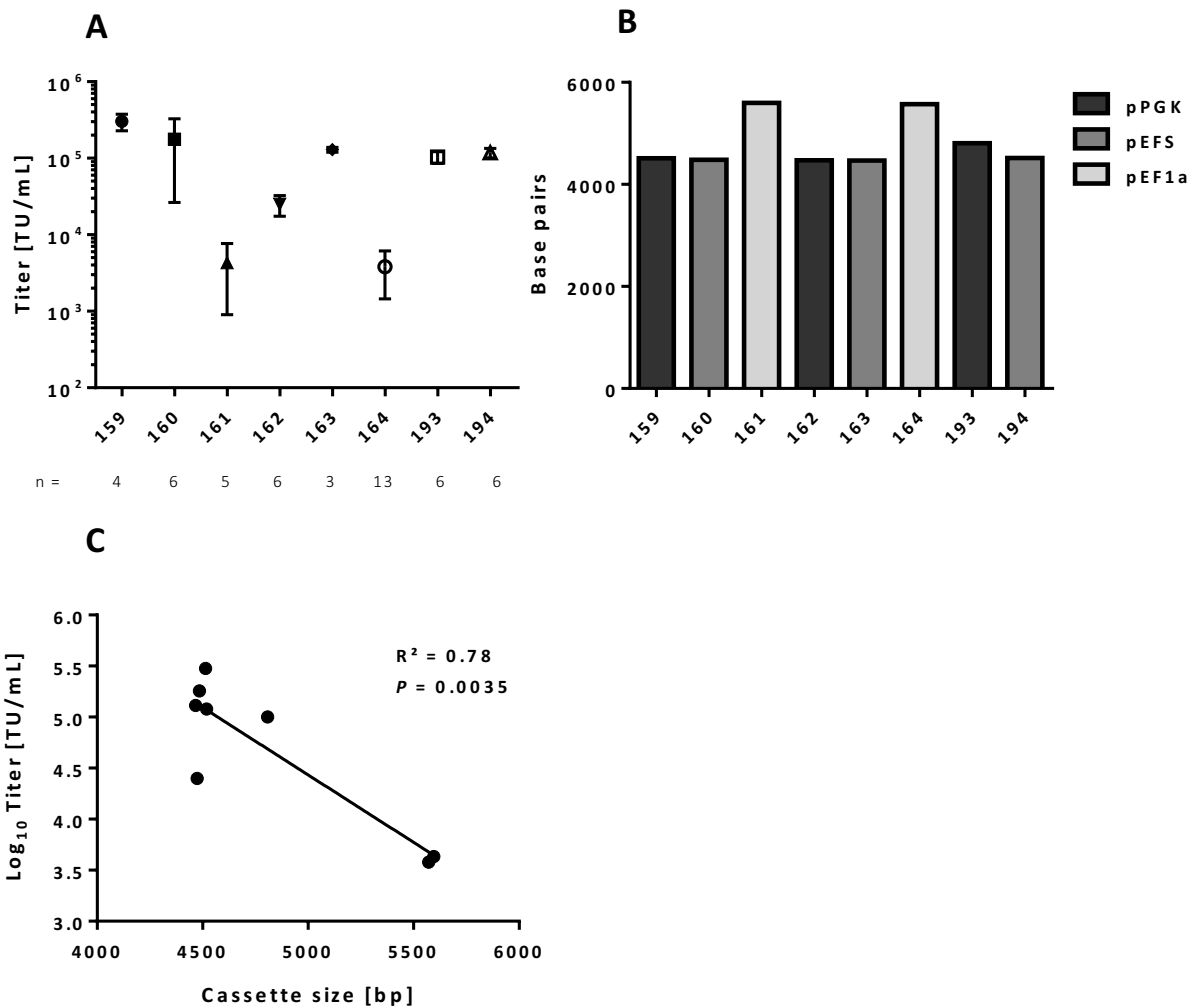
Figure 7: **Viral vectors are functional. A: Titers of viral supernatants #159-#194.** Constructs #159, #160, 163, #193, and #194 yielded comparable titers on HT1080 fibrosarcoma cells, while titers achieved with constructs #161 and 164 were almost two log units lower; titers of viral supernatant #162 were intermediate. Viral titers were determined by transduction of HT1080 cells and flow cytometry for intracellular AAT protein. Symbols represent average values from 4–13 independent transductions per viral vector ± standard deviation (SD). Small numbers below the graph indicate number of transductions performed for each supernatant. **B: Payload sizes of 2nd generation gamma-retroviral transfer constructs.** pEF1a plasmids are ~1kb larger than pPGK and pEFS vectors. Colors of bars represent the promoter driving *SERPINA1* (pPGK: dark gray; pEFS: medium gray; pEF1a: light gray). **C: Titers of viral supernatants and expression cassette sizes are inversely correlated.** Correlation analysis of expression cassette sizes and average viral titers revealed a negative correlation (R^2 = 0.78, P = 0.0035). Statistical correlation was determined by calculating the Pearson correlation coefficient. Gaussian distribution was confirmed using the D'Agostino & Pearson omnibus normality test.
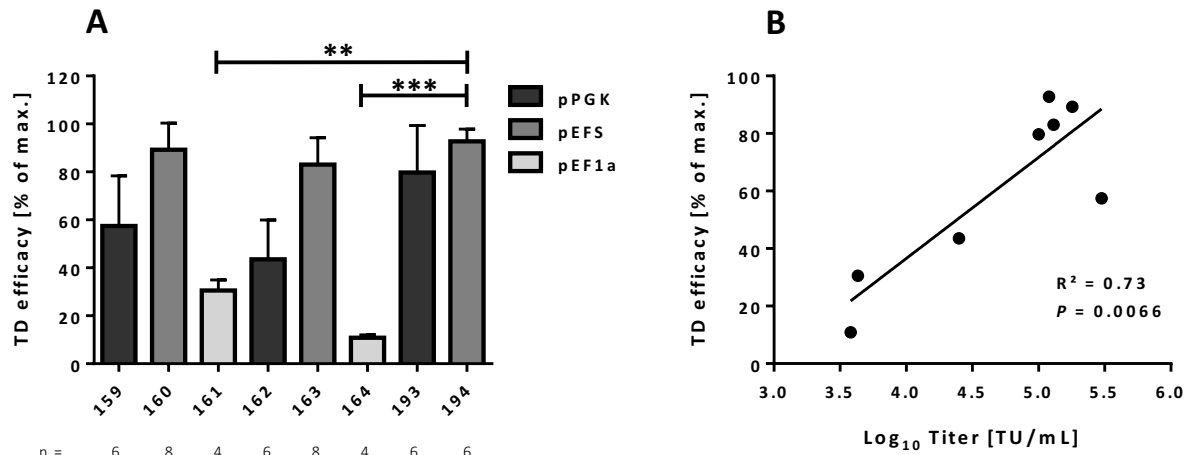
Figure 8: **Normalized transduction efficacies of primary human MSCs. A: Transduction efficacies are highest in MSCs transduced with viral supernatants #160, #163, #194, and #193.** Transduction of primary human MSCs was highest when supernatants #160, #163, #194 (constructs in which pEFS is driving *SERPINA1* expression), and #193 (pPGK_SERPINA1_IRES_pac) were used. Primary human MSCs derived from two healthy donors were transduced with viral supernatants #159–#194, and transduction efficacies were assessed by intracellular flow cytometry for AAT protein. Bars represent average values of 4–8 independent transduction experiments ± SD. Due to high variance in transduction results depending on the donor, values were normalized to the highest transduction achieved in each experiment (= 100%). Small numbers below the graph indicate the number of separate experiments performed for each viral construct. Statistical significance of differences between the construct yielding the highest value (#194) that was used as a control and all other constructs was calculated applying the Kruskal-Wallis test ($P < 0.0001$), followed by Dunn's multiple comparisons test (194 *vs.* 159: ns, 194 *vs.* 160: ns, 194 *vs.* 161: **, 194 *vs.* 162: *, 194 *vs.* 163: ns, 194 *vs.* 164: ***, 194 *vs.* 193: ns). * $P < 0.05$, ** $P < 0.01$, *** $P < 0.001$. **B: Transduction efficacies and viral titers are positively correlated.** Correlation analysis of expression cassette sizes and average viral titers revealed a strong correlation between these two variables (R^2 = 0.73, P = 0.0066). Statistical correlation was determined by calculating the Pearson correlation coefficient. Gaussian distribution was confirmed using the Kolmogorov-Smirnov test.

3.2.2.2. EF1a and EFS promoters yield higher AAT expression than pPGK

To analyze the strength of AAT expression yielded after transduction of human MSCs with the different constructs, expression of AAT in bulk MSC populations was assessed by flow cytometric analysis and mean fluorescence intensities (MFIs) of AAT-positive cells. All constructs in which *SERPINA1* was driven by either pEFS or pEF1a yielded comparable high MFIs, whereas AAT expression in cells transduced with constructs #159 and #162, in which *SERPINA1* is expressed from pPGK, was lower by about ~30% each ($P < 0.05$ and $P < 0.01$, respectively). Construct #193, in which *SERPINA1* was driven by pPGK, but using an IRES sequence instead of a second promoter, yielded AAT expression comparable to pEFS and pEF1a constructs (Figure 9).
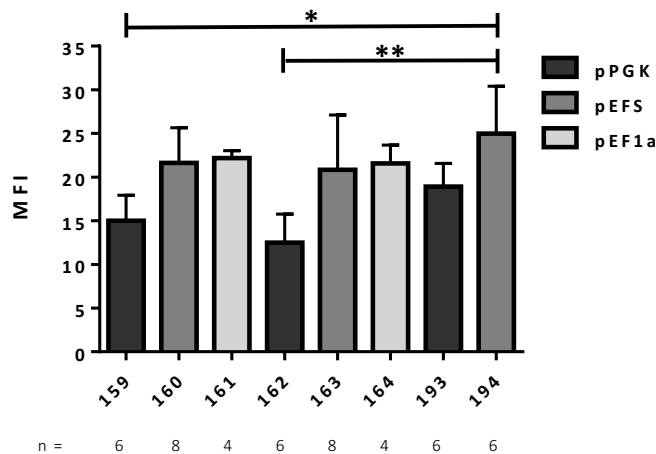
Figure 9: **AAT expression from pEF1a and pEFS is higher as compared to pPGK.** Transduction with viral supernatants generated from constructs in which *SEPRINA1* is driven by either pEF1a or pEFS resulted in higher AAT expression as compared to values achieved with pPGK. Primary human MSCs derived from two healthy donors were transduced with viral supernatants #159–#194, and MFIs were assessed by intracellular flow cytometry for AAT protein. Bars represent average values of 4–8 independent transduction experiments ± SD. Small numbers below the graph indicate the number of separate experiments performed for each viral construct. Statistical significance of differences between the construct yielding the highest MFI (#194) that was used as a control and all other constructs was calculated applying the Kruskal-Wallis test (P = 0.0009), followed by Dunn's multiple comparisons test (194 *vs.* 159: *, 194 *vs.* 160: ns, 194 *vs.* 161: ns, 194 *vs.* 162: **, 194 *vs.* 163: ns, 194 *vs.* 164: ns, 194 *vs.* 193: ns). * P < 0.05; ** P < 0.01.

3.2.3. Viral vectors allow for long-term modification of MSCs and sustained AAT expression after antibiotic selection and expansion

3.2.3.1. Constructs in which *SEPRINA1* and *pac* are linked via an IRES sequence yield highest VCNs after antibiotic selection and long-term culture of MSCs

After transduction efficacies and AAT expression were characterized in non-selected cells shortly after transduction, in a next set of experiments we wanted to analyze if transduction of primary human MSCs with the viral constructs led to stable genetic modification of the cells as well as long-lasting AAT expression after antibiotic selection and expansion of the cells. These processes are needed for the generation of a cell therapy product for clinical use. Thus, bulk populations of MSCs transduced with the eight different supernatants were subjected to antibiotic selection to yield pure populations of gene-modified cells. Figure 10 shows a representative example of intracellular flow cytometry stains of transduced cells before and after antibiotic selection.

After completion of the selection process, cells were expanded in Bio-M or Bio-1 for usually two weeks, when cell numbers sufficient to perform further experiments were reached. The DNA of selected cells was extracted, and VCNs were determined by qPCR and comparison with a reference cell clone containing a single viral integration as described in 2.2.15. MSCs transduced with supernatants #193, #194 (the two constructs containing an IRES sequence), and #160 (pEFS_SERPINA1_pPGK_pac) had the highest average values of ~4–5 viral integrations per cell,

followed by cells modified with supernatants #159, #162 (the two constructs in which *SERPINA1* is driven by pPGK), and #163 (pPGK_pac_pEFS_SEPRINA1) which had mean VCNs of 2.3, 2.8, and 3.2 (Figure 11). Average VCNs achieved with supernatant #161 (pEF1a_SERPINA1_pPGK_pac) were ~10-fold lower as compared to constructs #193 and #194 (*P* < 0.05), and only in one experiment out of four performed, was it possible to harvest cells for VCN measurement after antibiotic selection of cells transduced with supernatant #164 (pPGK_pac_pEFa1_SERPINA1); in the three other experiments no cells survived the antibiotic selection. Taken together, the VCN results generated after antibiotic selection and long-term culture of selected cells support the ones achieved by intracellular flow cytometry before selection and expansion, confirming that constructs #160, #163, #194 (all constructs in which pEFS is driving *SERPINA1* expression), and #194 (pPGK_SERPINA1_IRES_pac) resulted in the highest degree of genetic modification of the primary human MSCs, and thus, were further assessed to select the favored expression cassette.
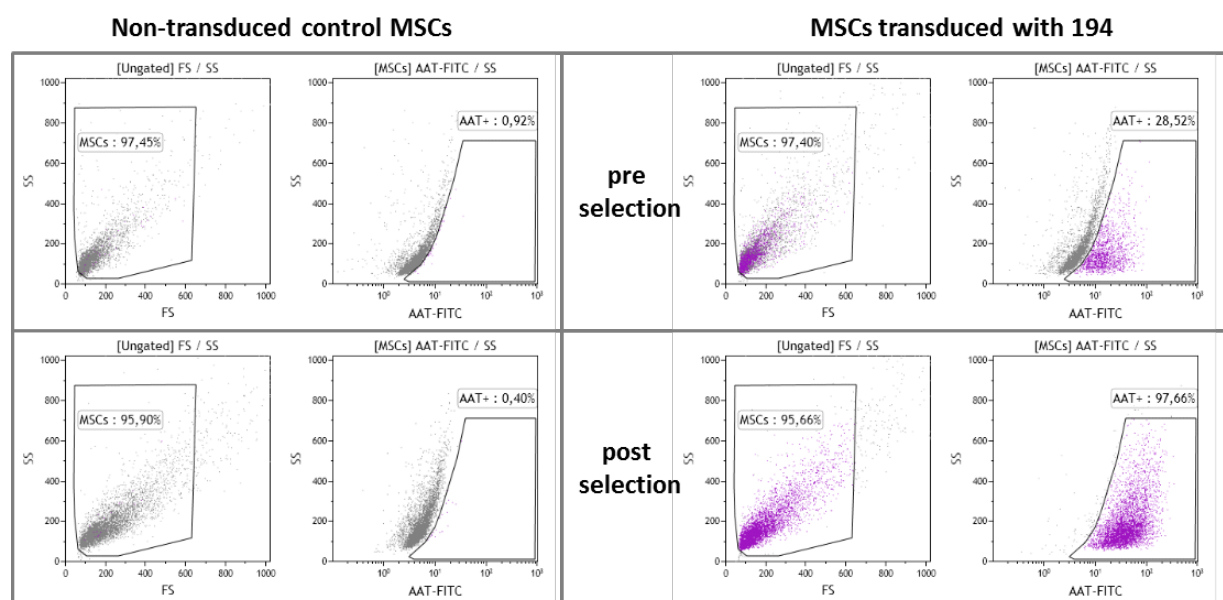
Figure 10: **Representative flow cytometry results for intracellular AAT stains achieved before and after antibiotic selection.** Antibiotic selection of transduced cells with puromycin yields >95% pure populations of MSCs expressing AAT. Primary human MSCs were transduced with viral vector #194, and intracellular staining for AAT and subsequent flow cytometric measurement were performed before and after a 5-day selection with [3µg/mL] puromycin. Representative flow cytometry plots show ~30% AAT+ cells 72 hours after transduction and a highly pure (>95% AAT+) population of AAT-expressing MSCs after selection. Non-transduced MSCs from the same donor were stained with the same antibody and used as negative controls for gating.
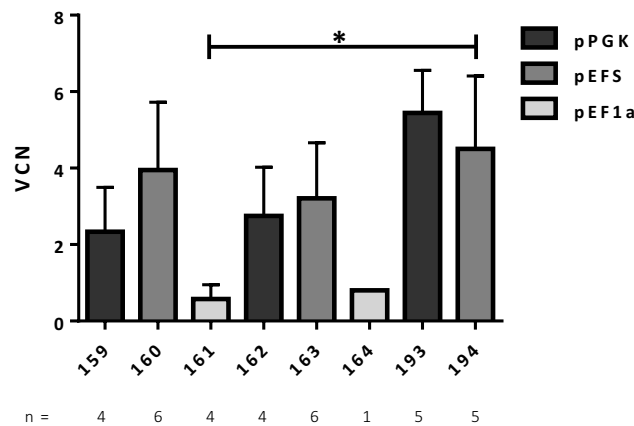
Figure 11: **Highest VCNs achieved in cells modified with supernatants #193 and #194.** Analysis of VCNs after antibiotic selection and long-term culture of the cells yielded highest values for MSCs transduced with viral supernatants #193 (pPGK_SERPINA1_IRES_pac) and #194 (pEFS_SERPINA1_IRES_pac), followed by #160, and #163 (constructs in which pEFS is driving *SERPINA1* expression, and a second promoter is used to drive *pac* expression). Primary human MSCs derived from two healthy donors were transduced with viral supernatants #159–#194, selected with puromycin, expanded, and harvested for DNA preparation. VCNs were determined by qPCR and comparison to a reference cell clone with a single viral integration. Bars represent average values of 1–6 independent experiments ± SD. Small numbers below the graph indicate the number of separate experiments performed for each viral construct. Statistical significance of differences between control construct #194 and all other constructs was calculated applying the Kruskal-Wallis test ($P = 0.0041$), followed by Dunn's multiple comparisons test (194 *vs.* 159: ns, 194 *vs.* 160: ns, 194 *vs.* 161: *, 194 *vs.* 162: ns, 194 *vs.* 163: ns, 194 *vs.* 164: ns, 194 *vs.* 193: ns). * $P < 0.05$.

3.2.3.2.   EF1a and EFS promoters lead to higher AAT expression than pPGK after antibiotic selection and long-term expansion of MSCs

In the next step the stability of AAT expression in transduced MSCs was determined after antibiotic selection and cell expansion. The AAT protein content in cell culture supernatants of selected and expanded MSCs was measured by ELISA and compared to flow cytometry expression data determined by MFI of intracellularly stained AAT in cells prior to antibiotic selection. MSCs derived from two donors were transduced with the eight gamma-retroviral supernatants, subjected to antibiotic selection, expanded, and seeded for harvest of supernatants. After 48 hours cell culture supernatants were collected, and the concentration of secreted AAT protein determined by ELISA. Consistent with MFI data measured before antibiotic selection, AAT expression after selection and long-term culture was highest in cell culture supernatants derived from cells transduced with viral vectors using either the EFS or the full-length EF1a promoter to drive *SERPINA1* expression, with an average AAT yield of ~500ng/1x10^5 cells/viral integration in 48 hours (Figure 12). AAT content in supernatants after transduction of MSCs with vectors #159 and #162 (constructs in which pPGK is driving *SERPINA1* expression) was significantly lower (~95ng/1x10^5 cells/VCN/48h; $P < 0.05$); viral supernatant #193 (pPGK_SERPINA1_IRES_pac) yielded intermediate results. In only one experiment out of four was it possible to determine AAT concentration in cell culture supernatants after

transduction with vector #164 (pPGK_pac_pEF1a_SERPINA1) as there was complete cell death of the

MSCs in the other three experiments.
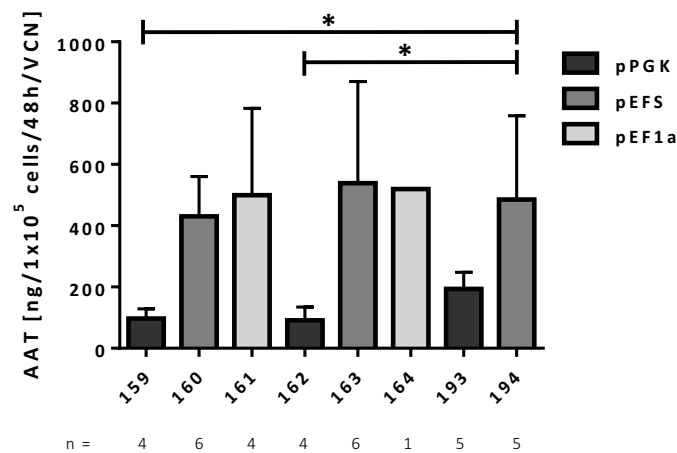
Figure 12: **AAT expression is markedly higher from pEF1a and pEFS as compared to pPGK as determined by ELISA.** Transduction of MSCs with viral supernatants generated from constructs in which *SERPINA1* is driven by either pEF1a or pEFS yielded higher amounts of AAT secreted into the cell culture supernatant as compared to constructs in which AAT is driven by pPGK after antibiotic selection and long-term expansion of selected cells. Primary human MSCs derived from two healthy donors were transduced with viral supernatants #159–#194, selected with puromycin, expanded and seeded at a concentration of $1x10^4$ cells and 250µL medium/cm². Cell culture supernatants were collected after 48 hours, and AAT protein content was assessed by ELISA. Bars represent average values of 1–6 independent transduction experiments ± SD, normalized to $1x10^5$ cells and divided by VCN. Small numbers below the graph indicate the number of separate experiments performed for each viral construct. Statistical significance of differences between control construct #194 and all other constructs was calculated applying the Kruskal-Wallis test (P = 0.0006), followed by Dunn's multiple comparisons test (194 *vs.* 159: *, 194 *vs.* 160: ns, 194 *vs.* 161: ns, 194 *vs.* 162: *, 194 *vs.* 163: ns, 194 *vs.* 164: ns, 194 *vs.* 193: ns). * P < 0.05.

Because AAT expression was lowest when transducing MSCs with vectors #159 and #162 (constructs in which pPGK is used to drive *SERPINA1* expression and which contain a second promoter to drive *pac* expression), and use of supernatants #161 and #164 (constructs in which *SERPINA1* is driven by pEF1a) led to low transduction efficacies and markedly decreased cell numbers after antibiotic selection (data not shown), these four constructs were excluded from subsequent experiments. Constructs #160, #163, and #194 (all three constructs in which *SERPINA1* is driven by pEFS) yielded comparable results regarding transduction efficacy and expression and were subjected to further evaluation. Construct #193 (pPGK_SERPINA1_IRES_pac) was also included as this vector had led to good results in previous experiments. It was the only remaining vector in which *SERPINA1* was driven by a promoter that is not EFS.

3.2.4.   Constructs containing an IRES sequence yield higher MSC numbers after antibiotic selection as compared to constructs containing two promoters

As described above, transduction efficacies and AAT expression were comparable among the remaining vectors #160, #163, #193, and #194 before and after antibiotic selection and long-term expansion of the selected cells. However, it had been noted that cell numbers after antibiotic selection varied markedly between the constructs even when transduction efficacies were similar. When generating an optimized cell product for clinical use, it is crucial to achieve a maximum cell yield. Thus, experiments were performed to assess MSC numbers achieved after transduction with the different viral supernatants at a constant MOI and subsequent selection with puromycin. MSCs were transduced with the four remaining gamma-retroviral supernatants #160, #163, #193, and #194 at MOI 0.25, subjected to antibiotic selection, and expanded until confluency was reached and cell numbers were determined by manual counting using a Neubauer hemocytometer in duplicate. Cell numbers after transduction with viral vectors containing an IRES sequence to link *SERPINA1* and *pac* genes (#193 and #194) were markedly higher as compared to those achieved after transduction with constructs in which *pac* was expressed from a second promoter (#160 and #163; Figure 13). The most striking difference was noticeable when comparing constructs #160 (pEFS_SERPINA1_pPGK_pac) and #194 (pEFS_SERPINA1_IRES_pac): Cell numbers were decreased by ~70% after transduction with viral vector #160 ($P < 0.01$).

Taken together, these results demonstrated that the retroviral expression plasmid #194 was best when compared to the other seven constructs tested with regards to transduction efficacy and AAT expression as well as cell yield. Thus, construct #194 was selected as the lead candidate for transgenic AAT expression in primary human MSCs and subjected to further testing.
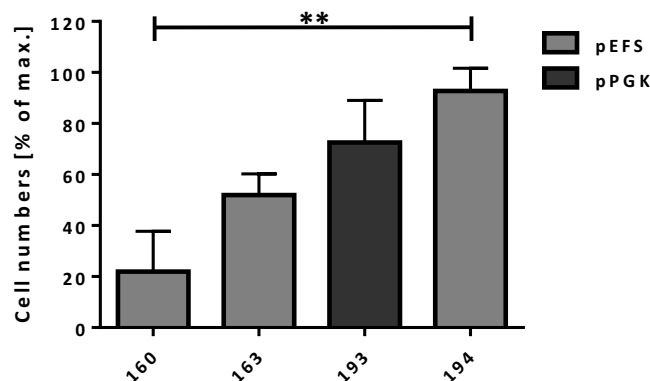
Figure 13: **Antibiotic selection of MSCs after transduction with supernatants #160, #163, #193, and #194 at comparable transduction efficacies results in different cell gain.** Transduction of MSCs with construct #194 results in higher cell yields after antibiotic selection when compared to cells transduced with #160, #163, and #193, despite similar transduction efficacies before selection. Primary human MSCs were transduced with viral supernatants #160, #163, #193, and #194, selected

with puromycin at a concentration of [3µg/mL], and expanded until confluency, when cells were counted. Bars represent average values of 4 independent transduction experiments ± SD. Due to different sizes of culture vessels used for expansion in different experiments, values were normalized to the highest cell number yielded in each experiment (= 100%). Statistical significance of differences between cell numbers recorded for control construct #194 and the three other constructs was calculated applying the Kruskal-Wallis test ($P < 0.0001$), followed by Dunn's multiple comparisons test (194 *vs.* 160: **, 194 *vs.* 163: ns, 194 *vs.* 193: ns). ** $P < 0.01$.

3.3. Comparison of best expression cassette in gamma-retroviral and lentiviral backbone

In the first stage of this work, the best performing expression cassette with regards to transduction, AAT expression, and cell yield was selected from the eight candidates. In the next step, we assessed if a different viral backbone could potentially further increase transduction efficacy and AAT expression. To this end, we chose a lentiviral system to compare with the gamma-retroviruses. Lentiviruses have the advantage of being able to transduce non-dividing cells, thus potentially enhancing transduction efficacies. Moreover, lentiviral vectors are used for clinical applications and – like gamma-retroviruses – also permanently integrate their genetic information into the genome of the host cell, thus allowing a stable genetic modification of the target cell and its progeny.

3.3.1. Titers achieved using the lentiviral backbone are four-fold higher

Accordingly, the expression cassette pEFS_SERPINA1_IRES_pac_oPRE was transferred from the gamma-retroviral backbone (pSERS11) to a lentiviral pCCL backbone by In-Fusion cloning as described in 2.2.1.2. Briefly, an expression cassette present in pCCL was removed by restriction enzyme digestion, homology arms were created 5' and 3' of the *SERPINA1-pac*-cassette by PCR, and the cassette was transferred to pCCL by recombination. A comparison of the schematic of both plasmids is depicted in Figure 14.
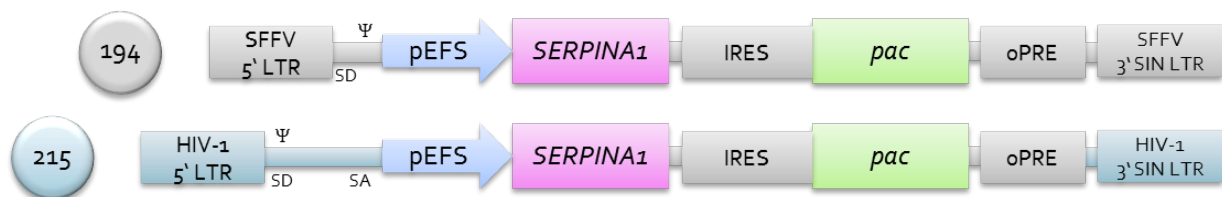
Figure 14: **Schematic representation of gamma-retroviral expression vector #194 and lentiviral expression vector #215.**

Two batches of viral supernatant #215 were produced by transient triple transfection of 293T cells and titers were determined on HT1080 fibrosarcoma cells as described in detail in 2.2.3 and 2.2.4. Two batches of viral supernatant #194 were generated for subsequent experiments. Consistent with published data [340], the average lentiviral titer was higher than the retroviral, in our case ~four-fold (#194: [2.9×10^5 TU/mL]; #215: [1.2×10^6 TU/mL]; Figure 15).
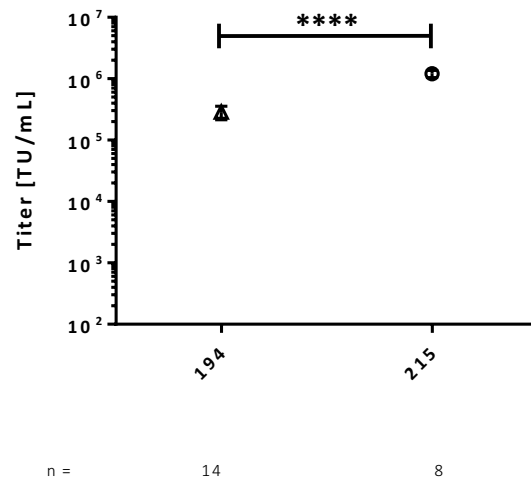
Figure 15: **For transfer plasmids containing the same expression cassette, lentiviral titers are higher than retroviral.** Viral titers determined on HT1080 cells were ~4-fold higher for the lentiviral vector as compared to the gamma-retroviral vector. Expression cassette pEFS_SERPINA1_IRES_pac_oPRE was cloned into the lentiviral pCCL backbone, 2 batches of supernatants of transfer plasmids #194 and #215 each were generated using the respective helper plasmids, and titers were determined on HT1080 cells. Symbols represent average values from 8–14 independent transductions per viral vector ± SD. Small numbers below the graph indicate numbers of independent transductions performed for each supernatant. Statistical significance was calculated using the unpaired t test with Welch's correction ($P < 0.0001$). **** $P < 0.0001$. Gaussian distribution of the data was confirmed by D'Agostino & Pearson omnibus normality test.

3.3.2. Transduction behavior differs between gamma-retro- and lentiviral vector

3.3.2.1. Transduction efficacy

To analyze potential differences in transduction efficacy between the gamma-retroviral and lentiviral vector and to assess a dose response, primary human MSCs derived from three donors were transduced with both viral supernatants at four MOIs, ranging from 0.25 to 5.0. Cells were analyzed by intracellular flow cytometry for AAT protein 72 hours after transduction. Due to high inter-donor variability in transduction, results were normalized to the highest transduction achieved in the respective experiment (= 100%). In all experiments performed, transduction efficacies at lower MOIs (0.25 and 0.75) were higher when the gamma-retroviral supernatant was used. At MOI 0.25, the average normalized transduction efficacy was ~50% of the maximal transduction achieved in each experiment using supernatant #194 and ~20% using vector #215 ($P < 0.05$; Figure 16). However, when MSCs were gene-modified at the ten-fold higher MOI of 2.5, average transduction efficacies achieved with the gamma-retroviral supernatant increased only modestly (from ~50% at MOI 0.25 to ~53% at MOI 2.5), whereas average normalized transduction was improved more than four-fold when cells were transduced with the lentiviral vector (from ~20% at MOI 0.25 to ~90% at MOI 2.5). Transduction of human MSCs at MOI 2.5 was thus almost twice as high with the lentiviral supernatant as compared to the gamma-retroviral vector ($P < 0.01$; Figure 16). Using lentiviral

supernatant #215 at the highest tested MOI of 5.0 resulted in absolute transduction efficacies as high as ~80% for two out of three donors analyzed (data not shown), while retroviral transduction did not increase to more than ¾ of what was reached with the lentiviral supernatant. When linear regression analysis was performed to assess if the two dose response curves generated by fitting the means were different, there was a significant distinction regarding the slope (P = 0.0006), indicating that transduction behavior differs markedly between gamma-retro- and lentiviral vectors.

Figure 16: **Dose response curve fits of average transduction values of human MSCs with gamma-retro- and lentiviral vectors at MOIs ranging from 0.25–5.0 are different.** At the lowest MOI (0.25), transduction with the gamma-retroviral supernatant was more than twice as high as the one achieved using the lentiviral vector (P < 0.05); however, using a 10-fold higher MOI, transduction efficacy with lentiviral supernatant #215 was increased more than 4-fold, resulting in transduction efficacies almost twice as high as the ones achieved with the gamma-retroviral vector #194 (P < 0.01). When comparing the 2 dose response curves, there was a statistically significant difference in the slopes (P = 0.0006). Symbols represent the average of 5 independent transduction experiments for MOIs 0.25, 0.75, and 2.5, and 3 for MOI 5.0 ± SD. Due to high variance in transduction results depending on the donor, values were normalized to the highest transduction achieved in each experiment (= 100%). Statistical significance of differences between transductions with both supernatants at the same MOI was calculated using Sidak's multiple comparisons test (194 *vs.* 215: MOI 0.25: *, MOI 0.75: ns, MOI 2.5: **, MOI 5.0: ns). * P < 0.05; ** P < 0.01.

3.3.2.2. Vector Copy Number

To assess the influence of the viral vector on transduced MSCs having undergone more *ex vivo* manipulation procedures and longer culture periods, the cells generated in the dose response experiment described above were subjected to antibiotic selection and long-term expansion; DNA was extracted, and VCNs were determined. A graphic representation of the results is shown in Figure 17. The data were congruent with the flow cytometry findings: Average VCNs were higher after transduction with the gamma-retroviral vector at lower MOIs (MOI 0.25: #194: 2.6, #215: 1.6; MOI 0.75: #194: 2.9, #215: 2.2); then, a trend reversal was observed. At the highest MOI of 5.0, transduction using the lentiviral supernatant yielded average VCNs almost twice as high as achieved with the retroviral vector (MOI 5.0: #194: 3.2, #215: 6.1; P < 0.01) while VCNs measured after transduction with the gamma-retroviral vector did not increase at all with increasing MOIs

(R² = 0.07). Linear regression analysis assessing if the two dose response curves generated by fitting the means were different confirmed that there was a significant distinction in the slope (*P* = 0.0003). Thus, VCN results support the transduction efficacy data described above, indicating that the gamma-retroviral and lentiviral AAT constructs display a significantly different transduction behavior in primary human MSCs: While retroviral transduction seems to be at the maximum already at MOI 0.25 and no further increase in VCN is achievable, lentiviral transduction follows a clear dose response curve (R² = 0.72).
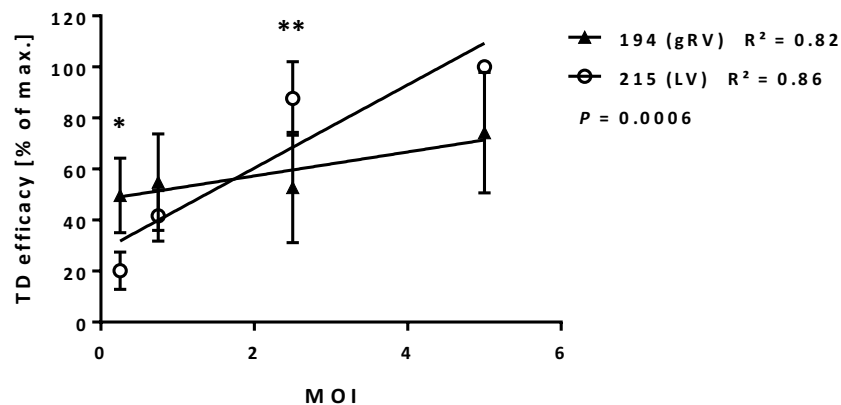

Figure 17: **Dose response curve fits of average VCNs after transduction of human MSCs with gamma-retro- and lentiviral vectors at MOIs ranging from 0.25–5.0 are different.** At the lowest MOI (0.25), transduction with the gamma-retroviral supernatant was ~1 vector copy higher than the one achieved using the lentiviral vector; however, using a 20-fold higher MOI of 5.0, transduction efficacy with #215 was increased ~4-fold as compared to MOI 0.25, resulting in VCNs almost twice as high as the ones achieved with #194 (*P* < 0.01). When comparing the two dose response curve fits, there was a statistically significant difference in the slopes (*P* = 0.0003). Symbols represent the average of 5 independent transduction experiments for MOIs 0.25, 0.75, and 2.5, and 3 for MOI 5.0 ± SD. Statistical significance of differences between transductions with both supernatants at the same MOI was calculated using Sidak's multiple comparisons test (194 *vs.* 215: MOI 0.25: ns, MOI 0.75: ns, MOI 2.5: ns, MOI 5.0: **). ** *P* < 0.01.

3.3.2.3. Expression of transgenic AAT

We next wanted to assess whether levels of AAT expression changed when using the same expression cassette in different viral backbones. AAT expression for both vectors was determined by analysis of the MFIs yielded in the dose response experiments described above. The results mirrored the results seen when comparing transduction efficacies: At the lower MOIs tested (0.25 and 0.75), AAT expression from the pEFS_SERPINA1_IRES_pac cassette in the gamma-retroviral backbone was higher (at MOI 0.25 ~85% of the maximum MFI yielded in each experiment as compared to ~55% for lentiviral vector #215, *P* < 0.001; 87% *vs.* 63% at MOI 0.75, *P* < 0.01), whereas at the highest MOI tested (5.0), AAT expression achieved using the lentiviral supernatant was highest in all experiments (100%), with even a minor decrease in MFI detected for vector #194 (82%, Figure 18). Again, when comparing the linear regression curves produced by fitting mean MFIs, there was a highly significant

difference between the vectors (P < 0.0001): For gamma-retroviral vector #194, there was no correlation between MOI and MFI achieved (R^2 = 0.51), indicating that AAT expression was the same no matter how many viral particles were used for transduction at MOIs ranging from 0.25–5.0, while MFIs after transduction with the lentiviral supernatant #215 followed a precise dose response (R^2 = 1.00).
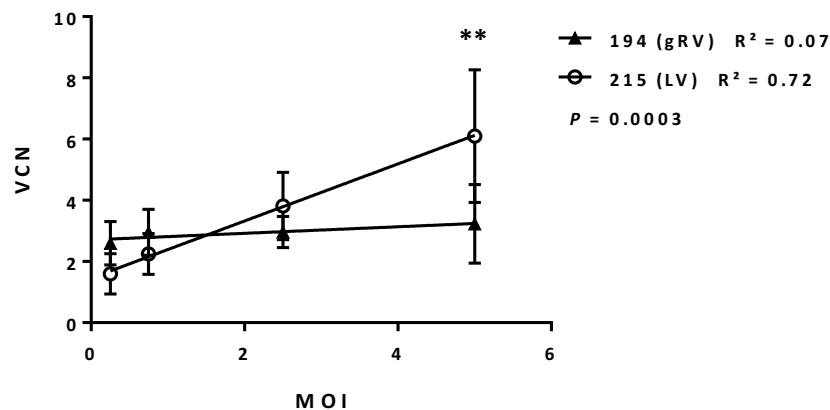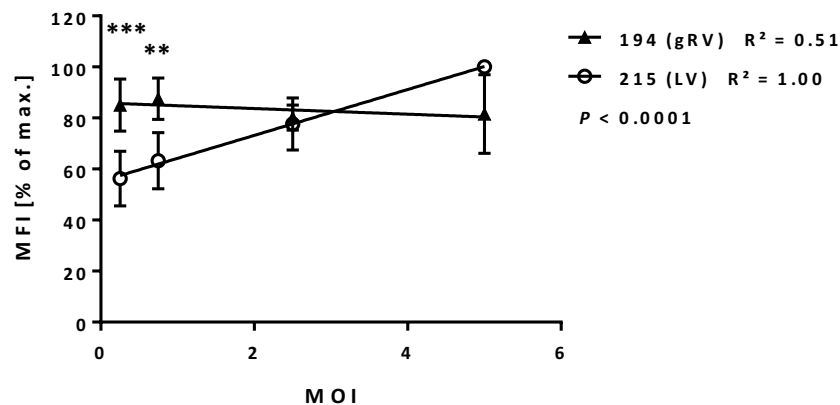

Figure 18: **Dose response curve fits of average AAT expression from human MSCs transduced with gamma-retro- and lentiviral vectors at MOIs ranging from 0.25–5.0 as measured by MFI are different.** At the lower MOIs analyzed (0.25 and 0.75), MFIs achieved with the gamma-retroviral supernatant were ~25% higher than the ones measured after transduction with the lentiviral vector (P < 0.01 and P < 0.001, respectively); however, MFIs were highest for MSCs transduced with lentiviral vector #215 at MOI 5.0 in all 3 experiments. When comparing the 2 linear regression curves, there was a statistically significant difference in the slopes (P < 0.0001). Symbols represent the average of 5 independent transduction experiments for MOIs 0.25, 0.75, and 2.5, and 3 for MOI 5.0 ± SD. Due to different flow cytometer settings used for acquiring the data in different experiments, values were normalized to the highest MFI measured in each experiment (= 100%). Statistical significance of differences between MFIs generated with both supernatants at the same MOI was calculated using Sidak's multiple comparisons test (194 *vs.* 215: MOI 0.25: ***, MOI 0.75: **, MOI 2.5: ns, MOI 5.0: ns). ** P < 0.01; *** P < 0.001.

In the next step, the expression data generated by flow cytometry was confirmed by measurement of transgenic AAT secreted from pure populations of transduced, selected MSCs after long-term expansion. As detailed in 2.2.16, selected cells were seeded at defined numbers, supernatants were collected after 48 hours, and AAT content was determined by ELISA. Figure 19 depicts a graphical representation of the results. AAT expression from selected MSCs measured by ELISA correlated well with MFI data. At lower MOIs, AAT expression from cells transduced with the gamma-retroviral vector was higher by the factor ~1.8 for MOI 0.25 and ~1.5 for MOI 0.75 when compared to the results achieved with the lentiviral supernatant. However, AAT expression seemed to be close to the maximum already at those MOIs for retrovirally transduced cells, and there was only a very modest increase in average AAT secretion observed with rising MOIs (from ~2200ng AAT/1×10^5 cells/48h at MOI 0.25 to ~2800ng AAT/1×10^5 cells/48h at MOI 5.0). In contrast, AAT yield increased more than

3.5-fold from ~1250ng AAT/1x10^5 cells/48h at MOI 0.25 to ~4500ng AAT/1x10^5 cells/48h at MOI 5.0 in supernatants harvested from lentivirally modified MSCs. However, none of the differences of AAT content at the same MOI for both vectors reached statistical significance, probably due to high inter-donor variability. However, when comparing the linear regression fits of the average AAT yields, there again was a significant difference between both regression curves, confirming the results described above in that there is a profound difference in gamma-retroviral and lentiviral transduction patterns (P = 0.0494).
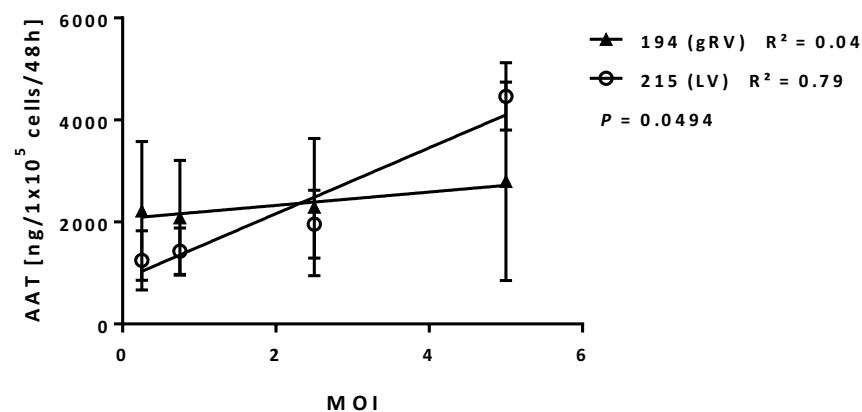
Figure 19: **Dose response curve fits of AAT yield [ng/1x10^5 cells/48h] from human MSCs transduced with gamma-retro- and lentiviral vectors at MOIs ranging from 0.25–5.0 as determined by ELISA are different.** At the lower MOIs analyzed (0.25 and 0.75), AAT contents achieved with the gamma-retroviral supernatant were higher than the ones measured after transduction with the lentiviral vector (by the factor of ~1.8 at MOI 0.25 and ~1.5 at MOI .075, respectively); however, AAT yield was highest for MSCs transduced with the lentiviral supernatant at MOI 5.0 in all experiments. When comparing the 2 linear regression curves, there was a statistically significant difference in the slopes (P = 0.0494). Symbols represent the average of 3 independent transduction experiments for MOIs 0.25, 0.75, and 2.5, and 2 for MOI 5.0 ± SD. Due to the accidental use of medium containing human plasma and thus AAT for the production of cell culture supernatants in one experiment, AAT expression data could not be generated for one of the donors tested in all previous experiments. Statistical significance of differences between AAT concentrations generated with both supernatants at the same MOI was calculated using Sidak's multiple comparisons test (194 *vs.* 215: MOI 0.25: ns, MOI 0.75: ns, MOI 2.5: ns, MOI 5.0: ns).

A further set of experiments sought to determine if AAT expression per viral integration differed depending on which vector backbone was used. Figure 20 shows a graphical representation of AAT expression data normalized to VCNs. Average AAT expression per vector copy in samples collected after gamma-retroviral transduction appeared slightly higher than that measured for the lentiviral vector (gamma-retroviral vector: [829ng AAT/1x10^5 cells/48h/VCN]; lentiviral vector: [754ng AAT/1x10^5 cells/48h/VCN]); however, the results did not reach statistical significance (P = 0.4856), indicating that once the transgene cassette is integrated into the host genome, gene expression is fairly independent of the viral backbone used. This finding is consistent with published data [329].
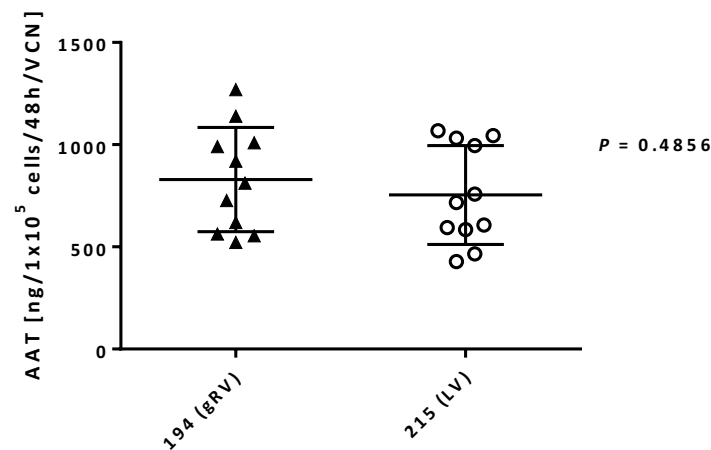
Figure 20: **AAT yield [ng/1x10^5 cells/48h] from human MSCs transduced with gamma-retro- and lentiviral vectors normalized to VCN is similar.** AAT content in supernatants derived from gamma-retrovirally and lentivirally transduced MSCs was determined by ELISA (Figure 19) and normalized to VCN (Figure 17). There was no statistically significant difference between AAT yields/VCN from both vectors. Symbols represent independent transduction experiments, and the horizontal lines denote mean. Statistical significance was calculated by unpaired two-tailed t test with Welch's correction (P = 0.4856). Gaussian distribution of the data was confirmed by D'Agostino & Pearson omnibus normality test.

3.3.2.4. Summary

These results demonstrate that transduction with, and AAT expression from, the gamma-retroviral vector #194 at varying MOIs follows a markedly different pattern as compared to the lentiviral vector #215 carrying the same expression cassette. Transduction with the latter shows a steep dose response curve with low transduction efficacies and VCNs at low MOIs and extremely high absolute transduction values of close to 80% and VCNs of up to eight using high MOIs. The same trend is true for AAT expression. In contrast, the dose response curve generated by transduction with the gamma-retroviral vector is flatter, indicating a less MOI-dependent mechanism of transduction: Transduction efficacies and VCNs were already considerably high even at low MOIs, reaching an average normalized value of ~50% of the maximum transduction possible and an average VCN of 2.6 at MOI 0.25; however, these values did not appreciably increase even when 20-fold more viral particles were used for genetic modification, suggesting that retroviral transduction was close to the maximum possible already at low MOIs. This pattern was reflected by the AAT expression data generated from gamma-retrovirally transduced MSCs as determined by MFI and AAT protein determination by ELISA. When analyzing AAT expression normalized to viral integrations, though, there was no difference between the vectors, indicating that the variations observed are solely resulting from differing transduction characteristics.

3.4. Confirmation of functionality of AAT expressed from MSCs

3.4.1. Transgenic AAT secreted from MSCs is functional

To assess if AAT secreted from transduced MSCs was functional with regards to its actions as a serine protease inhibitor, a neutrophil elastase inhibitor screening assay was performed as detailed in 2.2.17. Briefly, supernatants of gamma-retrovirally and lentivirally transduced MSCs were collected and incubated with neutrophil elastase before the addition of a fluorescent elastase substrate. In case of inhibition of neutrophil elastase by the supernatant, hydrolyzation of the substrate was reduced, resulting in a decreased RFU output. To compare transgenic AAT expressed from transduced MSCs to physiological, non-transgenic AAT, natural full length AAT from human serum was tested in the assay as a commensurable positive control; DMEM and supernatant from non-transduced MSCs served as negative controls.

During the establishment of the assay it was determined that for the test to yield reliable results, it was critical to generate cell culture supernatants free of serum as the neutrophil elastase included in the kit is inhibited by the bovine AAT present in FBS. Thus, the MSCs were subjected to five washes with PBS before serum-free DMEM was added. During the 16-24-hour incubation in serum-free DMEM many of the cells died, and AAT expression was ~four-fold lower as compared to the AAT protein content usually generated from the same number of plated cells in medium containing serum (data not shown). Hence, the supernatants were concentrated to a concentration of [≥2000ng AAT/mL] as measured by ELISA.

Supernatants collected from three different batches of MSCs transduced with viral vector #194 and #215, respectively, were analyzed using the neutrophil elastase inhibitor screening assay and compared to natural AAT from human plasma at concentrations ranging from [250–2000ng/mL]. In all experiments, AAT secreted from MSCs potently inhibited neutrophil elastase at values comparable to [2000ng/mL] natural AAT (Figure 21).
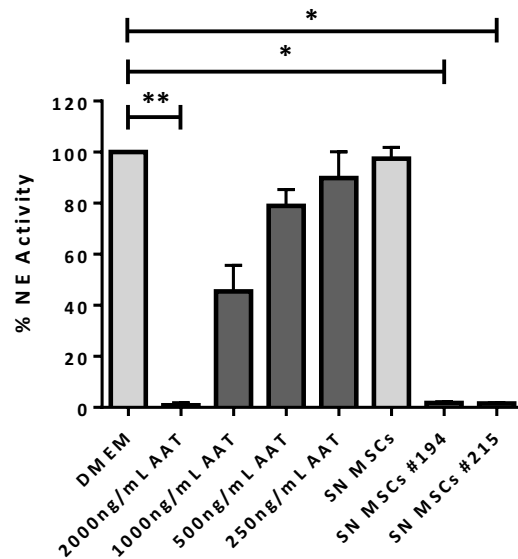
Figure 21: **Transgenic AAT secreted from primary human MSCs is functional.** Concentrated supernatants collected from MSCs transduced with vector #194 and #215, respectively, potently inhibit neutrophil elastase comparable to [2000ng/mL] natural human AAT. Supernatants harvested from transduced and native MSCs derived from two donors were analyzed using the neutrophil elastase inhibitor screening kit and compared to natural human full length AAT protein in concentrations from [250–2000ng/mL]. DMEM was used as a negative control yielding 100% neutrophil elastase activity. Bars represent average values from 3 independent transductions and 3–7 independent supernatant collections per viral vector ± SD. Statistical significance of differences between negative control DMEM and all other samples tested was calculated applying the Kruskal-Wallis test (P = 0.0002), followed by Dunn's multiple comparisons test (DMEM *vs.* [2000ng/mL AAT]: **, DMEM *vs.* [1000ng/mL AAT]: ns, DMEM *vs.* [500ng/mL AAT]: ns, DMEM *vs.* [250ng/mL AAT]: ns, DMEM *vs.* SN MSCs: ns, DMEM *vs.* SN MSCs #194: *, DMEM *vs.* SN MSCs #215: *). * $P < 0.05$; ** $P < 0.01$.

3.4.2. Transgenic AAT secreted from MSCs is as potent as natural AAT isolated from human plasma

After confirming that AAT expressed from MSCs was functional, we then analyzed whether there are differences in the potency of MSC-AAT as compared to natural AAT from human plasma. To this end, five dilutions of the MSC supernatant samples tested in 3.4.1 were generated and analyzed using the neutrophil elastase inhibitor screening assay. AAT contents in these samples as well as in natural human AAT dilution samples were determined by ELISA, and neutrophil elastase activity was plotted against AAT concentration. Figure 22 shows a graphic representation of the results. There was no difference seen in the log(inhibitor) *vs.* response curve fit between AAT derived from human plasma and AAT secreted from MSCs (P = 0.80), confirming that transgenic AAT expressed from human MSCs is equally potent as a serine protease inhibitor as natural AAT isolated from human plasma.
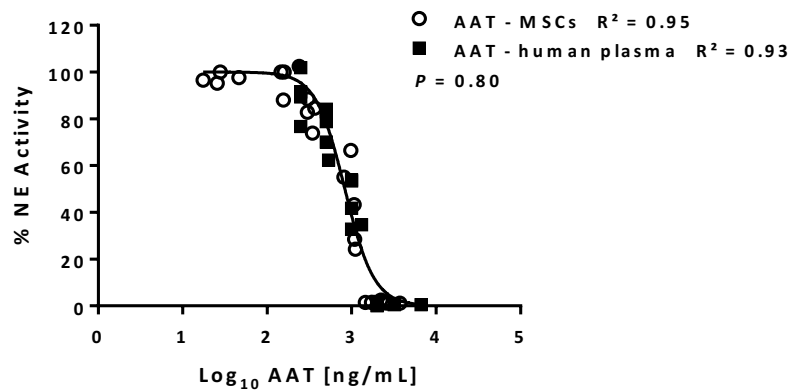
Figure 22: **Transgenic AAT secreted from transduced primary human MSCs is as potent as natural AAT isolated from human plasma.** Dilutions of supernatants collected from MSCs transduced with vector #194 and #215 were generated, and inhibition of neutrophil elastase was assessed. AAT protein content in diluted MSC supernatant samples and natural AAT samples was quantified by ELISA. Only samples were included in which neutrophil elastase inhibition values and AAT concentration were measurable for all 5 dilutions (MSC-AAT: n = 25; human plasma AAT: n = 20). Neutrophil elastase activity [%] was plotted against $\log_{10}$ of AAT concentration. Curves were fitted using the log(inhibitor) *vs.* response model (R^2 = 0.95 for AAT from MSCs; R^2 = 0.93 for AAT from human plasma). There was no statistical difference between both groups as determined by comparison of fits using the Extra sum-of-squares F test (*P* = 0.80).

3.5. Scale-up, batch generation and characterization

The next step was to assess if the transduction and cell expansion processes used in all previous experiments were scalable since the execution of *in vivo* studies requires large quantities of cells from the same batch. Thus, we next set out to produce large batches of native as well as gamma-retrovirally and lentivirally transduced MSCs from two donors to generate a supply of cells for subsequent animal studies. We also assessed if the MSCs at the end of the production process fulfilled specifications of MSC quality parameters (expression of typical surface markers, adipogenic and osteogenic differentiation, sterility, testing for Mollicutes). We also determined whether there was a difference between non-modified and gene-modified MSCs, and if the cell donor had an impact on the outcome of the aforementioned parameters.

3.5.1. Surface marker expression

Flow cytometric analyses of surface antigen expression revealed that values were comparable between the two donors, AP00158 and AP00208, as well as between non-modified and gene-modified MSCs, and that all four batches fulfilled surface marker specifications (Table 13). In all four batches, MSC content was well above 90% as measured by the expression of CD73, CD90, and CD105, and there were only traces of contaminating hematopoietic cells such as HSCs, lymphocytes, erythrocytes or thrombocytes as confirmed by the lack of cells expressing CD45, CD34, CD235a, CD41, CD3, CD19, and CD14.

Table 13: **Expression of MSC and hematopoietic surface markers on four MSC batches generated from 2 donors.** Native and transduced MSC batches from two donors (AP00158 and AP00208) consisted of >90% MSCs, and levels of contaminating hematopoietic cells were below 3% in all samples as analyzed by flow cytometry.

Parameter	Specification	AP00158 native	AP00158 TD #194	AP00208 native	AP00208 TD #215
Vital cells (7AAD-) [%]	>80	95.43	94.69	98.61	91.68
MSCs (CD73+/CD90+, CD34-/CD45-) [%]	>90	92.22	96.94	97.66	92.78
MSCs (CD105+, CD34-/CD45-) [%]	>90	95.77	95.57	98.42	95.71
HSCs (CD45+/CD34+) [%]	<10	0.05	0.07	0.00	0.00
Erythrocytes (CD235a+) [%]	<10	0.11	0.07	0.00	0.02
Thrombocytes (CD41+) [%]	<10	1.63	2.78	0.44	0.89
T-Lymphocytes (CD45+/CD3+) [%]	<10	0.00	0.03	0.00	0.00
B-Lymphocytes (CD45+/CD19+) [%]	<10	0.00	0.04	0.00	0.00
Monocytes (CD45+/CD14+) [%]	<10	0.00	0.01	0.00	0.00

Figure 23 depicts representative flow cytometry plots of native as well as gamma-retrovirally transduced MSCs from one donor stained with the different fluorescently labeled antibodies detecting MSC and hematopoietic surface antigens.

3.5.2. Adipogenic and osteogenic differentiation capability

After confirming that there were no differences in the MSC phenotype between the two donors and between non-modified and modified cells, adipogenic and osteogenic differentiation capabilities of the MSCs were analyzed as an additional measure of quality. Cells from all four batches were able to differentiate into adipocytes as determined by Oil Red O staining as well as into osteoblasts as assessed by Alizarin Red staining. These results suggest that the genetic modifications performed did not alter adipogenic and osteogenic differentiation capabilities of the engineered MSCs, and that donors AP00158 and AP00208 are comparable in that regard. Figure 24 shows representative pictures of native and gamma-retrovirally transduced MSCs from donor AP00158 after adipogenic and osteogenic differentiation.

3.5.3. Additional parameters

In a next step, we characterized the cell yields in the four batches produced. It was possible in all cases to produce quantities >1.5x10^8 MSCs (Table 14 and Table 15), sufficient for the execution of a series of *in vivo* studies, and to cryopreserve the cells in passage five. The batch of lentivirally transduced cells derived from donor AP00208 was expanded on six 5-layer cell stack systems; this explains the high cell yield of 4.63x10^8, about twice the amount of cells harvested for the gamma-retrovirally transduced batch (donor AP00158), which was expanded on three 5-layer cell stacks. The batches were tested for sterility and for the presence of Mollicutes as part of a standard panel of quality control assays for MSCs, and these specifications were also met. Batches of gamma-

retrovirally and lentivirally modified MSCs were additionally characterized regarding transduction efficacy, outcome of the antibiotic selection procedure, VCN in the bulk population of selected cells, AAT protein yield per 1×10^5 cells in 48 hours normalized to VCN, and the capacity to inhibit neutrophil elastase in comparison to natural AAT purified from human plasma.
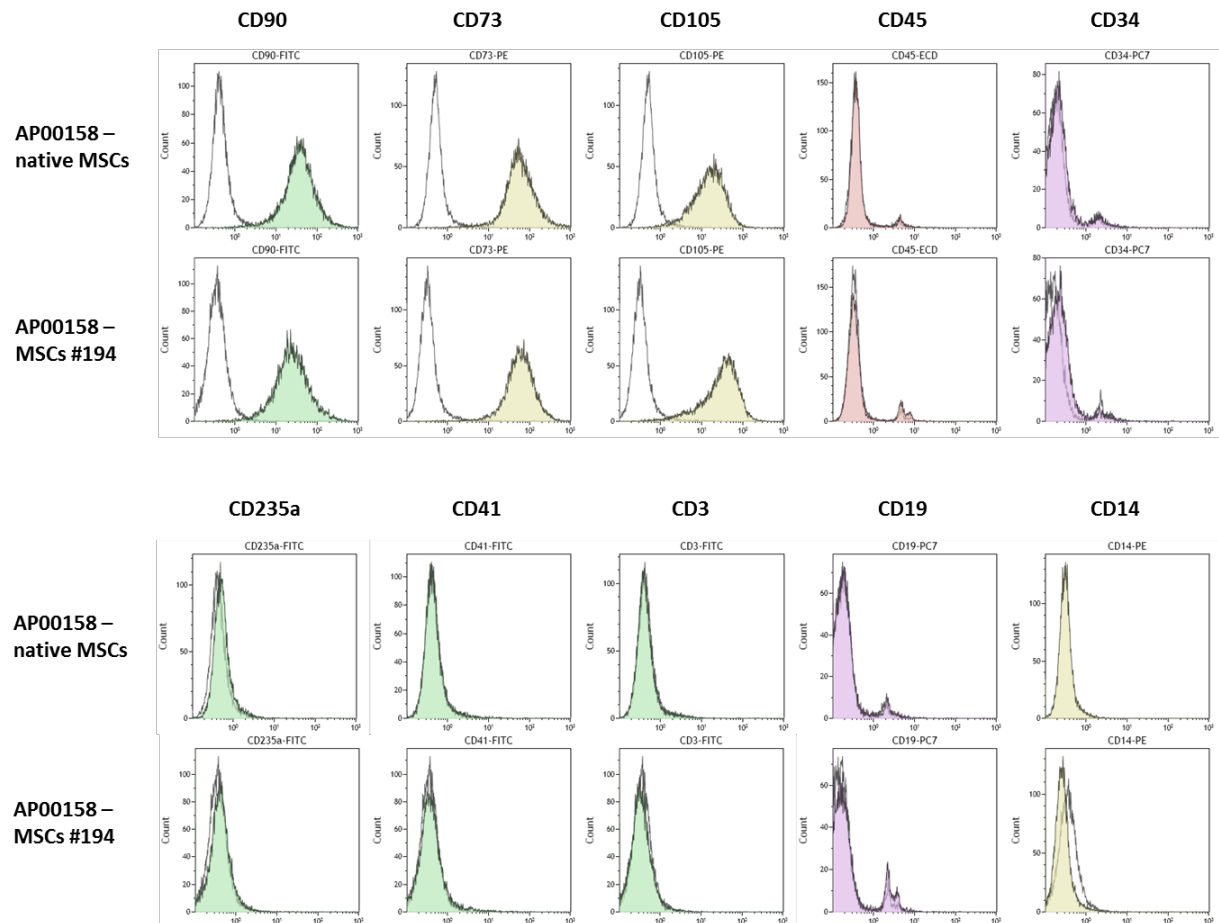
Figure 23: **Representative flow cytometry plots of native and gamma-retrovirally transduced MSCs from donor AP00158 stained for MSC and hematopoietic surface markers.** Native and gamma-retrovirally transduced cells were negative for hematopoietic markers (CD45, CD34, CD235a, CD41, CD3, CD19, and CD14), but positive for MSC markers (CD73, CD90, CD105). Histogram plots show an overlay of results generated by staining the cells with an isotype control antibody (white peak) and with an antibody specific to the antigen denominated in the graph above the histogram plot (colored peak). Colors represent the fluorochromes the respective antibodies are labeled with: green = fluorescein isothiocyanate (FITC), yellow = R-phycoerythrin (PE), orange = energy coupled dye (ECD), purple = phycoerythrin-cyanin-7 (PC7).
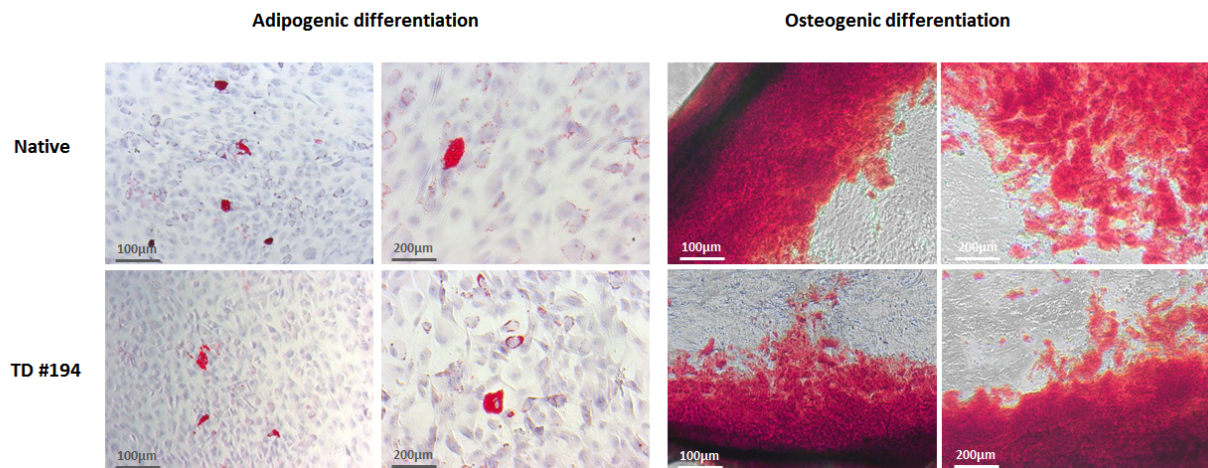
Figure 24: **Differentiation capabilities of native and gamma-retrovirally transduced MSCs are comparable.** No difference in the differentiation potential of native and transduced MSCs was seen after adipogenic and osteogenic differentiation and subsequent staining. Shown are representative pictures of cells derived from donor AP00158.

For the AAT-expressing MSCs there are at present no standard specifications regarding these parameters, thus specifications were chosen based on empirical "good" values generated in various previous experiments. As these genetically modified cells were to be used for in vivo studies at our collaborators' non-biosafety level (BSL) 2 facilities, transduced MSC batches were assayed for the presence of replication-competent retrovirus (RCR) and replication-competent lentivirus (RCL), respectively; both tested negative. The results of all tests performed are summarized in Table 14 and Table 15.

Table 14: **Characteristics of native MSC batches derived from donors AP00158 and AP00208.** MSCs fulfilled standard specifications regarding sterility, expression of surface markers, differentiation potential, and testing for Mollicutes; inter-donor variability was negligible for the parameters tested.

Native MSC batches			
Parameter	Specification	AP00158 native	AP00208 native
Donor		AP00158	AP00208
Number of cryopreserved cells [x10^6]	N.a.	245	164
Sterility	No growth of bacteria or fungi	No growth of bacteria and fungi	No growth of bacteria and fungi
Surface marker expression	All surface makers within specification (*cf.* Table 13)	Yes	Yes
Adipogenic differentiation	Several adipocytes visible	Yes	Yes
Osteogenic differentiation	Osteogenic mineralization visible	Yes	Yes
Testing for Mollicutes	Negative	Negative	Negative

Table 15: **Specifications of genetically modified MSC batches derived from donors AP00158 and AP00208.** MSCs fulfilled standard specifications regarding sterility, expression of surface markers, differentiation potential, and testing for Mollicutes; inter-donor variability was negligible for the parameters tested. Transduced MSCs also fulfilled self-chosen specifications for the values of %AAT-positive cells before and after antibiotic treatment, VCN, AAT protein yield, and the potential to inhibit neutrophil elastase.

Gene-modified MSC batches			
Parameter	Specification	AP00158 TD #194	AP00208 TD #215
Donor		AP00158	AP00208
Number of cryopreserved cells [x10^6]	N.a.	230	463
Sterility	No growth of bacteria or fungi	No growth of bacteria and fungi	No growth of bacteria and fungi
Surface marker expression	All surface makers within specification (*cf.* Table 13)	Yes	Yes
Adipogenic differentiation	Several adipocytes visible	Yes	Yes
Osteogenic differentiation	Osteogenic mineralization visible	Yes	Yes
Testing for Mollicutes	Negative	Negative	Negative
% AAT positive pre-selection	>25%	72,9	54,0
% AAT positive post-selection	>90%	96,2	93,9
VCN	1.0-5.0	1,7	2,4
AAT protein expression [ng/10^5 cells/48h/VCN]	>250	595	369
Neutrophil elastase inhibition assay	Neutrophil elastase inhibition comparable to AAT from human plasma	Yes	Yes
Testing for RCR/RCL	Negative	Negative	Negative

In summary, all batches fulfilled the specifications of the standard quality parameters. Values for native and genetically modified MSCs were comparable, and also inter-donor variability between AP00158 and AP00208 was limited for the parameters tested.

These results suggest that the development of a large scale procedure of transduction and expansion of AAT-modified MSCs was successful, and that genetic modification with gamma-retroviral or lentiviral vectors for expression of human AAT does not alter the established quality parameters from the panel of standard assays. Moreover, both gene-modified batches fulfilled all self-chosen specifications believed to be a reflection of "good" AAT-expressing MSCs, and differences between the batches were minor. Transduction efficacies were high for each batch; VCNs were well in the range of what has been considered safe in previous gene therapy clinical trial protocols [192]. AAT protein expression from both batches was above the threshold chosen to characterize "good" levels of AAT expression. Assaying of MSCs from both batches in the neutrophil elastase assay led to an inhibition of the elastase comparable to that yielded with natural AAT from human plasma at the

same concentration. Taken together, we can conclude that the scale-up of the processes and the production of comparable batches of native and AAT-expressing MSCs for use in *in vivo* experiments were successful.

3.6. *In vivo* proof of concept study

3.6.1. Elastase-induced lung emphysema – experimental design

The *in vivo* experiments described in this work were conducted in collaboration with Ali Önder Yildirim's group at the Comprehensive Pneumology Center at the Helmholtz Zentrum München.

To assess if native and AAT-MSCs were able to generate a therapeutical benefit in an inflammatory lung disease *in vivo*, the well-established model of elastase-induced lung emphysema [331,341] was applied in order to represent the emphysema observed in human COPD. Female C57BL/6N mice were divided into four groups consisting of six mice each (Table 12): Mice in group 1 served as negative controls and received PBS, while mice in all other groups were treated with a single intratracheal instillation of porcine pancreatic elastase on day 0. Mice in positive control group 2 additionally received an oropharyngeal application of saline on day 7, while mice in group 3 and 4 were oropharyngeally instilled with $5x10^5$ native MSCs, and $5x10^5$ MSCs modified to express AAT, respectively. On day 14, native and AAT-MSC application in groups 3 and 4 was repeated. Before the mice were sacrificed on day 21 for histological and BALF analysis, they were anesthetized, tracheostomized, and lung function measurements performed using the Buxco pulmonary function testing system. One mouse in the PBS-treated group had to be excluded from the analysis due to the development of spontaneous emphysema (probably resulting from a confusion of this mouse and subsequent inadvertent elastase instillation; A. Ö. Yildirim, personal communication), and one mouse died in each of the groups receiving elastase only, and elastase plus native MSCs. The mouse in the group receiving elastase only died shortly before completion of the pulmonary function analyses; however, it was possible to perform histological analyses. For that reason, pulmonary function measurements generated from five mice could be analyzed in the groups treated with PBS, elastase, and elastase plus native MSCs, and from six mice in the group receiving elastase plus AAT-MSCs; BALF and histology could be analyzed from five mice in the PBS and elastase plus native MSCs groups, and from six mice in the elastase only and elastase plus AAT-MSCs groups.

3.6.2. Amelioration of pulmonary function after treatment with AAT-MSCs

Instillation of porcine pancreatic elastase in mouse lungs is known to induce a breakdown of lung tissue and a severe destruction of small airways that is comparable to emphysema in COPD patients [342]. The model leads to the formation of large air pockets that replace lung tissue resulting in a dramatic increase of lung function parameters [343]. We observed this increase in pulmonary

measures in mice receiving a single application of elastase compared to PBS-treated animals in all parameters analyzed; however, all statistical analyses (Figure 25) were performed by comparing the results measured in groups 3 and 4 ("treatment groups" receiving native and AAT-MSCs, respectively) to the values measured in the elastase group ("disease group") in order to assess a potential therapeutic effect of MSC treatment – the main focus of the current work. We observed a statistically significant improvement in lung function as expressed by parameters measuring expiratory airflow (forced expiratory volume in 100ms (FEV_{100ms}): $P < 0.05$, forced vital capacity (FVC): $P < 0.01$; Figure 25A and Table 16), chord compliance (Cchord), a measure of the lung's ability to stretch and expand (Cchord: $P < 0.001$; Figure 25B and Table 16), as well as inspiratory capacity (IC: $P < 0.01$) and vital capacity (VC: $P < 0.05$, Figure 25C and Table 16) in the group in which mice were treated with AAT-MSCs in comparison to the elastase group. The most striking amelioration was seen in Cchord, from an average of $0.0929mL/cmH_2O$ in the elastase-treated group to 0.0718 in the AAT-MSC group (average in the PBS group = 0.0431), amounting to an improvement of this parameter by 42.3% assuming that values in the PBS group are equal to 100% improvement. FEV_{100ms} and FVC, the two parameters the diagnosis of human COPD is based on, were improved by 31.0% and 25.7%, respectively. The P-value for dynamic compliance (Cdyn) was not statistically significant ($P = 0.18$); however, the same trend towards an amelioration was visible as for the other parameters determined. In some of the parameters analyzed (*e.g.* FEV_{100ms}, IC) we could observe an indication that treatment with native MSCs might as well be beneficial, however, comparison of these results with the values measured in the elastase-treated group never reached statistical significance, indicating that AAT overexpression is required to achieve a clear therapeutic benefit in this model.

3.6.3. Amelioration of emphysema after treatment with AAT-MSCs

Next, it was assessed whether MSC treatment had an effect on the emphysema present in this model. To that end, airspace enlargement was quantified in H&E stained sections (Figure 26A) of lung tissue using an emphysema score from 0-5 (Figure 26B and Table 17). A noticeable amelioration of pulmonary tissue destruction was observed after treatment with native MSCs, as indicated by a decrease in the average emphysema score from 4.25 ± 0.61 in the elastase group to 3.50 ± 0.50 in the mouse group receiving native MSCs (equal to an amelioration of 17.6% assuming that the score of elastase-treated mice corresponds to 100%), suggesting that treatment with MSCs led to regeneration or repair of the injured lung tissue. However, a much more dramatic decrease in emphysema was noticed when mice were treated with AAT-MSCs (from 4.25 ± 0.61 in the elastase group to 2.17 ± 0.75; $P < 0.001$, equal to an amelioration of 49.0%), indicating that the combination of AAT and MSCs resulted in a more than additive beneficial effect that led to an enhanced amelioration of pulmonary tissue injury.
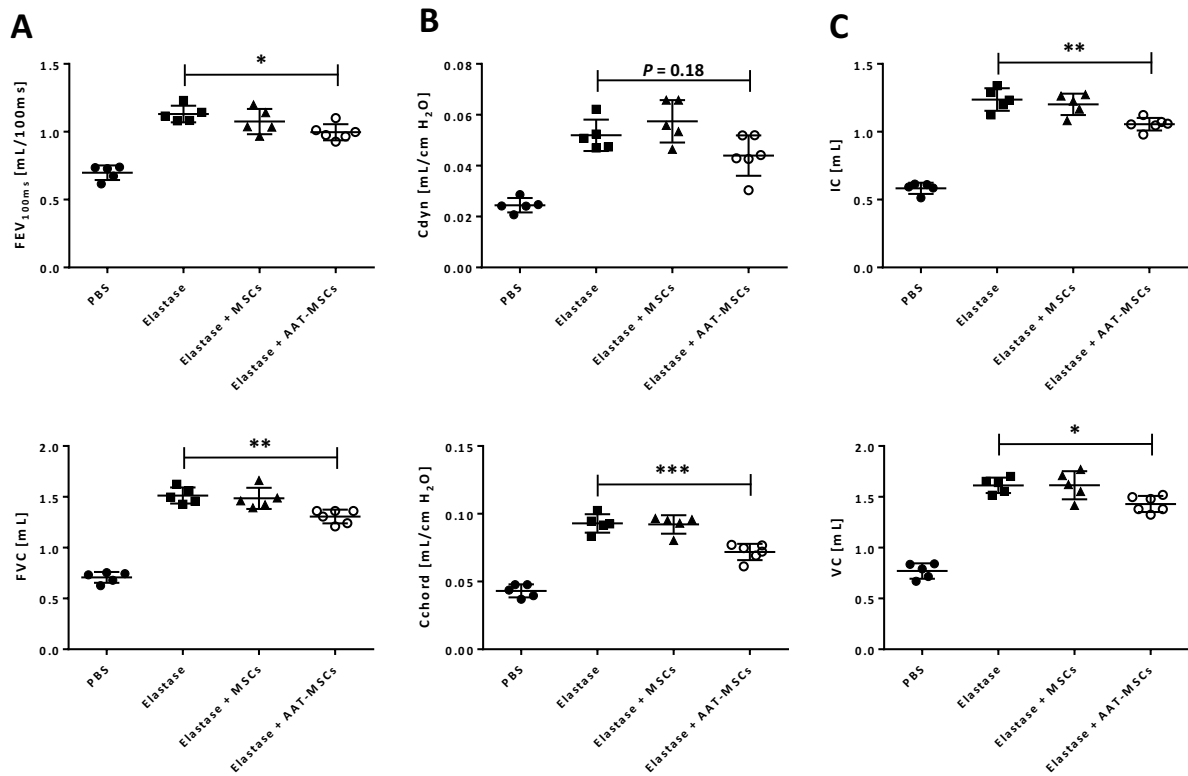
Figure 25: **Treatment with AAT-MSCs leads to improved pulmonary function in a model of elastase-induced emphysema (collaboration with A.Ö. Yildirim/CPC).** Lung function parameters were measured using the Buxco forced pulmonary maneuver system. **A: Expiratory airflow**. A statistically significant beneficial effect of treatment with AAT-MSCs was observed for both parameters describing expiratory airflow (FEV_{100ms}: $P < 0.05$, FVC: $P < 0.01$), equaling an amelioration of 31.0% and 25.7%, respectively. **B: Lung compliance.** While application of AAT-MSCs led to a highly statistically significant decrease in Cchord ($P < 0.001$; 42.3% improvement), a trend towards amelioration of Cdyn ($P = 0.18$) was observed after treatment with AAT-MSCs. **C: Inspiratory and vital capacity.** For IC as well as VC, a statistically significant improvement after treatment with AAT-MSCs was measured (IC: $P < 0.01$, VC: $P < 0.05$), equal to an amelioration of these parameters by 30.9% and 21.7%, respectively. MSC- and AAT-MSC-treated groups were compared to mice receiving elastase only for all parameters. Each symbol represents one mouse; the horizontal lines denote means. Statistical significance of differences between the elastase group and the groups treated with native MSCs and AAT-MSCs, respectively, was calculated applying ordinary one-way ANOVA, followed by Dunnett's multiple comparisons test. Normality of the data was confirmed by the Kolmogorov-Smirnov normality test. * $P < 0.05$; ** $P < 0.01$; *** $P < 0.001$. Only the clinically most significant parameters are presented in this figure; results for resistance (RI), peak expiratory flow (PEF), and expiratory reserve volume (ERV) are depicted in Supplemental figure 19.

Table 16: **Pulmonary function measurements (collaboration with A.Ö. Yildirim/CPC).** Shown are average values measured for FEV_{100ms}, FVC, Cdyn, Cchord, IC, and VC ± SD. n = 5 for the groups receiving PBS, elastase, and elastase + MSCs, and n = 6 for the group receiving elastase + AAT-MSCs.

	PBS		Elastase		Elastase + MSCs		Elastase + AAT-MSCs	
	Average	SD	Average	SD	Average	SD	Average	SD
FEV_{100ms}	0,6982	0,0534	1,1305	0,0616	1,0751	0,0927	0,9964	0,0591
FVC	0,7075	0,0538	1,5133	0,0797	1,4853	0,1044	1,3062	0,0672
Cdyn	0,0245	0,0028	0,0519	0,0061	0,0574	0,0084	0,0440	0,0079
Cchord	0,0431	0,0048	0,0929	0,0068	0,0921	0,0068	0,0718	0,0060
IC	0,5833	0,0414	1,2372	0,0828	1,2021	0,0789	1,0558	0,0462
VC	0,7702	0,0756	1,6131	0,0758	1,6139	0,1380	1,4299	0,0795
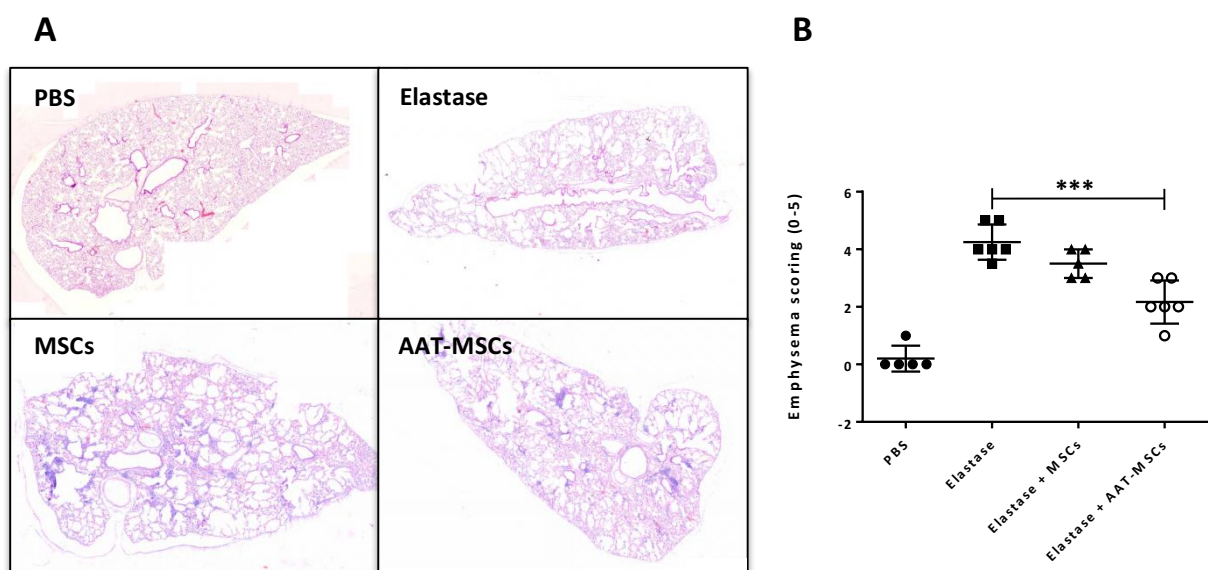
Figure 26: **Treatment with AAT-MSCs leads to significant lung tissue repair/regeneration (collaboration with A.Ö. Yildirim/CPC). A: Representative photomicrographs of H&E-stained lung sections.** Treatment with MSCs and AAT-MSCS led to repair and regeneration of lung tissue, as indicated by a decrease in airspace enlargement noticeable in the respective slides. Shown are representative slides from one mouse each treated with PBS, elastase, elastase plus native MSCs, and elastase plus AAT-MSCs. **B: Marked amelioration of emphysema in AAT-MSC-treated mice.** Airspace enlargement was assessed by using an emphysema scoring system ranging from 0–5. Each symbol represents one mouse; the horizontal lines denote means. Gaussian distribution of the data was analyzed by the Kolmogorov-Smirnov normality test. Statistical significance of differences between the elastase group and the groups treated with native MSCs and AAT-MSCs, respectively, was calculated applying ordinary one-way ANOVA, followed by Dunnett's multiple comparisons test. *** $P < 0.001$.

Table 17: **Emphysema scoring results (collaboration with A.Ö. Yildirim/CPC).** Shown are the emphysema scoring results for mice in all groups.

Mouse No.	PBS	Elastase	Elastase + MSCs	Elastase + AAT-MSCs
1	0,0	4,0	3,0	2,0
2	0,0	5,0	4,0	2,0
3	excluded	4,0	3,0	3,0
4	0,0	3,5	3,5	3,0
5	0,0	5,0	4,0	1,0
6	1,0	4,0	died	2,0

3.6.4. Increased inflammation scoring after treatment with MSCs

When designing this *in vivo* study, we were aware of the possibility that the administration of human cells expressing a human protein to immunocompetent mice might cause an immune response against the foreign antigens. Moreover, during the histopathologic examination of the H&E sections in the context of the assessment of the emphysema scoring an increase of inflammatory cell recruitment to the lungs of mice treated with MSCs and AAT-MSCs was observed (Figure 27A). Thus, in a next step an analysis of the inflammation score was performed using a scoring system ranging from 0–3 (Table 18). As graphically represented in Figure 27B, there was a marked increase in inflammation score from 0 ± 0 in the elastase group to 1.50 ± 1.0 in the group receiving MSCs ($P < 0.01$) and to 1.83 ± 0.75 in the group treated with AAT-MSCs ($P < 0.001$). It is possible that this inflammatory response results from the application of human MSCs and human MSCs expressing human AAT in immunocompetent mice, fostering an immune response against the foreign cells and protein.

3.6.5. Analysis of total and differential cell counts in the BALF

To further analyze the inflammation in the lungs of the mice, and to further assess if treatment with MSCs and AAT-MSCs had a beneficial effect on the inflammation caused by the elastase treatment, bronchoalveolar lavage (BAL) was performed by instilling the lungs of the mice with PBS. Total and differential cell counts analyzing the recruitment of inflammatory cells such as neutrophils, macrophages, and lymphocytes were measured. A graphical representation of the results is shown in Figure 28 and a summary of the data presented in Table 19. As for the pulmonary function parameters described in 3.6.2, we were mainly interested in the possible effect of our "treatment groups" in comparison to the "disease group". Thus, analyses of statistical significance were carried out by comparing values measured for the MSC-treated groups *vs.* the elastase only group. There was no significant difference in total cell numbers in these three groups; however, a statistically significant increase in absolute average lymphocyte and eosinophil counts in the mouse group

receiving AAT-MSCs as compared to the elastase only group (lymphocytes: from 4076 $\pm$ 2638 in the elastase group to 19240 $\pm$ 3499 in the AAT-MSC group; P < 0.001; eosinophils: from 0 to 19775 $\pm$ 11171; P < 0.01) was noted; a marked rise in these cell numbers was also observed in the groups treated with native MSCs, however, statistical significance was only reached for lymphocytes (P < 0.01). Concomitant with these results was a tendency towards decreased numbers of macrophages in both groups treated with MSCs (from 100778 $\pm$ 22579 in the elastase group to 75453 $\pm$ 39084 in the MSC-treated group, and to 78631 $\pm$ 23263 in the AAT-MSC group), as well as neutrophils in the AAT-MSC group (from 730 $\pm$ 390 in the elastase group to 450 $\pm$ 722 in the AAT-MSC group). Taken together, these results indicate that an immune reaction to the instilled cells might be happening in the mice that received MSCs, while at the same time a tendency towards a decrease of the cell types involved in emphysema development is noticeable.

Next, the relative proportions of each cell type were analyzed (Figure 29). As expected, percentages of lymphocytes and eosinophils were markedly increased in both mouse groups treated with MSCs compared to the group receiving elastase only (lymphocytes: MSCs: P < 0.0001, AAT-MSCs: P < 0.0001; eosinophils: MSCs: P < 0.05, AAT-MSCs: P < 0.001), and percentages of macrophages were significantly decreased (MSCs: P < 0.0001, AAT-MSCs: P < 0.0001).
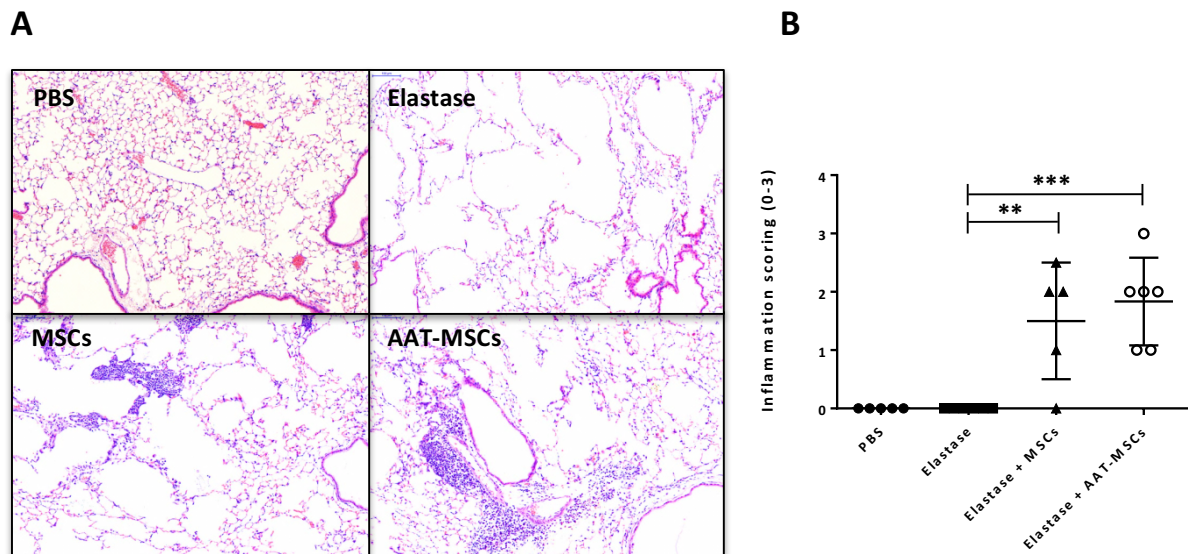
Figure 27: **Treatment with AAT-MSCs leads to significant increase in inflammation scoring (collaboration with A.Ö. Yildirim/CPC). A: Representative photomicrographs of H&E-stained lung sections.** Instillation of MSCs and AAT-MSCs leads to inflammatory cell recruitment to the mouse lungs. Shown are representative slides from one mouse each treated with PBS, elastase, elastase plus native MSCs, and elastase plus AAT-MSCs. **B: Significant increase of inflammation score in native and AAT-MSC-treated mice.** Inflammation score was assessed by using a scoring system ranging from 0–3. Each symbol represents one mouse; the horizontal lines denote means. Gaussian distribution of the data was analyzed by the Kolmogorov-Smirnov normality test. Statistical significance of differences between the elastase group and the groups treated with native MSCs and AAT-MSCs, respectively, was calculated applying ordinary one-way ANOVA, followed by Dunnett's multiple comparisons test. ** P < 0.01; *** P < 0.001.

Table 18: **Inflammation scoring results (collaboration with A.Ö. Yildirim/CPC).** Shown are the inflammation scoring results for mice in all groups.

Mouse No.	PBS	Elastase	Elastase + MSCs	Elastase + AAT-MSCs
1	0,0	0,0	0,0	1,0
2	0,0	0,0	2,0	2,0
3	excluded	0,0	1,0	2,0
4	0,0	0,0	2,0	3,0
5	0,0	0,0	2,5	1,0
6	0,0	0,0	died	2,0
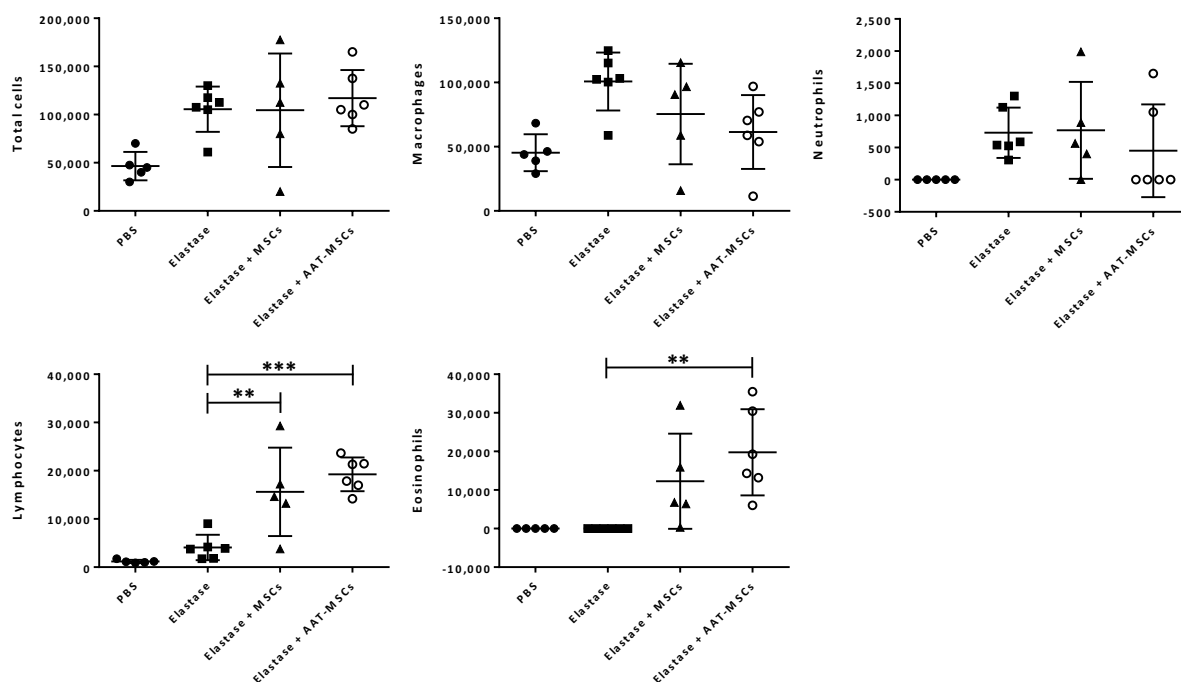
Figure 28: **Increase in absolute numbers of lymphocytes and eosinophils after treatment with AAT-MSCs (collaboration with A.Ö. Yildirim/CPC).** No significant difference in total cell numbers was noted. A statistically significant increase in the absolute number of lymphocytes and eosinophils in mice receiving AAT-MSCs in comparison to mice treated with elastase only was observed (lymphocytes: $P < 0.001$, eosinophils: $P < 0.01$). The same effect was noted for native MSCs; however, statistical significance was only reached for lymphocytes ($P < 0.01$). Accompanied by these results was a trend towards lower macrophage counts in both groups treated with MSCs, and neutrophil counts in the AAT-MSC groups. Mouse lungs were lavaged 3 times with PBS, cells were pelleted, and the pellet resuspended in medium for the total cell count. Cytospins of the cell suspension were prepared for differential cell counting. MSC-treated groups were compared to mice receiving elastase only for all cell types. Each symbol represents one mouse; the horizontal lines denote means. Gaussian distribution of the data was analyzed by the Kolmogorov-Smirnov normality test. Statistical significance of differences between the elastase group and the groups treated with native MSCs and AAT-MSCs, respectively, was calculated applying ordinary one-way ANOVA, followed by Dunnett's multiple comparisons test for total cells, macrophages, lymphocytes, and eosinophils, and Kruskal-Wallis test, followed by Dunn's multiple comparisons test for neutrophils. ** P < 0.01; *** P < 0.001.
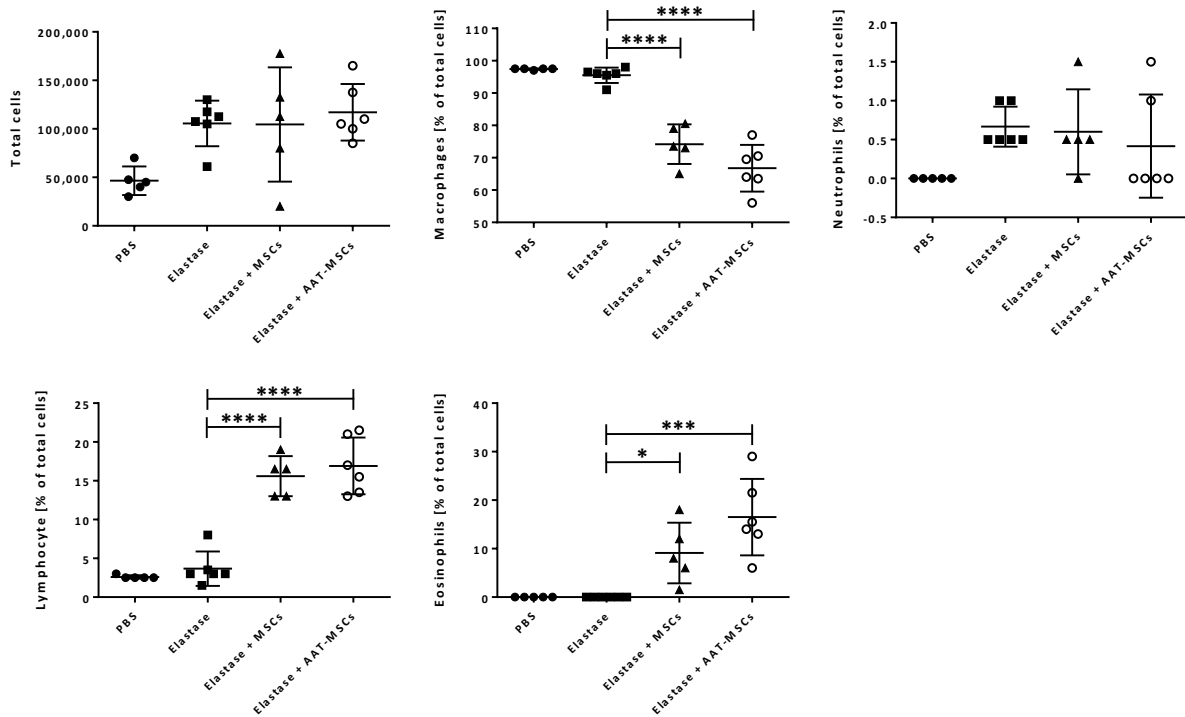
Figure 29: **Relative proportions of lymphocytes and eosinophils are increased, and percentages of macrophages are decreased after treatment with MSCs (collaboration with A.Ö. Yildirim/CPC).** A statistically significant increase in the relative proportions of lymphocytes and eosinophils in mice receiving either native MSCs or AAT-MSCs in comparison to mice treated with elastase only was observed (lymphocytes: MSCs: $P < 0.0001$, AAT-MSCs: $P < 0.0001$; eosinophils: MSCs: $P < 0.05$, AAT-MSCs: $P < 0.001$), while macrophage percentages were markedly decreased (MSCs: $P < 0.0001$, AAT-MSCs: $P < 0.0001$). Mouse lungs were lavaged 3 times with PBS, cells were pelleted and the pellet resuspended in medium for the total cell count. Cytospins of the cell suspension were prepared for differential cell counting. MSC-treated groups were compared to mice receiving elastase only for all cell types. Each symbol represents one mouse; the horizontal lines denote means. Gaussian distribution of the data was analyzed by the Kolmogorov-Smirnov normality test. Statistical significance of differences between the elastase group and the groups treated with native MSCs and AAT-MSCs, respectively, was calculated applying ordinary one-way ANOVA, followed by Dunnett's multiple comparisons test for total cells, macrophages, lymphocytes, and eosinophils, and Kruskal-Wallis test, followed by Dunn's multiple comparisons test for neutrophils. * $P < 0.05$; *** $P < 0.001$; **** $P < 0.0001$.

Table 19: **Cell counts in the BALF (collaboration with A.Ö. Yildirim/CPC).** Shown are average cell numbers counted in the BALF of the mice for total cells, macrophages, neutrophils, lymphocytes, and eosinophils ± SD. n = 5 for the groups receiving PBS, and elastase + MSCs, and n = 6 for the group receiving elastase and elastase + AAT-MSCs.

	PBS		Elastase		Elastase + MSCs		Elastase + AAT-MSCs	
	Average	SD	Average	SD	Average	SD	Average	SD
Total cells	46500	14748	105583	23570	104500	58986	117083	29087
Macrophages	45308	14421	100778	22579	75453	39084	78631	23263
Neutrophils	0	0	730	390	768	753	450	722
Lymphocytes	1193	331	4076	2638	15628	9164	19240	3499
Eosinophils	0	0	0	0	12260	12336	19775	11171

3.6.6. Summary

In summary, application of AAT-MSCs led to significantly improved respiratory function parameters and enhanced regeneration and repair of lung tissue as indicated by a dramatic decrease in emphysema scoring in a model of elastase-induced lung emphysema. However, treatment with native and AAT-MSCs also induced an inflammatory response in the mouse lungs as well as significant accumulation of lymphocytes and eosinophils in the BALF, which will need to be further investigated.

Taken together, this is, to the author's knowledge, the first proof of concept for the treatment of lung emphysema with MSCs virally modified to stably express the serine protease inhibitor AAT.

4. Discussion

4.1. Targeting construct

One major aim of the present work was to design an optimized transfer vector for the genetic modification of human MSCs to express the serine protease inhibitor AAT. Several considerations were taken into account for the design of this targeting construct. First, for construction of the *SERPINA1* expression cassette, transcript variant 1 out of 11 transcript variants published at NCBI's Nucleotide comprising the same coding sequence of 1254 bases was chosen. Variant 1 differs from the other 10 transcript variants only by the portion of the 5'UTR included in the published sequence, ranging from 240 (transcript variant 3, accession number NM_001002235.2) to 573 bases (transcript variant 5, accession number NM_001127701.1). The 5' UTR of transcript variant 1 has a relatively small size of 261 bases, as do the majority of the transcript variants. Therefore, it could easily be included in the expression construct without having to fear a major drop in viral titers. Our hypothesis was that the 5' UTR might contain sequences inducing cap-independent translation [344,345], serve as a natural site for the potential binding of regulatory factors such as miRNAs [346], or comprise other sequences possibly leading to enhanced protein expression [347,348]. The *SERPINA1* 3' UTR published at Nucleotide is the same for all 11 transcript variants and contains 1702 bases. Although there are papers describing that inclusion of the 3' UTR can lead to enhanced gene expression [349], it was not incorporated into the expression cassette due to size restrictions in the retroviral backbone. During the ordering process of the *SERPINA1* expression cassette from GeneArt, a modified Kozak consensus sequence [327] was inserted 5' of the *SERPINA1* start codon to ensure efficient initiation of translation, and the CDS was codon optimized [350,351] for *homo sapiens.* Although it might seem unnecessary and counterintuitive to codon optimize a human cDNA for *homo sapiens*, we performed this step as it has been shown that *homo sapiens* codon optimization of human genes could increase protein expression up to 200% in a gene therapy setting for hemophilia A [352].

The next important point to consider was the choice of promoters to be tested for the expression of *SERPINA1*. AAT is a protein that is highly expressed in the human body with an average production rate of 34mg/kg body weight per day [353]. Thus, the endogenous human AAT promoter would theoretically be well-suited to drive high-level expression of AAT in a gene therapy setting, as it has been described for the expression of transgenes in hepatocytes [354,355]. However, as it has also been published that the human AAT promoter is not active in bone marrow-derived MSCs [243], we refrained from including it in our list of promoters to be tested. Instead, we focused on the following constitutive promoters in order to assess the impact of different promoters on gene expression levels: The PGK and EF1a promoters are human physiological promoters normally driving the expression of ubiquitous proteins crucial for glycolysis [356,357] and protein translation [358], respectively,

processes that are essential for all living organisms. Thus, these proteins are constantly produced in all nucleated human cells at high levels, indicating that these promoters are capable of driving constant high gene expression. Furthermore, it has been described that pPGK and pEF1a when used in retroviral vectors are able to govern high-level gene expression also in stem cells such as HSCs [359], ESCs [360], and MSCs [361,362], and that expression of the transgene from physiological promoters such as pPGK and pEF1a is detectable over several weeks, while viral promoters are more prone to silencing [363,364]. Another reason to favor physiological promoters over strong viral promoters despite their high-level gene expression is safety: In all documented cases of insertional transformation that have occurred in gene therapy clinical trials to date, conventional LTR-driven gamma-retroviral vectors had been used to genetically modify the cells [185–187]. Physiological promoters in contrast have been shown to markedly reduce the risk of genotoxicity [365]. Based on these considerations, pPGK and pEF1a were chosen as test candidates to drive *SERPINA1* expression in our transfer constructs. The third promoter analyzed was pEFS (pEF1a short), the intron-less form of pEF1a described by Schambach and colleagues [329]. Comprising only 233 bases, it is almost six times shorter than the full length EF1a promoter, which is expected to be beneficial with regards to resulting viral titers, and expression from pEFS has been described to be approximately half of pEF1a in HSCs [329]. These features make pEFS a very attractive candidate promoter, and indeed is it presently being used in several gene therapy clinical trials worldwide [189,366,367]. The CAG promoter consists of the CMV early enhancer in combination with the chicken beta actin promoter and usually yields higher transgene expression as compared to the promoters described above [335]. Thus, it was included to serve as a positive control for high expression in early experiments. As expected, MFI values of AAT expressed from pCAG measured by flow cytometry for intracellular AAT were twice as high as *e.g.* MFIs measured for AAT driven from pEF1a. Transduction efficacies of primary MSCs, however, were unacceptably low using pCAG, probably due to very low viral titers, with the large size of the promoter of ~1600 bases most likely being the reason for these. Thus, pCAG was not included in any further experiments, and the three promoters tested for *SERPINA1* expression were pPGK, pEF1a, and pEFS.

In addition to *SERPINA1*, the *pac* gene was needed to be expressed in the targeting construct to allow for antibiotic selection of transduced cells. Thus, the next point to consider when designing our expression vector was how the *pac* gene should be co-expressed. Common strategies used to drive the expression of more than one gene per targeting construct make use of multiple promoters [368], IRES sequences [369], fusion proteins [370] or insertion of cleavage signals such as 2A peptides [371,372]. Among these strategies, multiple promoters and the utilization of IRES sequences are the most frequently employed [337]. Thus, we decided to assess both approaches and drive *pac* expression from either a second promoter or use the well described EMCV IRES sequence [332,333] to link both genes.

Due to pEF1a being the largest promoter under evaluation, and because we wanted to keep the construct sizes as small as possible, the choice was narrowed down to pPGK and pEFS promoters for *pac* expression in evaluation of the two promoter approach.

Another point of consideration regarding the use of two promoters was their configuration within the expression cassettes. It has been described that two active transcription units linked in *cis* can influence each other, usually in a suppressive manner, a phenomenon called promoter or transcriptional interference [336,337,373–376]. This suppressive effect can happen upstream or downstream of the nearby active gene and is dependent on the position and strength of the promoters involved, and among other things, the state of the chromatin surrounding the expression cassette [336,374,377,378]. The mechanisms leading to this perturbation of one transcription unit by another are diverse and include *e.g.* read-through from the upstream transcription unit into the downstream unit, thereby disrupting the binding of transcription factors and other DNA-binding proteins, competition between promoters for transcription factors, enhancers or their binding proteins or topological changes in the DNA induced by transcription such as supercoiling [337,373,374,379,380]. However, the interplay between all the *cis*-acting transcriptional elements is intricate, and a clear mechanism for this phenomenon has yet to be described. Because of this, it was hard to predict which promoter–gene combination and arrangement in the retroviral vector would lead to highest *SERPINA1* expression. Thus, a series of combinations were evaluated: *SERPINA1* driven from pPGK, pEF1a, and pEFS, and the expression cassette placed 5' of the *pac* cassette in some constructs, and 3' in others, resulting in a total of six gamma-retroviral transfer plasmids. As our focus was optimizing *SERPINA1* expression, permutations of different promoters were omitted for the *pac* gene. Instead, expression of the *pac* gene was driven by pEFS when *SERPINA1* was expressed from pPGK, and by pPGK when pEFS or pEF1a were used for *SERPINA1* expression. It was avoided to use the same promoter twice in the same construct to obviate possible unwanted recombination events.

As detailed above, the second strategy was to test the efficiency of bicistronic expression using the established EMCV IRES sequence to co-express *pac.* This strategy has been shown to function more efficiently in some cases than using a second internal promoter [333]. A second advantage of utilizing an IRES sequence is that all cells will express *pac* as well as *SERPINA1* after antibiotic selection because one long mRNA containing both genes is produced during transcription of the expression cassette. This is not necessarily the case when two promoters are used as only one of the transgenes may be expressed while the promoter of the second gene becomes silenced. However, concerns regarding the IRES approach were raised by the fact that oftentimes the gene downstream the IRES sequence is expressed at markedly lower levels compared to the upstream gene [381]. Thus, as maximizing AAT yield was our main focus, *SERPINA1* was only tested in a position 5' of the IRES sequence, and expression from pPGK and pEFS were compared in two constructs. The EF1a promoter was not used

in an IRES construct due to its large size and the fact that the IRES sequence by itself is larger than pPGK and pEFS combined. Thus, for this construct a massive drop in viral titers would have been expected, prompting us to refrain from cloning and testing this vector. Taken together, all these considerations led us to the construction of the eight gamma-retroviral transfer vectors depicted in Figure 6. Although making predictions regarding the expected performance of these constructs was almost impossible due to all the aforementioned factors influencing expression, from a hypothetical point of view, our best guess regarding the construct becoming the lead candidate among all the vectors designed was construct #194 due to several reasons: First, with a size of the expression cassette of ~4500 base pairs, it was one of the smallest constructs suggesting that resulting viral titers would most likely be higher than those of larger cassettes [338]. Second, as detailed above, it contains an IRES sequence instead of a second internal promoter, thus minimizing the risk of transcriptional interference on one hand, and guaranteeing expression of both transgenes after antibiotic selection on the other. And third, it has been described that pEF1a yields ~4-fold higher transgene expression than pPGK in primary MSCs as well as different cell lines [362,364]; assuming that expression from pEFS is about half of what can be achieved which full length EF1a [329], we were expecting that pEFS would still be more potent than pPGK, thus making construct #194 preferable to construct #193 in theory. Indeed, all these predictions proved to be accurate, which will be described in the following chapters in greater detail.

4.2. Viral titers

With regard to the viral titers obtained with the *SERPINA1* constructs, the highest value reached, [3×10^5 TU/mL], appears relatively low at first glance. However, the procedure of transduction included the use of adherent cells without the addition of compounds neutralizing negative charges, such as the cationic PLL. These chemicals are oftentimes added to improve transduction by minimizing repulsion between cells and viral particles [382–384]. Such being the case, the conditions we chose were suboptimal for transduction. However, we were interested in comparing the titers of the constructs in order to transduce our cells, primary human MSCs, with the same amount of viral particles in subsequent experiments. Thus, we chose the fastest and easiest way of transducing the cells, resulting in the lower absolute titers observed. A second issue regarding *SERPINA1* construct titers is the negative impact of a larger genetic payload on viral titers. This effect has been described for lentiviral vectors, with the reason for decreased titers linked to inefficient incapsidation of larger viral RNA genomes into infectious particles [338,339,385]. In these publications the addition of ~1000 bases to the provirus led to a ~10-fold decrease of lentiviral titers. For the retroviral vectors used here the effect was much more pronounced: In our hands, the addition of ~1000 bases to the expression cassette in constructs in which *SERPINA1* is driven from pEF1a results in a massive drop in

titers of close to two log units. This discrepancy may result from the different transduction characteristics of VSV.G-pseudotyped lentiviral vectors, and GaLV-pseudotyped retroviral vectors. Alternatively the suboptimal conditions used for transduction in the titration experiments may have a larger impact on viral supernatants which have low titers, leading to disproportionally low results. However, apart from the constructs containing pEF1a, all viral constructs yielded comparable titers.

4.3. Transduction of primary MSCs and expression of transgenic AAT

The transduction efficacy and transgenic AAT protein expression were assessed in two ways: First, the percentage of cells intracellularly staining positive for AAT as well as the MFI of these cells used as an indicator of expression strength were measured shortly after transduction by flow cytometry. Second, after pure populations of transduced cells were generated by antibiotic selection with puromycin and expanded in a long-term culture, the average number of viral integrations per cell in the bulk population was analyzed by qPCR, and AAT secretion from a defined number of plated cells in a distinct volume over a specified time period was measured by ELISA. This gave us an opportunity to compare the expression constructs at a time when the MSCs were in early passages following transduction, and at a point when the cells were in higher passages after culture for several weeks and subjected to *ex vivo* procedures such as cell expansion or antibiotic selection. This is important for the potential application of these cells in a gene therapy setting. The MSCs at higher passages having undergone these *ex vivo* manipulation steps more closely resemble the final cell product as compared to the cells analyzed shortly after transduction. The relative performance of the constructs tested stayed the same at different times, *i.e.* the same constructs yielded good results in all experiments, and the "bad" vectors were inferior in all analyses. It was thus possible for us to conclude that the results observed were constant over time and not influenced by MSC expansion or treatments such as antibiotic selection, mirroring the properties of the expression constructs. This was reassuring regarding our choice of lead construct: Since our transduction and expression results did not appear to be affected by outside influences such as selection or expansion processes, it was fair to assume that the vector in which *SERPINA1* is driven by the EFS promoter and *pac* linked via an IRES sequence would probably yield good results under all circumstances.

Culturing cells for extended culture time as described above would most likely have enabled us to observe any potential unwanted effects such as silencing of gene expression [386] or cytotoxicity of AAT overexpression. We could not detect these phenomena in any of the experiments performed, thus we could assume that genetic modification of primary human MSCs with our retroviral vectors leads to non-cytotoxic, long-term transgenic AAT expression. This is of great importance for a cell-based gene therapy approach, since the therapeutic benefit relies on stable expression of the therapeutic transgene over a prolonged period of time. As of yet, it is not clear how long MSCs persist in the

human body after administration, but data generated in animal models indicate that human MSCs can live in rat lungs for several weeks [387]. Thus, it was crucial to confirm stable AAT expression from our transduced cells over a longer period of time. This result was also supported by data generated later in this project during the production process of large MSC batches for *in vivo* experiments: AAT levels were constant even after cryopreservation of transduced and selected MSCs, thawing of the cells and expansion, indicating that transgene silencing is not a problem in our approach. As mentioned above, it is also critical that long-term transgene expression is not toxic for the cells. In some preclinical gene therapy studies, significant toxicity of the therapeutic transgene necessitated the use of complex expression systems [388]; AAT however, is used in extremely high doses in clinical studies for AAT deficiency without any signs of toxicity of the protein [321,389]. Also in our case, when AAT is permanently overexpressed from constitutive promoters in MSCs, we did not perceive any signs of toxicity, even during prolonged culture periods: During the generation of large MSC batches, AAT-MSCs fulfilled all quality specifications for MSCs, viability was constantly >90%, and results were comparable to the ones generated from non-transduced MSCs, thus making AAT-MSCs a well-suited candidate for the use in a gene therapy approach.

Another important point is that when transducing primary MSCs with our eight retroviral supernatants, it was striking that although the cells had been treated with the same amount of viral particles for each construct, transduction efficacies were not similar as might have been expected (Figure 8): MSCs transduced with supernatants #161 and #164 (in which *SERPINA1* expression is driven from pEF1a) only reached transduction efficacies of about 10–30% of the ones measured with #160, #163, #194 (all three constructs which contain pEFS to express *SERPINA1*) or #193 (pPGK_SERPINA1_IRES_pac), while #159 and #162 (constructs in which *SERPINA1* expression is driven by pPGK) yielded intermediate results. As the constructs producing these low results were also the ones having the lowest titers, we speculate that there might be a correlation between titers and transduction efficacies. In order to treat MSCs with the same amount of viral particles per construct, very different volumes of viral supernatant were used in these experiments: For supernatants with high viral titers such as #160, #163, #193 or #194, only a few microliters were pipetted onto the cells, whereas almost pure viral supernatant was needed for constructs #161 and #164 to reach the same MOI. Viral supernatant is basically DMEM containing 10% FBS that has been incubated on a confluent layer of 293T cells for 24–36 hours. Thus, it is depleted of nutrients but full of byproducts secreted from the cells that might be inhibitory to transduction as it has been described for empty envelope proteins shed from packaging cells or non-transducing viral particles [390]. Adding pure viral supernatant to the MSCs might create an unhealthy environment for the cells, and the waste products present in the supernatant might impede transduction, both factors together possibly giving an explanation why transduction efficacies of constructs #161 and #164 were that low.

Another issue was that although the titers of the remaining supernatants were similar, transduction efficacies were not; there appeared to be a dependence of the results on the promoter used: All constructs containing pEFS reached similar high values, while the results achieved with pPGK vectors tended to be lower. Furthermore, we showed that AAT expression from pPGK-based constructs is also lower in MSCs than that seen from pEFS-based vectors (Figure 9). This might have led to cells expressing low levels of AAT ending up in the negative gate during flow cytometry analysis. If this was the case, the transduction efficacies of pPGK constructs would have been underestimated, potentially explaining the results observed. The AAT expression seen from vector #193, a construct containing the PGK promoter and an IRES sequence instead of a second promoter, was higher, and transduction efficacies obtained with this construct were more similar to that seen with pEFS constructs, which would support the abovementioned hypothesis. VCN data from bulk populations of transduced and selected MSCs, however, contradict this idea. Also in these analyses, which are independent of the strength of AAT expression, pPGK-based constructs, especially the ones containing a second promoter, fared poorly (Figure 11), thus confirming the flow cytometry data and indicating that these constructs indeed lead to lower transduction efficacies.

Due to high donor-to-donor variability, in order to compare transduction efficacies as described above, it was necessary to normalize the values determined in each experiment to the highest result measured in the same run. The fact that MSCs derived from different donors yield very diverse results when the same experiment is performed, is a common problem in MSC research [391,392]. A representative example of the impact of the cell donor on transduction efficacies is shown in Figure 30. A 5-fold difference was seen in transduction efficacies when using the same viral supernatant on cells derived from different donors. It is worth mentioning, however, that despite the variability in absolute numbers, the relative pattern of the results was the same, no matter which donor was used.
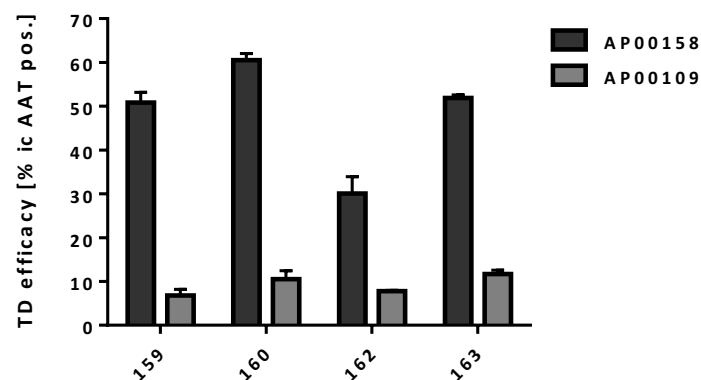

Figure 30: **Impact of cell donor on transduction efficacies achieved with constructs #159, #160, #162, and #163.** Normalized transduction efficacies differed by the factor 5 between 2 cell donors. Primary human MSCs derived from 2 healthy donors (AP00109 and AP00158) were transduced with viral supernatants #159, #160, #162, and #163 at MOI 0.25, and transduction efficacies were

assessed by intracellular staining for AAT and subsequent flow cytometric measurement 72 hours after transduction. Bars represent average values of 2 independent transduction experiments ± SD.

In the present study we also compared the various constructs by values not impaired by donor variability, but depending solely on the expression construct: As all flow cytometry experiments performed to compare the eight gamma-retroviral constructs were measured using the same settings, absolute MFI values of AAT-positive cells could be compared as a measure of expression strength. The same is true for VCN determination which was performed after antibiotic selection of the bulk cell population; as such, the selection and subsequent expansion processes compensate for the different transduction efficacies. Moreover, for determination of AAT content in cell culture supernatants by ELISA, the same experimental scheme was applied in all experiments: The same numbers of cells per cm^2 were plated, the same volume of medium was added and incubated for the same time on the cells before AAT protein content was determined. Thus, the (absolute and relative) transduction and expression results generated provided a good platform for characterizing the system.

Subsequent experiments led us to exclude pEF1a-driven constructs. As described above, transduction efficacies achieved on primary MSCs with these supernatants were extremely low, probably due to very low viral titers resulting from larger genetic payload sizes as compared to the other constructs. The low transduction efficacies suggest that a high percentage of cells harvested from a healthy donor will not get gene-modified and thus be eliminated during antibiotic selection. This is bad not only from an economic point of view, but also implies that the remaining transduced cells will have to undergo more population doublings to reach cell numbers sufficient for treating a patient. This should be avoided as cells in lower passages are thought to produce better outcomes in clinical trials for inflammatory diseases including GvHD [393]. To accept all these disadvantages and still use the pEF1a-driven constructs would only have made sense if AAT expression would have been markedly higher in comparison to the other constructs. Although it has been described that the first intron of pEF1a is required for high gene expression [394,395], and the intron-less EFS promoter has been shown to yield expression approximately half of what is achievable with the full-length promoter in HSCs [329], in our hands both promoters were performing equally regarding AAT expression, suggesting that the lack of the first intron has no influence on transgene expression in human bone-marrow MSCs. Viral titers and transduction efficacies were highest in pEFS constructs. Thus, there was no reason to further evaluate constructs comprising pEF1a. While performing these experiments, it also became clear that expression vectors using pPGK were not as efficient as pEFS-based constructs, at least when two promoters were used: Transduction efficacies and AAT expression were lower than those achieved with pEFS constructs in all cases. Only the pPGK construct that used an IRES sequence for bicistronic *pac* gene expression yielded transduction efficacies comparable to pEFS vectors, thus this

construct was further characterized to include at least one construct in which *SERPINA1* was not driven from pEFS. The remaining four constructs (#160, #163, #193, and #194) achieved similar results with respect to transduction and AAT expression, thus it was difficult to select a lead candidate based only on these parameters. However, the cell numbers after transduction with these supernatants and antibiotic selection varied greatly. Despite transduction efficacies being similar for all constructs, both IRES vectors yielded similar cell numbers after selection, while MSC content was markedly decreased for the supernatants in which the two genes were expressed from two different promoters (Figure 13). This suggested that in these constructs *pac* gene expression was too low for the cells to survive antibiotic selection with puromycin at the used concentration. Another fact supporting this idea was that for the IRES constructs cell numbers also agreed well with transduction efficacies determined, *i.e.* 50% transduction efficacy would result in approximately 50% of the transduced cells surviving the selection process during the first days of selection, while the percentage of surviving cells was much lower for the two promoter constructs. These results suggest that the two transcription units present in these vectors perturbed one another, a phenomenon fairly common in gene therapy settings called transcriptional or promoter interference [373,374,379,380]. It has *e.g.* been described that during the development of a polycistronic vector for liver-directed gene therapy, a pronounced decrease in expression of the transgenes was observed, and that this drop in expression was found to be due to promoter interference between the CMV and the EF1a promoter [337]. While in this publication the effect was bidirectional, *i.e.* the upstream promoter impaired transgene expression from the downstream promoter and *vice versa*, in our case the effect was unidirectional. *SERPINA1* expression was the same for all three pEFS constructs, indicating that the pPGK_pac transcription unit did not have an impact on the pEFS_SERPINA1 unit. Thus, the differences in *pac* expression seen may result from pEFS, which is very strongly activated in MSCs, competing with the weaker PGK promoter for the binding of transcription factors, enhancers or other DNA-binding proteins, resulting in a decrease in *pac* expression in the constructs comprising two promoters. The fact that the IRES constructs were not affected by this phenomenon of transcriptional interference in our setting would support this hypothesis. Although *pac* expression might be lower than *SERPINA1* expression in the IRES-based constructs as described for gene expression downstream of an IRES sequence [381], it was sufficient for the selection process.

Another aspect we analyzed was if different configurations of the expression units (5' *vs.* 3') in the expression cassette could have an influence on AAT expression. Swapping the position of the *SERPINA1* unit in the expression cassette did not seem to have an impact on AAT expression. This may be because pEFS is considerably strong in MSCs, so that possible effects on AAT expression caused by the position of the transcription units are too minor to be noticed. Cell numbers obtained after antibiotic selection (Figure 13), however, suggest a position effect. Transduction efficacies for

cells transduced with constructs #160 and #163 were similar. Average cell numbers after antibiotic selection were different for these two constructs by more than factor 2, suggesting that the position of the *pac* unit in relation to the *SERPINA1* unit might play a role in how strong transcriptional interference impairs *pac* gene expression.

Based on these results, construct #194 (pEFS_SERPINA1_IRES_pac) was selected as our lead candidate for preclinical evaluation.

4.4. Comparison of gamma-retroviral with lentiviral vector

Another aim of this study was to further optimize AAT expression by evaluating a second viral backbone. In addition to gamma-retroviral vectors, lentiviral vectors are the only viral vectors currently used for clinical applications leading to stable integration of genetic information into the host genome and a permanent modification of the host cell and its progeny [396,397]. Since MSCs are dividing relatively rapidly, transient cell modification would result in a dilution effect fairly quickly, so that only by applying permanent modification techniques a long-lasting therapeutical effect can be achieved. Lentiviruses such as HIV-1 belong to the same family of *Retroviridae* as gamma-retroviruses and are also single stranded, positive-sense RNA viruses. Both viral vectors can transfer genetic payloads of approximately 7–10kb [398,399]. The production of gamma-retro- and lentiviral supernatants is similar, as are the transduction procedures. All these factors enable a direct comparison of both vector systems. Our lead expression cassette was subcloned into the pCCL backbone, and viral supernatants were generated. Although the genetic payload of the lentiviral vector is approximately 1kb larger due to more regulatory viral sequences being included between the LTRs, the titers achieved on HT1080 cells were higher than those seen for the retroviral supernatants. The main difference between these two viral vectors is that while gamma-retroviruses need dissolution of the nuclear membrane of the host cell for successful insertion of their genome into the host DNA, lentiviruses transfer their pre-integration complex into the nucleus through the intact nuclear envelope. Because of this, retroviral transduction is limited to mitotic cells, while lentiviral vectors can also transduce growth-arrested and terminally differentiated cells [400–402]. This phenomenon was observed in the transduction experiments performed using MOIs ranging from 0.25–5.0: While for the gamma-retroviral supernatant, there was only a very slight increase in normalized transduction efficacy when the MOI was increased 10-fold (from ~50% of the maximum transduction achieved in each experiment at MOI 0.25 to ~53% at MOI 2.5), lentiviral transduction went from ~20% of maximum at MOI 0.25 to ~90% at MOI 2.5, indicating that at MOI 0.25 almost all dividing cells were transduced with the retroviral supernatant, so that the maximum transduction possible was reached. With the lentiviral supernatant, transduction efficacies were less than half of that seen with the retroviral vector at the lowest MOI, but rose in a dose-dependent manner when more viral particles

were added to the cells, until at the highest MOI tested more than 80% of MSCs were gene-modified. It is possible that 100% of the MSCs could be transduced using the lentiviral vector when using higher MOIs.

Analyses of VCNs in the bulk population of cells after selection, of MFIs in non-selected cells, and of AAT expression in pure populations of selected MSCs revealed the same pattern as seen for transduction efficacies: a plateau of values generated with the gamma-retroviral vector and a dose-dependent increase measured after transduction with the lentiviral supernatant. This suggests that transduction and transgene expression follow the same pattern and that the retroviral vector has a different transduction behavior from the lentiviral vector. No increase in VCNs or AAT expression after transduction with the gamma-retroviral supernatant at higher MOIs was seen, although this would have been expected, since in theory the mitotic cells should have acquired more copies of the transgene per cell with increasing MOIs. As this plateau effect was observed for cells derived from all three donors tested and therefore did not appear to be influenced by the MSCs or their source, we hypothesized that it was linked to the gamma-retroviral supernatant. Indeed it has been described that molecules present in retroviral supernatants such as free envelope glycoproteins or negatively charged molecules secreted from the producer cell line such as glycosaminoglycans or proteoglycans can interfere with transduction at high MOIs [384,390,403–405]. For transductions at lower MOIs, the volume of viral supernatant used was low, suggesting that potential repressive effects on transduction would have been lower; at high MOIs, however, when larger volumes of supernatant were used, a higher amount of inhibitory factors could be present potentially resulting in the non-linear transduction observed with the gamma-retroviral supernatant.

Considering the results generated in comparing the gamma-retroviral and lentiviral vectors, it still is not clear which vector system is optimal in this setting. If maximum transduction efficacy and highest AAT expression were desired, and scalable transduction was an aim, the lentiviral vector appears preferable to the gamma-retroviral. However, if the goal was not to reach maximum transduction levels, but if a well-balanced ratio between AAT expression and number of integrations per cell was required, the gamma-retroviral system appears to be superior, since much less viral supernatant would be needed employing the gamma-retroviral system to yield this result.

Importantly, regulatory agencies are less likely to approve a cell therapy product having high levels of vector integrations due to safety concerns: The more viral integrations, the higher the chance that regulatory elements such as promoters or enhancers included in the provirus may interfere with the surrounding chromatin of the host cell, which could lead to deregulation of nearby oncogenes and insertional transformation [185–187]. The lentiviral integration pattern is thought to be safer than the retroviral [406–411]. However, to the author's knowledge, no case of genotoxicity has been described for

human MSCs, for either vector types used in the present study, SIN gamma-retroviral and SIN lentiviral vectors.

With regards to economic factors: If the desired outcome was maximum transduction, the lentiviral supernatant at an MOI of 5.0 was most sufficient. However, much more viral supernatant would be needed in this approach as compared to aiming for transduction efficacies of about half and expression levels of ~2/3 of the maximum, which required 20-fold less volume of gamma-retroviral supernatant in our preclinical experiments. The first approach would therefore be more expensive, while it is unknown if maximum transduction and expression are required to achieve a therapeutic benefit. Also, in a clinical gene therapy setting, it is preferable to treat as many patients as possible with the same batch of viral supernatant to ensure optimal comparability of the results. Using producer cell lines expressing the MLV gagpol and the GaLV env, as it is commonly done for the generation of gamma-retroviral supernatants, it is possible to produce batches of high-titer supernatants in liter volumes for clinical trials [412–414]. To establish such scale-up production processes is more difficult for lentiviral vectors, since due to the toxicity of the VSV.G protein there are no GMP-compliant packaging cell lines for VSV.G-pseudotyped lentiviral vectors available to date [415]. Taken together, both viral vectors have advantages and disadvantages, and further experiments, especially assessing the amount of MSCs and AAT needed to achieve a therapeutic benefit, need to be performed to be able to select the viral vector that is better suited for the present application.

4.5. Functionality of transgenic AAT

The next aim was to confirm the functionality of transgenically expressed AAT. AAT is normally primarily expressed in hepatocytes (70–80%), but neutrophils, mononuclear phagocytes, intestinal epithelial and lung alveolar cells are also able to synthesize small amounts of the protein [217,257]. Bone marrow derived MSCs, however, are not thought to produce AAT naturally [243]. AAT is a glycoprotein with a highly ordered tertiary structure that is co- and posttranslationally modified, and whose function depends on a conformational transition from "stressed" to "relaxed" during binding to proteases [231,251,416,417]. Because it is a secreted protein, it contains a targeting signal that is cleaved by signal peptidase, allowing secretion. To confirm that AAT expression in MSCs results in a correctly cleaved, N-glycosylated and folded protein, thereby preserving AAT functionality, a functional assay of neutrophil elastase inhibition by AAT was used. The assay confirmed that concentrated supernatants from serum free cultures efficiently inhibited neutrophil elastase, demonstrating that AAT secreted from transduced MSCs is functional. MSC-derived AAT was also found to inhibit neutrophil elastase with approximately the same efficiency as natural AAT isolated from human plasma, currently used in clinical trials of AAT augmentation for AAT deficiency [321].

4.6. *In vivo* mouse model of elastase-induced lung emphysema

We next set out to demonstrate a proof of principle for AAT-MSC-based treatment of inflammatory lung diseases using an *in vivo* model.

COPD is an extremely heterogeneous disease with many different pathophysiological aspects such as a chronic inflammatory response to inhaled irritants, emphysema, small airway fibrosis and mucus hypersecretion, leading to an irreversible, progressive airflow limitation and loss of lung function over time [8,11]. It is extremely difficult to mimic all these symptoms in one animal model at once, especially because the pathology of the small airways is hard to reproduce in mouse models due to the limited airway branching seen in small animals [418]. The standard *in vivo* model used for COPD is a cigarette smoke-induced model, since the injury is caused by the same insult as in humans, and many symptoms that are comparable to the human disease such as chronic lung inflammation, impaired lung function, emphysema, mucus hypersecretion, and small airway wall thickening and remodeling are induced [8]. However, this model requires several months of exposure to cigarette smoke before emphysematous changes and alterations in lung function occur, thus making it very expensive and also not suitable. More importantly, it cannot fully reproduce the severity of the human disease, but resembles a fairly mild COPD instead (comparable to GOLD stage 1 or 2), while in humans the morbidity and mortality occurs in higher GOLD stage diseases [418]. For example, pulmonary lesions do not appear to progress after discontinuation of smoke exposure in the murine model, but this is the case in human disease [418].

A second commonly applied *in vivo* COPD model is the elastase-induced emphysema model. This model was developed based on two observations: First, it was described in the 1960s that patients suffering from AAT deficiency develop early emphysema and COPD [200,419]. And second, around the same time, the induction of emphysema in rats by installation of the protease papain was reported [201]. It is generally accepted that a protease-antiprotease imbalance is one of the major pathogenetic factors for the development of smoke-induced emphysema in COPD patients. The underlying hypothesis is that proteases, which are released from inflammatory cells recruited to the small airways by cigarette smoke, destroy the parenchymal matrix of the lung, leading to emphysema [3,418,420]. On these grounds, the elastase-induced model was thought to be appropriate as a proof of concept study of AAT-MSCs. Moreover, the elastase model is a rapidly inducible short-term model, thus allowing a quick assessment of the potential therapeutic benefit of a treatment; mice can be analyzed after 21 days in this model. In addition, the elastase model generates emphysema from a single application of elastase, while in the smoke-induced model mice usually have to be subjected to cigarette smoke twice daily [421,422]. The elastase model is preferable when therapeutic agents for alveolar repair and regeneration are evaluated: In contrast to lesions in the smoke-induced model, emphysema in the elastase model is permanent and additionally more

severe, and has been described to even continue progressing for more than five months after instillation of elastase [341,342], making it possible to assess a potential therapeutic benefit more easily [418,420].

MSCs have been described to contribute to lung regeneration in various diseases [142]. Thus, we tested the therapeutic effect of two applications of AAT-MSCs in the porcine pancreatic elastase (PPE)-induced emphysema model in comparison to non-modified MSCs [133]. Our hypothesis was that AAT-MSCs will have an improved therapeutic effect based on an additive, or more than additive action of AAT and MSCs in comparison to non-modified MSCs.

It is surprising that even though the diagnosis of COPD in humans as defined by GOLD guidelines is based on pulmonary function measurements, specifically FEV and FVC, these parameters are oftentimes not analyzed when performing *in vivo* COPD models [343]. Non-invasive methods to analyze lung function parameters like whole body plethysmography have been criticized by some researchers as being flawed for the analysis of airway mechanics [423]. In contrast, invasive methods are believed to produce more sensitive and specific results [343]. Through collaboration with the Comprehensive Pneumology Center, we were able to employ invasive lung measurements using the Buxco system to determine parameters such as FEV_{100ms} (which is the murine equivalent to FEV_1 in humans), FVC, Cdyn and Cchord (both measures for lung compliance), as well as IC and VC in order to analyze the outcome of the treatment in our *in vivo* model [343].

The experimental group of mice that received only PBS served as the negative control in our study, and thus was excluded from statistical analysis since comparing the other groups with this group would yield statistically significant results without contributing additional information regarding a therapeutic potential of the treatment *vs.* the disease groups, which was the main focus of our analyses.

We did observe a statistically significant amelioration of five out of six important pulmonary function parameters analyzed when mice were treated with elastase plus AAT-MSCs as compared to elastase only. These parameters included FEV and FVC, on which the diagnosis of human COPD is based, thus providing an indication that these results might be highly relevant for the human disease. We also saw a dramatic improvement in the two factors describing lung volumes, IC and VC, as well as Cchord, which is a measure for compliance, representing the ability of the lung to stretch and expand. Due to the breakdown of lung tissue and the resulting airspace enlargement in emphysema, this parameter is drastically increased in the model we employed, and treatment with AAT-MSCs reversed this increase by >40% (mean Cchord: PBS: 0.0431; elastase: 0.09291; elastase + AAT-MSCs: 0.07182). The only pulmonary function parameter that did not reach statistical significance is the second measure for compliance, Cdyn; however, the same trend towards an amelioration after treatment with AAT-MSCs was clearly visible. Treatment with non-modified MSCs did not result in a

statistically significant improvement of any of the lung function parameters analyzed, confirming that the genetic modification of MSCs with AAT created an additional beneficial effect and improved the efficacy of MSC treatment.

As for pulmonary functions, application of AAT-MSCs resulted in a clear improvement of the emphysema score of ~50% that was also statistically significant ($P < 0.001$). Again, the effect seen with non-modified MSCs was substantially smaller, and did not reach statistical significance. This indicates that AAT has not only an additional beneficial effect on lung function when combined with MSCs, but also on repair and regeneration of pulmonary tissue. This finding could shed light onto the mode of action of AAT in this model. It has been described that the elastase used to induce emphysema is cleared from the mouse lungs within 24 hours [424], but that the airspace enlargement continues even when the elastase is long gone [331,425]. Together, this suggests that the beneficial effect of AAT in this model is not solely due to protease inhibition, but has an additional immunomodulatory component as well, a very well recognized phenomenon in protease biology [216,257,426].

During analysis of the lung sections it was seen that apart from the amelioration of lung destruction in mice treated with AAT-MSCs, there was also a profound increase in inflammatory cells in the tissue, reflected by a significantly higher inflammation score when compared to mice receiving elastase alone. This was true for both mouse groups receiving MSCs (MSCs: $P < 0.01$; AAT-MSCs: $P < 0.001$). This finding was corroborated by analysis of total and differential cell counts in the BALF of the mice, which revealed a drastic increase in absolute and relative lymphocyte and eosinophil counts in all mice receiving either MSCs or AAT-MSCs. The inflammatory response was more distinct in the group receiving AAT-MSCs, suggesting that the murine immune cells may be reacting against the human MSCs, and potentially against the human AAT protein being secreted from the cells. Indeed, it has been described that the repeated administration of human AAT and human albumin is immunogenic in immunocompetent mice [427]. However, since MSCs have been described to be immune-evasive in many studies [99,428–430], an alternative hypothesis would be that the inflammatory infiltrate is needed to effect tissue repair and regeneration [431]. Thus, further studies to analyze this inflammatory response are underway, *e.g.* a repetition of the same model with murine MSCs expressing murine AAT.

Interestingly, despite the increase in lymphocytes and eosinophils, total cell numbers in the BALF of mice receiving MSCs did not change significantly as compared to the mice treated with elastase only. When analyzing absolute differential cell numbers, there was a trend towards lower macrophage counts in both MSC groups; however, these differences did not reach statistical significance. Still, when calculating relative proportions of the cells in the BALF, there was a significant decrease in macrophages, which are one of the major cell types involved in the pathogenesis of COPD, in both

mouse groups receiving MSCs compared to the elastase group. The second effector cell type in COPD is neutrophilic granulocytes. In this model of emphysema these cells were drastically increased after elastase instillation. Remarkably, four out of six mice had no neutrophils in their BALF after treatment with AAT-MSCs. These observations suggest that human MSCs, and even more human MSCs expressing human AAT, appear to exert immunomodulatory effects on the major cell types involved in the pathogenesis of the lung disease.

Native MSCs showed only a mild improvement of emphysema, and had a very minor effect on lung function parameters. This is in contrast to published studies [133,164,432,433], which describe a clear beneficial effect of MSC treatment in elastase-induced emphysema in mice. This discrepancy might be due to different experimental setups [133,164], diverging MSC numbers used [433], and different MSC sources analyzed [164]. Also, pulmonary function measurements were not always performed, the assessment of an amelioration of the disease was based on histological findings, where the effect of MSCs seems to be more pronounced (also in our case).

The model employed here is very stringent, since it is a model of treatment and not prevention. In our case, the first application of the cells was made seven days after elastase instillation when the animals had full-blown disease as compared *e.g.* to Tibboel and colleagues, who injected the cells either 24 hours before or after elastase treatment as a preventive measure at a time when the mice had not developed emphysema yet [432]. These factors may help explain the diverging results observed with non-modified MSCs in models of elastase-induced emphysema.

A question raised by the positive results obtained with AAT-MSCs is why the relatively moderate additional human AAT expressed from the MSCs led to such a dramatic improvement of lung function, as well as emphysema, as compared to the treatment with non-modified MSCs, when these mice were not AAT-deficient and had physiological AAT levels in their plasma. Average physiological AAT concentrations in the blood of female C57BL/6 mice have been described to be [~3mg/mL] [434]. The average amount of AAT produced *in vitro* by cells from the very batch of AAT-MSCs used in this *in vivo* study is ~1000ng/$1x10^5$ cells/48h as determined by ELISA. Considering that $5x10^5$ cells were instilled into the mice twice, one time on day 7, a second time on day 14, and the mice were sacrificed on day 21, the total amount of secreted AAT would be ~50µg, not considering half-life of the protein or cell death. The blood volume of mice is in the range of 1.5–2.5mL [435], thus the maximum systemic human AAT concentration without calculating any losses would be ~25µg/mL, which is still ~100-fold lower than physiological murine AAT concentrations, thus making it very unlikely that the results seen are due to actions of additional systemic AAT. Instead, our hypothesis is that the therapeutic effect observed in our work results from the locally increased levels of human AAT expressed from MSCs in the lungs of the mice, working its effects at the site of inflammation and injury. It has been suggested that AAT serum concentrations reaching 20% of physiological serum

levels are sufficient to protect the alveoli in humans [436]. Moreover, it has been also found that in humans, the distribution of AAT is fairly heterogeneous, and that *e.g.* in the epithelial lining fluid of the lower respiratory tract, AAT levels are only 10% of serum levels under physiological conditions [217], indicating that the addition of even small amounts of extra AAT might have even stronger effects in this tissue. Thus, we hypothesize that due to the instillation of the cells directly into the lung, the homing of the MSCs to the most damaged and inflamed sites, and the cumulative expression of AAT there, levels high enough to exceed the threshold for a beneficial effect could be achieved locally in the present study, leading to the therapeutic effects we observed. Another factor to consider is that physiological AAT levels in the mouse are twofold higher than the average levels in humans, which range between 0.9–1.75mg/mL [216]. Since we saw such impressive therapeutic results in the mouse, the therapeutic benefits in humans might be even stronger.

The efficacy of AAT-MSCs for the treatment of inflammatory lung diseases needs to be confirmed in additional *in vivo* models such as bleomycin-induced lung fibrosis or smoke-induced COPD, and the mechanisms by which AAT-MSCs are able to ameliorate lung function and effect pulmonary tissue repair and regeneration better understood. The inflammatory response elicited in the mouse lungs after treatment with MSCs should be studied in detail, *e.g.* by conducting a study with murine MSCs expressing murine AAT.

An interesting question that also needs clarification is how strong the additive effect of AAT and MSCs is in comparison to AAT protein isolated from human plasma alone in an efficacy model. Moreover, crucial questions regarding biodistribution and tumorigenicity of the cells after application as well as dosing and treatment regime have to be clarified in further studies.

It would also be interesting to assess the therapeutic potential of extracellular vesicles derived from AAT-MSCs. These microvesicles or exosomes, as already mentioned briefly in the introduction, are circular membrane fragments released from MSCs, that are involved in the transfer of cellular material and in cell-cell communication, and have recently emerged as a mechanism of MSC-mediated functions [437,438]. Since microvesicles have been described to maintain the functional phenotype of the parent cell [438], it is likely that they also exert beneficial functions in regard to inflammation and tissue damage. Indeed, MSC-derived microvesicles have been recently described to ameliorate acute lung injury and hypoxic pulmonary arterial hypertension in mice [167,439]. Thus, testing this approach might be worthwhile in the future.

In summary, this study provides the first proof of concept for the treatment of inflammatory lung diseases with MSCs transduced to express AAT. Application of these cells in a murine model of elastase-induced emphysema resulted not only in impressive repair and regeneration of lung tissue, but moreover also in significantly improved pulmonary function parameters, giving a first indication that this gene-modified MSC cell product might be well-suited for the treatment of COPD.

5. References

1.   Honeyman, M. & Harrison, L. Chronic Disease and Public Health. *Health (Irvine. Calif).* 23–44 (2011).

2.   WHO. The top 10 causes of death. Retrieved June 13, 2016. *Fact sheet N°310 (Updated May 2014)* (2014). at <http://www.who.int/mediacentre/factsheets/fs310/en/>

3.   Lomas, D. A. Does Protease-Antiprotease Imbalance Explain Chronic Obstructive Pulmonary Disease? *Ann. Am. Thorac. Soc.* **13 Suppl 2,** S130–7 (2016).

4.   Vos, T. *et al.* Years lived with disability (YLDs) for 1160 sequelae of 289 diseases and injuries 1990–2010: a systematic analysis for the Global Burden of Disease Study 2010. *Lancet* **380,** 2163–2196 (2012).

5.   Vos, T. *et al.* Global, regional, and national incidence, prevalence, and years lived with disability for 301 acute and chronic diseases and injuries in 188 countries, 1990–2013: a systematic analysis for the Global Burden of Disease Study 2013. *Lancet* **386,** 743–800 (2015).

6.   Bloom, D. E. *et al.* The Global Economic Burden of Noncommunicable Diseases. *World Econ. Forum* 1–46 (2011). at <http://ideas.repec.org/p/gdm/wpaper/8712.html>

7.   Global Initiative for Chronic Obstructive Lung Disease, I. Global Initiative for Chronic Obstructive Lung Disease: Global Strategy for The Diagnosis, Management, and Prevention of Chronic Obstructive Lung Disease. (2016). at <http://goldcopd.org/global-strategy-diagnosis-management-prevention-copd-2016/>

8.   Vlahos, R. & Bozinovski, S. Recent advances in pre-clinical mouse models of COPD. *Clin. Sci. (Lond).* **126,** 253–65 (2014).

9.   Morjaria, J. B., Malerba, M. & Polosa, R. Biologic and pharmacologic therapies in clinical development for the inflammatory response in COPD. *Drug Discov. Today* **15,** 396–405 (2010).

10.   Rennard, S. I. & Drummond, M. B. Early chronic obstructive pulmonary disease: definition, assessment, and prevention. *Lancet (London, England)* **385,** 1778–88 (2015).

11.   Groneberg, D. A. & Chung, K. F. Models of chronic obstructive pulmonary disease. *Respir. Res.* **5,** 18 (2004).

12.   Woodruff, P. G., Agusti, A., Roche, N., Singh, D. & Martinez, F. J. Current concepts in targeting chronic obstructive pulmonary disease pharmacotherapy: making progress towards personalised management. *Lancet (London, England)* **385,** 1789–98 (2015).

13.   Vestbo, J. *et al.* Global strategy for the diagnosis, management, and prevention of chronic obstructive pulmonary disease GOLD executive summary. *American Journal of Respiratory and Critical Care Medicine* **187,** 347–365 (2013).

14.   Barnes, P. J., Shapiro, S. D. & Pauwels, R. A. Chronic obstructive pulmonary disease: molecular and cellular mechanisms. *Eur. Respir. J.* **22,** 672–88 (2003).

15.   Roth, M. Pathogenesis of COPD. Part III. Inflammation in COPD. *Int. J. Tuberc. Lung Dis.* **12,** 375–80 (2008).

16.   Teramoto, S. 1. COPD pathogenesis from the viewpoint of risk factors. *Intern. Med.* **46,** 77–9 (2007).

17.   Molfino, N. A. Current thinking on genetics of chronic obstructive pulmonary disease. *Curr. Opin. Pulm. Med.* **13,** 107–13 (2007).

18.   Sampsonas, F., Karkoulias, K., Kaparianos, A. & Spiropoulos, K. Genetics of chronic obstructive pulmonary disease, beyond a1-antitrypsin deficiency. *Curr. Med. Chem.* **13,** 2857–73 (2006).

19.   Logan, W. P. D. Mortality in the London Fog Incident. *Lancet* **261,** 336–338 (1953).

20.   Ulvestad, B. *et al.* Increased risk of obstructive pulmonary disease in tunnel workers. *Thorax* **55,** 277–82 (2000).

21.   Peto, R., Chen, Z. M. & Boreham, J. Tobacco--the growing epidemic. *Nat. Med.* **5,** 15–7 (1999).

22.   Kiraz, K. *et al.* Chronic pulmonary disease in rural women exposed to biomass fumes. *Clin. Investig. Med. Médecine Clin. Exp.* **26,** 243–8 (2003).

23.   Mannino, D. M. & Buist, A. S. Global burden of COPD: risk factors, prevalence, and future trends. *Lancet (London, England)* **370,** 765–73 (2007).

24.   Heguy, A. *et al.* Gene expression profiling of human alveolar macrophages of phenotypically normal smokers and nonsmokers reveals a previously unrecognized subset of genes modulated by cigarette smoking. *J. Mol. Med. (Berl).* **84,** 318–28 (2006).

25.   Pierrou, S. *et al.* Expression of genes involved in oxidative stress responses in airway epithelial cells of smokers with chronic obstructive pulmonary disease. *Am. J. Respir. Crit. Care Med.* **175,** 577–86 (2007).

26.   Zandvoort, A. *et al.* High ICAM-1 gene expression in pulmonary fibroblasts of COPD patients: a reflection of an enhanced immunological function. *Eur. Respir. J.* **28,** 113–22 (2006).

27.   Løkke, A., Lange, P., Scharling, H., Fabricius, P. & Vestbo, J. Developing COPD: a 25 year follow up study of the general population. *Thorax* **61,** 935–9 (2006).

28.   Lomas, D. A. The selective advantage of alpha1-antitrypsin deficiency. *Am. J. Respir. Crit. Care Med.* **173,** 1072–7 (2006).

29.   Chorostowska-Wynimko, J. Targeted screening programmes in COPD: how to identify individuals with α1-antitrypsin deficiency. *Eur. Respir. Rev.* **24,** 40–5 (2015).

30.   Traclet, J., Delaval, P., Terrioux, P. & Mornex, J.-F. Augmentation therapy of alpha-1 antitrypsin deficiency associated emphysema. *Rev. Mal. Respir.* **32,** 435–46 (2015).

31.   Greulich, T. & Vogelmeier, C. F. Alpha-1-antitrypsin deficiency: increasing awareness and improving diagnosis. *Ther. Adv. Respir. Dis.* **10,** 72–84 (2016).

32.   Sakao, S. & Tatsumi, K. The importance of epigenetics in the development of chronic obstructive pulmonary disease. *Respirology* **16,** 1056–63 (2011).

33.   Smolonska, J., Wijmenga, C., Postma, D. S. & Boezen, H. M. Meta-analyses on Suspected Chronic Obstructive Pulmonary Disease Genes. *Am. J. Respir. Crit. Care Med.* **180,** 618–631 (2009).

34.   Keatings, V. M., Collins, P. D., Scott, D. M. & Barnes, P. J. Differences in interleukin-8 and tumor necrosis factor-alpha in induced sputum from patients with chronic obstructive pulmonary disease or asthma. *Am. J. Respir. Crit. Care Med.* **153,** 530–4 (1996).

35.   Pesci, A. *et al.* Inflammatory cells and mediators in bronchial lavage of patients with chronic obstructive pulmonary disease. *Eur. Respir. J.* **12,** 380–6 (1998).

36.   MacNee, W. Pathogenesis of chronic obstructive pulmonary disease. *Proc. Am. Thorac. Soc.* **2,** 258–66; discussion 290–1 (2005).

37.   Stănescu, D. *et al.* Airways obstruction, chronic expectoration, and rapid decline of FEV1 in smokers are associated with increased levels of sputum neutrophils. *Thorax* **51,** 267–71 (1996).

38.   Stockley, J. A., Walton, G. M., Lord, J. M. & Sapey, E. Aberrant neutrophil functions in stable chronic obstructive pulmonary disease: the neutrophil as an immunotherapeutic target. *Int. Immunopharmacol.* **17,** 1211–7 (2013).

39.   Stockley, R. A. Neutrophils and protease/antiprotease imbalance. *Am. J. Respir. Crit. Care Med.* **160,** S49–52 (1999).

40.   Hogg, J. C. *et al.* The nature of small-airway obstruction in chronic obstructive pulmonary disease. *N. Engl. J. Med.* **350,** 2645–53 (2004).

41.   Vernooy, J. H. *et al.* Local and systemic inflammation in patients with chronic obstructive pulmonary disease: soluble tumor necrosis factor receptors are increased in sputum. *Am. J. Respir. Crit. Care Med.* **166,** 1218–24 (2002).

42.   Rahman, I. Pharmacological antioxidant strategies as therapeutic interventions for COPD. *Biochim. Biophys. Acta* **1822,** 714–28 (2012).

43.   Rahman, I. & Adcock, I. M. Oxidative stress and redox regulation of lung inflammation in COPD. *Eur. Respir. J.* **28,** 219–42 (2006).

44.   Taggart, C. *et al.* Oxidation of either methionine 351 or methionine 358 in alpha 1-antitrypsin causes loss of anti-neutrophil elastase activity. *J. Biol. Chem.* **275,** 27258–65 (2000).

45.   Carp, H., Miller, F., Hoidal, J. R. & Janoff, A. Potential mechanism of emphysema: alpha 1-proteinase inhibitor recovered from lungs of cigarette smokers contains oxidized methionine and has decreased elastase inhibitory capacity. *Proc. Natl. Acad. Sci. U. S. A.* **79,** 2041–5 (1982).

46.   Janoff, A., Carp, H., Laurent, P. & Raju, L. The role of oxidative processes in emphysema. *Am. Rev. Respir. Dis.* **127,** S31–8 (1983).

47.   Shapiro, S. D. Proteolysis in the lung. *Eur. Respir. J. Suppl.* **44,** 30s–32s (2003).

48.   Shapiro, S. D. Proteinases in chronic obstructive pulmonary disease. *Biochem. Soc. Trans.* **30,** 98–102 (2002).

49.   Parks, W. C. & Shapiro, S. D. Matrix metalloproteinases in lung biology. *Respir. Res.* **2,** 10–9 (2001).

50.   Chorostowska-Wynimko, J. Disease Modification in Emphysema Related to Alpha-1 Antitrypsin Deficiency. *COPD J. Chronic Obstr. Pulm. Dis.* **2555,** 1–9 (2016).

51.   Pirozzi, C. & Scholand, M. B. Smoking Cessation and Environmental Hygiene. *Med. Clin. North Am.* **96,** 849–867 (2012).

52.   Rigotti, N. A. Smoking cessation in patients with respiratory disease: existing treatments and future directions. *Lancet. Respir. Med.* **1,** 241–50 (2013).

53.   Tønnesen, P. *et al.* Smoking cessation and COPD. *Eur. Respir. Rev.* **22,** 37–43 (2013).

54.   Poole, P. J., Chacko, E., Wood-Baker, R. W. B. & Cates, C. J. Influenza vaccine for patients with chronic obstructive pulmonary disease. *Cochrane database Syst. Rev.* CD002733 (2006).

55.   Mackay, A. J. & Hurst, J. R. COPD Exacerbations: Causes, Prevention, and Treatment. *Med. Clin. North Am.* **96,** 789–809 (2012).

56.   Rabe, K. F. *et al.* Global Strategy for the Diagnosis, Management, and Prevention of Chronic Obstructive Pulmonary Disease. *Am. J. Respir. Crit. Care Med.* **176,** 532–555 (2007).

57.   Decramer, M. *et al.* Chronic obstructive pulmonary disease. *Lancet* **379,** 1341–1351 (2012).

58.   Drummond, M. B. *et al.* Inhaled Corticosteroids in Patients With Stable Chronic Obstructive Pulmonary Disease. *JAMA* **300,** 2407 (2008).

59.   Liesker, J. J. W. *et al.* A Systematic Review of the Effects of Bronchodilators on Exercise Capacity in Patients With COPD. *Chest* **121,** 597–608 (2002).

60.   van Dijk, W. D., van den Bemt, L. & van Weel, C. Megatrials for Bronchodilators in Chronic Obstructive Pulmonary Disease (COPD) Treatment: Time to Reflect. *J. Am. Board Fam. Med.* **26,** 221–224 (2013).

61.   Gartlehner, G., Hansen, R. A., Carson, S. S. & Lohr, K. N. Efficacy and Safety of Inhaled Corticosteroids in Patients With COPD: A Systematic Review and Meta-Analysis of Health Outcomes. *Ann. Fam. Med.* **4,** 253–262 (2006).

62.   Herath, S. C. & Poole, P. Prophylactic antibiotic therapy for chronic obstructive pulmonary disease (COPD). *Cochrane database Syst. Rev.* **11,** CD009764 (2013).

63.   Mammen, M. J. & Sethi, S. Macrolide therapy for the prevention of acute exacerbations in chronic obstructive pulmonary disease. *Pol. Arch. Med. Wewnętrznej* **122,** 54–9 (2012).

64.   Marchetti, N. & Criner, G. J. Surgical Approaches to Treating Emphysema: Lung Volume Reduction Surgery, Bullectomy, and Lung Transplantation. *Semin. Respir. Crit. Care Med.* **36,** 592–608 (2015).

65.   Mulhall, P. & Criner, G. Non-pharmacological treatments for COPD. *Respirology* (2016).

66.   Aigner, C. Retransplantation. *Curr. Opin. Organ Transplant.* **20,** 521–526 (2015).

67.   Rennard, S. I. *et al.* The safety and efficacy of infliximab in moderate to severe chronic obstructive pulmonary disease. *Am. J. Respir. Crit. Care Med.* **175,** 926–34 (2007).

68.   Dentener, M. A. *et al.* Effect of infliximab on local and systemic inflammation in chronic obstructive pulmonary disease: a pilot study. *Respiration.* **76,** 275–82 (2008).

69.   van der Vaart, H., Koëter, G. H., Postma, D. S., Kauffman, H. F. & ten Hacken, N. H. T. First study of infliximab treatment in patients with chronic obstructive pulmonary disease. *Am. J. Respir. Crit. Care Med.* **172,** 465–9 (2005).

70.   Mahler, D. A., Huang, S., Tabrizi, M. & Bell, G. M. Efficacy and safety of a monoclonal antibody recognizing interleukin-8 in COPD: a pilot study. *Chest* **126,** 926–34 (2004).

71.   Thomas, E. D., Lochte, H. L., Cannon, J. H., Sahler, O. D. & Ferrebee, J. W. Supralethal whole body irradiation and isologous marrow transplantation in man. *J. Clin. Invest.* **38,** 1709–1716 (1959).

72.   Trounson, A. & McDonald, C. Stem Cell Therapies in Clinical Trials: Progress and Challenges. *Cell Stem Cell* **17,** 11–22 (2015).

73.   Schwartz, S. D. *et al.* Embryonic stem cell trials for macular degeneration: a preliminary report. *Lancet (London, England)* **379,** 713–20 (2012).

74.   Schwartz, S. D. *et al.* Human embryonic stem cell-derived retinal pigment epithelium in patients with age-related macular degeneration and Stargardt's macular dystrophy: follow-up of two open-label phase 1/2 studies. *Lancet (London, England)* **385,** 509–16 (2015).

75.   Reardon, S. & Cyranoski, D. Japan stem-cell trial stirs envy. *Nature* **513,** 287–8 (2014).

76.   Rama, P. *et al.* Limbal Stem-Cell Therapy and Long-Term Corneal Regeneration. *N. Engl. J. Med.* **363,** 147–155 (2010).

77.   Selden, N. R. *et al.* Central nervous system stem cell transplantation for children with neuronal ceroid lipofuscinosis. *J. Neurosurg. Pediatr.* **11,** 643–652 (2013).

78.   Gupta, N. *et al.* Neural stem cell engraftment and myelination in the human brain. *Sci. Transl. Med.* **4,** 155ra137 (2012).

79.   Kinoshita, M. *et al.* Long-term clinical outcome after intramuscular transplantation of granulocyte colony stimulating factor-mobilized CD34 positive cells in patients with critical limb ischemia. *Atherosclerosis* **224,** 440–445 (2012).

80.   Kawamoto, A. *et al.* Intramuscular Transplantation of G-CSF-Mobilized CD34 [+] Cells in Patients With Critical Limb Ischemia: A Phase I/IIa, Multicenter, Single-Blinded, Dose-Escalation Clinical Trial. *Stem Cells* **27,** 2857–2864 (2009).

81.   Ma, S. *et al.* Immunobiology of mesenchymal stem cells. *Cell Death Differ.* **21,** 216–225 (2014).

82.   Laurent, L. C. *et al.* Dynamic changes in the copy number of pluripotency and cell proliferation genes in human ESCs and iPSCs during reprogramming and time in culture. *Cell Stem Cell* **8,** 106–18 (2011).

83.   ClinicalTrials.gov a. Bethesda (MD): National Library of Medicine (US). 2000 Feb 29 – [retrieved 2016 Jun 15]. Search for Studies: Mesenchymal stem cell OR mesenchymal stromal cell. *ClinicalTrials.gov* at <https://clinicaltrials.gov/ct2/results?term=mesenchymal+stem+cell+OR+mesenchymal+stromal+cell&no_unk=Y>

84.   Prasad, V. K. *et al.* Efficacy and Safety of Ex Vivo Cultured Adult Human Mesenchymal Stem Cells (Prochymal[TM]) in Pediatric Patients with Severe Refractory Acute Graft-Versus-Host Disease in a Compassionate Use Study. *Biol. Blood Marrow Transplant.* **17,** 534–541 (2011).

85.   Le Blanc, K. *et al.* Mesenchymal stem cells for treatment of steroid-resistant, severe, acute graft-versus-host disease: a phase II study. *Lancet* **371,** 1579–1586 (2008).

86.   Carlsson, P.-O., Schwarcz, E., Korsgren, O. & Le Blanc, K. Preserved β-cell function in type 1 diabetes by mesenchymal stromal cells. *Diabetes* **64,** 587–92 (2015).

87.   Reinders, M. E. *et al.* Autologous bone marrow derived mesenchymal stromal cell therapy in combination with everolimus to preserve renal structure and function in renal transplant recipients. *J. Transl. Med.* **12,** 331 (2014).

88.   Reinders, M. E. J. *et al.* Autologous Bone Marrow-Derived Mesenchymal Stromal Cells for the Treatment of Allograft Rejection After Renal Transplantation: Results of a Phase I Study. *Stem Cells Transl. Med.* **2,** 107–111 (2013).

89.   Hare, J. M. *et al.* A Randomized, Double-Blind, Placebo-Controlled, Dose-Escalation Study of Intravenous Adult Human Mesenchymal Stem Cells (Prochymal) After Acute Myocardial Infarction. *J. Am. Coll. Cardiol.* **54,** 2277–2286 (2009).

90.   Hare, J. M. *et al.* Comparison of Allogeneic vs Autologous Bone Marrow–Derived Mesenchymal Stem Cells Delivered by Transendocardial Injection in Patients With Ischemic Cardiomyopathy. *JAMA* **308,** 2369 (2012).

91.   Forbes, G. M. *et al.* A phase 2 study of allogeneic mesenchymal stromal cells for luminal Crohn's disease refractory to biologic therapy. *Clin. Gastroenterol. Hepatol.* **12,** 64–71 (2014).

92.   Duijvestein, M. *et al.* Autologous bone marrow-derived mesenchymal stromal cell treatment for refractory luminal Crohn's disease: results of a phase I study. *Gut* **59,** 1662–9 (2010).

93.   Wilson, J. G. *et al.* Mesenchymal stem (stromal) cells for treatment of ARDS: a phase 1 clinical trial. *Lancet. Respir. Med.* **3,** 24–32 (2015).

94.   Weiss, D. J., Casaburi, R., Flannery, R., LeRoux-Williams, M. & Tashkin, D. P. A placebo-controlled, randomized trial of mesenchymal stem cells in COPD. *Chest* **143,** 1590–8 (2013).

95.   Friedenstein, A. J., Chailakhjan, R. K. & Lalykina, K. S. The development of fibroblast colonies in monolayer cultures of guinea-pig bone marrow and spleen cells. *Cell Tissue Kinet.* **3,** 393–403 (1970).

96.   Friedenstein, A. J., Piatetzky-Shapiro, I. I. & Petrakova, K. V. Osteogenesis in transplants of bone marrow cells. *J. Embryol. Exp. Morphol.* **16,** 381–90 (1966).

97. Friedenstein, A. J., Petrakova, K. V, Kurolesova, A. I. & Frolova, G. P. Heterotopic of bone marrow. Analysis of precursor cells for osteogenic and hematopoietic tissues. *Transplantation* **6,** 230–47 (1968).

98. Caplan, A. I. Mesenchymal stem cells. *J. Orthop. Res.* **9,** 641–50 (1991).

99. Ankrum, J. A., Ong, J. F. & Karp, J. M. Mesenchymal stem cells: immune evasive, not immune privileged. *Nat. Biotechnol.* **32,** 252–260 (2014).

100. Horwitz, E. M. *et al.* Clarification of the nomenclature for MSC: The International Society for Cellular Therapy position statement. *Cytotherapy* **7,** 393–5 (2005).

101. Stanko, P., Kaiserova, K., Altanerova, V. & Altaner, C. Comparison of human mesenchymal stem cells derived from dental pulp, bone marrow, adipose tissue, and umbilical cord tissue by gene expression. *Biomed. Pap. Med. Fac. Univ. Palacký, Olomouc, Czechoslov.* **158,** 373–7 (2014).

102. Portmann-Lanz, C. B. *et al.* Placental mesenchymal stem cells as potential autologous graft for pre- and perinatal neuroregeneration. *Am. J. Obstet. Gynecol.* **194,** 664–73 (2006).

103. Crisan, M. *et al.* A Perivascular Origin for Mesenchymal Stem Cells in Multiple Human Organs. *Cell Stem Cell* **3,** 301–313 (2008).

104. da Silva Meirelles, L., Chagastelles, P. C. & Nardi, N. B. Mesenchymal stem cells reside in virtually all post-natal organs and tissues. *J. Cell Sci.* **119,** 2204–13 (2006).

105. Fajardo-Orduña, G. R., Mayani, H. & Montesinos, J. J. Hematopoietic Support Capacity of Mesenchymal Stem Cells: Biology and Clinical Potential. *Arch. Med. Res.* **46,** 589–96 (2015).

106. Lama, V. N. *et al.* Evidence for tissue-resident mesenchymal stem cells in human adult lung from studies of transplanted allografts. *J. Clin. Invest.* **117,** 989–96 (2007).

107. Rolandsson, S. *et al.* Primary mesenchymal stem cells in human transplanted lungs are CD90/CD105 perivascularly located tissue-resident cells. *BMJ open Respir. Res.* **1,** e000027 (2014).

108. Dominici, M. *et al.* Minimal criteria for defining multipotent mesenchymal stromal cells. The International Society for Cellular Therapy position statement. *Cytotherapy* **8,** 315–317 (2006).

109. Prockop, D. J. & Oh, J. Y. Medical therapies with adult stem/progenitor cells (MSCs): A backward journey from dramatic results in vivo to the cellular and molecular explanations. *J. Cell. Biochem.* **113,** 1460–1469 (2012).

110. Günther, C., Hauser, A. & Huss, R. *Advances in pharmaceutical cell therapy : principles of cell-based biopharmaceuticals. ISBN 9789814616782*. (WORLD SCIENTIFIC, 2015).

111. Keating, A. Mesenchymal stromal cells: new directions. *Cell Stem Cell* **10,** 709–716 (2012).

112. Phinney, D. G. *et al.* MSCs: Science and Trials. *Nat. Med.* **19,** 812–812 (2013).

113. Pittenger, M. F. MSCs: science and trials. *Nat. Med.* **19,** 811 (2013).

114. Caplan, A. I. & Correa, D. The MSC: an injury drugstore. *Cell Stem Cell* **9,** 11–5 (2011).

115. von Bahr, L. *et al.* Analysis of Tissues Following Mesenchymal Stromal Cell Therapy in Humans Indicates Limited Long-Term Engraftment and No Ectopic Tissue Formation. *Stem Cells* **30,** 1575–1578 (2012).

116. Liu, S. *et al.* MSC Transplantation Improves Osteopenia via Epigenetic Regulation of Notch Signaling in Lupus. *Cell Metab.* **22,** 606–618 (2015).

117. Dos Santos, C. C. *et al.* Network analysis of transcriptional responses induced by mesenchymal stem cell treatment of experimental sepsis. *Am. J. Pathol.* **181,** 1681–1692 (2012).

118.   Shi, Y. *et al.* Mesenchymal stem cells: a new strategy for immunosuppression and tissue repair. *Cell Res.* **20,** 510–8 (2010).

119.   Pandolfi, F., Altamura, S., Frosali, S. & Conti, P. Key Role of DAMP in Inflammation, Cancer, and Tissue Repair. *Clin. Ther.* **38,** 1017–28 (2016).

120.   Luster, A. D., Alon, R. & von Andrian, U. H. Immune cell migration in inflammation: present and future therapeutic targets. *Nat. Immunol.* **6,** 1182–90 (2005).

121.   Eming, S. A., Krieg, T. & Davidson, J. M. Inflammation in wound repair: molecular and cellular mechanisms. *J. Invest. Dermatol.* **127,** 514–25 (2007).

122.   Hung, S.-P., Yang, M.-H., Tseng, K.-F. & Lee, O. K. Hypoxia-induced secretion of TGF-β1 in mesenchymal stem cell promotes breast cancer cell progression. *Cell Transplant.* **22,** 1869–82 (2013).

123.   Aguilar, S. *et al.* Bone marrow stem cells expressing keratinocyte growth factor via an inducible lentivirus protects against bleomycin-induced pulmonary fibrosis. *PLoS One* **4,** e8013 (2009).

124.   Ma, X. *et al.* Human mesenchymal stem cells increases expression of α-tubulin and angiopoietin 1 and 2 in focal cerebral ischemia and reperfusion. *Curr. Neurovasc. Res.* **10,** 103–11 (2013).

125.   Shi, Y. *et al.* How mesenchymal stem cells interact with tissue immune responses. *Trends Immunol.* **33,** 136–43 (2012).

126.   Kim, S.-W., Zhang, H.-Z., Guo, L., Kim, J.-M. & Kim, M. H. Amniotic mesenchymal stem cells enhance wound healing in diabetic NOD/SCID mice through high angiogenic and engraftment capabilities. *PLoS One* **7,** e41105 (2012).

127.   Yang, M. *et al.* Bone marrow-derived mesenchymal stem cells transplantation accelerates tissue expansion by promoting skin regeneration during expansion. *Ann. Surg.* **253,** 202–9 (2011).

128.   Houchen, C. W., George, R. J., Sturmoski, M. A. & Cohn, S. M. FGF-2 enhances intestinal stem cell survival and its expression is induced after radiation injury. *Am. J. Physiol.* **276,** G249–58 (1999).

129.   Yoon, B. S. *et al.* Secretory profiles and wound healing effects of human amniotic fluid-derived mesenchymal stem cells. *Stem Cells Dev.* **19,** 887–902 (2010).

130.   Beckermann, B. M. *et al.* VEGF expression by mesenchymal stem cells contributes to angiogenesis in pancreatic carcinoma. *Br. J. Cancer* **99,** 622–31 (2008).

131.   Wu, Y., Chen, L., Scott, P. G. & Tredget, E. E. Mesenchymal stem cells enhance wound healing through differentiation and angiogenesis. *Stem Cells* **25,** 2648–59 (2007).

132.   Tropea, K. A. *et al.* Bronchioalveolar stem cells increase after mesenchymal stromal cell treatment in a mouse model of bronchopulmonary dysplasia. *Am. J. Physiol. Lung Cell. Mol. Physiol.* **302,** L829–37 (2012).

133.   Katsha, A. M. *et al.* Paracrine factors of multipotent stromal cells ameliorate lung injury in an elastase-induced emphysema model. *Mol. Ther.* **19,** 196–203 (2011).

134.   Lan, Y.-W. *et al.* Hypoxia-preconditioned mesenchymal stem cells attenuate bleomycin-induced pulmonary fibrosis. *Stem Cell Res. Ther.* **6,** 97 (2015).

135.   Chen, Q.-H., Liu, A.-R., Qiu, H.-B. & Yang, Y. Interaction between mesenchymal stem cells and endothelial cells restores endothelial permeability via paracrine hepatocyte growth factor in vitro. *Stem Cell Res. Ther.* **6,** 44 (2015).

136. Tadokoro, T. *et al.* IL-6/STAT3 promotes regeneration of airway ciliated cells from basal stem cells. *Proc. Natl. Acad. Sci. U. S. A.* **111,** E3641–9 (2014).

137. Krasnodembskaya, A. *et al.* Antibacterial effect of human mesenchymal stem cells is mediated in part from secretion of the antimicrobial peptide LL-37. *Stem Cells* **28,** 2229–2238 (2010).

138. Fang, X. *et al.* Human Mesenchymal Stem (Stromal) Cells Promote the Resolution of Acute Lung Injury in Part through Lipoxin A4. *J. Immunol.* **195,** 875–881 (2015).

139. Wang, Y., Chen, X., Cao, W. & Shi, Y. Plasticity of mesenchymal stem cells in immunomodulation: pathological and therapeutic implications. *Nat. Immunol.* **15,** 1009–1016 (2014).

140. Uccelli, A. & de Rosbo, N. K. The immunomodulatory function of mesenchymal stem cells: mode of action and pathways. *Ann. N. Y. Acad. Sci.* **1351,** 114–26 (2015).

141. Bernardo, M. E. & Fibbe, W. E. Mesenchymal Stromal Cells: Sensors and Switchers of Inflammation. *Cell Stem Cell* **13,** 392–402 (2013).

142. Savukinas, U. B., Enes, S. R., Sjöland, A. A. & Westergren-Thorsson, G. The Bystander Effect: MSC-Mediated Lung Repair. *Stem Cells* (2016).

143. Le Blanc, K. & Mougiakakos, D. Multipotent mesenchymal stromal cells and the innate immune system. *Nat. Rev. Immunol.* **12,** 383–96 (2012).

144. Ortiz, L. A. *et al.* Interleukin 1 receptor antagonist mediates the antiinflammatory and antifibrotic effect of mesenchymal stem cells during lung injury. *Proc. Natl. Acad. Sci. U. S. A.* **104,** 11002–7 (2007).

145. Wang, L., Zhao, Y. & Shi, S. Interplay between mesenchymal stem cells and lymphocytes: implications for immunotherapy and tissue regeneration. *J. Dent. Res.* **91,** 1003–10 (2012).

146. Chinnadurai, R., Copland, I. B., Patel, S. R. & Galipeau, J. IDO-independent suppression of T cell effector function by IFN-γ-licensed human mesenchymal stromal cells. *J. Immunol.* **192,** 1491–501 (2014).

147. Glennie, S., Soeiro, I., Dyson, P. J., Lam, E. W.-F. & Dazzi, F. Bone marrow mesenchymal stem cells induce division arrest anergy of activated T cells. *Blood* **105,** 2821–7 (2005).

148. Benvenuto, F. *et al.* Human mesenchymal stem cells promote survival of T cells in a quiescent state. *Stem Cells* **25,** 1753–60 (2007).

149. Burr, S. P., Dazzi, F. & Garden, O. A. Mesenchymal stromal cells and regulatory T cells: the Yin and Yang of peripheral tolerance? *Immunol. Cell Biol.* **91,** 12–8 (2013).

150. Ghannam, S. *et al.* Mesenchymal stem cells inhibit human Th17 cell differentiation and function and induce a T regulatory cell phenotype. *J. Immunol.* **185,** 302–12 (2010).

151. Goodwin, M. *et al.* Bone marrow-derived mesenchymal stromal cells inhibit Th2-mediated allergic airways inflammation in mice. *Stem Cells* **29,** 1137–48 (2011).

152. Kavanagh, H. & Mahon, B. P. Allogeneic mesenchymal stem cells prevent allergic airway inflammation by inducing murine regulatory T cells. *Allergy* **66,** 523–31 (2011).

153. Akiyama, K. *et al.* Mesenchymal-stem-cell-induced immunoregulation involves FAS-ligand-/FAS-mediated T cell apoptosis. *Cell Stem Cell* **10,** 544–555 (2012).

154. Asari, S. *et al.* Mesenchymal stem cells suppress B-cell terminal differentiation. *Exp. Hematol.* **37,** 604–15 (2009).

155. Franquesa, M., Hoogduijn, M. J., Bestard, O. & Grinyó, J. M. Immunomodulatory effect of mesenchymal stem cells on B cells. *Front. Immunol.* **3,** 212 (2012).

156. Franquesa, M. *et al.* Human adipose tissue-derived mesenchymal stem cells abrogate plasmablast formation and induce regulatory B cells independently of T helper cells. *Stem Cells* **33,** 880–91 (2015).

157. Chen, P.-M. *et al.* Induction of immunomodulatory monocytes by human mesenchymal stem cell-derived hepatocyte growth factor through ERK1/2. *J. Leukoc. Biol.* **96,** 295–303 (2014).

158. Chen, H.-W. *et al.* Mesenchymal stem cells tune the development of monocyte-derived dendritic cells toward a myeloid-derived suppressive phenotype through growth-regulated oncogene chemokines. *J. Immunol.* **190,** 5065–77 (2013).

159. Hof-Nahor, I. *et al.* Human mesenchymal stem cells shift CD8+ T cells towards a suppressive phenotype by inducing tolerogenic monocytes. *J. Cell Sci.* **125,** 4640–50 (2012).

160. Prockop, D. J. Concise review: Two negative feedback loops place mesenchymal stem/stromal cells at the center of early regulators of inflammation. *Stem Cells* **31,** 2042–2046 (2013).

161. Abumaree, M. H. *et al.* Human placental mesenchymal stem cells (pMSCs) play a role as immune suppressive cells by shifting macrophage differentiation from inflammatory M1 to anti-inflammatory M2 macrophages. *Stem Cell Rev.* **9,** 620–41 (2013).

162. Gu, W. *et al.* Mesenchymal stem cells alleviate airway inflammation and emphysema in COPD through down-regulation of cyclooxygenase-2 via p38 and ERK MAPK pathways. *Sci. Rep.* **5,** 8733 (2015).

163. Casey, A. *et al.* Bone marrow-derived multipotent stromal cells attenuate inflammation in obliterative airway disease in mouse tracheal allografts. *Stem Cells Int.* **2014,** 468927 (2014).

164. Antunes, M. A. *et al.* Effects of different mesenchymal stromal cell sources and delivery routes in experimental emphysema. *Respir. Res.* **15,** 118 (2014).

165. Jiang, D. *et al.* Suppression of Neutrophil-Mediated Tissue Damage - A Novel Skill of Mesenchymal Stem Cells. *Stem Cells* (2016).

166. Valadi, H. *et al.* Exosome-mediated transfer of mRNAs and microRNAs is a novel mechanism of genetic exchange between cells. *Nat. Cell Biol.* **9,** 654–9 (2007).

167. Zhu, Y.-G. *et al.* Human mesenchymal stem cell microvesicles for treatment of Escherichia coli endotoxin-induced acute lung injury in mice. *Stem Cells* **32,** 116–25 (2014).

168. Schuster, J. A. *et al.* Expansion of hematopoietic stem cells for transplantation: current perspectives. *Exp. Hematol. Oncol.* **1,** 12 (2012).

169. Caplan, A. I. All MSCs Are Pericytes? *Cell Stem Cell* **3,** 229–230 (2008).

170. Prockop, D. J. *et al.* Defining the risks of mesenchymal stromal cell therapy. *Cytotherapy* **12,** 576–8 (2010).

171. Ankrum, J. & Karp, J. M. Mesenchymal stem cell therapy: Two steps forward, one step back. *Trends Mol. Med.* **16,** 203–209 (2010).

172. Lalu, M. M. *et al.* Safety of cell therapy with mesenchymal stromal cells (SafeCell): a systematic review and meta-analysis of clinical trials. *PLoS One* **7,** e47559 (2012).

173. Jonasch, E. & Haluska, F. G. Interferon in Oncological Practice: Review of Interferon Biology, Clinical Applications, and Toxicities. *Oncologist* **6,** 34–55 (2001).

174. Levy, O. *et al.* mRNA-engineered mesenchymal stem cells for targeted delivery of interleukin-10 to sites of inflammation. *Blood* **122,** e23–32 (2013).

175. Ng, K. S., Kuncewicz, T. M. & Karp, J. M. Beyond Hit-and-Run: Stem Cells Leave a Lasting Memory. *Cell Metab.* **22,** 541–3 (2015).

176. Naldini, L. Ex vivo gene transfer and correction for cell-based therapies. *Nat. Rev. Genet.* **12,** 301–315 (2011).

177. Naldini, L. Gene therapy returns to centre stage. *Nature* **526,** 351–60 (2015).

178. Terheggen, H. G., Lowenthal, A., Lavinha, F., Colombo, J. P. & Rogers, S. Unsuccessful trial of gene replacement in arginase deficiency. *Zeitschrift für Kinderheilkd.* **119,** 1–3 (1975).

179. Rogers, S. & Pfuderer, P. Use of viruses as carriers of added genetic information. *Nature* **219,** 749–51 (1968).

180. Rogers, S., Lowenthal, A., Terheggen, H. G. & Columbo, J. P. Induction of arginase activity with the Shope papilloma virus in tissue culture cells from an argininemic patient. *J. Exp. Med.* **137,** 1091–6 (1973).

181. Friedmann, T. Stanfield Rogers: insights into virus vectors and failure of an early gene therapy model. *Mol. Ther.* **4,** 285–8 (2001).

182. GSK. StrimvelisTM receives European marketing authorisation to treat very rare disease, ADA-SCID [Press release] (27 May 2016). Retrieved June 21, 2016. (2016). at <http://www.gsk.com/en-gb/media/press-releases/2016/strimvelistm-receives-european-marketing-authorisation-to-treat-very-rare-disease-ada-scid/>

183. Aiuti, A. *et al.* Correction of ADA-SCID by stem cell gene therapy combined with nonmyeloablative conditioning. *Science* **296,** 2410–3 (2002).

184. Candotti, F. *et al.* Gene therapy for adenosine deaminase-deficient severe combined immune deficiency: Clinical comparison of retroviral vectors and treatment plans. *Blood* **120,** 3635–3646 (2012).

185. Stein, S. *et al.* Genomic instability and myelodysplasia with monosomy 7 consequent to EVI1 activation after gene therapy for chronic granulomatous disease. *Nat. Med.* **16,** 198–204 (2010).

186. Hacein-Bey-Abina, S. *et al.* LMO2-associated clonal T cell proliferation in two patients after gene therapy for SCID-X1. *Science* **302,** 415–9 (2003).

187. Braun, C. J. *et al.* Gene Therapy for Wiskott-Aldrich Syndrome--Long-Term Efficacy and Genotoxicity. *Sci. Transl. Med.* **6,** 227ra33–227ra33 (2014).

188. Aiuti, A. *et al.* Multilineage hematopoietic reconstitution without clonal selection in ADA-SCID patients treated with stem cell gene therapy. *J. Clin. Invest.* **117,** 2233–40 (2007).

189. Hacein-Bey-Abina, S. *et al.* A modified γ-retrovirus vector for X-linked severe combined immunodeficiency. *N. Engl. J. Med.* **371,** 1407–17 (2014).

190. Aiuti, A. *et al.* Lentiviral Hematopoietic Stem Cell Gene Therapy in Patients with Wiskott-Aldrich Syndrome. *Science (80-.).* **341,** 1233151–1233151 (2013).

191. Cavazzana-Calvo, M. *et al.* Transfusion independence and HMGA2 activation after gene therapy of human β-thalassaemia. *Nature* **467,** 318–322 (2010).

192. Biffi, A. *et al.* Lentiviral Hematopoietic Stem Cell Gene Therapy Benefits Metachromatic Leukodystrophy. *Science (80-.).* **341,** 1233158–1233158 (2013).

193. Cartier, N. *et al.* Hematopoietic stem cell gene therapy with a lentiviral vector in X-linked adrenoleukodystrophy. *Science (80-.).* **326,** 818–823 (2009).

194. Dull, T. *et al.* A third-generation lentivirus vector with a conditional packaging system. *J. Virol.* **72,** 8463–71 (1998).

195. Zufferey, R. *et al.* Self-inactivating lentivirus vector for safe and efficient in vivo gene delivery. *J. Virol.* **72,** 9873–9880 (1998).

196. Niess, H. *et al.* Treatment of advanced gastrointestinal tumors with genetically modified autologous mesenchymal stromal cells (TREAT-ME1): study protocol of a phase I/II clinical trial. *BMC Cancer* **15,** 1–13 (2015).

197. Fermi, C. & Pernossi, L. Ueber die Enzyme. *Zeitschrift für Hyg. und Infekt.* **18,** 83–127 (1894).

198. Schultze, H. E. ., Göllner, I., Heide, K., Schönenberger, M. & Schwick, G. Zur Kenntnis der α-Globuline des menschlichen Normalserums. *Zeitschrift für Naturforsch. B* **10,** 463–473 (1955).

199. Eriksson, S., Laurell, C.-B., Stewart, J. W. & Takahashi, M. A New Abnormal Serum Globulin alpha1-Antitrypsin. *Acta Chem. Scand.* **17 supl.,** 150–153 (1963).

200. Eriksson, S. Studies in alpha 1-antitrypsin deficiency. *Acta Med. Scand. Suppl.* **432,** 1–85 (1965).

201. Gross, P., Babyak, M. A., Tolker, E. & Kaschak, M. Enzymatically produced emphysema; a preliminary report. *J. Occup. Med.* **6,** 481–4 (1964).

202. Stockley, R. A. The multiple facets of alpha-1-antitrypsin. *Ann. Transl. Med.* **3,** 130 (2015).

203. Turino, G. M. *et al.* Serum elastase inhibitor deficiency and alpha 1-antitrypsin deficiency in patients with obstructive emphysema. *Science* **165,** 709–11 (1969).

204. Laurell, C. B. Is emphysema in alpha 1 -antitrypsin deficiency a result of autodigestion? *Scand. J. Clin. Lab. Invest.* **28,** 1–3 (1971).

205. James, H. L. & Cohen, A. B. Mechanism of inhibition of porcine elastase by human alpha-1-antitrypsin. *J. Clin. Invest.* **62,** 1344–53 (1978).

206. Kidokoro, Y., Kravis, T. C., Moser, K. M., Taylor, J. C. & Crawford, I. P. Relationship of leukocyte elastase concentration to severity of emphysema in homozygous alpha1-antitrypsin-deficient persons. *Am. Rev. Respir. Dis.* **115,** 793–803 (1977).

207. Larsson, C., Eriksson, S. & Dirksen, H. Smoking and intermediate alpha1-antitrypsin deficiency and lung function in middle-aged men. *Br. Med. J.* **2,** 922–5 (1977).

208. Larsson, C. Natural history and life expectancy in severe alpha1-antitrypsin deficiency, Pi Z. *Acta Med. Scand.* **204,** 345–51 (1978).

209. Carp, H. & Janoff, A. Possible mechanisms of emphysema in smokers. In vitro suppression of serum elastase-inhibitory capacity by fresh cigarette smoke and its prevention by antioxidants. *Am. Rev. Respir. Dis.* **118,** 617–21 (1978).

210. Janoff, A., Carp, H., Lee, D. K. & Drew, R. T. Cigarette smoke inhalation decreases alpha 1-antitrypsin activity in rat lung. *Science* **206,** 1313–4 (1979).

211. Gadek, J. E., Klein, H. G., Holland, P. V & Crystal, R. G. Replacement therapy of alpha 1-antitrypsin deficiency. Reversal of protease-antiprotease imbalance within the alveolar structures of PiZ subjects. *J. Clin. Invest.* **68,** 1158–65 (1981).

212. Wewers, M. D. *et al.* Replacement therapy for alpha 1-antitrypsin deficiency associated with emphysema. *N. Engl. J. Med.* **316,** 1055–62 (1987).

213. Hubbard, R. C., Sellers, S., Czerski, D., Stephens, L. & Crystal, R. G. Biochemical efficacy and safety of monthly augmentation therapy for alpha 1-antitrypsin deficiency. *JAMA* **260,** 1259–64 (1988).

214. Stoller, J. K. & Aboussouan, L. S. A Review of α 1 -Antitrypsin Deficiency. *Am. J. Respir. Crit. Care Med.* **185,** 246–259 (2012).

215. de Serres, F. J. & Blanco, I. Prevalence of α1-antitrypsin deficiency alleles PI*S and PI*Z worldwide and effective screening for each of the five phenotypic classes PI*MS, PI*MZ, PI*SS, PI*SZ, and PI*ZZ: a comprehensive review. *Ther. Adv. Respir. Dis.* **6,** 277–95 (2012).

216. Lewis, E. C. Expanding the clinical indications for α(1)-antitrypsin therapy. *Mol. Med.* **18,** 957–70 (2012).

217. Janciauskiene, S. M. *et al.* The discovery of α1-antitrypsin and its role in health and disease. *Respir. Med.* **105,** 1129–39 (2011).

218. Wanner, A., Arce, A. De & Pardee, E. Novel therapeutic uses of alpha-1 antitrypsin: a window to the future. *COPD* **9,** 583–8 (2012).

219. Stoller, J. K. & Aboussouan, L. S. α1-antitrypsin deficiency. in *Lancet* **365,** 2225–2236 (2005).

220. Lomas, D. A., Hurst, J. R. & Gooptu, B. Update on alpha-1 antitrypsin deficiency: new therapies. *J. Hepatol.* (2016).

221. Gooptu, B., Dickens, J. A. & Lomas, D. A. The molecular and cellular pathology of α₁-antitrypsin deficiency. *Trends Mol. Med.* **20,** 116–27 (2014).

222. Wanner, A. Chairman's Summary: Can Cystic Fibrosis and Alpha-1 Antitrypsin Deficiency Inform Chronic Obstructive Pulmonary Disease? *Ann. Am. Thorac. Soc.* **13 Suppl 2,** S112–3 (2016).

223. Fregonese, L. & Stolk, J. Hereditary alpha-1-antitrypsin deficiency and its clinical consequences. *Orphanet J. Rare Dis.* **3,** 16 (2008).

224. Eriksson, S., Carlson, J. & Velez, R. Risk of cirrhosis and primary liver cancer in alpha 1-antitrypsin deficiency. *N. Engl. J. Med.* **314,** 736–9 (1986).

225. Dawwas, M. F., Davies, S. E., Griffiths, W. J. H., Lomas, D. A. & Alexander, G. J. Prevalence and risk factors for liver involvement in individuals with PiZZ-related lung disease. *Am. J. Respir. Crit. Care Med.* **187,** 502–8 (2013).

226. Stone, H., Pye, a. & Stockley, R. a. Disease associations in alpha-1-antitrypsin deficiency. *Respir. Med.* **108,** 338–343 (2014).

227. Stockley, R. A. α1-antitrypsin: a polyfunctional protein? *Lancet. Respir. Med.* **3,** 341–3 (2015).

228. Kurachi, K. *et al.* Cloning and sequence of cDNA coding for alpha 1-antitrypsin. *Proc. Natl. Acad. Sci. U. S. A.* **78,** 6826–30 (1981).

229. de Serres, F. & Blanco, I. Role of alpha-1 antitrypsin in human health and disease. *J. Intern. Med.* **276,** 311–335 (2014).

230. Huber, R. & Carrell, R. W. Implications of the three-dimensional structure of alpha 1-antitrypsin for structure and function of serpins. *Biochemistry* **28,** 8951–66 (1989).

231. Stein, P. E. & Carrell, R. W. What do dysfunctional serpins tell us about molecular mobility and disease? *Nat. Struct. Biol.* **2,** 96–113 (1995).

232. Kang, S., Barak, Y., Lamed, R., Bayer, E. A. & Morrison, M. The functional repertoire of prokaryote cellulosomes includes the serpin superfamily of serine proteinase inhibitors. *Mol. Microbiol.* **60,** 1344–54 (2006).

233. Ogushi, F., Hubbard, R. C., Vogelmeier, C., Fells, G. A. & Crystal, R. G. Risk factors for emphysema. Cigarette smoking is associated with a reduction in the association rate constant of lung alpha 1-antitrypsin for neutrophil elastase. *J. Clin. Invest.* **87,** 1060–5 (1991).

234. Gooptu, B. & Lomas, D. A. Conformational pathology of the serpins: themes, variations, and therapeutic strategies. *Annu. Rev. Biochem.* **78,** 147–76 (2009).

235. Luo, L.-Y. & Jiang, W. Inhibition profiles of human tissue kallikreins by serine protease inhibitors. *Biol. Chem.* **387,** 813–6 (2006).

236. Janciauskiene, S. *et al.* Alpha1-antitrypsin inhibits the activity of the matriptase catalytic domain in vitro. *Am. J. Respir. Cell Mol. Biol.* **39,** 631–7 (2008).

237. Petrache, I. *et al.* Alpha-1 antitrypsin inhibits caspase-3 activity, preventing lung endothelial cell apoptosis. *Am. J. Pathol.* **169,** 1155–66 (2006).

238. Geboes, K. *et al.* Morphological identification of alpha-I-antitrypsin in the human small intestine. *Histopathology* **6,** 55–60 (1982).

239. Ray, M. B., Geboes, K., Callea, F. & Desmet, V. J. Alpha-1-antitrypsin immunoreactivity in gastric carcinoid. *Histopathology* **6,** 289–97 (1982).

240. Perlmutter, D. H. *et al.* The cellular defect in alpha 1-proteinase inhibitor (alpha 1-PI) deficiency is expressed in human monocytes and in Xenopus oocytes injected with human liver mRNA. *Proc. Natl. Acad. Sci. U. S. A.* **82,** 6918–21 (1985).

241. Higashiyama, M., Doi, O., Kodama, K., Yokouchi, H. & Tateishi, R. An evaluation of the prognostic significance of alpha-1-antitrypsin expression in adenocarcinomas of the lung: an immunohistochemical analysis. *Br. J. Cancer* **65,** 300–2 (1992).

242. Fleixo-Lima, G. *et al.* Mechanistic evidence in support of alpha1-antitrypsin as a therapeutic approach for type 1 diabetes. *J. Diabetes Sci. Technol.* **8,** 1193–203 (2014).

243. Zemel, R., Bachmetov, L., Ad-El, D., Abraham, A. & Tur-Kaspa, R. Expression of liver-specific markers in naïve adipose-derived mesenchymal stem cells. *Liver Int.* **29,** 1326–1337 (2009).

244. Chung, H.-S., Kim, J.-S., Lee, S. M. & Park, S. J. Additional N-glycosylation in the N-terminal region of recombinant human alpha-1 antitrypsin enhances the circulatory half-life in Sprague-Dawley rats. *Glycoconj. J.* **33,** 201–8 (2016).

245. Lee, K. J. *et al.* N-glycan analysis of human α1-antitrypsin produced in Chinese hamster ovary cells. *Glycoconj. J.* **30,** 537–47 (2013).

246. Chowanadisai, W. & Lönnerdal, B. Alpha(1)-antitrypsin and antichymotrypsin in human milk: origin, concentrations, and stability. *Am. J. Clin. Nutr.* **76,** 828–33 (2002).

247. Berman, M. B., Barber, J. C., Talamo, R. C. & Langley, C. E. Corneal ulceration and the serum antiproteases. I. Alpha 1-antitrypsin. *Invest. Ophthalmol.* **12,** 759–70 (1973).

248. Huang, H. *et al.* Alpha1-antitrypsin inhibits angiogenesis and tumor growth. *Int. J. Cancer* **112,** 1042–8 (2004).

249. Janciauskiene, S., Toth, E., Sahlin, S. & Eriksson, S. Immunochemical and functional properties of biliary alpha-1-antitrypsin. *Scand. J. Clin. Lab. Invest.* **56,** 597–608 (1996).

250. Eden, E. Asthma and COPD in alpha-1 antitrypsin deficiency. Evidence for the Dutch hypothesis. *COPD* **7,** 366–74 (2010).

251. Janciauskiene, S. Conformational properties of serine proteinase inhibitors (serpins) confer multiple pathophysiological roles. *Biochim. Biophys. Acta* **1535,** 221–35 (2001).

252. PeproTechFocus. Serpins, Serpinopathies, and Conformational Diseases. Retrieved June 3, 2016. at <https://www.peprotech.com/Lists/PTPublications/Serpins, Serpinopathies and Conformational Diseases.pdf>

253. Stein, P. E. *et al.* Crystal structure of ovalbumin as a model for the reactive centre of serpins. *Nature* **347,** 99–102 (1990).

254. Loebermann, H., Tokuoka, R., Deisenhofer, J. & Huber, R. Human alpha 1-proteinase inhibitor. Crystal structure analysis of two crystal modifications, molecular model and preliminary analysis of the implications for function. *J. Mol. Biol.* **177,** 531–57 (1984).

255. Brantly, M., Nukiwa, T. & Crystal, R. G. Molecular basis of alpha-1-antitrypsin deficiency. *Am. J. Med.* **84,** 13–31 (1988).

256. Silverman, G. A. *et al.* The serpins are an expanding superfamily of structurally similar but functionally diverse proteins. Evolution, mechanism of inhibition, novel functions, and a revised nomenclature. *J. Biol. Chem.* **276,** 33293–6 (2001).

257. Ehlers, M. R. Immune-modulating effects of alpha-1 antitrypsin. *Biol. Chem.* **395,** 1187–93 (2014).

258. Guttman, O. *et al.* Acute-phase protein α1-anti-trypsin: diverting injurious innate and adaptive immune responses from non-authentic threats. *Clin. Exp. Immunol.* **179,** 161–72 (2015).

259. Bosković, G. & Twining, S. S. Retinol and retinaldehyde specifically increase alpha1-proteinase inhibitor in the human cornea. *Biochem. J.* **322 (Pt 3,** 751–6 (1997).

260. Faust, D., Hormann, S., Friedrich-Sander, M., Milovic, V. & Stein, J. Butyrate and the cytokine-induced alpha1-proteinase inhibitor release in intestinal epithelial cells. *Eur. J. Clin. Invest.* **31,** 1060–3 (2001).

261. Bosco, D. *et al.* Expression and secretion of alpha1-proteinase inhibitor are regulated by proinflammatory cytokines in human pancreatic islet cells. *Diabetologia* **48,** 1523–33 (2005).

262. Knoell, D. L., Ralston, D. R., Coulter, K. R. & Wewers, M. D. Alpha 1-antitrypsin and protease complexation is induced by lipopolysaccharide, interleukin-1beta, and tumor necrosis factor-alpha in monocytes. *Am. J. Respir. Crit. Care Med.* **157,** 246–55 (1998).

263. Perlmutter, D. H. & Punsal, P. I. Distinct and additive effects of elastase and endotoxin on expression of alpha 1 proteinase inhibitor in mononuclear phagocytes. *J. Biol. Chem.* **263,** 16499–503 (1988).

264. Larsson, A., Palm, M., Hansson, L.-O., Basu, S. & Axelsson, O. Reference values for alpha1-acid glycoprotein, alpha1-antitrypsin, albumin, haptoglobin, C-reactive protein, IgA, IgG and IgM during pregnancy. *Acta Obstet. Gynecol. Scand.* **87,** 1084–8 (2008).

265. Kobayashi, Y., Oppenheim, J. J. & Matsushima, K. Human pre-interleukin 1 alpha and beta: structural features revealed by limited proteolysis. *Chem. Pharm. Bull. (Tokyo).* **39,** 1513–7 (1991).

266. Crotty Alexander, L. E., Shin, S. & Hwang, J. H. Inflammatory Diseases of the Lung Induced by Conventional Cigarette Smoke: A Review. *Chest* **148,** 1307–22 (2015).

267. Shah, R. Protease-activated receptors in cardiovascular health and diseases. *Am. Heart J.* **157,** 253–62 (2009).

268. Shpacovitch, V., Feld, M., Hollenberg, M. D., Luger, T. A. & Steinhoff, M. Role of protease-activated receptors in inflammatory responses, innate and adaptive immunity. *J. Leukoc. Biol.* **83,** 1309–22 (2008).

269. Fields, R. C. *et al.* Protease-activated receptor-2 signaling triggers dendritic cell development. *Am. J. Pathol.* **162,** 1817–22 (2003).

270. Vergnolle, N. *et al.* A role for proteinase-activated receptor-1 in inflammatory bowel diseases. *J. Clin. Invest.* **116,** 2056 (2006).

271. Noorbakhsh, F. *et al.* Proteinase-activated receptor 2 modulates neuroinflammation in experimental autoimmune encephalomyelitis and multiple sclerosis. *J. Exp. Med.* **203,** 425–35 (2006).

272. Yoshida, K. *et al.* Aggrecanase-1 (ADAMTS-4) interacts with alpha1-antitrypsin. *Biochim. Biophys. Acta* **1725,** 152–9 (2005).

273. Liu, Z. *et al.* The serpin alpha1-proteinase inhibitor is a critical substrate for gelatinase B/MMP-9 in vivo. *Cell* **102,** 647–55 (2000).

274. Muroski, M. E. *et al.* Matrix metalloproteinase-9/gelatinase B is a putative therapeutic target of chronic obstructive pulmonary disease and multiple sclerosis. *Curr. Pharm. Biotechnol.* **9,** 34–46 (2008).

275. Bergin, D. a *et al.* AAT regulates human neutrophil chemotaxis induced by soluble immune complexes and Il - 8. *J. Clin. Invest.* **120,** (2010).

276. Finotti, P. & Pagetta, A. A heat shock protein70 fusion protein with alpha1-antitrypsin in plasma of type 1 diabetic subjects. *Biochem. Biophys. Res. Commun.* **315,** 297–305 (2004).

277. Ochayon, D. E., Mizrahi, M., Shahaf, G., Baranovski, B. M. & Lewis, E. C. Human α1-Antitrypsin Binds to Heat-Shock Protein gp96 and Protects from Endogenous gp96-Mediated Injury In vivo. *Front. Immunol.* **4,** 320 (2013).

278. Bergin, D. A. *et al.* The circulating proteinase inhibitor α-1 antitrypsin regulates neutrophil degranulation and autoimmunity. *Sci. Transl. Med.* **6,** 217ra1 (2014).

279. Tilg, H., Vannier, E., Vachino, G., Dinarello, C. A. & Mier, J. W. Antiinflammatory properties of hepatic acute phase proteins: preferential induction of interleukin 1 (IL-1) receptor antagonist over IL-1 beta synthesis by human peripheral blood mononuclear cells. *J. Exp. Med.* **178,** 1629–36 (1993).

280. Janciauskiene, S. *et al.* Inhibition of lipopolysaccharide-mediated human monocyte activation, in vitro, by alpha1-antitrypsin. *Biochem. Biophys. Res. Commun.* **321,** 592–600 (2004).

281. Nita, I. M., Serapinas, D. & Janciauskiene, S. M. alpha1-Antitrypsin regulates CD14 expression and soluble CD14 levels in human monocytes in vitro. *Int. J. Biochem. Cell Biol.* **39,** 1165–76 (2007).

282. Janciauskiene, S. M., Nita, I. M. & Stevens, T. Alpha1-antitrypsin, old dog, new tricks. Alpha1-antitrypsin exerts in vitro anti-inflammatory activity in human monocytes by elevating cAMP. *J. Biol. Chem.* **282,** 8573–82 (2007).

283. Pott, G. B., Chan, E. D., Dinarello, C. A. & Shapiro, L. Alpha-1-antitrypsin is an endogenous inhibitor of proinflammatory cytokine production in whole blood. *J. Leukoc. Biol.* **85,** 886–95 (2009).

284. Nita, I., Hollander, C., Westin, U. & Janciauskiene, S.-M. Prolastin, a pharmaceutical preparation of purified human alpha1-antitrypsin, blocks endotoxin-mediated cytokine release. *Respir. Res.* **6,** 12 (2005).

285. Lewis, E. C. *et al.* alpha1-Antitrypsin monotherapy induces immune tolerance during islet allograft transplantation in mice. *Proc. Natl. Acad. Sci. U. S. A.* **105,** 16236–16241 (2008).

286. Koulmanda, M. *et al.* Curative and beta cell regenerative effects of alpha1-antitrypsin treatment in autoimmune diabetic NOD mice. *Proc. Natl. Acad. Sci. U. S. A.* **105,** 16242–7 (2008).

287. Jonigk, D. *et al.* Anti-inflammatory and immunomodulatory properties of 1-antitrypsin without inhibition of elastase. *Proc. Natl. Acad. Sci.* **110,** 15007–15012 (2013).

288. Bucurenci, N., Blake, D. R., Chidwick, K. & Winyard, P. G. Inhibition of neutrophil superoxide production by human plasma alpha 1-antitrypsin. *FEBS Lett.* **300,** 21–4 (1992).

289. Stockley, R. A., Shaw, J., Afford, S. C., Morrison, H. M. & Burnett, D. Effect of alpha-1-proteinase inhibitor on neutrophil chemotaxis. *Am. J. Respir. Cell Mol. Biol.* **2,** 163–70 (1990).

290. Ozeri, E., Mizrahi, M., Shahaf, G. & Lewis, E. C. α1 Antitrypsin Promotes Semimature, IL-10-Producing and Readily Migrating Tolerogenic Dendritic Cells. *J. Immunol.* **189,** 146–153 (2012).

291. Vivier, E. *et al.* Innate or adaptive immunity? The example of natural killer cells. *Science* **331,** 44–9 (2011).

292. Ko, F. W. *et al.* Acute exacerbation of COPD. *Respirology* (2016).

293. Guttman, O., Yossef, R., Freixo-lima, G., Porgador, A. & Lewis, E. C. a 1-Antitrypsin modifies general natural killer cell interactions with dendritic cells and specific interactions with islet b - cells in favour of protection from autoimmune diabetes. 530–539 (2014).

294. Yang, P. *et al.* Alpha1-antitrypsin deficiency carriers, tobacco smoke, chronic obstructive pulmonary disease, and lung cancer risk. *Arch. Intern. Med.* **168,** 1097–103 (2008).

295. Sun, Z. & Yang, P. Role of imbalance between neutrophil elastase and alpha 1-antitrypsin in cancer development and progression. *Lancet. Oncol.* **5,** 182–90 (2004).

296. Yang, P. *et al.* Alpha1-antitrypsin and neutrophil elastase imbalance and lung cancer risk. *Chest* **128,** 445–52 (2005).

297. Xu, Y. *et al.* Curcumin inhibits tumor proliferation induced by neutrophil elastase through the upregulation of α1-antitrypsin in lung cancer. *Mol. Oncol.* **6,** 405–17 (2012).

298. Münch, J. *et al.* Discovery and optimization of a natural HIV-1 entry inhibitor targeting the gp41 fusion peptide. *Cell* **129,** 263–75 (2007).

299. Ferreira, T. C. da S. *et al.* Increased prevalence of the alpha-1-antitrypsin (A1AT) deficiency-related S gene in patients infected with human immunodeficiency virus type 1. *J. Med. Virol.* **86,** 23–9 (2014).

300. Bristow, C. L. *et al.* A feedback regulatory pathway between LDL and alpha-1 proteinase inhibitor in chronic inflammation and infection. *Discov. Med.* **16,** 201–18 (2013).

301. Lewis, E. C., Shapiro, L., Bowers, O. J. & Dinarello, C. A. Alpha1-antitrypsin monotherapy prolongs islet allograft survival in mice. *Proc. Natl. Acad. Sci. U. S. A.* **102,** 12153–8 (2005).

302. Zhang, B. *et al.* Alpha1-antitrypsin protects beta-cells from apoptosis. *Diabetes* **56,** 1316–23 (2007).

303. Subramanian, S. *et al.* Sustained expression of circulating human alpha-1 antitrypsin reduces inflammation, increases CD4+FoxP3+ Treg cell population and prevents signs of experimental autoimmune encephalomyelitis in mice. *Metab. Brain Dis.* **26,** 107–13 (2011).

304. Wang, Y. *et al.* The immunoregulation effect of alpha 1-antitrypsin prolong β-cell survival after transplantation. *PLoS One* **9,** e94548 (2014).

305. Grimstein, C. *et al.* Alpha-1 antitrypsin protein and gene therapies decrease autoimmunity and delay arthritis development in mouse model. *J. Transl. Med.* **9,** 21 (2011).

306. Tawara, I. *et al.* Alpha-1-antitrypsin monotherapy reduces graft-versus-host disease after experimental allogeneic bone marrow transplantation. *Proc. Natl. Acad. Sci. U. S. A.* **109,** 564–9 (2012).

307. Mizrahi, M. *et al.* Human α1-antitrypsin modifies B-lymphocyte responses during allograft transplantation. *Immunology* **140,** 362–73 (2013).

308. Redfield, R. R. *et al.* Essential role for B cells in transplantation tolerance. *Curr. Opin. Immunol.* **23,** 685–91 (2011).

309. Petrache, I. *et al.* A novel antiapoptotic role for alpha1-antitrypsin in the prevention of pulmonary emphysema. *Am. J. Respir. Crit. Care Med.* **173,** 1222–8 (2006).

310. Stockley, R. A. *et al.* Therapeutic efficacy of α-1 antitrypsin augmentation therapy on the loss of lung tissue: an integrated analysis of 2 randomised clinical trials using computed tomography densitometry. *Respir. Res.* **11,** 136 (2010).

311.   Ikari, Y., Mulvihill, E. & Schwartz, S. M. alpha 1-Proteinase inhibitor, alpha 1-antichymotrypsin, and alpha 2-macroglobulin are the antiapoptotic factors of vascular smooth muscle cells. *J. Biol. Chem.* **276,** 11798–803 (2001).

312.   Lockett, A. D. *et al.* α_1-Antitrypsin modulates lung endothelial cell inflammatory responses to TNF-α. *Am. J. Respir. Cell Mol. Biol.* **49,** 143–50 (2013).

313.   Serban, K. A. & Petrache, I. Alpha-1 Antitrypsin and Lung Cell Apoptosis. *Ann. Am. Thorac. Soc.* **13 Suppl 2,** S146–9 (2016).

314.   Zelvyte, I., Stevens, T., Westin, U. & Janciauskiene, S. alpha1-antitrypsin and its C-terminal fragment attenuate effects of degranulated neutrophil-conditioned medium on lung cancer HCC cells, in vitro. *Cancer Cell Int.* **4,** 7 (2004).

315.   Bellacen, K., Kalay, N., Ozeri, E., Shahaf, G. & Lewis, E. C. Revascularization of pancreatic islet allografts is enhanced by α-1-antitrypsin under anti-inflammatory conditions. *Cell Transplant.* **22,** 2119–33 (2013).

316.   Shapiro, L., Pott, G. B. & Ralston, A. H. Alpha-1-antitrypsin inhibits human immunodeficiency virus type 1. *FASEB J.* **15,** 115–122 (2001).

317.   Bryan, C. L. *et al.* HIV infection is associated with reduced serum alpha-1-antitrypsin concentrations. *Clin. Investig. Med. Médecine Clin. Exp.* **33,** E384–9 (2010).

318.   Cantin, A. M. & Woods, D. E. Aerosolized prolastin suppresses bacterial proliferation in a model of chronic Pseudomonas aeruginosa lung infection. *Am. J. Respir. Crit. Care Med.* **160,** 1130–5 (1999).

319.   Griese, M. *et al.* alpha1-Antitrypsin inhalation reduces airway inflammation in cystic fibrosis patients. *Eur. Respir. J.* **29,** 240–50 (2007).

320.   Knappstein, S., Ide, T., Schmidt, M. A. & Heusipp, G. Alpha 1-antitrypsin binds to and interferes with functionality of EspB from atypical and typical enteropathogenic Escherichia coli strains. *Infect. Immun.* **72,** 4344–50 (2004).

321.   Chapman, K. R. *et al.* Intravenous augmentation treatment and lung density in severe $\alpha1$ antitrypsin deficiency (RAPID): a randomised, double-blind, placebo-controlled trial. *Lancet* **386,** 360–368 (2015).

322.   Abbate, A. *et al.* Effects of Prolastin C (Plasma-Derived Alpha-1 Antitrypsin) on the acute inflammatory response in patients with ST-segment elevation myocardial infarction (from the VCU-alpha 1-RT pilot study). *Am. J. Cardiol.* **115,** 8–12 (2015).

323.   Gottlieb, P. A. *et al.* $\alpha1$-Antitrypsin therapy downregulates toll-like receptor-induced IL-1β responses in monocytes and myeloid dendritic cells and may improve islet function in recently diagnosed patients with type 1 diabetes. *J. Clin. Endocrinol. Metab.* **99,** E1418–26 (2014).

324.   ClinicalTrials.gov b. Bethesda (MD): National Library of Medicine (US). 2000 Feb 29 – [retrieved 2016 Jun 07]. Search for Studies: Antitrypsin. *ClinicalTrials.gov* at <https://clinicaltrials.gov/ct2/results?term=antitrypsin&Search=Search>

325.   Ylä-Herttuala, S. ADA-SCID Gene Therapy Endorsed By European Medicines Agency For Marketing Authorization. *Mol. Ther.* **24,** 1013–1014 (2016).

326.   Dieffenbach, C. W., Lowe, T. M. & Dveksler, G. S. General concepts for PCR primer design. *PCR Methods Appl.* **3,** S30–7 (1993).

327.   Kozak, M. Point mutations define a sequence flanking the AUG initiator codon that modulates translation by eukaryotic ribosomes. *Cell* **44,** 283–92 (1986).

328.   Stein, S., Grez, M. & Schambach, A. Gene therapy of chronic granulomatous disease. EP 2019134 A1, priority date 2007-07-26, issue date 2009-01-28. *Patent* (2007). at <https://www.google.com/patents/EP2019134A1?cl=da>

329.   Schambach, A. *et al.* Equal potency of gammaretroviral and lentiviral SIN vectors for expression of O6-methylguanine-DNA methyltransferase in hematopoietic cells. *Mol. Ther.* **13,** 391–400 (2006).

330.   Naldini, L., Dull, T., Farson, D. A. & Witt, R. Method and means for producing high titer, safe, recombinant lentivirus vectors. US 5994136 A, priority date 1997-12-12, issue date 1999-11-30. *Patent* (1997). at <http://www.google.de/patents/US5994136>

331.   Yildirim, A. O. *et al.* Palifermin induces alveolar maintenance programs in emphysematous mice. *Am. J. Respir. Crit. Care Med.* **181,** 705–17 (2010).

332.   Bochkov, Y. A. & Palmenberg, A. C. Translational efficiency of EMCV IRES in bicistronic vectors is dependent upon IRES sequence and gene location. *Biotechniques* **41,** 283–4, 286, 288 passim (2006).

333.   Ghattas, I. R., Sanes, J. R. & Majors, J. E. The encephalomyocarditis virus internal ribosome entry site allows efficient coexpression of two genes from a recombinant provirus in cultured cells and in embryos. *Mol. Cell. Biol.* **11,** 5848–59 (1991).

334.   Schambach, a *et al.* Woodchuck hepatitis virus post-transcriptional regulatory element deleted from X protein and promoter sequences enhances retroviral vector titer and expression. *Gene Ther.* **13,** 641–645 (2006).

335.   Powell, S. K., Rivera-Soto, R. & Gray, S. J. Viral expression cassette elements to enhance transgene target specificity and expression in gene therapy. *Discov. Med.* **19,** 49–57 (2015).

336.   Hasegawa, K. & Nakatsuji, N. Insulators prevent transcriptional interference between two promoters in a double gene construct for transgenesis. *FEBS Lett.* **520,** 47–52 (2002).

337.   Curtin, J. A., Dane, A. P., Swanson, A., Alexander, I. E. & Ginn, S. L. Bidirectional promoter interference between two widely used internal heterologous promoters in a late-generation lentiviral construct. *Gene Ther.* **15,** 384–90 (2008).

338.   Kumar, M., Keller, B., Makalou, N. & Sutton, R. E. Systematic determination of the packaging limit of lentiviral vectors. *Hum. Gene Ther.* **12,** 1893–905 (2001).

339.   al Yacoub, N., Romanowska, M., Haritonova, N. & Foerster, J. Optimized production and concentration of lentiviral vectors containing large inserts. *J. Gene Med.* **9,** 579–84 (2007).

340.   Cooper, A. R. *et al.* Highly efficient large-scale lentiviral vector concentration by tandem tangential flow filtration. *J. Virol. Methods* **177,** 1–9 (2011).

341.   Sarker, R. S. J. *et al.* Coactivator-Associated Arginine Methyltransferase-1 Function in Alveolar Epithelial Senescence and Elastase-Induced Emphysema Susceptibility. *Am. J. Respir. Cell Mol. Biol.* **53,** 769–81 (2015).

342.   Conlon, T. M. *et al.* Metabolomics screening identifies reduced L-carnitine to be associated with progressive emphysema. *Clin. Sci. (Lond).* **130,** 273–87 (2016).

343.   Vanoirbeek, J. A. J. *et al.* Noninvasive and invasive pulmonary function in mouse models of obstructive and restrictive respiratory diseases. *Am. J. Respir. Cell Mol. Biol.* **42,** 96–104 (2010).

344.   Stein, I. *et al.* Translation of vascular endothelial growth factor mRNA by internal ribosome entry: implications for translation under hypoxia. *Mol. Cell. Biol.* **18,** 3112–3119 (1998).

345.   Weingarten-Gabbay, S. *et al.* Comparative genetics. Systematic discovery of cap-independent translation sequences in human and viral genomes. *Science* **351,** (2016).

346. Ørom, U. A., Nielsen, F. C. & Lund, A. H. MicroRNA-10a binds the 5'UTR of ribosomal protein mRNAs and enhances their translation. *Mol. Cell* **30,** 460–71 (2008).

347. Chung, B. Y. W., Simons, C., Firth, A. E., Brown, C. M. & Hellens, R. P. Effect of 5'UTR introns on gene expression in Arabidopsis thaliana. *BMC Genomics* **7,** 120 (2006).

348. Falcone, D. & Andrews, D. W. Both the 5' untranslated region and the sequences surrounding the start site contribute to efficient initiation of translation in vitro. *Mol. Cell. Biol.* **11,** 2656–2664 (1991).

349. Miao, C. H. *et al.* Inclusion of the hepatic locus control region, an intron, and untranslated region increases and stabilizes hepatic factor IX gene expression in vivo but not in vitro. *Mol. Ther.* **1,** 522–32 (2000).

350. Makoff, A. J., Oxer, M. D., Romanos, M. A., Fairweather, N. F. & Ballantine, S. Expression of tetanus toxin fragment C in E. coli: high level expression by removing rare codons. *Nucleic Acids Res.* **17,** 10191–202 (1989).

351. Kim, C. H., Oh, Y. & Lee, T. H. Codon optimization for high-level expression of human erythropoietin (EPO) in mammalian cells. *Gene* **199,** 293–301 (1997).

352. Ward, N. J. *et al.* Codon optimization of human factor VIII cDNAs leads to high-level expression. *Blood* **117,** 798–807 (2011).

353. Primhak, R. A. & Tanner, M. S. Alpha-1 antitrypsin deficiency. *Arch. Dis. Child.* **85,** 2–5 (2001).

354. Van Linthout, S., Collen, D. & De Geest, B. Effect of promoters and enhancers on expression, transgene DNA persistence, and hepatotoxicity after adenoviral gene transfer of human apolipoprotein A-I. *Hum. Gene Ther.* **13,** 829–40 (2002).

355. Miao, C. H., Thompson, A. R., Loeb, K. & Ye, X. Long-term and therapeutic-level hepatic gene expression of human factor IX after naked plasmid transfer in vivo. *Mol. Ther.* **3,** 947–57 (2001).

356. Watson, H. C. *et al.* Sequence and structure of yeast phosphoglycerate kinase. *EMBO J.* **1,** 1635–40 (1982).

357. Chiarelli, L. R. *et al.* Molecular insights on pathogenic effects of mutations causing phosphoglycerate kinase deficiency. *PLoS One* **7,** e32065 (2012).

358. Merrick, W. C. Mechanism and regulation of eukaryotic protein synthesis. *Microbiol. Rev.* **56,** 291–315 (1992).

359. Salmon, P. *et al.* High-level transgene expression in human hematopoietic progenitors and differentiated blood lineages after transduction with improved lentiviral vectors. *Blood* **96,** 3392–8 (2000).

360. Chen, C., Krohn, J., Bhattacharya, S. & Davies, B. A Comparison of Exogenous Promoter Activity at the ROSA26 Locus Using a PhiC31 Integrase Mediated Cassette Exchange Approach in Mouse ES Cells. *PLoS One* **6,** e23376 (2011).

361. Lee, C. I., Kohn, D. B., Ekert, J. E. & Tarantal, A. F. Morphological analysis and lentiviral transduction of fetal monkey bone marrow-derived mesenchymal stem cells. *Mol. Ther.* **9,** 112–23 (2004).

362. Qin, J. Y. *et al.* Systematic Comparison of Constitutive Promoters and the Doxycycline-Inducible Promoter. *PLoS One* **5,** e10611 (2010).

363. Norrman, K. *et al.* Quantitative comparison of constitutive promoters in human ES cells. *PLoS One* **5,** (2010).

364. Ramezani, A., Hawley, T. S. & Hawley, R. G. Lentiviral vectors for enhanced gene expression in human hematopoietic cells. *Mol. Ther.* **2,** 458–69 (2000).

365.   Zychlinski, D. *et al.* Physiological Promoters Reduce the Genotoxic Risk of Integrating Gene Vectors. *Mol. Ther.* **16,** 718–725 (2008).

366.   De Ravin, S. S. *et al.* Lentiviral hematopoietic stem cell gene therapy for X-linked severe combined immunodeficiency. *Sci. Transl. Med.* **8,** 335ra57–335ra57 (2016).

367.   ClinicalTrials.gov c. Bethesda (MD): National Library of Medicine (US). 2000 Feb 29 – [retrieved 2016 Jun 24]. Clinical trial NCT01852071. *ClinicalTrials.gov c* at <https://clinicaltrials.gov/ct2/results?term=NCT01852071&Search=Search>

368.   Zhong, S., Liu, C., Haviland, D., Doris, P. A. & Teng, B.-B. Simultaneous expression of apolipoprotein B mRNA editing enzyme and scavenger receptor BI mediated by a therapeutic gene expression system. *Atherosclerosis* **184,** 264–75 (2006).

369.   Ngoi, S. M., Chien, A. C. & Lee, C. G. L. Exploiting internal ribosome entry sites in gene therapy vector design. *Curr. Gene Ther.* **4,** 15–31 (2004).

370.   Germann, U. A., Chin, K. V, Pastan, I. & Gottesman, M. M. Retroviral transfer of a chimeric multidrug resistance-adenosine deaminase gene. *FASEB J.* **4,** 1501–7 (1990).

371.   Kim, J. H. *et al.* High cleavage efficiency of a 2A peptide derived from porcine teschovirus-1 in human cell lines, zebrafish and mice. *PLoS One* **6,** e18556 (2011).

372.   Szymczak, A. L. & Vignali, D. A. A. Development of 2A peptide-based strategies in the design of multicistronic vectors. *Expert Opin. Biol. Ther.* **5,** 627–38 (2005).

373.   Eszterhas, S. K., Bouhassira, E. E., Martin, D. I. K. & Fiering, S. Transcriptional interference by independently regulated genes occurs in any relative arrangement of the genes and is influenced by chromosomal integration position. *Mol. Cell. Biol.* **22,** 469–79 (2002).

374.   Emerman, M. & Temin, H. M. Genes with promoters in retrovirus vectors can be independently suppressed by an epigenetic mechanism. *Cell* **39,** 449–67 (1984).

375.   Kadesch, T. & Berg, P. Effects of the position of the simian virus 40 enhancer on expression of multiple transcription units in a single plasmid. *Mol. Cell. Biol.* **6,** 2593–601 (1986).

376.   Proudfoot, N. J. Transcriptional interference and termination between duplicated alpha-globin gene constructs suggests a novel mechanism for gene regulation. *Nature* **322,** 562–5 (1986).

377.   West, A. G., Gaszner, M. & Felsenfeld, G. Insulators: many functions, many mechanisms. *Genes Dev.* **16,** 271–88 (2002).

378.   Tolmachov, O., Subkhankulova, T. & Tolmachova, T. Silencing of Transgene Expression: A Gene Therapy Perspective. *Gene Ther. - Tools Potential Appl.* (2013).

379.   Palmer, A. C., Egan, J. B. & Shearwin, K. E. Transcriptional interference by RNA polymerase pausing and dislodgement of transcription factors. *Transcription* **2,** 9–14 (2011).

380.   Shearwin, K. E., Callen, B. P. & Egan, J. B. Transcriptional interference--a crash course. *Trends Genet.* **21,** 339–45 (2005).

381.   Mizuguchi, H., Xu, Z., Ishii-Watabe, A., Uchida, E. & Hayakawa, T. IRES-dependent second gene expression is significantly lower than cap-dependent first gene expression in a bicistronic vector. *Mol. Ther.* **1,** 376–82 (2000).

382.   Davis, H. E., Rosinski, M., Morgan, J. R. & Yarmush, M. L. Charged polymers modulate retrovirus transduction via membrane charge neutralization and virus aggregation. *Biophys. J.* **86,** 1234–42 (2004).

383.   Katakura, H. *et al.* Improvement of retroviral vectors by coating with poly(ethylene glycol)-poly(L-lysine) block copolymer (PEG-PLL). *J. Gene Med.* **6,** 471–7 (2004).

384. Le Doux, J. M., Morgan, J. R. & Yarmush, M. L. Differential inhibition of retrovirus transduction by proteoglycans and free glycosaminoglycans. *Biotechnol. Prog.* **15,** 397–406 (1999).

385. Terwilliger, E. F., Godin, B., Sodroski, J. G. & Haseltine, W. A. Construction and use of a replication-competent human immunodeficiency virus (HIV-1) that expresses the chloramphenicol acetyltransferase enzyme. *Proc. Natl. Acad. Sci. U. S. A.* **86,** 3857–61 (1989).

386. Antoniou, M. N., Skipper, K. A. & Anakok, O. Optimizing retroviral gene expression for effective therapies. *Hum. Gene Ther.* **24,** 363–74 (2013).

387. Ahn, S. Y. *et al.* Long-term (postnatal day 70) outcome and safety of intratracheal transplantation of human umbilical cord blood-derived mesenchymal stem cells in neonatal hyperoxic lung injury. *Yonsei Med. J.* **54,** 416–24 (2013).

388. De Palma, M. *et al.* Tumor-targeted interferon-alpha delivery by Tie2-expressing monocytes inhibits tumor growth and metastasis. *Cancer Cell* **14,** 299–311 (2008).

389. Flotte, T. R. & Mueller, C. Gene therapy for alpha-1 antitrypsin deficiency. *Hum. Mol. Genet.* **20,** R87–R92 (2011).

390. Slingsby, J. H. *et al.* Analysis of 4070A envelope levels in retroviral preparations and effect on target cell transduction efficiency. *Hum. Gene Ther.* **11,** 1439–51 (2000).

391. Lavoie, J. R. *et al.* EMILIN-1 and ILK are Novel Markers of Islet Regenerative Function in Human Multipotent Mesenchymal Stromal Cells. *Stem Cells* (2016). doi:10.1002/stem.2385

392. Lee, R. H. *et al.* TSG-6 as a biomarker to predict efficacy of human mesenchymal stem/progenitor cells (hMSCs) in modulating sterile inflammation in vivo. *Proc. Natl. Acad. Sci. U. S. A.* **111,** 16766–71 (2014).

393. von Bahr, L. *et al.* Long-term complications, immunologic effects, and role of passage for outcome in mesenchymal stromal cell therapy. *Biol. Blood Marrow Transplant.* **18,** 557–64 (2012).

394. Kim, D. W., Uetsuki, T., Kaziro, Y., Yamaguchi, N. & Sugano, S. Use of the human elongation factor 1 alpha promoter as a versatile and efficient expression system. *Gene* **91,** 217–23 (1990).

395. Kim, S.-Y., Lee, J.-H., Shin, H.-S., Kang, H.-J. & Kim, Y.-S. The human elongation factor 1 alpha (EF-1 alpha) first intron highly enhances expression of foreign genes from the murine cytomegalovirus promoter. *J. Biotechnol.* **93,** 183–7 (2002).

396. Somia, N. & Verma, I. M. Gene therapy: trials and tribulations. *Nat. Rev. Genet.* **1,** 91–99 (2000).

397. Thomas, C. E., Ehrhardt, A. & Kay, M. a. Progress and problems with the use of viral vectors for gene therapy. *Nat. Rev. Genet.* **4,** 346–58 (2003).

398. Kay, M. A., Glorioso, J. C. & Naldini, L. Viral vectors for gene therapy: the art of turning infectious agents into vehicles of therapeutics. *Nat. Med.* **7,** 33–40 (2001).

399. Schmidt, F. & Grimm, D. CRISPR genome engineering and viral gene delivery: a case of mutual attraction. *Biotechnol. J.* **10,** 258–72 (2015).

400. Miller, D. G., Adam, M. a & Miller, a D. Gene transfer by retrovirus vectors occurs only in cells that are actively replicating at the time of infection. *Mol. Cell. Biol.* **10,** 4239–4242 (1990).

401. Roe, T., Reynolds, T. C., Yu, G. & Brown, P. O. Integration of murine leukemia virus DNA depends on mitosis. *EMBO J.* **12,** 2099–2108 (1993).

402. Piller, S. C., Caly, L. & Jans, D. A. Nuclear import of the pre-integration complex (PIC): the Achilles heel of HIV? *Curr. Drug Targets* **4,** 409–29 (2003).

403. Le Doux, J. M., Morgan, J. R., Snow, R. G. & Yarmush, M. L. Proteoglycans secreted by packaging cell lines inhibit retrovirus infection. *J. Virol.* **70,** 6468–73 (1996).

404. Landázuri, N. & Le Doux, J. M. Complexation with chondroitin sulfate C and Polybrene rapidly purifies retrovirus from inhibitors of transduction and substantially enhances gene transfer. *Biotechnol. Bioeng.* **93,** 146–58 (2006).

405. Landazuri, N., Krishna, D., Gupta, M. & Le Doux, J. M. Retrovirus-polymer complexes: study of the factors affecting the dose response of transduction. *Biotechnol. Prog.* **23,** 480–7 (2007).

406. Rothe, M., Modlich, U. & Schambach, A. Biosafety challenges for use of lentiviral vectors in gene therapy. *Curr. Gene Ther.* **13,** 453–68 (2013).

407. Schröder, a. R. W. *et al.* HIV-1 integration in the human genome favors active genes and local hotspots. *Cell* **110,** 521–529 (2002).

408. Wu, X., Li, Y., Crise, B. & Burgess, S. M. Transcription start regions in the human genome are favored targets for MLV integration. *Science* **300,** 1749–51 (2003).

409. Wang, G. P. *et al.* Analysis of Lentiviral Vector Integration in HIV+ Study Subjects Receiving Autologous Infusions of Gene Modified CD4+ T Cells. *Mol. Ther.* **17,** 844–850 (2009).

410. Moiani, A. *et al.* Genome-wide analysis of alpharetroviral integration in human hematopoietic stem/progenitor cells. *Genes (Basel).* **5,** 415–429 (2014).

411. Cattoglio, C. *et al.* High-definition mapping of retroviral integration sites identifies active regulatory elements in human multipotent hematopoietic progenitors. *Blood* **116,** 5507–17 (2010).

412. Miller, a D. *et al.* Construction and properties of retrovirus packaging cells based on gibbon ape leukemia virus. *J. Virol.* **65,** 2220–4 (1991).

413. Zhan, H. *et al.* Production and first-in-man use of T cells engineered to express a HSVTK-CD34 sort-suicide gene. *PLoS One* **8,** e77106 (2013).

414. Parente, M. K. & Wolfe, J. H. Production of increased titer retrovirus vectors from stable producer cell lines by superinfection and concentration. *Gene Ther.* **3,** 756–60 (1996).

415. Humbert, O. *et al.* Development of 3(rd) Generation Cocal Envelope Producer Cell Lines for Robust Lentiviral Gene Transfer into Hematopoietic Stem Cells and T Cells. *Mol. Ther.* (2016). doi:10.1038/mt.2016.70

416. Marques, P. I. *et al.* SERPINA2 is a novel gene with a divergent function from SERPINA1. *PLoS One* **8,** e66889 (2013).

417. Lomas, D. A. & Carrell, R. W. Serpinopathies and the conformational dementias. *Nat. Rev. Genet.* **3,** 759–68 (2002).

418. Wright, J. L., Cosio, M. & Churg, A. Animal models of chronic obstructive pulmonary disease. *Am. J. Physiol. Lung Cell. Mol. Physiol.* **295,** L1–15 (2008).

419. Laurell, C.-B. & Eriksson, S. The electrophoretic α1-globulin pattern of serum in α1-antitrypsin deficiency. 1963. *COPD* **10 Suppl 1,** 3–8 (2013).

420. Fujita, M. & Nakanishi, Y. The pathogenesis of COPD: lessons learned from in vivo animal models. *Med. Sci. Monit.* **13,** RA19–24 (2007).

421. Dau, T., Sarker, R. S. J., Yildirim, A. O., Eickelberg, O. & Jenne, D. E. Autoprocessing of neutrophil elastase near its active site reduces the efficiency of natural and synthetic elastase inhibitors. *Nat. Commun.* **6,** 6722 (2015).

422. John-Schuster, G. *et al.* Inflammaging increases susceptibility to cigarette smoke-induced COPD. *Oncotarget* **5,** (2015).

423. Lundblad, L. K. A., Irvin, C. G., Adler, A. & Bates, J. H. T. A reevaluation of the validity of unrestrained plethysmography in mice. *J. Appl. Physiol.* **93,** 1198–207 (2002).

424. Stone, P. J. *et al.* Defenses of the hamster lung against human neutrophil and porcine pancreatic elastase. *Respiration.* **54,** 1–15 (1988).

425. Lucey, E. C., Keane, J., Kuang, P.-P., Snider, G. L. & Goldstein, R. H. Severity of elastase-induced emphysema is decreased in tumor necrosis factor-alpha and interleukin-1beta receptor-deficient mice. *Lab. Invest.* **82,** 79–85 (2002).

426. Henry, C. M. *et al.* Neutrophil-Derived Proteases Escalate Inflammation through Activation of IL-36 Family Cytokines. *Cell Rep.* **14,** 708–22 (2016).

427. Lu, Y. *et al.* Human alpha 1-antitrypsin therapy induces fatal anaphylaxis in non-obese diabetic mice. *Clin. Exp. Immunol.* **154,** 15–21 (2008).

428. Le Blanc, K., Tammki, L., Sundberg, B., Haynesworth, S. E. & Ringden, O. Mesenchymal stem cells inhibit and stimulate mixed lymphocyte cultures and mitogenic response independently of the major histocompatibility complex. *Scand J Immunol* **57,** 11–20 (2003).

429. Klyushnenkova, E. *et al.* T cell responses to allogeneic human mesenchymal stem cells: immunogenicity, tolerance, and suppression. *J. Biomed. Sci.* **12,** 47–57 (2005).

430. Mo, M., Wang, S., Zhou, Y., Li, H. & Wu, Y. Mesenchymal stem cell subpopulations: phenotype, property and therapeutic potential. *Cell. Mol. Life Sci.* (2016). doi:10.1007/s00018-016-2229-7

431. Yamada, M. *et al.* Inflammatory responses in the initiation of lung repair and regeneration: their role in stimulating lung resident stem cells. *Inflamm. Regen. 2016 361* **36,** 584–591 (2016).

432. Tibboel, J., Keijzer, R., Reiss, I., de Jongste, J. C. & Post, M. Intravenous and intratracheal mesenchymal stromal cell injection in a mouse model of pulmonary emphysema. *COPD* **11,** 310–8 (2014).

433. Kim, Y.-S. *et al.* The Therapeutic Effects of Optimal Dose of Mesenchymal Stem Cells in a Murine Model of an Elastase Induced-Emphysema. *Tuberc. Respir. Dis. (Seoul).* **78,** 239–45 (2015).

434. Minnich, M., Kueppers, F. & James, H. Alpha-1-antitrypsin from mouse serum isolation and characterization. *Comp. Biochem. Physiol. B.* **78,** 413–9 (1984).

435. Riches, A. C., Sharp, J. G., Thomas, D. B. & Smith, S. V. Blood volume determination in the mouse. *J. Physiol.* **228,** 279–84 (1973).

436. Kay, M. A., Graham, F., Leland, F. & Woo, S. L. Therapeutic serum concentrations of human alpha-1-antitrypsin after adenoviral-mediated gene transfer into mouse hepatocytes. *Hepatology* **21,** 815–9 (1995).

437. Konala, V. B. R. *et al.* The current landscape of the mesenchymal stromal cell secretome: A new paradigm for cell-free regeneration. *Cytotherapy* **18,** 13–24 (2016).

438. Rani, S., Ryan, A. E., Griffin, M. D. & Ritter, T. Mesenchymal Stem Cell-derived Extracellular Vesicles: Toward Cell-free Therapeutic Applications. *Mol. Ther.* **23,** 812–23 (2015).

439. Lee, C. *et al.* Exosomes mediate the cytoprotective action of mesenchymal stromal cells on hypoxia-induced pulmonary hypertension. *Circulation* **126,** 2601–11 (2012).

6. Supplemental material

6.1. Sequences

SERPINA1 CDS: Bases 262 to 1518 of the full reference sequence published at http://www.ncbi.nlm.nih.gov/nuccore/NM_000295.4.

```
                         262 atgccgtct tctgtctcgt ggggcatcct cctgctggca
     301 ggcctgtgct gcctggtccc tgtctccctg gctgaggatc cccagggaga tgctgcccag
     361 aagacagata catcccacca tgatcaggat cacccaacct tcaacaagat cacccccaac
     421 ctggctgagt tcgccttcag cctataccgc cagctggcac accagtccaa cagcaccaat
     481 atcttcttct ccccagtgag catcgctaca gcctttgcaa tgctctccct ggggaccaag
     541 gctgacactc acgatgaaat cctggagggc ctgaatttca acctcacgga gattccggag
     601 gctcagatcc atgaaggctt ccaggaactc ctccgtaccc tcaaccagcc agacagccag
     661 ctccagctga ccaccggcaa tggcctgttc ctcagcgagg gcctgaagct agtggataag
     721 tttttggagg atgttaaaaa gttgtaccac tcagaagcct tcactgtcaa cttcgggggac
     781 accgaagagg ccaagaaaca gatcaacgat tacgtggaga agggtactca agggaaaatt
     841 gtggatttgg tcaaggagct tgacagagac acagtttttg ctctggtgaa ttacatcttc
     901 tttaaaggca aatgggagag acccttttgaa gtcaaggaca ccgaggaaga ggacttccac
     961 gtggaccagg tgaccaccgt gaaggtgcct atgatgaagc gtttaggcat gtttaacatc
    1021 cagcactgta agaagctgtc cagctgggtg ctgctgatga aatacctggg caatgccacc
    1081 gccatcttct tcctgcctga tgaggggaaa ctacagcacc tggaaaatga actcacccac
    1141 gatatcatca ccaagttcct ggaaaatgaa gacagaaggt ctgccagctt acatttaccc
    1201 aaactgtcca ttactggaac ctatgatctg aagagcgtcc tgggtcaact gggcatcact
    1261 aaggtcttca gcaatggggc tgacctctcc ggggtcacag aggaggcacc cctgaagctc
    1321 tccaaggccg tgcataaggc tgtgctgacc atcgacgaga aagggactga agctgctggg
    1381 gccatgtttt tagaggccat acccatgtct atcccccccg aggtcaagtt caacaaaccc
    1441 tttgtcttct taatgattga acaaaatacc aagtctcccc tcttcatggg aaaagtggtg
    1501 aatcccaccc aaaaataa
```

The SERPINA1 CDS was codon optimized for *homo sapiens* to increase protein production. The CDS after codon optimization reads as follows:

```
ATGCCCAGCAGCGTGTCCTGGGGAATTCTGCTGCTGGCCGGCCTGTGTTGTCTGGTGCCTGTGTCTCT
GGCCGAGGACCCTCAGGGGGATGCCGCCCAGAAAACCGATACCAGCCACCACGACCAGGACCACCCCA
CCTTCAACAAGATCACCCCCAACCTGGCCGAGTTCGCCTTCAGCCTGTACAGACAGCTGGCCCACCAG
AGCAACAGCACCAACATCTTTTTTCAGCCCCGTGTCTATCGCCACCGCCTTCGCCATGCTGAGCCTGGG
CACAAAGGCCGACACCCACGACGAGATCCTGGAAGGCCTGAACTTCAACCTGACCGAGATCCCCGAGG
CCCAGATCCACGAGGGCTTCCAGGAACTGCTGCGGACCCTGAACCAGCCCGATAGCCAGCTGCAGCTG
ACAACCGGCAACGGCCTGTTTCTGAGCGAGGGACTGAAGCTGGTGGACAAGTTTCTGGAAGATGTGAA
GAAGCTGTATCACAGCGAGGCCTTCACCGTGAACTTCGGCGACACCGAGGAAGCCAAGAAGCAGATCA
ACGACTACGTGGAAAAGGGCACCCAGGGCAAGATCGTGGACCTCGTGAAAGAGCTGGACCGGGACACC
GTGTTCGCCCTCGTGAACTACATCTTCTTCAAGGGCAAGTGGGAGCGGCCCTTCGAAGTGAAGGACAC
AGAGGAAGAGGACTTTCACGTGGACCAAGTGACCACCGTGAAGGTGCCCATGATGAAGAGACTGGGCA
TGTTCAACATCCAGCACTGCAAGAAACTGAGCAGCTGGGTGCTGCTGATGAAGTACCTGGGCAACGCT
ACCGCCATATTCTTTCTGCCCGACGAGGGCAAGCTGCAGCACCTGGAAAACGAGCTGACCCACGACAT
CATCACCAAATTTCTGGAAAATGAGGACCGGCGGAGCGCCAGCCTGCATCTGCCTAAGCTGTCTATCA
CCGGCACCTACGACCTGAAGTCCGTGCTGGGACAGCTGGGCATCACCAAGGTGTTCAGCAACGGCGCC
GATCTGAGCGGCGTGACAGAAGAGGCCCCTCTGAAGCTGTCCAAGGCCGTGCACAAAGCCGTGCTGAC
CATCGACGAGAAGGGCACCGAAGCCGCTGGCGCCATGTTTCTGGAAGCCATCCCCATGAGCATCCCCC
CTGAAGTGAAGTTCAACAAGCCCTTCGTGTTCCTGATGATCGAGCAGAACACCAAGAGCCCCCTGTTC
ATGGGCAAGGTCGTGAACCCCACCCAGAAA
```
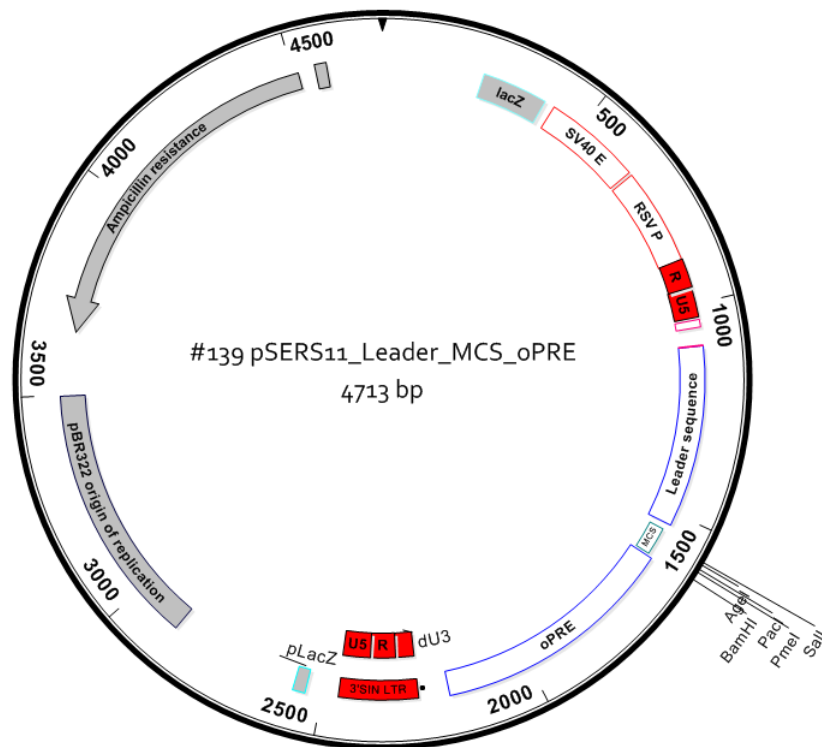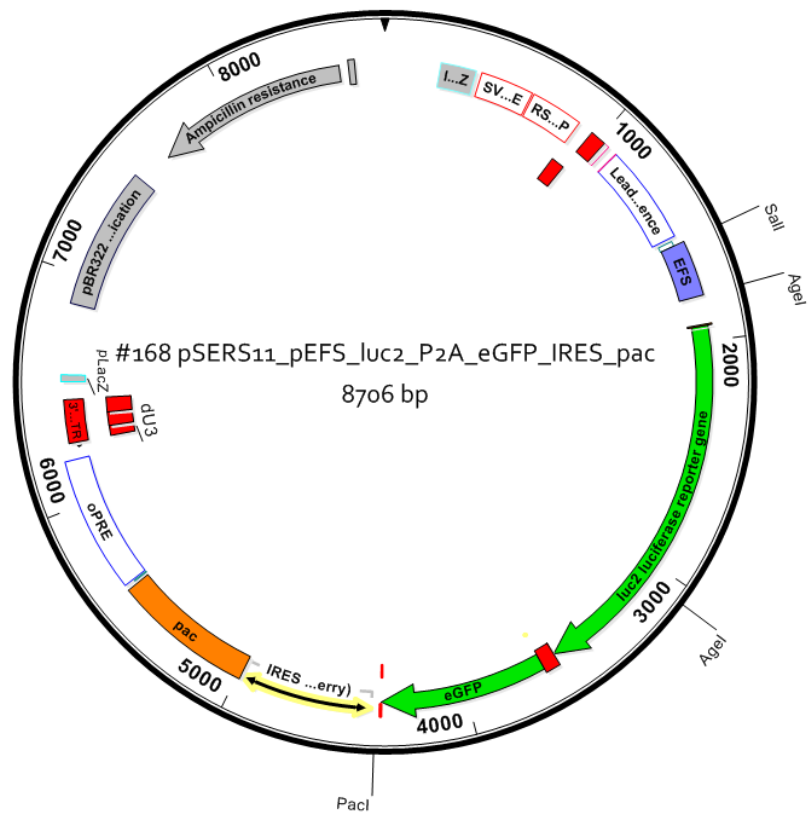
6.2. Plasmid maps – intermediate constructs
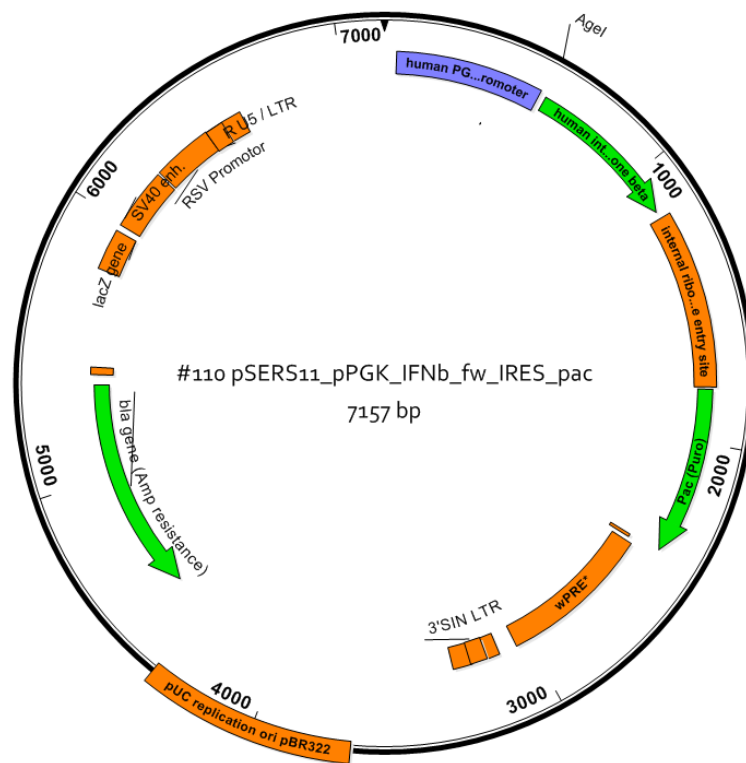
Supplemental figure 1: Plasmid map of plasmid #110 pSERS11_pPGK_IFNb_fw_IRES_pac
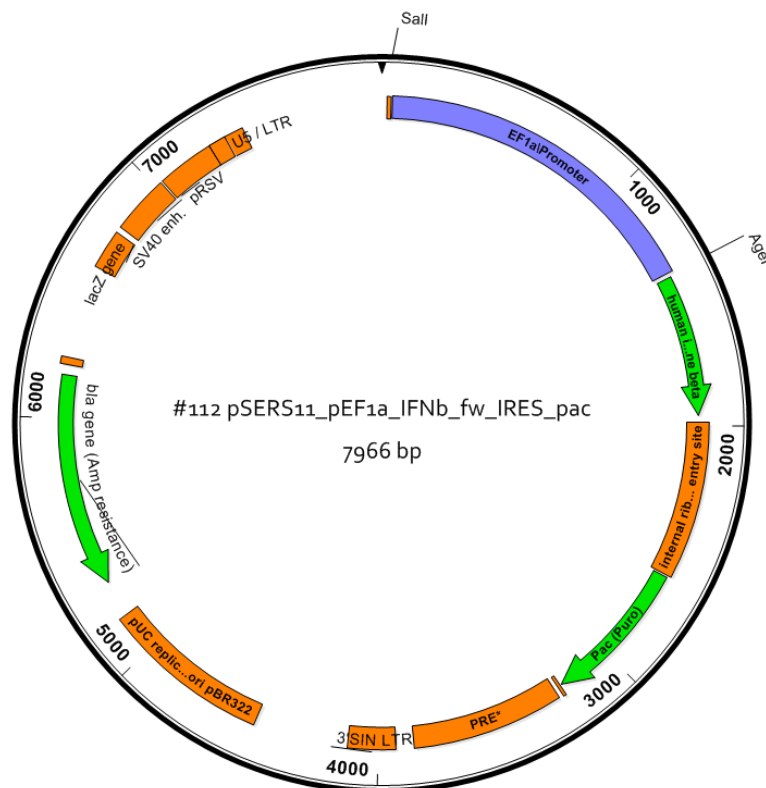
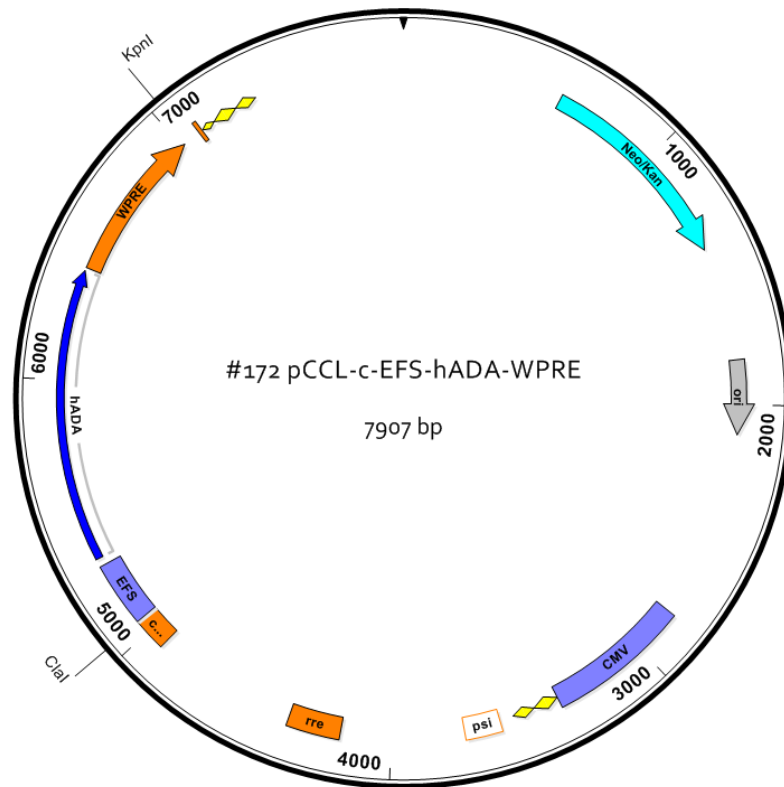Supplemental figure 2: Plasmid mag of plasmid #112 pSERS11_pEF1a_IFNb_fw_IRES_pac

Supplemental figure 3: Plasmid map of plasmid #139 pSERS11_Leader_MCS_oPRE

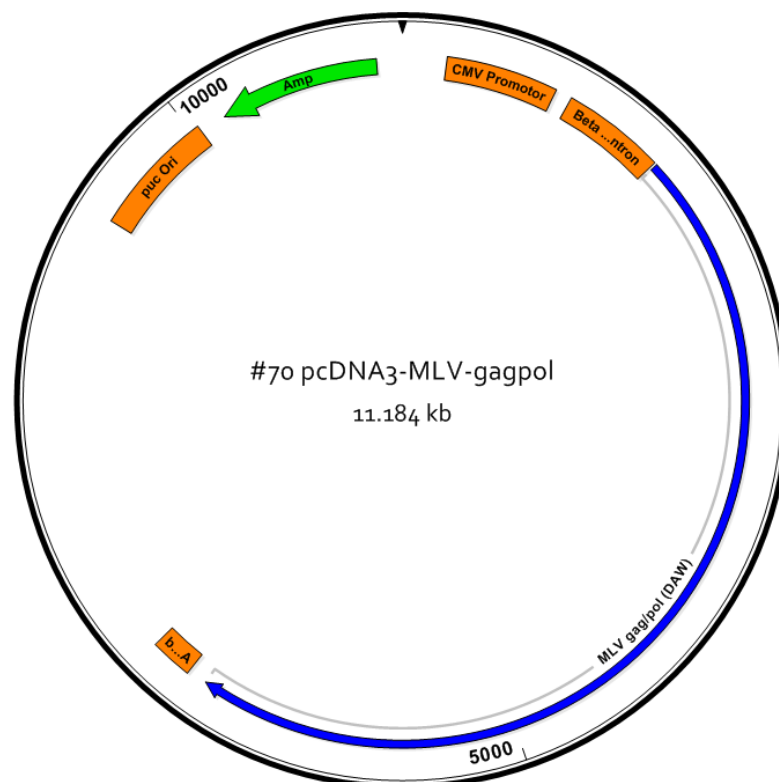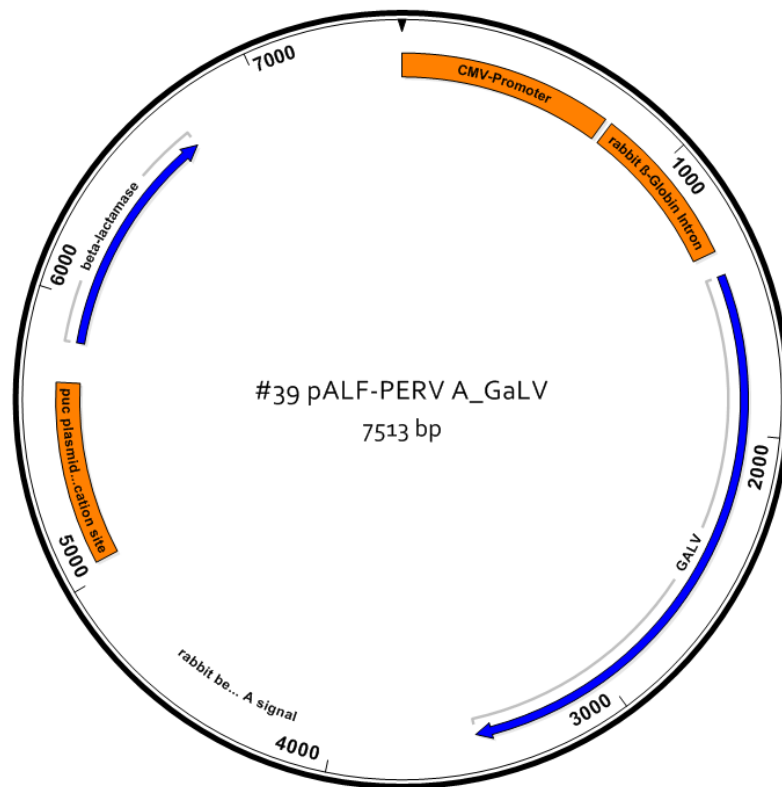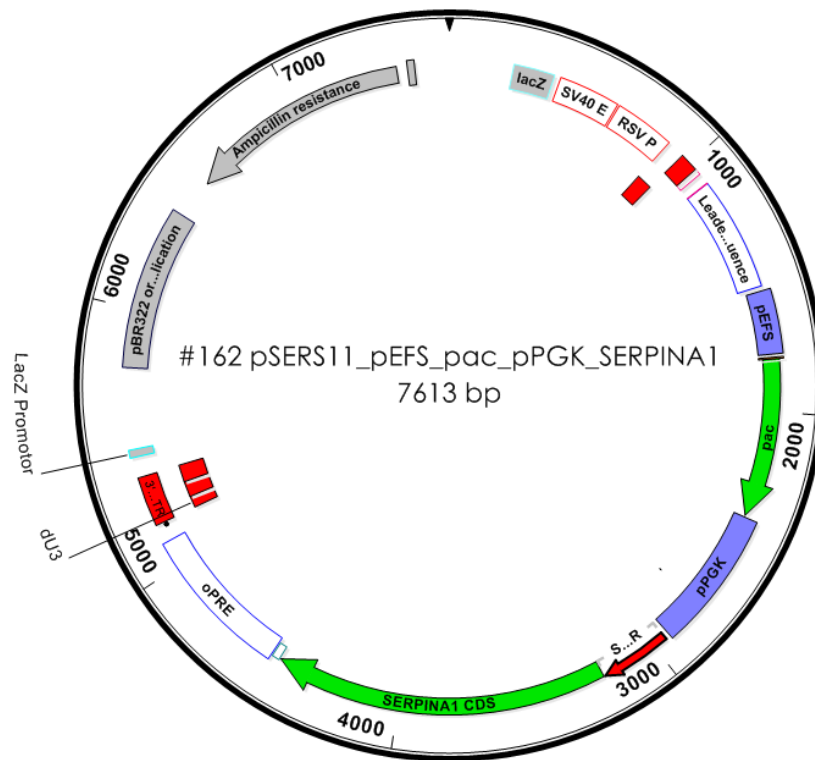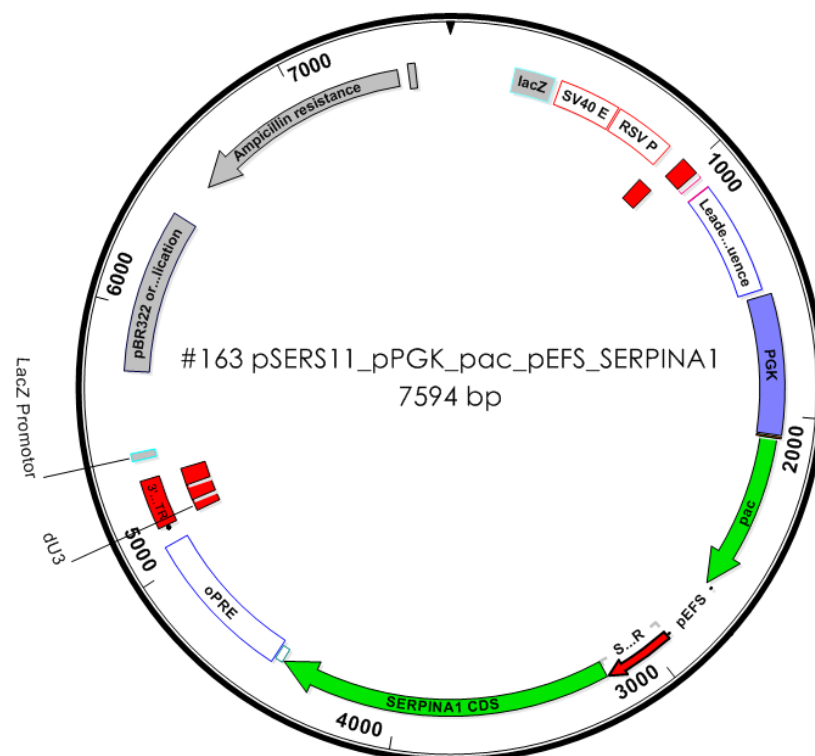Supplemental figure 4: Plasmid map of plasmid #168 pSERS11_pEFS_luc2_P2A_eGPF_IRES_pac

Supplemental figure 5: Plasmid map of plasmid #172 pCCL-c-EFS-hADA_WPRE

6.3. Plasmid maps – helper plasmids

6.3.1. Gamma-retroviral helper plasmids

Supplemental figure 6: Plasmid map of plasmid #70 pcDNA3-MLV-gagpol

Supplemental figure 7: Plasmid map of plasmid #39 pALF-PERV A_GaLV

6.3.2. Lentiviral helper plasmids
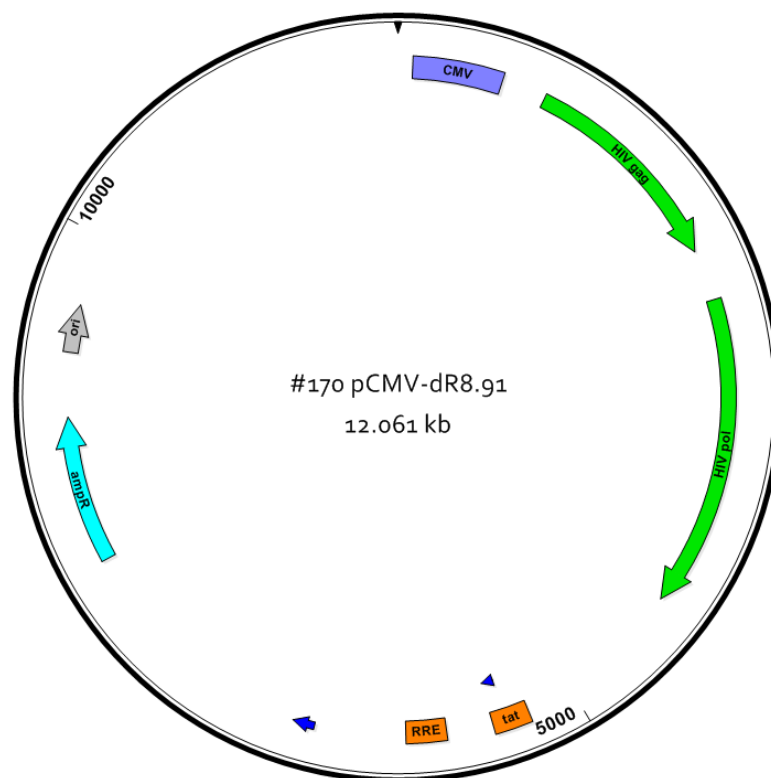
Supplemental figure 8: Plasmid map of plasmid #170 pCMV-dR8.91
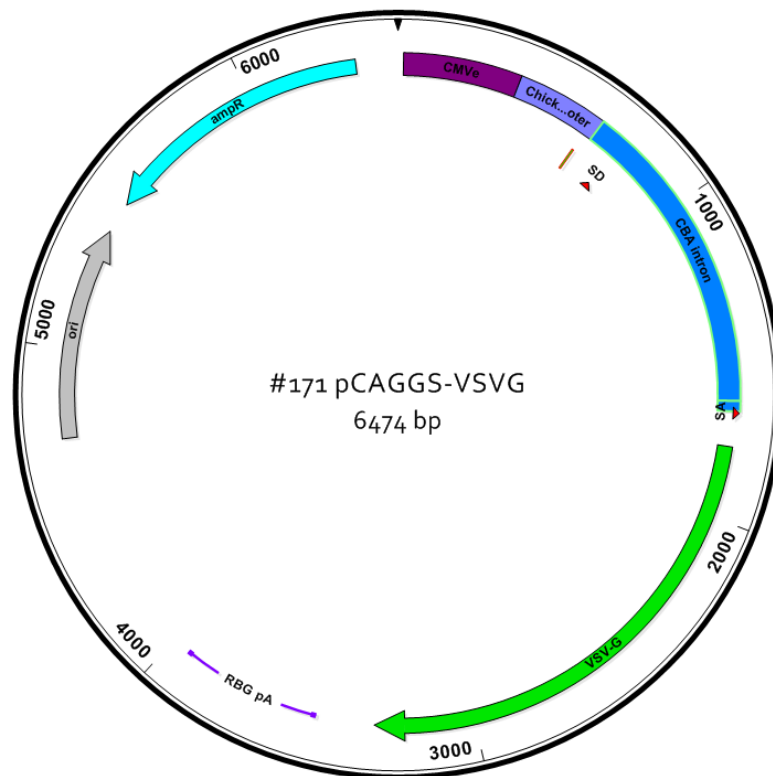
Supplemental figure 9: Plasmid map of plasmid #171 pCAGGS-VSVG

6.4. Plasmid maps – gamma-retroviral AAT expression constructs
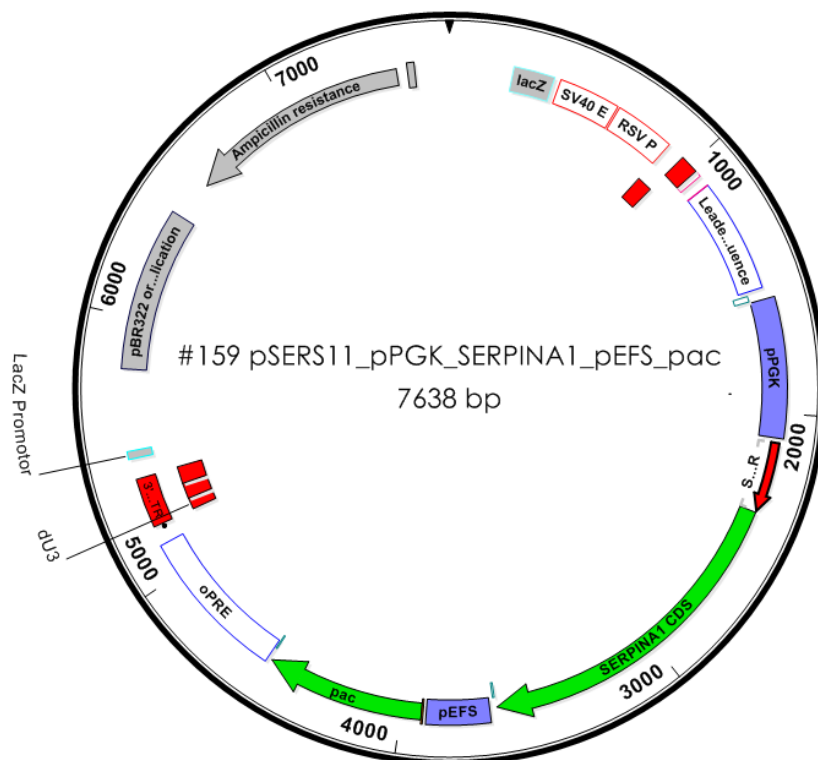
Supplemental figure 10: Plasmid map of plasmid #159 pSERS11_pPGK_SERPINA1_pEFS_pac
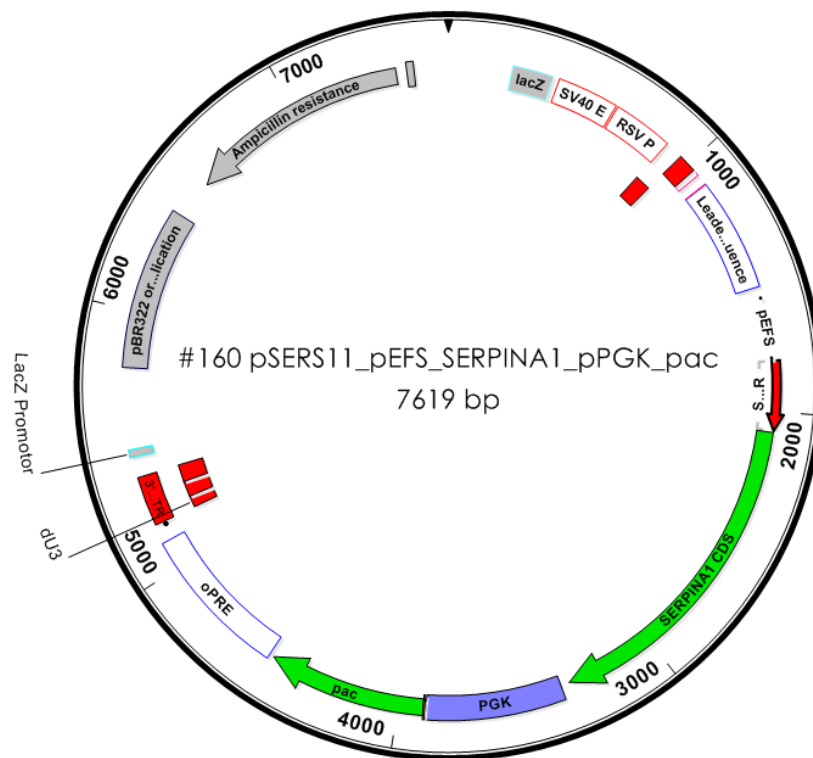
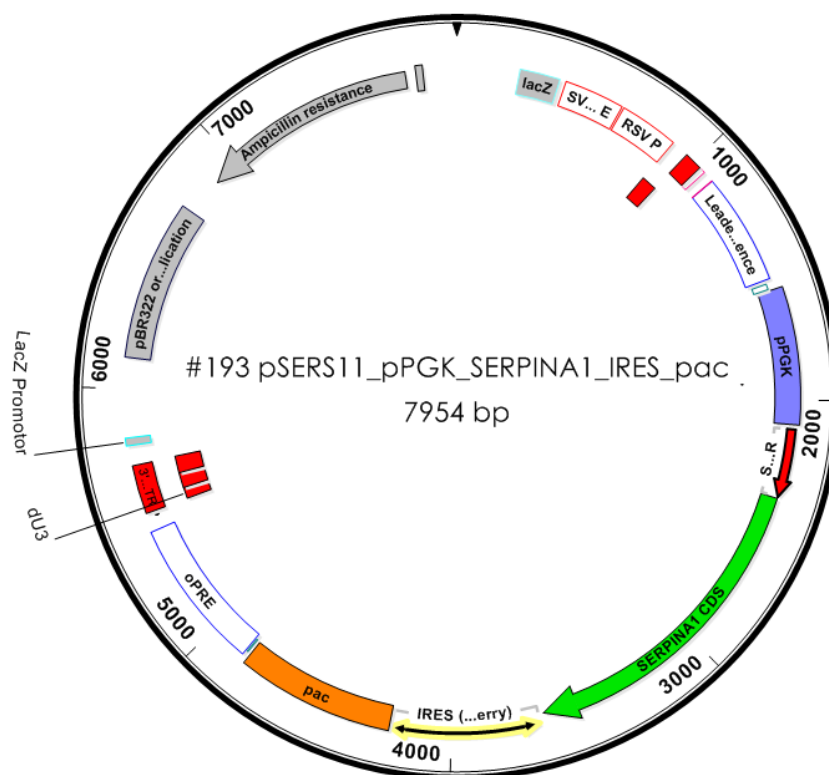Supplemental figure 11: Plasmid map of plasmid #160 pSERS11_pEFS_SERPINA1_pPGK_pac
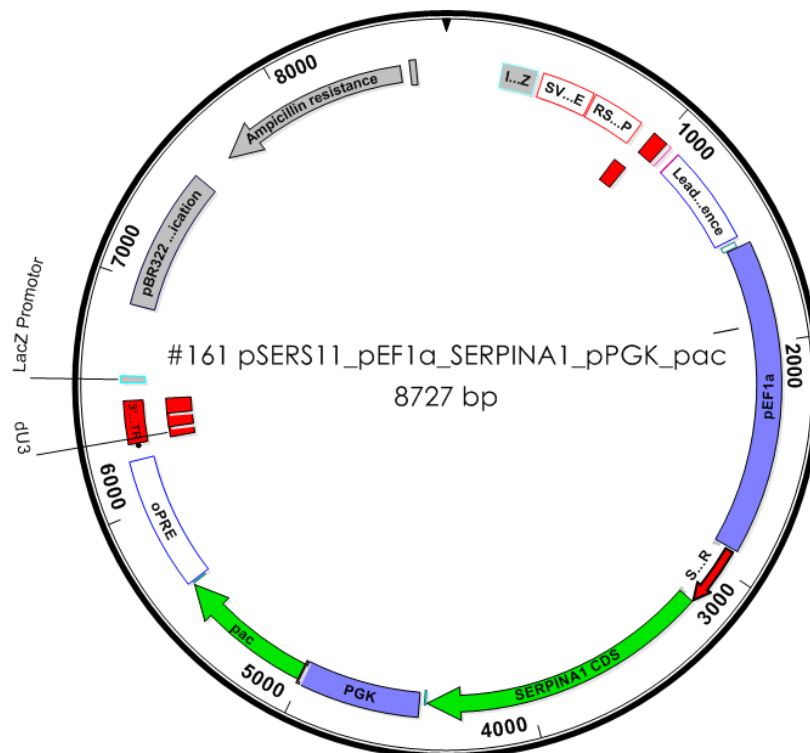
Supplemental figure 12: Plasmid map of plasmid #161 pSERS11_pEF1a_SERPINA1_pPGK_pac

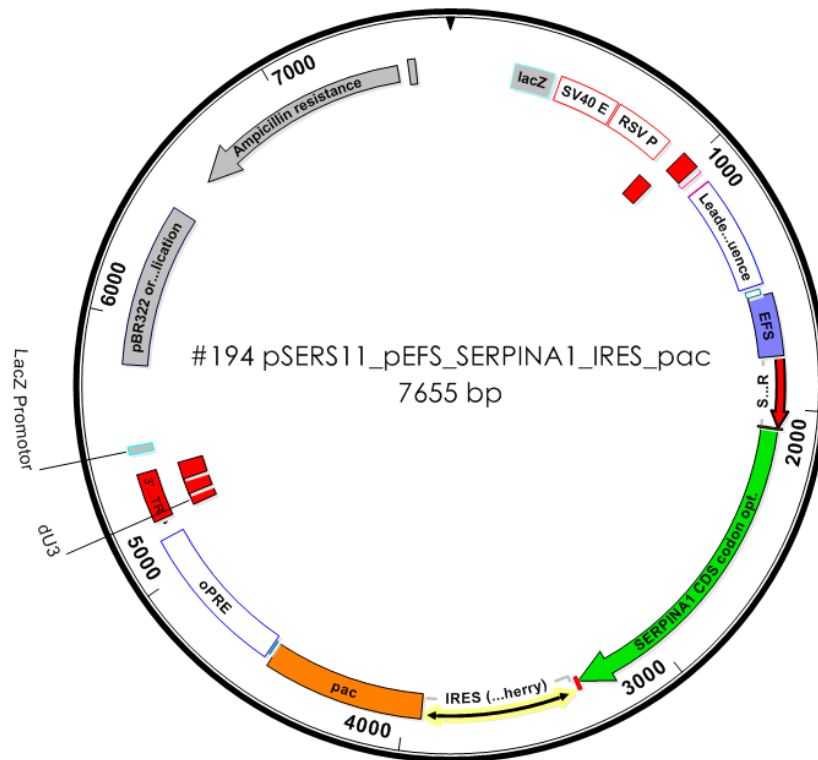Supplemental figure 13: Plasmid map of plasmid #162 pSERS11_pEFS_pac_pPGK_SERPINA1

Supplemental figure 14: Plasmid map of plasmid #163 pSERS11_pPGK_pac_pEFS_SERPINA1
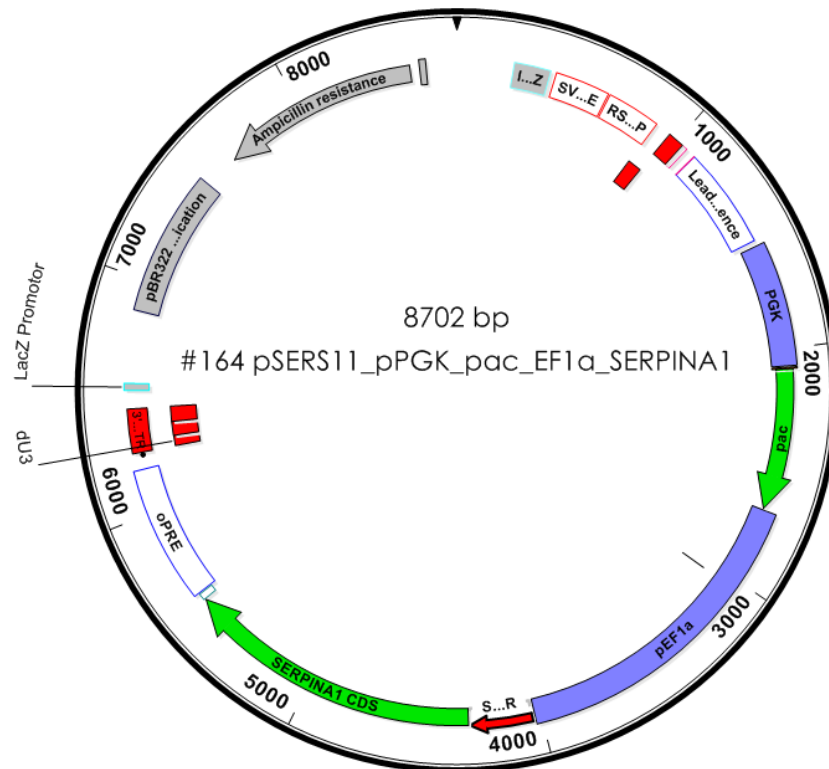
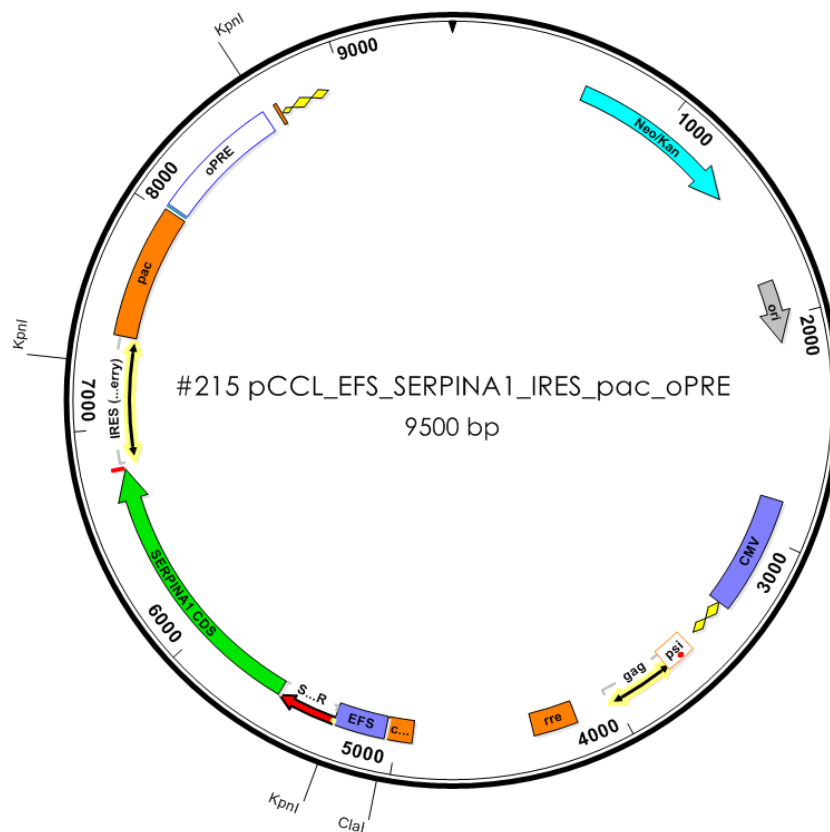Supplemental figure 15: Plasmid map of plasmid #164 pSERS11_pPGK_pac_pEF1a_SERPINA1

Supplemental figure 16: Plasmid map of plasmid #193 pSERS11_pPGK_SERPINA1_IRES_pac

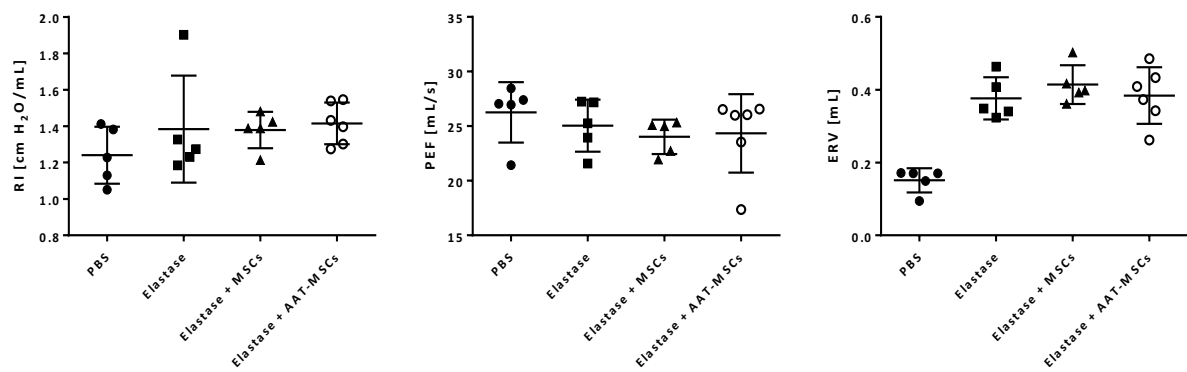Supplemental figure 17: Plasmid map of plasmid #194 pSERS11_pEFS_SERPINA1_IRES_pac

6.5. Plasmid maps – lentiviral AAT expression construct

Supplemental figure 18: Plasmid map of plasmid #215 pCCL_pEFS_SERPINA1_IRES_pac

6.6. Additional pulmonary function parameters

Supplemental figure 19: **Invasive lung function measurements using the Buxco forced pulmonary maneuver system.** Lung function parameters were measured applying the Fast Flow Volume (FV) and the Quasistatic Pressure Volume (PV) tests. Invasive pulmonary function analyses of resistance (RI), peak expiratory flow (PEF), and expiratory reserve volume (ERV).